



U F *m* G

Biomechanical and mechanobiological model of the midpalatal suture formation process, by computational simulation

Ph.D. Thesis by
José Alejandro Guerrero Vargas

Thesis supervisors:
Ph.D., Estevam Barbosa de Las Casas
Ph.D., Diego Alexander Garzón Alvarado

Universidad Nacional de Colombia
Department of Mechanical and Mechatronics Engineering
Universidade Federal de Minas Gerais
School of Mechanical Engineering
October - 2019

Biomechanical and mechanobiological model of the midpalatal suture formation process, by computational simulation

José Alejandro Guerrero Vargas

Co-tutelle Ph.D. Thesis to obtain the degree of Doctor in:

Engineering - Mechanical and Mechatronics Engineering
Universidad Nacional de Colombia
Bogotá (Colombia)

and

Mechanical Engineering
Universidade Federal de Minas Gerais
Belo Horizonte (Brazil)

G934b Guerrero Vargas, Jos  Alejandro.
Biomechanical and mechanobiological model of the midpalatal suture formation process, by computational simulation [recurso eletr nico] / Jos  Alejandro Guerrero Vargas. - 2019.
1 recurso online (xvi, 122 f. : il., color.) : pdf.

Orientador: Diego Alexander Garz n Alvarado.
Coorientador: Estevam Barbosa de Las Casas.

Tese (doutorado) - Universidade Federal de Minas Gerais, Escola de Engenharia.

Ap ndices: f. 84-110.

Bibliografia: f. 111-122.
Exig ncias do sistema: Adobe Acrobat Reader.

1. Engenharia mec nica - Teses. 2. Biomec nica - Teses. 3. M todo dos elementos finitos - Teses. 4. Simula...  o (Computadores) Teses.
I. Garz n Alvarado, Diego Alexander. II. Las Casas, Estevam Barbosa de. III. Universidade Federal de Minas Gerais. Escola de Engenharia.
IV. T tulo.

CDU: 621(043)



UNIVERSIDADE FEDERAL DE MINAS GERAIS
PROGRAMA DE PÓS-GRADUAÇÃO EM
ENGENHARIA MECÂNICA
Av. Antônio Carlos, 6627 - Campus Universitário
31270-901 - Belo Horizonte - MG
Tela: +55 31 3409.5145
E-mail: epneca@ufmg.br

**"BIOMECHANICAL AND MECHANOBIOLOGICAL MODEL OF THE
MIDPALATAL SUTURE FORMATION PROCESS, BY
COMPUTATIONAL SIMULATION"**

JOSE ALEJANDRO GUERRERO VARGAS

Tese submetida à Banca Examinadora designada pelo Colegiado do Programa de Pós-Graduação em Engenharia Mecânica da Universidade Federal de Minas Gerais, como parte dos requisitos necessários a obtenção do título de "Doutor em Engenharia Mecânica", na área de concentração de "Bioengenharia".

Tese aprovada no dia 09 de outubro de 2019.

Por:

Prof. Estevam Barbosa de las Casas
Orientador - Departamento de Engenharia de Estruturas UFMG

Prof. Soraiá Macari
Departamento de Odontopediatria e Ortodontia UFMG

Prof. Dan Romanick
University of Alberta

Prof. Flávio Augusto Prieto Ortiz
Universidad Nacional de Colombia

Prof. Henry Octavio Cortés Ramos
Universidad Nacional de Colombia

Prof. Diego Alexander Gayzón Alvarado
Universidad Nacional de Colombia

To my mother who has always been there, who has always supported me, who has always believed in me. She who, regardless the day or time, continues giving support to this son who loves her.

To my beloved Laura who had the right word to give me peace of mind in the moments where I lost my way. To her who came to my life to show me multiple ways of being happy.

To my sisters, my nephews and all my family and friends who have always wanted the best for my life. They who have motivated many of my decisions and have shared and lived moments with me, making them a fundamental part of my life.

I dedicate this work done with a lot of effort and love to all of them and I hope to continue providing them with joys and good memories.

Acknowledgments

The PhD thesis is a path full of experiences and learning and its development has become one of the most important stages of my life. This thesis, product of an arduous effort, would not have been possible if I had not crossed paths with people who with their support, knowledge or friendship made it possible to achieve this goal. Many thanks to all those who as teachers, as colleagues, as family or as friends contributed to this work. Thank God for having put them in my way, for having assigned me this project and for having given me the opportunities and the strength to bring it to a successful conclusion.

I would like to acknowledge my thesis advisor in Colombia, Dr. Diego Alexander Garzón Alvarado, for the teachings, for the patience and for sharing his knowledge for the development of this work. Thanks for the words, for the friendship and for the orientation that has marked a great part of my academic and professional life. I would like to acknowledge my thesis advisor in Brazil, Dr. Estevam Barbosa de Las Casas, for all the valuable contributions to each of the analyzes developed, for having received me in such a beautiful country as Brazil is and for having given me the opportunity to have a great academic experience at the UFMG.

Thanks to Prof. Angel Yobany, the people linked to the pathology laboratory and the postgraduate department of the Universidad Nacional. Thanks to Prof. Soraia, Prof. Tarcília, Breno, the staff of the biological sciences institute and the graduate department of the UFMG. In both cases, the contributions and support received during the development of this work was fundamental.

Thanks to my friends from the Group of Modeling and Numerical Methods in Engineering of the Universidad Nacional de Colombia and from the Group of Biomechanics of the Universidade Federal de Minas Gerais for allowing me to work as a team with you, for helping me when I needed it and for sharing moments in these last years that I will always remember with joy.

Finally, I would like to thank COLCIENCIAS–COLFUTURO for the financial support that I received through the scholarship program for national doctorates, No. 617 of 2013.

Contents

Acknowledgments	vii
Table of Contents	viii
List of Figures	x
List of Tables	xiii
Abstract	xiv
Resumen	xv
Resumo	xvi
1 Introduction	1
1.1 State of the art	2
1.1.1 Descriptive analyzes	3
1.1.2 Experimental analyzes	4
1.1.3 Mechanobiological models	5
1.1.4 Biomechanical models	7
1.2 Objectives	11
1.3 Thesis Outline	11
2 Experimental model	12
2.1 Conceptual Framework	12
2.2 Materials and Methods	15
2.2.1 MicroCT imaging	17
2.2.2 Histological analysis	17
2.2.3 Quantitative Polymerase Chain Reaction (qPCR)	18
2.2.4 Statistical analysis	18
2.3 Results	18
2.3.1 MicroCT imaging	18
2.3.2 Histological analysis	20
2.3.3 Quantitative Polymerase Chain Reaction (qPCR)	22
2.4 Discussion	23
2.5 Conclusions	25

3	Mechanobiological model	27
3.1	Reaction–diffusion systems	27
3.1.1	Reaction–diffusion equation	27
3.1.2	Biological models	28
3.2	Materials and Methods	29
3.2.1	Mathematical model proposed	29
3.2.2	Numerical Solution	32
3.2.3	Parameters selection	36
3.2.4	Numerical implementation	38
3.3	Results	39
3.3.1	Simulation results of the mice MPS	39
3.3.2	Simulation results of the human MPS	46
3.4	Discussion	52
3.5	Conclusions	53
4	Biomechanical 2D model	55
4.1	Materials and Methods	55
4.2	Results	58
4.3	Discussion	62
4.4	Conclusions	63
5	Biomechanical 3D model	64
5.1	Materials and Methods	64
5.2	Results	68
5.2.1	Dental anchorage models (DA)	68
5.2.2	Dento–skeletal anchorage models (DSA)	70
5.2.3	Skeletal anchorage models (SA)	72
5.2.4	Models with the variation of the conventional Hyrax (HVDA)	74
5.3	Discussion	76
5.4	Conclusions	81
6	Conclusions and future work	82
A	Certificate of ethical approval of the experimental protocol	84
B	Results of the tests carried out to calculate the diffusion coefficients	85
C	Graphical results obtained for the biomechanical 2D model	100
	Bibliography	111

List of Figures

1-1	Considerations to understand the transverse maxillary deficiency	1
1-2	Components of greater relevance in the cranial cavity	3
1-3	Maturation states of the MPS	3
1-4	Anchorage types for RME	4
1-5	Description of the Khonsari's model.	6
1-6	Outline of the two-dimensional model proposed by Zollikofer <i>et al.</i>	6
1-7	Results of the reaction-diffusion model developed by Miura <i>et al.</i>	7
1-8	Example of results obtained by Yoshimura <i>et al.</i>	7
1-9	Results obtained by Burgos <i>et al.</i>	8
2-1	Sections of the Midpalatal Suture	13
2-2	Morphological changes of the MPS during growth	13
2-3	Biological stages of the MPS in response to a external stimuli	14
2-4	Calibration of the expansion load	16
2-5	Experimental procedure to apply the expansion force	17
2-6	Anthropomorphic results of the maxillary transverse dimension	19
2-7	Anthropomorphic results of the suture space	19
2-8	Bone density results	20
2-9	Histological results of H&E analysis in the 7-day period	20
2-10	Histological results of H&E analysis in the 14-day period	21
2-11	Histological results of the cellular activity in the MPS	21
2-12	Quantitative Polymerase Chain Reaction results	22
2-12	Quantitative Polymerase Chain Reaction results (Continued)	23
2-12	Quantitative Polymerase Chain Reaction results (Continued)	24
3-1	Outline of the cell migration process caused by mechanical stimuli	30
3-2	Outline of the bone remodeling process at the bone margins	32
3-3	Domains developed for the mechanobiological model of the midpalatal suture	38
3-4	Molecular factors concentrations found in the mice MPS	39
3-4	Molecular factors concentrations found in the mice MPS (Continued)	40
3-5	Mice MPS formation without external loads and with (1, 1) vibration mode	41
3-6	Mice MPS formation without external loads and with (2, 0) vibration mode	41
3-7	Results comparison of the mice MPS without external loads	42
3-8	Mice MPS formation with expansion load and (1, 1) vibration mode	43
3-9	Mice MPS formation with expansion load and (2, 0) vibration mode	44
3-10	Results comparison of the mice MPS with expansion load	45
3-11	Molecular factors concentrations found in the human MPS	47
3-11	Molecular factors concentrations found in the human MPS (Continued)	48

3-12	Human MPS formation without external loads and with (1, 1) vibration mode	48
3-13	Human MPS formation without external loads and with (1, 1) vibration mode	49
3-14	Results comparison of the human MPS without external loads	50
3-15	Human MPS formation with expansion load and (1, 1) vibration mode	51
3-16	Results comparison of the human MPS morphology	52
4-1	Idealized models of the bone-suture-bone interface	56
4-2	Collagen fibers in the MPS	57
4-3	Boundary conditions to the biomechanical 2D model	58
4-4	Behavior of the first principal stress in the biomechanical 2D model	58
4-5	Behavior of the first principal strain in the biomechanical 2D model	59
4-6	Comparative analysis between the model with and without suture	61
4-7	Comparative graphics of the MPS mechanical behavior in the different configurations	62
5-1	Geometric model of the bone structure obtained from the reconstruction process	65
5-2	Geometric models of the sutures obtained from the bone structure	65
5-3	Final geometric models with null interdigitation and the expander devices	66
5-4	Boundary conditions for the finite element analysis	67
5-5	Maximum Principal Stresses (<i>MPa</i>) obtained for the bone structure in DA models	68
5-6	Results obtained for the midpalatal suture in DA models	69
5-7	Equivalent stresses (<i>MPa</i>) obtained for the conventional Hyrax	69
5-8	Maximum Principal Stresses (<i>MPa</i>) obtained for the bone structure in DSA models	70
5-9	Results obtained for the midpalatal suture in DSA models	71
5-10	Equivalent stresses (<i>MPa</i>) obtained for the hybrid Hyrax	71
5-11	Maximum Principal Stresses (<i>MPa</i>) obtained for the bone structure in SA models	72
5-12	Results obtained for the midpalatal suture in SA models	73
5-13	Equivalent stresses (<i>MPa</i>) obtained for the Hyrax with skeletal anchorage	73
5-14	Maximum Principal Stresses (<i>MPa</i>) obtained for the bone structure in HVDA models	74
5-15	Results obtained for the midpalatal suture in HVDA models	75
5-16	Equivalent stresses (<i>MPa</i>) obtained for the the variation of the conventional Hyrax	75
5-17	Comparative graphs of the stress behavior in the oral cavity	77
5-18	Comparative graphs of the stress behavior in the bone–suture interface	78
5-19	Comparative graphs of the MPS displacements and inclination teeth	79
5-20	Comparative graphs of the desplacement behavior in the bone–suture interface	80
A-1	Certificate of ethical approval of the experimental protocol	84
B-1	Results obtained for the chemoattractant concentration with $D_p = 0.1$	85
B-2	Results obtained for the cellular migration with $D_p = 0.1$	86
B-3	Results obtained for the ossification with $D_p = 0.1$	87
B-4	Results obtained for the chemoattractant concentration with $D_p = 0.4$	88
B-5	Results obtained for the cellular migration with $D_p = 0.4$	89
B-6	Results obtained for the ossification with $D_p = 0.4$	90
B-7	Results obtained for the chemoattractant concentration with $D_p = 0.5$	91
B-8	Results obtained for the cellular migration with $D_p = 0.5$	92
B-9	Results obtained for the ossification with $D_p = 0.5$	93
B-10	Results obtained for the chemoattractant concentration with $D_p = 0.7$	94
B-11	Results obtained for the cellular migration with $D_p = 0.7$	95
B-12	Results obtained for the ossification with $D_p = 0.7$	96

B-13	Results obtained for the chemoattractant concentration with $D_p = 1.0$	97
B-14	Results obtained for the cellular migration with $D_p = 1.0$	98
B-15	Results obtained for the ossification with $D_p = 1.0$	99
C-1	First principal stress obtained for the models in tension	100
C-1	First principal stress obtained for the models in tension (Continued)	101
C-2	Second principal stress obtained for the models in tension	101
C-2	Second principal stress obtained for the models in tension (Continued)	102
C-3	First principal strain obtained for the models in tension	103
C-3	First principal strain obtained for the models in tension (Continued)	104
C-4	Second principal strain obtained for the models in tension	104
C-4	Second principal strain obtained for the models in tension (Continued)	105
C-5	First principal stress obtained for the models in compression	105
C-5	First principal stress obtained for the models in compression (Continued)	106
C-6	Second principal stress obtained for the models in compression	107
C-6	Second principal stress obtained for the models in compression (Continued)	108
C-7	First principal strain obtained for the models in compression	108
C-7	First principal strain obtained for the models in compression (Continued)	109
C-8	Second principal strain obtained for the models in compression	109
C-8	Second principal strain obtained for the models in compression (Continued)	110

List of Tables

2-1	Explanation of the symbols used in Figure 2-3	14
2-2	Typical factors that have been related to bone cells activity in sutures	15
2-3	Groups distribution for the experimental procedure	16
3-1	Modes of vibrations (m,n) for different values of d and γ	37
4-1	Elastic modulus of the collagen fibers obtained for each model	57
4-2	Values obtained for the models in tension	60
4-3	Values obtained for the models in compression	60
4-4	Percentage variation of the values obtained inside the MPS	61

Abstract

Maxillary expansion is an orthodontic procedure that is used to treat the transverse maxillary deficiency. This procedure increases the transversal measurement of the maxilla taking advantage of the presence of the fibrous tissue that joins the two horizontal portions of the palate, known as midpalatal suture. To overcome some adverse effects that are generated with this treatment, or to make changes in the technique, it is necessary to understand the behavior of the suture and the surrounding tissues. Consequently, this work seeks to evaluate the midpalatal suture formation processes, and its response to the presence of external loads such as those generated during the expansion, from both an experimental and computational perspective. Therefore, the project was developed by means of an experimental model, a computational mechanobiological model, a biomechanical computational model in *2D* and a biomechanical computational model in *3D*. For the development of the experimental model, an *in vivo* procedure was standardized to observe the effect of tensile loads on cellular activity inside the suture and on the expressions of some molecular factors located at the bone–suture–bone interface. The procedure can be used as a reference for future research on this suture. With respect to the mechanobiological model, the mathematical model proposed achieves to reproduce the cellular migration phenomena that are carried out as a consequence of the expansion loads application and simulates the remodeling processes that occur at the bone margins, replicating the initial states of the midpalatal suture morphology in humans and generating more complex interdigitation patterns in expanded sutures. In relation to the biomechanical models, it was possible to evaluate the influence of certain parameters, such as the interdigitation degree and the anchorage type used, in the structural behavior of the oral cavity when it is subjected to an maxillary expansion treatment. The experimentally findings and the biomechanical models derived from this research can be used by dentists and clinicians to understand some events that happen into the oral cavity during the period of treatment. On the other hand, the mechanobiological model could be the first approach looking for reproduce the molecular and cellular interaction into the midpalatal suture, when a maxillary expansion is applied, by a combination of a basic chemotaxis model and a reaction–diffusion model.

Resumen

La expansión del maxilar es un procedimiento ortodóntico que se utiliza para tratar la deficiencia transversal del maxilar. Este procedimiento incrementa la medida transversal del maxilar aprovechando la presencia del tejido fibroso que une las dos porciones horizontales del paladar, conocido como sutura medial palatina. Para superar algunos efectos adversos que se generan con este tratamiento, o realizar cambios en la técnica, es necesario entender el comportamiento de la sutura y de los tejidos que la rodean. En consecuencia, este trabajo busca evaluar los procesos de formación de la sutura medial palatina, y su respuesta a la presencia de cargas externas como aquellas generadas durante la expansión, desde una perspectiva tanto experimental como computacional. Por lo tanto, el proyecto fue desarrollado por medio de un modelo experimental, un modelo computacional mecanobiológico, un modelo computacional biomecánico en 2D y un modelo computacional biomecánico en 3D. Para el desarrollo del modelo experimental se estandarizó un procedimiento *in vivo* que permitió observar el efecto de las cargas de tensión sobre la actividad celular al interior de la sutura y sobre las expresiones de algunos factores moleculares localizados en la interfaz hueso–sutura–hueso. El procedimiento podrá ser utilizado como referencia para la realización de futuras investigaciones en esta sutura. Con respecto al modelo mecanobiológico, el modelo matemático planteado logra reproducir los fenómenos de migración celular que se producen como consecuencia de la aplicación de cargas de expansión y simula los procesos de remodelado que acontecen en los márgenes óseos, replicando los estados iniciales de la morfología de la sutura medial palatina en humanos y generando patrones de interdigitación de mayor complejidad en suturas expandidas. En relación a los modelos biomecánicos, fue posible evaluar la influencia de ciertos parámetros, como el grado de interdigitación y el tipo de anclaje empleado, en el comportamiento estructural de la cavidad oral cuando es sometida a un tratamiento de expansión del maxilar. Los hallazgos experimentales y los modelos biomecánicos derivados de esta investigación pueden ser utilizados por odontólogos y clínicos para comprender algunos eventos que ocurren en la cavidad oral durante el período del tratamiento. Por otro lado, el modelo mecanobiológico podría ser el primer enfoque que busca reproducir la interacción molecular y celular en la sutura medial palatina, cuando se aplica una expansión del maxilar, mediante una combinación de un modelo de quimiotaxis básico y un modelo de reacción–difusión.

Resumo

A expansão maxilar é um procedimento ortodôntico usado para tratar a deficiência transversal maxilar. Este procedimento aumenta a medida transversal da maxila aproveitando a presença do tecido fibroso que une as duas porções horizontais do palato, conhecido como sutura palatina mediana. Para superar alguns efeitos adversos que são gerados com este tratamento, ou para fazer mudanças na técnica, é necessário entender o comportamento da sutura e dos tecidos adjacentes. Consequentemente, este trabalho procura avaliar os processos de formação da sutura palatina mediana e sua resposta à presença de cargas externas, como as geradas durante a expansão, tanto do ponto de vista experimental quanto computacional. Portanto, o projeto foi desenvolvido por meio de um modelo experimental, um modelo mecanobiológico computacional, um modelo biomecânico computacional em $2D$ e um modelo biomecânico computacional em $3D$. Para o desenvolvimento do modelo experimental, se padronizou um procedimento *in vivo* para observar o efeito das cargas de tração sobre a atividade celular no interior da sutura e sobre as expressões de alguns fatores moleculares localizados na interface osso-sutura-osso. O procedimento pode ser usado como referência para futuras pesquisas sobre essa sutura. Com relação ao modelo mecanobiológico, o modelo matemático proposto consegue reproduzir os fenômenos de migração celular que ocorrem como consequência da aplicação de cargas de expansão e simula os processos de remodelação que acontecem nas margens ósseas, replicando os estados iniciais da morfologia da sutura palatina mediana em humanos e gerando padrões de interdigitação mais complexos em suturas expandidas. Em relação aos modelos biomecânicos, foi possível avaliar a influência de determinados parâmetros, como o grau de interdigitação e o tipo de ancoragem utilizado, no comportamento estrutural da cavidade bucal quando esta é submetida a um tratamento de expansão da maxila. Os resultados experimentais e os modelos biomecânicos derivados desta investigação podem ser utilizados por dentistas e clínicos para entender alguns eventos que ocorrem na cavidade bucal durante o período do tratamento. Por outro lado, o modelo mecanobiológico poderia ser a primeira abordagem que procura reproduzir a interação molecular e celular na sutura palatina mediana, quando se aplica uma expansão da maxila, através de uma combinação de um modelo quimiotáxico básico e um modelo de reação-difusão.

Chapter 1

Introduction

Transverse maxillary deficiency is an oral pathology associated with dento-skeletal alterations and characterized by a less transverse dimension in the maxilla (Dimension D, Figure 1.1(a)). This pathology generates some problems such as malocclusion (Figure 1.1(c)), crowding of the anterior teeth, aesthetic problems or, in more advanced cases, respiratory problems (with an incidence of 3 – 18%) [1–3]. A way to treat this pathology is by Maxillary Expansion (ME) [4], an orthopedic procedure that employs a device (Figure 1.1(a)), conventionally a palatal expander, fixed to the posterior teeth to separate the two maxillary bones [5, 6]. For the expansion, the mechanism has a screw that is normally activated daily until the desired distance is achieved; after that, the device is kept in the patient as a retainer for a period of 3 to 18 months [4]. This treatment is possible due to presence of a facial suture known as Midpalatal Suture (MPS). It is the line that joins the horizontal portions of the two palatine bones (Figure 1.1(b)) [7]. Normally, the MPS is highly sensitive to mechanical stimulus [8] and changes its morphology during growth, taking a rough and sinuous shape, until forming an interdigitated pattern [9–11]. According to the literature, with the ME, the opening range of the suture can reach values from 1.6 to 4.3mm in the anterior region and from 1.2 to 4.4mm in the posterior one [4]. However, even though the ME is the most common treatment to the transverse maxillary deficiency, it presents some complications such as alveolar flexion processes and dental tipping of the posterior region in the vestibular direction [2, 4, 12–14], reduction of the cortical bone height [14] and alveolar plate [15], possible generation of root resorption [16], periodontal complications [2], among others.

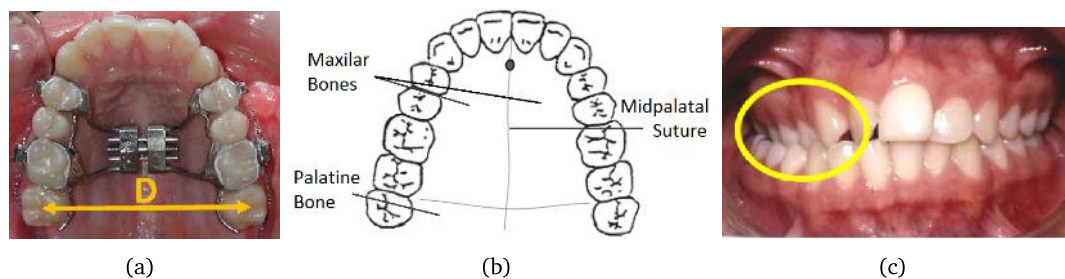


Figure 1-1: Considerations to understand the transverse maxillary deficiency: a) Transverse dimension in the maxilla (D). Adapted from [17]. b) Midpalatal Suture (MPS). Adapted from [18]. c) Example of malocclusion problems. Adapted from [19].

To approach the ME problems, and propose modifications to this treatment, like to incorporate the skeletal anchorage, it is necessary to understand the behavior of the suture and tissues that surround it. Therefore, the study presented here employed a computational simulation to represent the biome-

chanical and mechanobiological response of the tissues involved to mechanical stimulus. Consequently, the study was divided in three parts: the experimental, the mechanobiological and the biomechanical part. The first one was an experimental analysis on the mice MPS, where the molecular and cellular response to external mechanical loads were observed. The second one was a mechanobiological model that tries to reproduce the cellular and molecular behavior that was observed in the experimental part and a proposed extrapolation to the human MPS. The third one was a biomechanical model where the influence of the suture interdigitation pattern, the devices used for the expansion and the anchorage type were evaluated.

The experimental results showed a high dependence between the molecular and cellular behavior and the mechanical stimulus. It was possible to identify some of the molecular factors that are activated when an expansion force is applied over the suture and the cellular response to this phenomenon. Based on the literature, a methodology to characterize the expansion force and evaluate the consequence of variations on the force value was also developed. The mechanobiological results showed a good approximation of the events that take place inside the suture and that were described by the experimental model and by some authors like Hou *et al.* [8], Ennes *et al.* [10] and Consolaro *et al.* [20]. Finally, the biomechanical results showed the influence of the suture interdigitation on the bone and suture stress distribution and the effect of the expander and anchorage type in the mechanical response of the whole structure.

1.1 State of the art

The human skull is a complex and multifunctional structure composed of approximately 29 bones and can be divided in viscerocranium and neurocranium [21,22]. The viscerocranium is composed of the facial bones and originates, mainly, in the cartilage of the first two pharyngeal arches. The neurocranium, formed by the bones that support and protect the brain, develops from the mesenchymal tissue [21–23]. The cranial bones are joined by sutures, which are composed of multiple lineages of connective tissue cells such as mesenchymal, fibroblastic, osteoblastic, osteoclastic and vascular cells [24–27]. The bones that limit the sutures are usually of intramembranous origin and grow by ossifying the suture boundaries [24]. Figure 1-2 shows the principal sutures of the cranial cavity: the coronal (between the frontal and parietal bones), the midsagittal suture (which divides the two parietal bones), the lamboid suture (between the occipital bone and the anterior part of the parietal bones) and the temporo–parietal suture (located between the temporal and parietal bones) [23, 28–30]. The suture of interest in this work is the midpalatal suture. As mentioned earlier, it is the line that joins the palatine bones [7] and it has an important role when performing a maxillary expansion.

The Midpalatal Suture and the Maxillary Expansion have been analyzed since the 1970s [12]. The developed studies can be classified as descriptive, experimental, mechanobiological and biomechanical models. The first ones seek to evaluate medical images or clinical procedures to describe aspects such as suture morphologies, collateral effects of the ME application, effectiveness of the treatment, etc. The experimental studies aim at evaluating the biological response of the tissues when the mechanical environment is changed; for example, when the expansion forces are applied. The mechanobiological models try to represent the cellular and molecular behavior and its effect in the evolution of the suture morphology under mechanical stimuli. Finally, the biomechanical models are related with the structural response of the oral cavity; suture material behavior, treatment effectiveness, stress and displacement distributions, among other parameters have been analyzed. Next, a brief description of the state of the art will be provided.

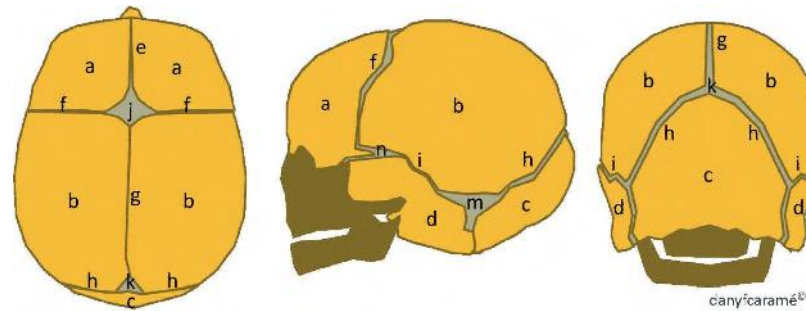


Figure 1-2: Components of greater relevance in the cranial cavity. a: frontal bone (right and left); b: parietal bone (right and left); c: occipital bone; d: temporal bone (right and left); e: frontal suture; f: coronal suture (right and left); g: sagittal suture; h: lambdoid suture; i: temporo-parietal suture; j: anterior fontanelle; k: posterior fontanelle; m: mastoid fontanelle; n: sphenoidal fontanelle. Taken from [29].

1.1.1 Descriptive analyzes

One purpose of the investigations based on medical images and clinical studies is to evaluate the ossification state of the suture in search of a criteria about the convenience of the ME treatment. Thus, it has been possible to establish that the MPS ossification begins, mainly, in the adulthood at the posterior region [31] and that ossification is less than 50% in patients under 25 years old [32]. Angelieri *et al.* found that the MPS can be classified, according to its maturation, in five states (Figure 1-3). In the state A, the suture is a straight line with high density and without interdigitation. In the state B the MPS takes a scalloped shape and maintains the density. The state C is characterized by two scalloped lines close to each other with some spaces of low density. Finally, states D and E are evident when the suture fusion in the palatine bone and in the anterior part of the maxilla occurs, respectively [9].

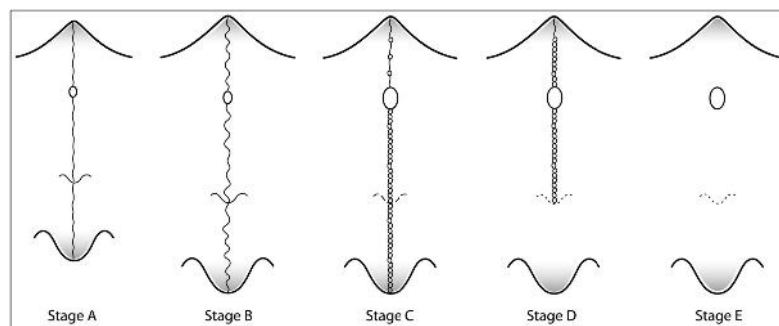


Figure 1-3: Maturation states of the MPS proposed by Angelieri *et al.* [9]. Taken from [9].

On the other hand, some studies are focused on the tissues response and the side effects of the ME application. Franchi *et al.* [33], Schauseil *et al.* [34] and da Silva Filho *et al.* [35] evaluated the retention period, after the ME application, as a function of the density tissue inside the suture. They concluded that the minimum time lapse of retention should be six months because it is the necessary time for the tissue reorganization and for the recovery of the density values. For their part, Lione *et al.* [4], McNamara *et al.* [36] and Pereira-Filho [3] investigated the morphological changes in the craniofacial complex due to the expansion. The first group found the opening range (1.6 to 4.3mm in the anterior region and 1.2 to 4.4mm in the posterior region), the teeth tipping range (3.4° to 9.2°) and the alveolar bone bending range (5.1° to 11.3°) generated during the treatment [4]. The second authors

associated transverse maxillary deficiency not just with oral problems, like teeth crowding, but with respiratory pathologies, like apnea, and they suggested that an early ME could reduce its symptoms [36]. In contrast, when the last research group studied the effectiveness of the ME in the apnea treatment, they observed that the ME isolated does not produce significant changes in the airway dimension [3]. In relation to the side effects, the authors used cephalometric measurements and they agreed that the unwanted effects are minimal in the long term [4, 37, 38]

Finally, other topic of interest is the variations that the ME treatment could have; normally, variations related to the expander and to the anchorage type. Sandikçioğlu *et al.* [39] and Ciambotti *et al.* [13] analyzed different types of expander to evaluate their behavior and effectiveness. Sandikçioğlu *et al.* used devices that generate slow, semirapid and rapid expansions and found that the three types produce similar skeletal and dental results with the greater effect in the transverse plane. Therefore, the authors recommend the semirapid and rapid expansion due to the treatment period [39]. Ciambotti *et al.* compared a conventional Hyrax and a nickel titanium expander, demonstrating that the first one produced a more reliable expansion while the second generated more dental tipping and dental rotation [13]. Regarding the anchorage types, the studies have assessed devices that are supported on the teeth (dental anchorage, Figure 1.4(a)), on the bone (skeletal anchorage, Figure 1.4(b)) and on the both parts (hybrid anchorage, Figure 1.4(c)). According to the literature, the different types of anchorage produce similar results in the transverse dimension [40–43] and it seems that the hybrid anchorage is a good alternative to dental anchorage due to avoids the side effects of the treatment [34, 42, 44].

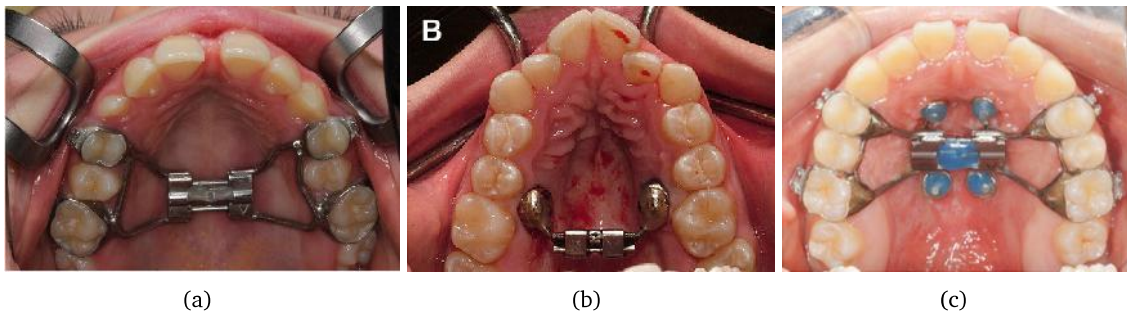


Figure 1-4: Anchorage types for ME: a) Dental anchorage. Taken from [45]. b) Skeletal anchorage. Taken from [40]. c) Hybrid anchorage. Taken from [46].

1.1.2 Experimental analyzes

The experimental investigations were developed in both *in vivo* and *in vitro* studies. From a mechanical point of view, the analyzes seeked to explore the relationship between the mechanical environment and the bone and sutural tissue response. Henderson *et al.* made a tracking of the changes in the geometric, structural and material properties of rat sutures during their first 60 days of life. The results showed that the cranial expansion modifies the sagittal suture and, for this reason, the width and stiffness of the suture are age-depend properties [47]. Parr *et al.* analyzed the viability to employ endosseous implants to perform expansion procedures on animals. They observed that low forces, applied on this type of implants, caused a decrease in the percentage of the bone volume and an increase in the percentage of the suture volume, which could be interpreted as a successful expansion [48]. Liu *et al.* applied constant loads of 0, 50, 100 and 200gf on the New Zeland rabbits midsagittal suture and quantified the sutural separation, the movement of the anchorage and the advance of the bone margins. The findings revealed a relationship between the force magnitude, the sutural separation and the bone formation in

the suture [49]. Peptan *et al.*, Vij *et al.* and Oppenheimer *et al.* evaluated the influence of the cyclical loads on the bone and sutures behavior. They concluded that this type of mechanical stimulus promotes the osteoblastic and osteoclastic differentiation and, with it, the bone remodeling processes and bone deposition into the suture, even reaching the fusion [26, 27, 50]. Tanaka *et al.* performed two studies on rats and they look for the type III collagen reaction to a constant load. The interest in this particular collagen is because it is the main component of the sutural fibrous tissue. The authors could see that the presence and duration of tensile stress are related with the location of type III collagen and with the biomechanical behavior of the suture [51, 52].

The biochemical activity is a key factor to understand the regulation of the ossification process [22, 53–56], the pathogenesis of some bone diseases [57–59] and the tissue response and adaptation to external signals, like mechanical stimulus [60, 61]. Roth *et al.* demonstrated that the Transforming Growth Factors ($TGF - \beta$) are present into the suture, more intensively in the margins where the osteoblasts are differentiating themselves in bone. However, $TGF - \beta 3$ were detected at higher levels in the margins of the unfused suture, which could be interpreted as the responsible for inhibiting the ossification [62]. For their part, Sawada *et al.* and Liu *et al.* focused on the factors that promote the bone formation and found that the factors involved in this process are $TGF - \beta 1$ and $rhBMP - 2$ [63, 64]. In addition to this, the investigation developed by Hirukawa established that tension loads increase the production of growth factors (such as IGF) causing the proliferation of the osteoblastic and fibroblastic cells [65].

So far, the aforementioned investigations have been developed in cranial sutures; however, some interesting analyzes for this investigation are those directed to the midpalatal suture, as such. Hou *et al.* described two projects in order to track the cellular response into the suture when subjected to expansion loads. To this end, they made morphological studies to establish the general behavior of collagen fibers and other cells such as chondrocytes. They analyzed cell proliferation, osteoblastic activity, type I collagen expression and the role of the Polycystic kidney disease 1 ($Pkd1$) in the mechanotransduction process. As a result of this research, it was possible to observe that the expansion forces promote the osteoclasts activation and the proliferation and differentiation of periosteal cells, which can represent a bone remodeling process. The expansion also demonstrates the $Pkd1$ relevance on the cellular response; for example, the absence of this protein increased the chondroprogenitor apoptosis. An important fact is that, after expansion, the suture returns to a width and structure similar to the original suture [8, 66]. On the other hand, Burn *et al.* worked on young pigs and evaluated the effects of reducing chewing forces on the growth and morphology of the MPS. They concluded that the modification of the diet in the animals affected the bone margins development and the suture ossification, observing less bone in pigs with a soft diet than with a normal diet [67].

1.1.3 Mechanobiological models

The mechanobiology studies the tissues response to biophysical stimuli in a cellular scale. Factors like molecular signaling, cellular production and differentiation and the effects of external forces have been evaluated [68–70]. A way to treat these type of analysis is by the use of mathematical models, which are a representation of reality in mathematical language [71]. For example, Khonsari *et al.* argue that the growth and pattern of craniofacial sutures is subjected to the effect of mechanical stress. They propose a theoretical model based on the orientation of collagen fibers in response to local stress. The model establishes that, at the beginning, the osteogenic cells are in the center of the mesenchymal area and the collagen fibers do not have a defined orientation (Figure 1.5(a)). Then, when the suture is subjected to loading, the collagen fibers are organized in the load direction, from the convex to the concave. During this process, the osteogenic cells migrate towards the suture boundary preferring to

locate in the convex areas, generating deposition, and avoiding the concave ones, producing resorption (Figure 1.5(b)). For the development of this study, a transport–diffusion model was used, which was limited to the beginning of interdigitation, without reaching ossification (Figure 1.5(c)). A reason to this is that they did not know how to maintain the relationship between the load and the generation of the interdigitation pattern, due to its viscoelastic nature [25].

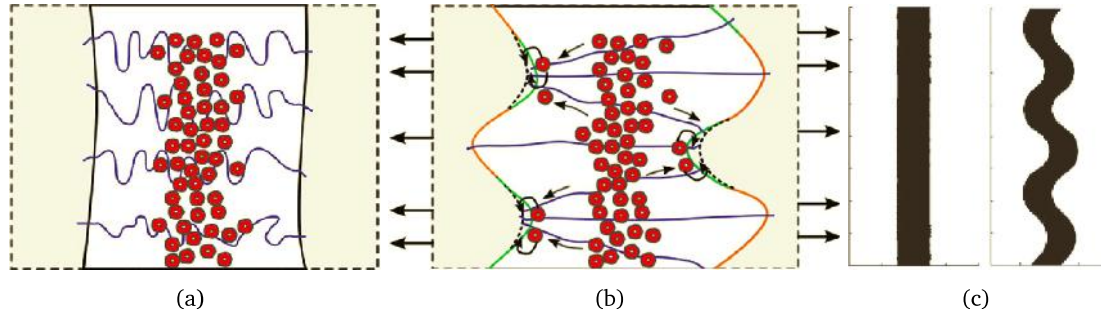


Figure 1-5: Description of the Khonsari's model: distribution of collagen fibers (blue lines) and location of osteogenic cells (red circles) in the mesenchymal tissue a) at the process beginning and b) after load application. c) Initial and final state of the suture. Taken from [25].

A different approach was developed by Zollikofer *et al.* based on the suture morphology. They performed a bidimensional model that reproduces a diversity of sagittal suture morphologies, generating the morpho–space, and selecting the parameters that reproduce the shape that best fits a real suture. According to the study, the sutural growth corresponds to a deposition and reabsorption processes as a function of the local strain gradient. For this, they divided the domain into two coupled systems (Figure 1-6) which allowed, simultaneously, the presence of reabsorption in one side and deposition in the other one, and vice versa [72].

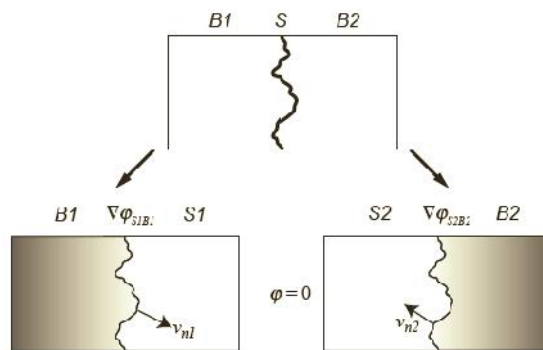


Figure 1-6: Outline of the two–dimensional model proposed by Zollikofer *et al.*. Taken from [72].

On the other hand, Miura *et al.* sought to explain the suture ossification from a reaction–diffusion system. The model represents the cellular tissue behavior and shows the evolution of the suture morphology, first as a straight line and then with an interdigitation pattern, reaching levels of fractality. According to the authors, the presented model reproduces the maintenance of suture thickness in the early stages, the subsequent modification of the straight suture to interdigitated bone forms and the formation of fractal structures. It should be noted that the model reproduces the non–ossified sectors, such as those highlighted with red circles (Figure 1-7). In addition, they performed an *in vitro* study where bone resorption was observed, without the presence of explanted tissue growth. This suggests

that the interdigitation process occurs independently of the brain growth and the calvary expansion. That is, they propose that mechanical loads are not the only ones that influence the interdigitated patterns formation [73]. The investigation presented by Yoshimura *et al.* also uses a reaction–diffusion system. The authors based their work in the Allen–Cahn equation and point out that it was the first model capable to simulate the formation of the interdigitation pattern without establishing the final thin of the suture tissue before starting the interdigitation process. Figure 1-8 shows an example of the results obtained by Yoshimura *et al.* [74].

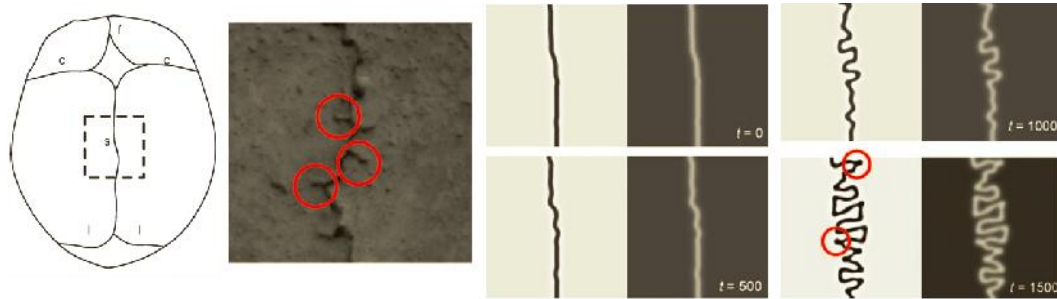


Figure 1-7: Results of the reaction–diffusion model developed by Miura *et al.*. Taken from [73].

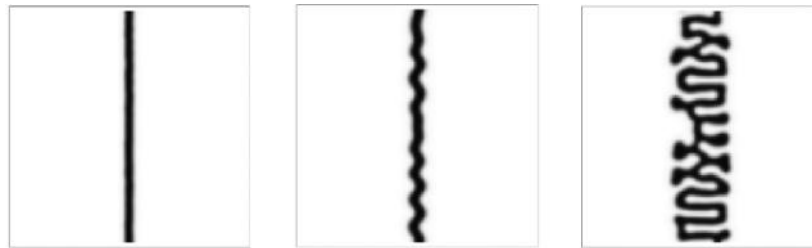


Figure 1-8: Example of results obtained by Yoshimura *et al.*. Taken from [74].

Finally, another interesting work was developed by Burgos *et al.* where the suture interdigitation study was analyzed not just like an isolated system but a whole 3D model, taking into account a simplified skull morphology and the presence of multiple sutures at the same time [75]. The model is presented in two stages: the formation of the flat bones in the calvaria and the generation of the interdigitated pattern. The first one is based on the Garzón-Alvarado *et al.* investigations [22, 76]. This part of the model identifies the primary ossification centers of the skull in formation and their subsequent growth to form the flat bones and suture spaces. The second one reproduces how the bone margins advance toward each other to form the irregular shapes known as interdigitation. The mathematical conception is based on the formation of Turing patterns through reaction–diffusion systems [77]. The model has the ability to reproduce the interaction between two molecular factors that control the differentiation of mesenchymal cells and estimates the bone formation at different stages. The results showed a high similarity between the modeled skull and a real one (Figure 1-9) [75].

1.1.4 Biomechanical models

Biomechanics studies the behavior of tissues and living beings when they are subjected to different types of loads, either static and dynamic [78–80]. Focused on living beings, it evaluates aspects such as the mechanical behavior of the structures that constitute the body, the interaction between different components that are part of a mechanism or system, the response to external phenomena, the tissues ability

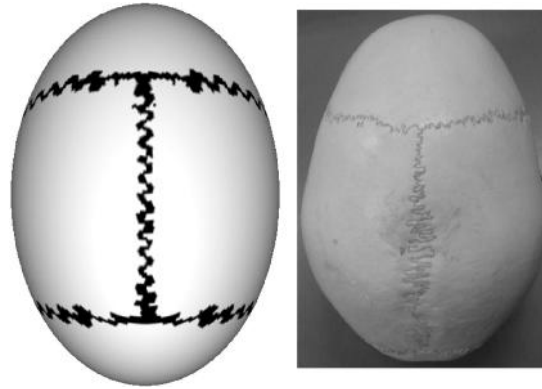


Figure 1-9: Results obtained by Burgos *et al.*. Taken from [75].

to associate themselves with non-biological materials, among others [79,81]. From the biomechanical point of view, the MPS and the ME have been studied with different purposes: to evaluate the mechanical response of the oral cavity to ME, to analyze the material properties of the suture, to observe the influence of the interdigitation in the results treatment, to compare the possible types of anchorage for expander devices, to establish the effect that could have variations in the design and in the position of the expander.

According to Romanyk *et al.*, four types of assumptions are normally made about the suture material: assuming no material, assuming bone mechanical properties or soft tissue properties and, by last, assuming a viscoelastic material behavior [82]. Priyadarshini *et al.* reconstructed a Computed Tomography (CT) and applied expansion forces in the premolars and first molar to evaluate the stresses and displacements distribution on the cranial bones and sutures. A linear material behavior was considered for all domain components. The displacement results showed higher values in the oral side than in the nasal and the maximum equivalent stresses were found in sutures such as the midpalatal and pterygo-maxillary sutures [83]. For their part, Lee *et al.* developed a model with a palatal structure made up just by one solid, a model with palatal structure made up by suture and bone components, with the same elastic modulus, and a model without the presence of the suture. The intention of the study was to evaluate the ME with different suture stage in an attempt to explain some clinical observations. They found that the first two models had similar stress patterns and the third model translated the stress to the nasal cavity [84]. Nevertheless, some authors like Provatidis *et al.*, Tanaka *et al.*, Ludwig *et al.* and Romanyk *et al.*, looking for more reliable representations, have employed viscoelastic constitutive models to describe the suture material behavior [5, 52, 85–88]. Provatidis *et al.* analyzed the expansion taking into account the whole skull and the unfused and fused states of the sutures, with elastic modulus of $1MPa$ and $13700MPa$, respectively. In addition to this, the authors set up another scenario with a “pseudo-viscoelastic” behavior, where the stress was set to zero between each activation. The findings showed that the displacements were larger in the models with non-ossified sutures; however, the model that showed the best behavior was that with all sutures ossified, except the midpalatal and the midsagittal suture. They concluded that the relaxation phenomena should be taken into account to calculate the stress distributions into the craniofacial complex [5]. Ludwig *et al.* took a CT scan of a 16 years old patient, before and after the expansion, performed a simulation with linear and viscoelastic properties and compared the accuracy of the displacements simulated in relation to the expansion reached in the patient. In a similar way to Provatidis *et al.* [5], the viscoelastic model just accounted for the relaxation process. As an interesting aspect in this study, this model was not applied to the suture due to it was considered like a void, so the viscoelastic properties was assigned to the bone. According

to the authors, the linear model did not correspond to the clinical reality while the viscoelastic model did [88]. Tanaka *et al.*, as mentioned before, had interest in type III collagen. They used a Kelvin model in a finite element analysis to describe the material behavior to compare the simulated results with the experimental ones. The data obtained showed similarity between the displacements found experimentally and those calculated computationally [52].

Romanyk *et al.* focused on determining the mathematical model that describes the viscoelastic nature of the MPS, considering both the creep and relaxation phenomena [85–87]. They used the data presented by Liu *et al.* in the sagittal suture of New Zealand white rabbits [49]. In a first attempt, they found a viscoelastic model capable of predicting the creep behavior with only one set of constants for different loads applied [87]. Then, the authors established the relationship between the creep and relaxation behavior and obtained the functions that describe the relaxation response of the tissue. According to these models, after a few minutes, the mechanical stresses values decayed to less than 0.1MPa which indicates that, in a common protocol, the superposition of stresses between activations does not happen [85]. Finally, they analyzed the suture response when is subjected to a constant displacement or a constant expansion load, taking into account the viscoelastic properties. It was evident that the suture is capable to resist a screw activation without damage and that the models that best describe the clinical procedure are the relaxation models, as the screw generates a constant deformation [86]. The consideration of a model to describe the viscoelastic behavior is necessary only if the concern is the transient response on a scale of minutes or less. If the concern is the response in a longer period, the linear properties could be considered for an adequate result [82]. Another alternative to describe the material behavior of the suture was presented by Carvalho *et al.* [89]. They proposed a bilinear model where the suture elastic modulus changes when the tissue experiences a stress above 0.1MPa . This could be interpreted as the suture initial state corresponding to an organized connective tissue and, when the resistance to displacement is overcome, the tissue loses its order and can be represented by a lower elastic modulus. The findings showed that the bilinear assumption produces results that agree with clinical data, providing a simple material model for the suture without losing reliability [89].

Another factor of interest in the suture investigations is the influence of the interdigitation pattern in the mechanical response of the bone–suture–bone interface. Jasinowski *et al.* made a geometrical representation of the suture with three degrees of interdigitation; those degrees corresponds to a null, moderate and complex interdigitation. They modeled the suture with isotropic and orthotropic properties and considered the presence of the collagen fibers aligned in the load direction. Then, they applied compression and tension forces on the domain and evaluated the mechanical behavior. The findings showed that, independent of the collagen fibers, a decrease of the interdigitation index produces a decrease in the bone strain energy and an increase of the interdigitation index causes lower stress values at the apices and higher stress values at the suture limbs [90]. Additionally, Jasinowski *et al.*, in a later work, took the results of the previously research presented and compared them with a response obtained in a study with suture viscoelastic properties and chewing loads. The authors reaffirmed the relationship between strain energy and interdigitation index and found that the viscoelastic properties effect decreases with the increment of the frequency loads, suggesting that these properties could be not necessary for chewing loads analysis [91]. The study developed by Maloul *et al.* used a simplified 3D models of the suture, with interdigitation index similar to Jasinowski *et al.* [90, 91], and a suture obtained from a computed tomography. The results obtained with the simplified models agreed with the obtained in the TC model. Also, with respect to the research reported by Jasinowski *et al.* [90], the results also agree; which is an interesting aspect because the model of Jasinowski *et al.* [90] was developed in two dimensions. This similarity in the results is due to the fact that the 2D model was configured in a plane stress state and took into account the third dimension as an inherent constant during the problem resolution [24].

By their part, Lee *et al.* performed an analysis with a model that had the same interdigitation index but a different irregularity degree of the suture morphology. The findings demonstrated that the increment in the degree of irregularity helps the structure to withstand greater deformations before the damage occurs [92].

Some authors have focused their investigations on analyzing variations in the procedure or in the expander devices during a ME treatment. For example, Han *et al.* developed a finite element analysis to evaluate the effect of performing surgical procedures, before the application of the expansion, on the final displacement outcomes. The research revealed that the osteotomy procedures help to increase the maxillary expansion and to reduce the mechanical resistance that the bone structure makes, avoiding the side effects [93]. De Sousa Araugio *et al.* studied the position of the expansion screw in relation to the vertical distance with respect to the palate. The reference point was the resistance center of the first molars, so the models were developed to locate the screw above, below and at that point. The results showed the existence of a relationship between the screw height and the dental side effects; the authors concluded that the ideal position is a little above the resistance center [94]. Corroborating the investigation aforementioned, Matsuyama *et al.* sought to assess the influence of the palate depth and certain device modifications on the expansion results. They found that the greater the depth of the palate, the smaller the effect of the expansion. Also, they showed that variations on the device arms could produce efficient expansions and reduce the strain in the arms [95].

The way in which the expansion device is attached to the oral cavity is another variable of study. As a mentioned before, the most common anchorage types are dental, skeletal and hybrid anchorage (Figure 1-4). Carvalho *et al.* compared the stress and displacement distributions generated by dental and skeletal anchorage during the ME. They found that the devices with palatal support produce greater ME effectiveness, coinciding with Matsuyama *et al.* [95], but generate significant increases in the stress and strain values; it is a result that need to be taken into account for the expansion protocols [96]. In the same line, the models proposed by Jain *et al.* and MacGinnis *et al.* showed higher stresses and less side effects when the expander is supported by implants than when it is supported on the teeth [97,98]. Particularly, MacGinnis *et al.* concluded that the skeletal anchorage could be beneficial for patients who require transfer the mechanical stimulus directly to the midpalatal region, like those with some ossification degree of the suture [98]. Lee H. *et al.* developed four models with different configurations for the devices: skeletal and hybrid anchorage with implants near to the MPS, skeletal anchorage with implants near to the roots of the teeth and dental anchorage with conventional Hyrax and surgical assistance. The results showed higher expansion values in the posterior than in the anterior region for all models; however, the hybrid anchorage seems to be the most effective device and a good choice to treat the transverse maxillary deficiency [99]. At last, Lee S. *et al.* performed an analysis with the purpose to evaluate the influences of surgical assistance in ME treatment with skeletal anchorage. In a similar way that reported by Han *et al.* [93], surgical procedure translate into greater transverse displacements. Additionally, the different structures of the domain experienced the highest stress levels in the model without the surgical assistance. Therefore, the authors suggested that procedure when the skeletal anchorage is used [100].

1.2 Objectives

- General aim:
To develop a biomechanical and mechanobiological model that describes the midpalatal suture formation process, by the use of computational simulation.
- Specific aims:
 1. To formulate the biomechanical and mechanobiological model for the midpalatal suture formation process, free of pathologies and external loads.
 2. To implement the biomechanical and mechanobiological model, which describes the midpalatal suture formation process when subjected to external expansion loads.
 3. To evaluate, through the use of the developed model, the midpalatal suture behavior when it is subjected to a Maxillary Expansion treatment, with dental and skeletal anchorage.

1.3 Thesis Outline

This thesis document is made up of six chapters. **Chapter 1** corresponds to this introductory chapter and aims to introduce the reader to the conceptual framework of the Maxillary Expansion and Midpalatal Suture through a presentation of multiple works obtained from the literature. Also, the objectives to achieve are presented. In **Chapter 2**, a description of the theoretical biological behavior of the suture when it is exposed to a mechanical stimulus are made. After that, the experimental model that was developed looking to observe the molecular and cellular response to tensile loads is described. By last, the results of the microcomputer tomography, histological and qPCR analysis are showed and discussed.

In **Chapter 3** a brief explanation of the Shnakenberg, Glycolysis and Chemotaxis models are performed. Then, a mechanobiological model of the suture behavior is proposed and developed based on the experimental findings and on the Turing patterns theory. Later, the model application in the mice and human MPS is presented; both with and without external loads. Subsequently, the results obtained, the model validation with the experimental data and literature and the discussion are described.

Chapter 4 and **Chapter 5** are focused on the biomechanical behavior of the suture when submitted to a ME treatment. **Chapter 4** presents the analysis done, on a simplified domain, to find the mechanical response of the suture with different interdigitation index. **Chapter 5** shows the biomechanical model developed to evaluate the influence of the interdigitation pattern in a more realistic scenario. Also, in that chapter, a study about the devices used for the expansion and the anchorage type was described. As in other chapters, in the last part of each one, all results are presented and discussed.

Finally, in **Chapter 6**, the main conclusions obtained from the results of this work are described, as well as some possible recommendations for future work. It is important to note that the content described in **Chapter 2** is currently submitted to “*Journal of Biomechanics*” and it is in the “under review” state. Additionally, **Chapter 5** is currently published in the Journal “*Computer Methods and Programs in Biomedicine*” (<https://doi.org/10.1016/j.cmpb.2019.05.007>).

Chapter 2

Experimental model

The biomechanical and mechanobiological models that will be described in Chapters 3 to 5 seek to characterize the midpalatal suture (MPS) mechanical behavior when it is subjected to an expansion treatment. Particularly, the mechanobiological simulation tries to establish, through a proposed mathematical model, an approximate relationship between the molecular and cellular events involved in the MPS formation process and the biological response to a mechanical stimuli, such as those present in maxillary expansions. These type of models usually require both input data to feed the model and information to assure that the results obtained in the simulation implemented correspond to the equivalents in the real phenomenon. Therefore, in this chapter, the *in vivo* experimental procedure developed on Five-week-old wild-type (*WT*)(*C57BL/6*) mice is presented. The objectives of this experiment are:

- To observe morphological changes in the bone–suture–bone interface caused by bone distraction.
- To identify variations in the osteoblasts and osteoclasts activity at the bone–suture–bone interface associated with different loading levels applied to bone distraction.
- To analyze variations in the expression of molecules related to the bone cells activity in the MPS, during bone distraction.

This part of the work was developed in collaboration with the departments of Clinical, Pathology and Dental Surgery and Pediatric Dentistry and Orthodontics of the Faculty of Dentistry of the Universidade Federal de Minas Gerais and with the Pathology Laboratory of the Faculty of Medicine of the Universidad Nacional de Colombia. The ethical approval certificate of the experimental protocol #152/2016 can be seen in the Appendix A. In the following sections a conceptual framework that will allow to understand in greater depth the midpalatal suture and its biological response to external loads will be presented, the methodology used for the development of the experiment will be explained and, by last, the results obtained will be shown and discussed.

2.1 Conceptual Framework

Sutures can be defined as fibrous tissues between the cranial bones acting as joints [26, 53–55, 101]. These tissues restrict the movement of adjacent bones, which convert them into synarthrosis articulations [102, 103]. Particularly, the midpalatal suture is the line that joins the two horizontal halves of the maxilla [8, 102] and can be divided in anterior (between the upper interdental point and the anterior section of the incisive fossa), middle (from the posterior section of the incisive fossa to the intersection with transverse palatine suture) and posterior part (from the transverse suture to the posterior nasal

spine) (Figure 2-1) [10]. This suture changes its morphology during growth; initially it is characterized by a Y-shape morphology (Figure 2.2(a)) and, then, it evolves to take a sinuous shape or meandering interdigitation (Figure 2.2(b)) [6, 104–108]. Nevertheless, it is from the third decade that the palate reaches its maximum width [109] and the suture starts to change its ossification percentage [105, 107]; according to Knaup *et al.*, that percentage is almost zero before 25 years old and takes a median value of 3.11% after that age [105].

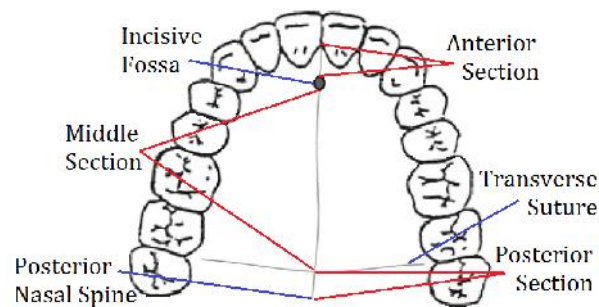


Figure 2-1: Sections of the Midpalatal Suture. Adapted from [18].

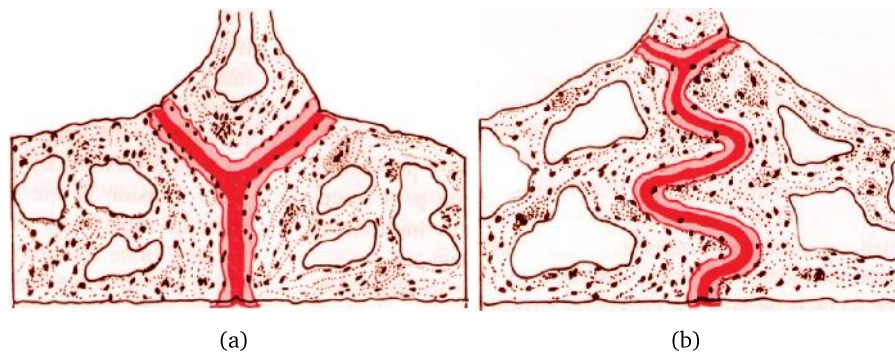


Figure 2-2: Morphological changes of the MPS during growth: a) Initial state with Y-shape and b) Sinuous shape in early adolescence. Taken from [6].

The midpalatal suture is highly sensitive to its mechanical environment [8] and can be exposed to different types of loads such as the forces produced during chewing, those generated by the expansion of adjacent tissues [57, 67, 110] or produced by orthodontic procedures like the Maxillary Expansion [6, 11, 111]. In general, the MPS is a dense connective tissue located between the palatal bones and limited by a periosteal layer, rich in osteogenic cells, both in the nasal and oral side. Without the presence of external forces, the connective tissue is composed by two layers of osteoblastic cells adjacent to the bone margins and another central layer of mesenchymal tissue formed by osteoblasts, fibroblasts, collagen fibers and blood vessels (Stage 1, Figure 2.3(a)) [10, 20, 26, 102]. With the application of the expansion load, the suture tissue becomes disorganized, the collagen fibers and some blood vessels are broken and the osteogenic cells migrate from the periosteum into the suture. In response to the tissue damage generated, the inflammatory exudate is formed with a high concentration of fibrins and the immune system, preventing the presence of possible bacteria, invades the region with neutrophils. Then, neutrophils disappear and give space to macrophages who are responsible for eliminating cellular waste and fibrin excess and, along with vascularization, release the molecular signaling that will regulate the tissue recovery. All this is developed in a period of time that ranges between 24 and 48 hours

(Stage 2, Figure 2.3(b)). After this stage, fibroblasts and undifferentiated cells work to recover the extracellular matrix while the osteoblastic cells organize themselves to produce immature bone that covers the empty spaces; bone that is subsequently reabsorbed and replaced by fibrous tissue (Stage 3, Figure 2.3(c)). Once the macrophages finish their phagocytosis process, the pH is normalized, which the osteoblastic cells interpret as a signal to move again to the suture margins and produce new bony layers that restore the approximate size and shape that the suture had before the expansion (Stage 4, Figure 2.3(d)) [10, 20, 102, 110, 112].

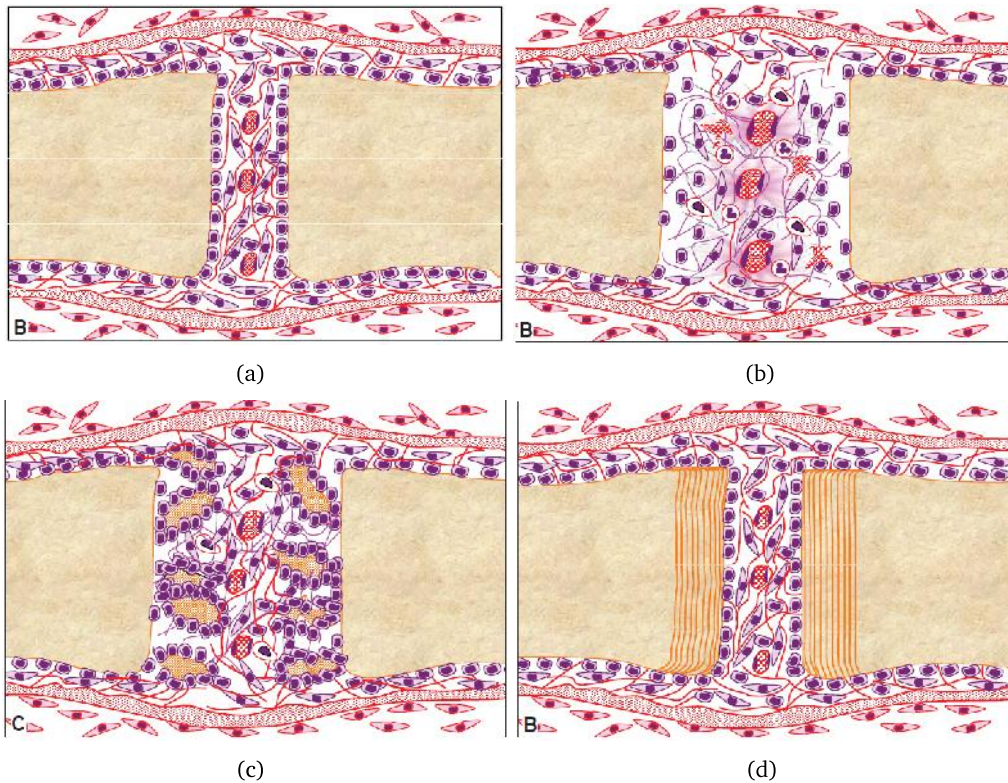


Figure 2-3: Biological stages of the MPS in response to an external stimulus: a) Stage 1, b) Stage 2, c) Stage 3 and d) Stage 4. Taken from [20].

	Mature bone		Neutrophils		Blood vessel
	Periosteum		Macrophages		New bone
	Osteoblasts		Collagen fibers		Fasciculated bone
	Fibroblasts		Fibrin network		

Table 2-1: Explanation of the symbols used in Figure 2-3. Taken from [20].

As to the biochemical activity that regulate the different stages before mentioned, many growth and transcription factors, like $TGF - \beta$, FGF , $BMPs$, $Twist$, and $Runx2$, are present in the bone–suture–bone interface and have different functions in the cellular activity. For example, it is proven that the $TGF - \beta1$, $TGF - \beta2$, $BMP2$ and $BMP4$ promote the bone formation while the $TGF - \beta3$, $BMP3$,

Shh and *Ptc* inhibit the ossification process or contribute in suture patency [53, 55, 57, 58, 103, 112, 113]. Table 2-2 presents the typical factors that have been related to the suture formation process and its response to mechanical stimuli. Nevertheless, according to the literature review, the studies are normally developed on cranial sutures, that differs in key aspects such as the presence of the Dura Mater, and the investigations specifically focused on the MPS are limited [66, 114]. This is the motivation of the third objective of this chapter.

Factor	Supposed function	Reference(s)
<i>IGF - I</i>	Increase the osteoblast and fibroblast proliferation	[55, 56, 110, 112]
<i>IGF - IR</i>	Increase the osteoblast and fibroblast proliferation	[112]
<i>TGF - β1</i>	Promotes bone production	[53, 73, 112]
<i>TGF - β2</i>	Promotes bone production	[55, 56, 73, 75]
<i>TGF - β3</i>	Inhibits bone production	[53, 55, 75]
<i>TGF - βR(1 - 2)</i>	Promotes bone production	[103]
<i>FGFs</i>	Promotes bone production	[55-57, 73, 110, 112]
<i>FGFRs(1 - 3)</i>	Promotes osteoblast differentiation	[53, 55, 73, 103]
<i>FGFR2</i>	Promotes the proliferation of stem cells	[57, 58, 73, 110]
<i>BMPs</i>	Promotes bone production	[53, 56, 57, 73, 110, 112]
<i>Twist</i>	Promotes bone production	[57, 73, 103, 112]
<i>Msx2</i>	Promotes bone production	[53, 55, 57, 73, 112]
<i>Runx2</i>	Promotes bone production	[55, 56, 73, 75, 112]
<i>Tbx2</i>	Inhibits bone production	[110, 112]
<i>RANKL</i>	Promotes osteoclast differentiation and suture patency	[8, 55]
<i>MMPs</i>	Promotes bone production and remodeling	[110, 114]
<i>TIMP - 1</i>	Inhibits the effect of <i>MMP - 2</i>	[114]
<i>Shh</i>	Regulates the intramembranous bone formation	[55, 103]
<i>PC1</i>	Mechanotransduction function	[57, 66]
<i>Wnt</i>	Promotes the differentiation process of mesenchymal cells in osteoblasts	[56, 57]
<i>Noggin</i>	Inhibits the effect of <i>BMPs</i>	[57, 73]

Table 2-2: Typical factors that have been related to bone cells activity in sutures

2.2 Materials and Methods

This procedure was based on the studies reported by Hou *et al.* who analyzed the influence of loads on bone remodeling processes and the *PC1* protein on the mechanotransduction process in the oral cavity [8, 66]. The experiment sought to evaluate the morphological, cellular and molecular changes produce by ME in two time points, at 7 and 14 days. Each period of time was divided into 4 groups, one of control and 3 experimental. The groups were formed of 6 animals for a total sample size of 48 mice; Table 2-3 shows the groups distribution. The conditions to which the animals were submitted during the experiment were normal conditions of light (12h light/dark cycle) and temperature ($24 \pm 2^\circ C$). Due to the possible discomfort that the animals could experience after the expansion procedure, the type of feed supplied was commercial concentrate moistened and crushed to have a pasty consistency. Drinking water was freely available.

Time	Load	Number of animals
7 days	Control	6
	0.56N	6
	0.42N	6
	0.28N	6
14 days	Control	6
	0.56N	6
	0.42N	6
	0.28N	6

Table 2-3: Groups distribution for the experimental procedure

A 0.014in stainless steel orthodontic wire (GAC International Inc., Bohemia, NY) was used to apply the expansion force; the load values were 0.28N, 0.42N and 0.56N and were calibrated using a tension gauge (Shimpo Instruments, Itasca, Ill) (Figure 2-4).



Figure 2-4: Calibration of the expansion load

For the procedure, a combination of xylazine (10 mg/Kg) and ketamine (100 mg/Kg) solution was used to anesthetize the animal. Mice were placed on the surgery table fixing their limbs and head. Subsequently, a mouth-opener, a stereomicroscope (Quimis Aparelhos Científicos Ltd, Diadema, São Paulo, Brazil) and an optical light system (Multi-Position Fiber Optic Illuminator system, Cole-Parmer Instrument Company Ltd., London, England) were used to ensure full visibility of oral cavity. Then, the area where the force would be applied (first and second maxillary molars) was cleaned using acetone and etched using a self-etching primer (Unitek/3 M, Minneapolis, USA) and the appliances were bonded on the occlusal surface of the teeth using a light-cured resin (Transbond, Unitek/3 M, Monrovia, CA, USA) (Figure 2-5). Finally, mice were euthanized by decapitation in the two time-points established and the different analysis were performed.

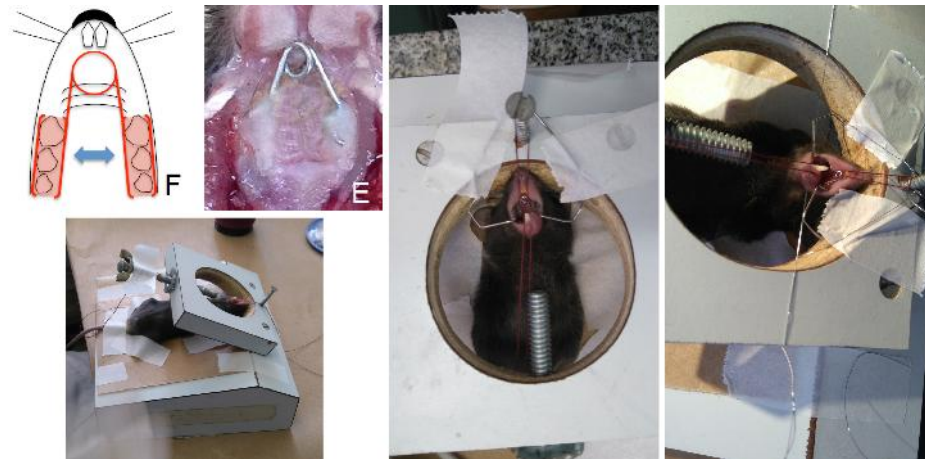


Figure 2-5: Experimental procedure to apply the expansion force

2.2.1 MicroCT imaging

The maxillary samples were dissected and fixed in 10% buffered formalin with a pH of 7.4. They were scanned using a 0.5mm aluminium filter and a compact desktop micro-CT scanner (SkyScan 1174, Bruker micro-CT, Belgium), with 50kV of source voltage, 800 μ A source current and 12.18 μ m pixel size. Samples were attached to a stage that rotated 180° with images acquired every 0.7°. To measure the maxillary width, the images were reconstructed using NRecon software (Bruker-MicroCT, Belgium), the sample position was determined by Dataviewer software (Bruker-MicroCT, Belgium) and analyzed using CTan software (Bruker-MicroCT, Belgium). For the bone density analysis, the software used was Mimics 10.01 (Materialize, Belgium).

Two variables were calculated to establish the anthropometric effect of the expansion in the maxilla: the transverse dimension of the palate and the suture space. The first variable was measured in the transverse plane as the mean distance between: (1) the occlusal third and middle third obtained at the vestibular surface of the mesio-vestibular root of the first molar; (2) middle third and apical third obtained at the palatal root canal of the first molar. For the second variable, the measurement of the 3D volume was made in the antero-posterior direction along the entire suture. Another variable of interest was the mineral density variation in the bone–suture–bone interface. The Hounsfield Units (HU) were used as a unit of measurement of that variable [115]. Therefore, at the level of the first molars, on the coronal plane, a filter corresponding to bone (226 – 2746HU) was applied. Then, the density was calculated as the average of 10 measurements that were taken on the bone, five on each side of the suture.

2.2.2 Histological analysis

Once the MicroCT were taken, the samples were decalcified in 14% EDTA with a pH of 7.4 for 21 days with daily solution changes. The maxillary samples were washed for 4 hours in running water and the dehydration was done in increasing series of 70%, 80%, 90% and absolute alcohol, 30 minutes in each. After that, the samples were clarified in 3 xylol baths (Mono Fabric Processor 2000, Lupe Industria e Comércio Ltda, São Carlos, Brazil). Finally, the samples were included in paraffin where the maxillae were cut in the coronal axis keeping the molars perpendicular to the occlusal plane. The blocks were sectioned cutting them each 4 μ m using a rotating microtome (Leica, Histocut 820, Germany). The count of the osteoblasts and osteoclasts was carried out by means of a Masson's trichrome stain and

a hematoxylin and eosin stain (H&E), respectively. The cell counting was performed in the marginal bone contouring the maxillary suture at the level of the palatal root of the first molar. At least five serial vertical sections containing the above mentioned structures were evaluated for each animal for each analysis.

2.2.3 Quantitative Polymerase Chain Reaction (qPCR)

Total RNA was extracted (RNeasy FFPE kit; Qiagen Inc., Valencia, CA), according to the manufacturer's instructions. The integrity of RNA samples was checked by analyzing 1mg of total RNA on 2100 Bioanalyzer (Agilent Technologies, Santa Clara, CA, USA). The complementary DNA (cDNA) was synthesized using 3μg of RNA through a reverse transcription reaction using QuantiTectRTkit (Qiagen Inc, Valencia, CA). Real-Time PCR array was performed in a Viia7 instrument (Life Technologies) using TaqMan chemistry (Invitrogen) associated with inventoried optimized primers/probes sets (Invitrogen), for bone morphogenetic protein 2 (*BMP2*); transforming growth factor beta 1, 2 and 3 (*TGF-β1, 2 and 3*); sclerostin (*SOST*); catenin beta like 1 (*Ctnnbl1*); Wnt family member 3, 3a and 5a (*Wnt3, 3a and 5a*); myostatin (*Mtsn*); receptor activator of nuclear factor kappa B (*RANK*); receptor activator of nuclear factor kappa B ligand (*RANKL*); osteoprotegerin (*OPG*); cathepsin K (*CTSK*); matrix metalloproteinases 9 and 13 (*MMP9 and 13*); runt-related transcription factor 2 (*RUNX2*); alkaline phosphatase (*ALP*); osteocalcin (*OCN*); collagen, type I alpha 1 (*COL1A1*); tissue inhibitor of metalloproteinases-1 (*TIMP1*); dentin matrix acidic phosphoprotein 1 (*DMP1*); with basic reaction conditions of 50°C (20s), 95°C (10min), (40cycles) 95°C (15s) and 60°C (1min). The mean threshold cycle values from duplicate measurements were used to calculate expression of the target gene, with normalization to an internal control (β -actin) using the $2^{-\Delta\Delta C_t}$ method.

2.2.4 Statistical analysis

Results were expressed as mean \pm standard error of the mean (SEM), considering that data sets presented a normal distribution (Kolmogorov-Smirnov). Two-way ANOVA followed by the Bonferroni post-hoc test were used to analyze differences among groups. The data obtained from all evaluations were processed with GraphPad Prism version 5.01 (GraphPad Software, San Diego, CA). The level of significance for all statistical tests was predetermined at 5%.

2.3 Results

2.3.1 MicroCT imaging

The anthropomorphic analysis showed a successful expansion of the maxilla for all groups; regardless of the load value or the period of time of the treatment. It is possible to see that the data presents similar values for the three applied loads and the two time points. Figure 2-6 displays the maxillary transverse dimension results obtained at the first (Figure 2.6(a)) and second (Figure 2.6(b)) measurement point, described in section 2.2.1. Also, in Figure 2-7 it is possible to see the results obtained about the suture space.

The results of the bone density analysis are showed by two comparative graphics in Figure 2-8. *P1* (left) and *P10* (right) correspond to the points furthest from the MPS, while *P5* (left) and *P6* (right) correspond to the points closest to the suture. In all cases the mineral density has a tendency to decrease from the extremes toward the center. As an interesting aspect, the density values of the control group on the seventh day were relatively lower than the values found for the groups of 0.42N and 0.56N

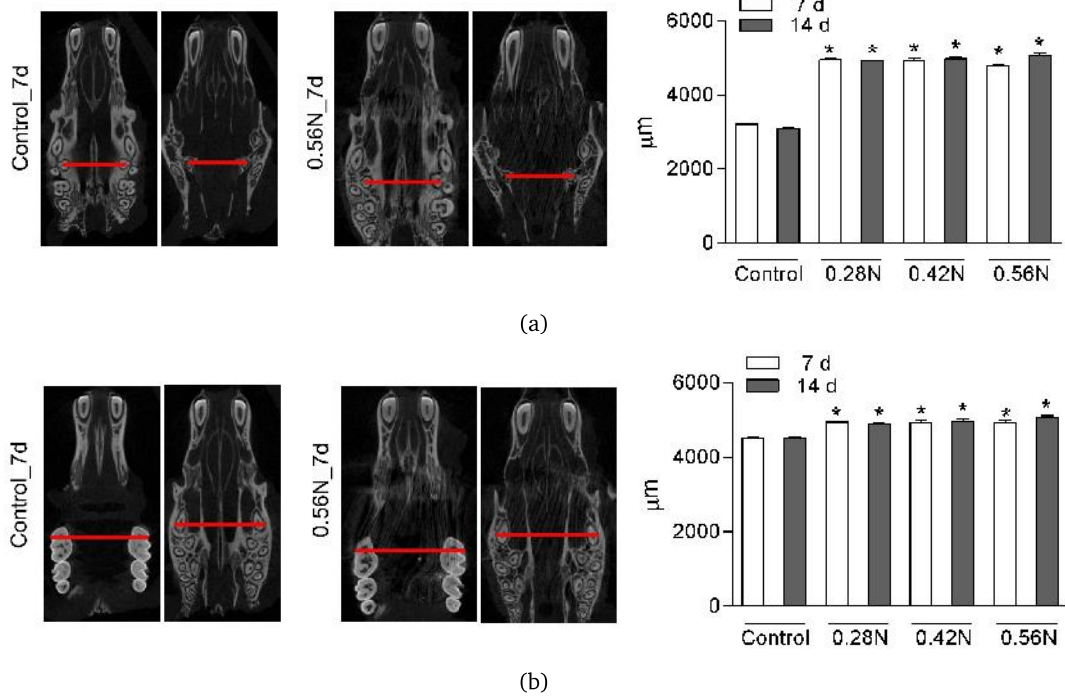


Figure 2-6: Anthropomorphic results of the maxillary transverse dimension: a) at the first measurement point b) at the second measurement point. Data were expressed as means SEM. * $P < 0.05$.

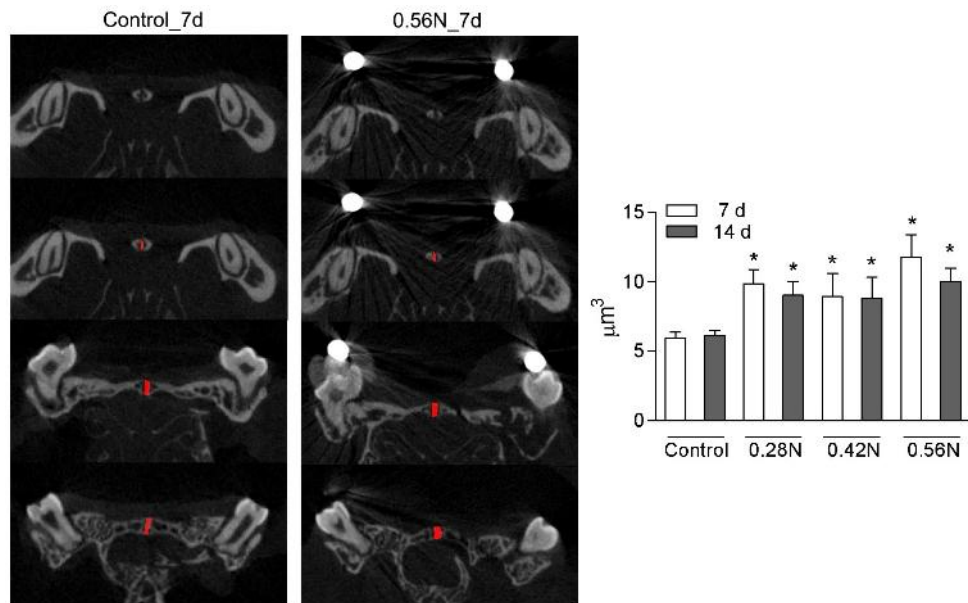


Figure 2-7: Anthropomorphic results of the suture space in the coronal plane along the anteroposterior direction. Data were expressed as means SEM. * $P < 0.05$.

and slightly higher compared to the 0.28N group. On the other hand, on day 14, the control group presented a little higher values than the other groups.

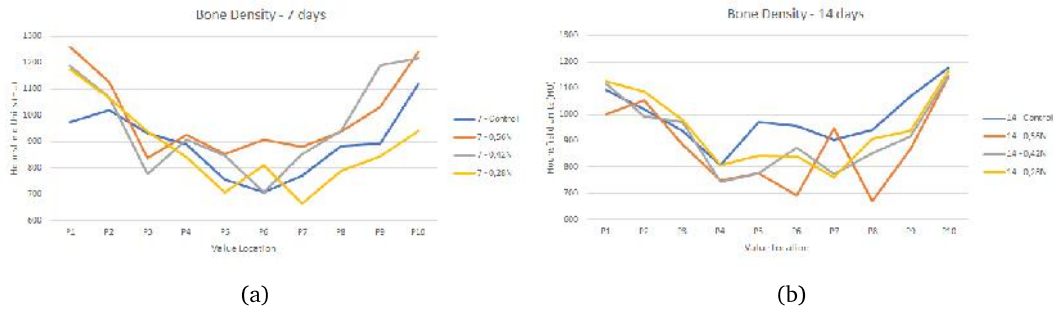


Figure 2-8: Bone density results: a) at 7 days ($SD = 4.97\%$) b) at 14 days ($SD = 4.53\%$)

2.3.2 Histological analysis

In relation to the cellular activity, the analysis was made both qualitatively and quantitatively. Figures 2-9 and 2-10 allow to compare the cellular activity inside the suture, in response to different load values applied, on days 7 and 14, respectively. It is possible to observe that the expansion loads generated both an increase of the area corresponding to the conjunctive tissue and an activation of the cellular migration from the ends (both nasal and buccal) towards the interior of the suture. In addition to this, qualitatively, a proportionality relation is perceived between the load magnitude, the migration size and the number of cells organized at the bone margins; the greater the load, the larger the migration size through the buccal end of the suture and the greater the number of cells located at the bone margins. At last, on day 14, a greater number of cells is perceived inside the connective tissue compared to day 7. Quantitatively, Figure 2-11 presents the osteoblastic and osteoclastic response to the expansion application. As it is possible appreciate, there is an increase in the number of osteoblasts when the suture is subjected to a tensile force (Figure 2.11(a)). On the other hand, no significant variations were found in the osteoclastic activity (Figure 2.11(a)). Comparing the values obtained for the different groups, it can be seen that the behavior was very similar for the three load magnitudes and time periods.

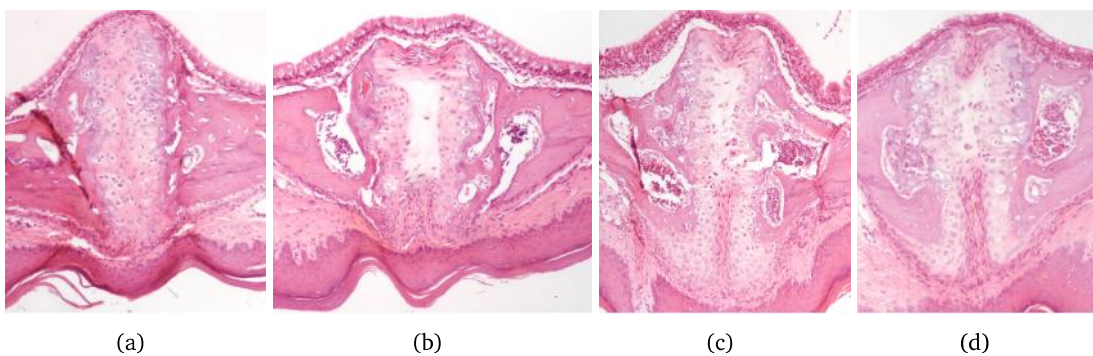


Figure 2-9: Histological results of H&E analysis in the 7-day period with loads of: a) Control, b) 0.28N, c) 0.42N and d) 0.56N

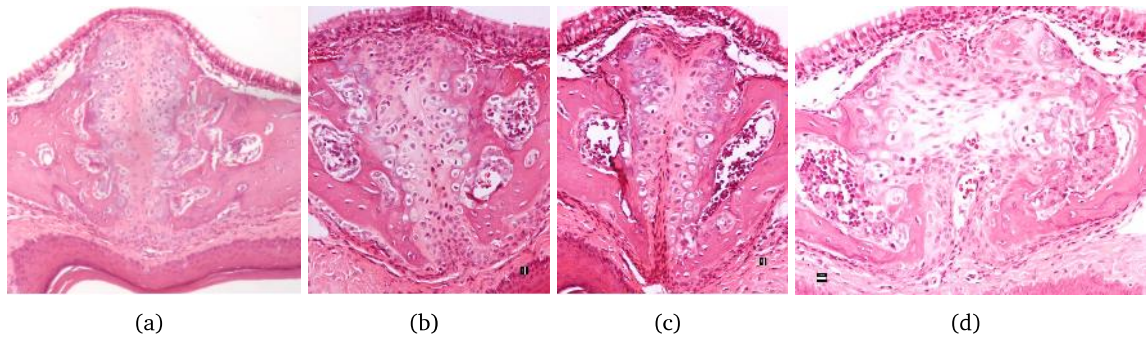


Figure 2-10: Histological results of H&E analysis in the 14-day period with loads of: a) Control, b) 0.28N, c) 0.42N and d) 0.56N

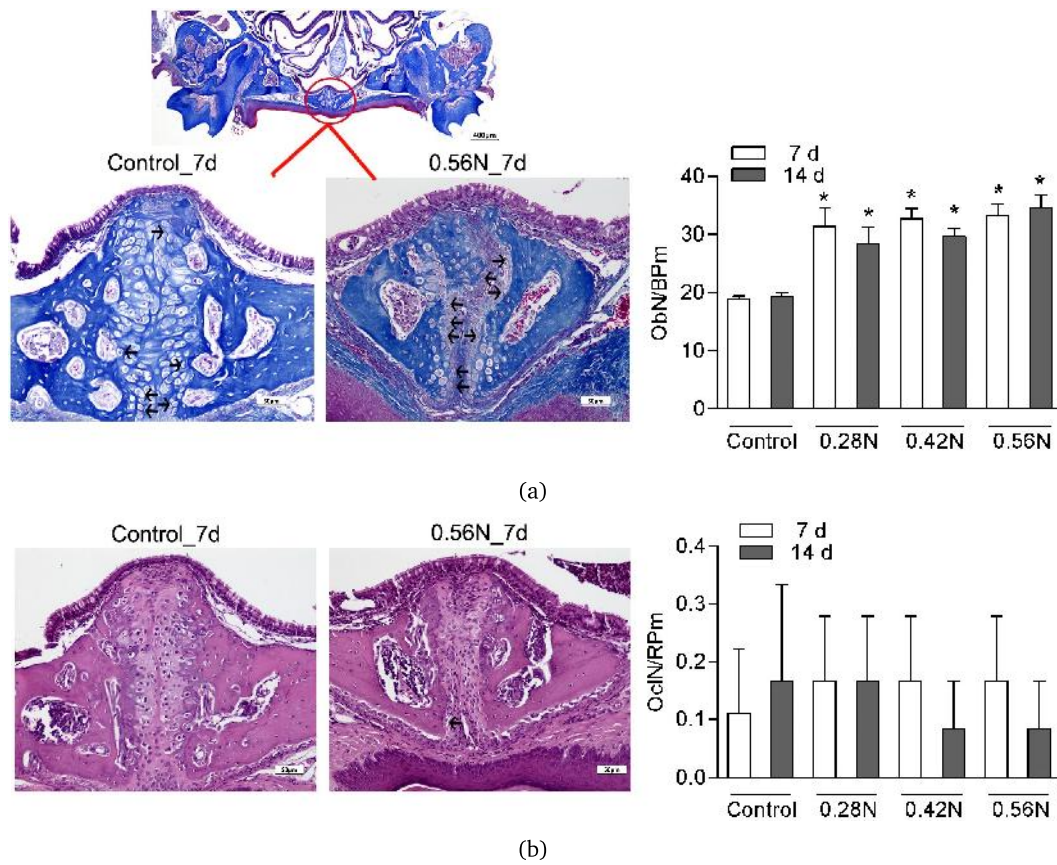


Figure 2-11: Histological results of the cellular activity in the MPS: a) osteoblastic activity and b) osteoclastic activity. Data were expressed as means SEM. * $P < 0.05$.

2.3.3 Quantitative Polymerase Chain Reaction (qPCR)

Regarding the qPCR analysis, Figure 2-12 shows the response of the molecular factors analyzed during the experiment. With respect to the osteoblastic markers (Figure 2.12(a)), the values of the expressions tended to increase with the application of the expansion loads; only the factors *RUNX2* and *ALP* had no significant variations compared to the control group when the applied load was 0.28N. Significant differences between groups with 0.42N and 0.56N loads were only perceived in *RUNX2* and *COL1A1*. Comparing the behavior of the factors between the two periods of time, it can be seen that the *COL1A1* was the only one that decreased (for 0.28N) or that did not present significant changes (for 0.42N) between days 7 and 14; the other factors showed higher values in the longer period of time.

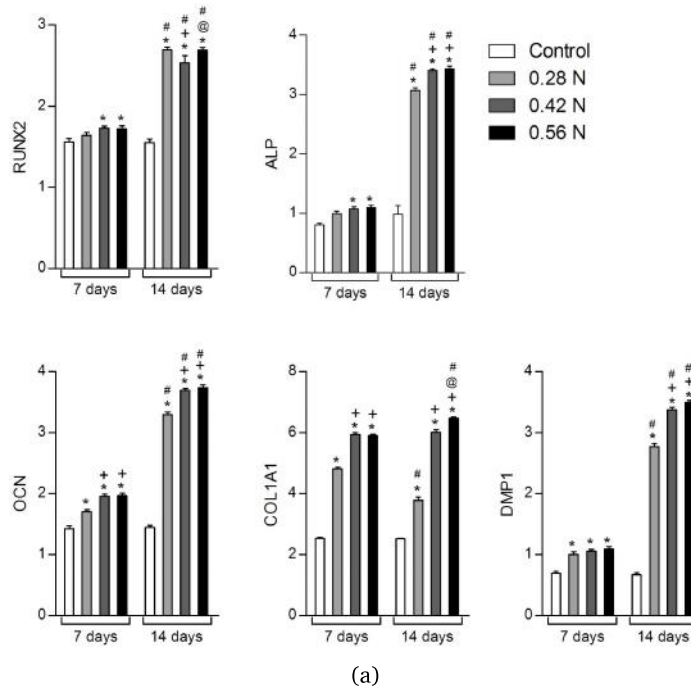


Figure 2-12: Quantitative Polymerase Chain Reaction results. * $P < 0.05$ comparing experimental with the control group, + $P < 0.05$ with 0.28N and @ $P < 0.05$ with 0.42N at the same time point; # $P < 0.05$ comparing with 7 days of mechanical loading under the same force. Data were expressed as means SEM.

Comparing with the control groups, osteoclastic markers increased their values when a tensile load was applied; except for the *RANKL/OPG* ratio, that at 14 days decreased in presence of the 0.28N load and showed no significant differences with the other force values. Nevertheless, it is not possible to generalize the behavior between the two periods of time. As seen in Figure 2.13(b), *CTSK* and *TIMP1* factors had a behavior that contrasted with *MMP9* and *MMP13* factors. While *CTSK* and *TIMP1* decreased their values compared to day 7, the expressions of *MMP9* and *MMP13* increased. In this four cases, the 0.28N load produced the lowest values and no significant differences were appreciated between 0.42N and 0.56N. In the particular case of *RANK*, just the 0.56N load at 14 days generated significant higher values than the other loads, regardless of the period of time.

Finally, Figure 2.13(c) shows the results obtained for the last factors analyzed that are related to the bone formation or remodeling process. The only factor that showed no significant differences, comparing with the control group, was the *TGF- β 3* at 14 days with 0.28N. *BMP2*, *TGF- β 2*, *TGF- β 3*

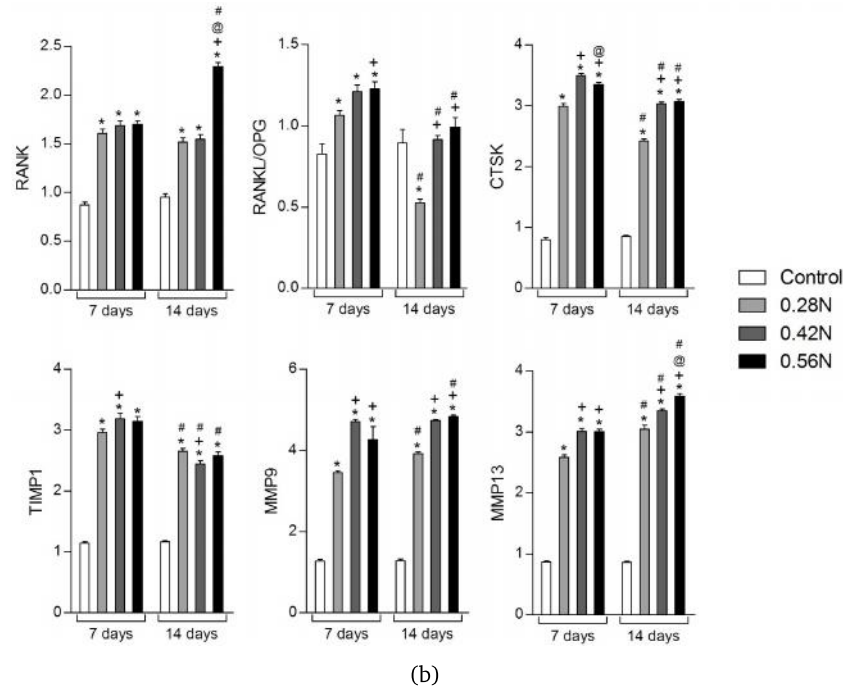


Figure 2-12 (Continued): Quantitative Polymerase Chain Reaction results. * $P < 0.05$ comparing experimental with the control group, + $P < 0.05$ with 0.28N and @ $P < 0.05$ with 0.42N at the same time point; # $P < 0.05$ comparing with 7 days of mechanical loading under the same force. Data were expressed as means SEM.

and *Ctnnb1* decreased their expressions at seventh day in relation to the 14 day, for the three load values. On the other hand, *SOST* and *Wnt3A* presented a behavior with higher values at 14 day than 7 day. The other factors showed no significant differences between the periods of time. In relation to the force magnitude, 0.42N and 0.56N loads had a very similar effect and, normally, promoted greater expression responses than the 0.28N load; aspect that was more evident on day 14 than on day 7.

2.4 Discussion

The experimental procedure performed on Five-week-old wild-type (WT) (C57BL/6) mice was designed to evaluate the effect of expansion loads in the morphology and in the cellular and molecular activity of the bone–suture–bone interface. Thus, an experimental procedure based on previous studies [8,66] was proposed and a MicroCT, a histological and a qPCR analysis were carried out. The anthropomorphic and histological analysis show that the expansion was successful for all experimental groups; it means that independently of the load or the period of time, the palate gained width with the treatment application.

As seen in the figures 2-9 and 2-10, the load applied impacted directly in the cellular activity. Qualitatively, it is observed that higher load values produce higher levels of cell migration and a higher concentration of cells located in the bone margins; suggesting the active beginning of the formation of new bone layers as established by Consolaro *et al.* [20] and Ennes *et al.* [10] and as was observed in the study of Hou *et al.* [8]. This was verified, quantitatively, both by the count of osteoblastic cells present inside the suture and by the behavior of the osteoblastic markers expression. Reaffirming what was

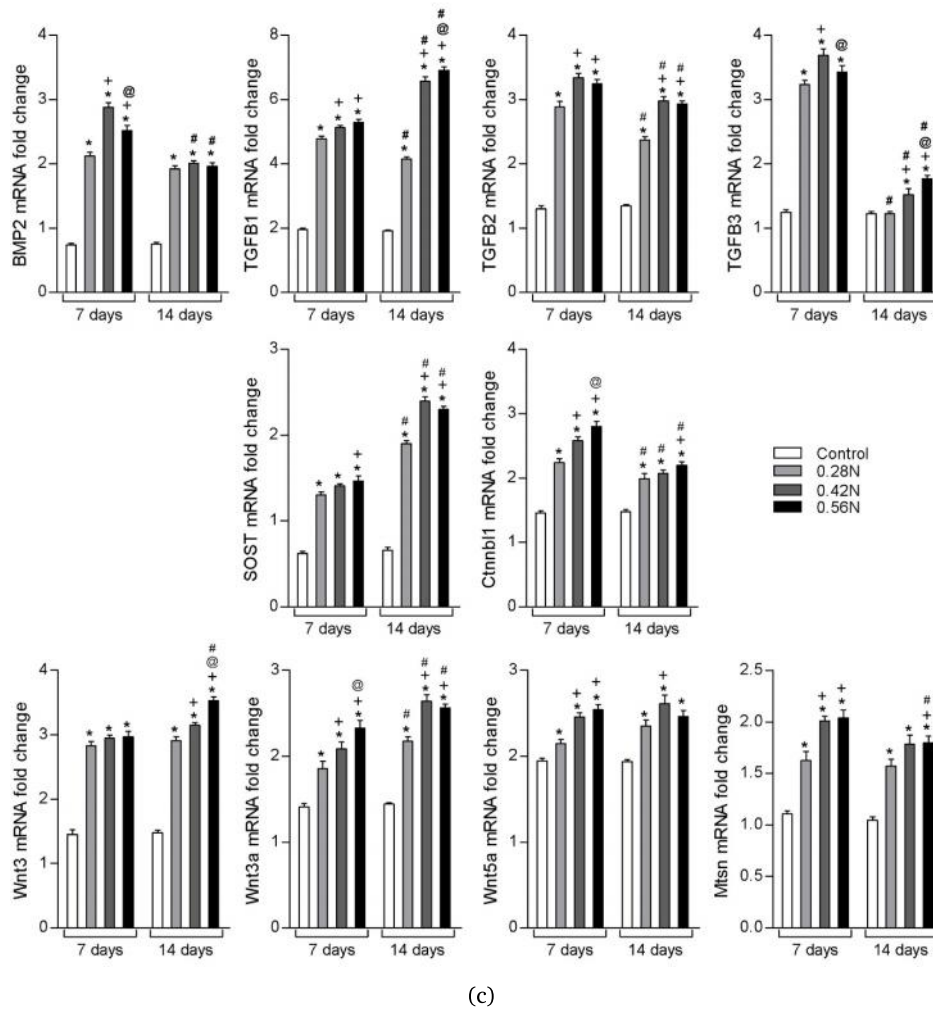


Figure 2-12 (Continued): Quantitative Polymerase Chain Reaction results. $*P < 0.05$ comparing experimental with the control group, $+P < 0.05$ with $0.28N$ and $@P < 0.05$ with $0.42N$ at the same time point; $\#P < 0.05$ comparing with 7 days of mechanical loading under the same force. Data were expressed as means SEM.

reported by Cheng *et al.* [116], the histological analysis shows a significant increase in the osteoblasts when the expansion load was present. The expression of the molecular factors related to the proliferation and differentiation of this type of cells also increased. Some of these factors had been analyzed by other authors such as the *ALP* and *COL1A1* studied by Hou *et al.* [8] and the *OCN* studied by Wu *et al.* [117]; in both cases, the behavior was similar to that found in this work. A particular case is the *RUNX2* factor, which, according to Hou *et al.* [66], showed no significant difference with the load application; what differs from the results presented in this research. The foregoing may be due to the fact that the author carried out the analysis in the nasal cartilage, while here the palate bone was taken into account.

In addition to bone formation, the experimental procedure also sought to evaluate the bone remodeling process. Therefore, the histological analysis of the osteoclastic activity and the qPCR analysis of the osteoclastic markers expression were performed. In agreement with Wu *et al.* [117], there is no evidence of the significant variations in the number of osteoclasts inside the suture when the expansion treatment is applied, regardless the force value or period of time. Nevertheless, the expressions of molecular factors related with the osteoclastic activity had a different behavior. For example, the *RANK*, *RANKL* and *OPG* factors were increased under load; this fact is important because these factors are involved in the osteoclastogenesis process [118, 119]. Additionally, another factors that controlled the bone resorption process, like *CTSK*, *MMP9*, *MMP13* and *TIMP1* [120, 121], were augmented too; the last one agrees with the study reported by Chen *et al.* [114]. The difference between the cellular and molecular results can be attributed to the place where the cell count was carried out. According to the research developed by Hou *et al.* [8], when the cell count is performed in the nasal cartilage, the number of osteoclasts increases; the foregoing could suggest that the stimulation of osteoclastic activity in these cases is made indirectly [122].

Finally, it is important to highlight two additional aspects that were obtained from this experimentation. The first one is related to the third group of molecular factors that were analyzed within the experimental procedure (Figure 2.13(c)). These factors have been commonly studied by other authors who have focused on investigating cranial sutures [52, 53, 63–65]. As it could be evidenced, all of them reacted by increasing their expression level when the expansion load was applied. This aspect is of great importance since it allows to relate the results obtained in cranial sutures with the events that occur inside the facial sutures; even when there are key differences such as the absence of the Dura Mater. For example, according to the results, it could be suggested that $TGF - \beta 1$ and $TGF - \beta 2$ are contributing to bone formation while $TGF - \beta 3$ is helping to the suture patency, as in the case of cranial sutures [53, 55, 73, 75]. The second one has to do with the development of the maxillary expansion procedure in mice. So far, there are very few studies conducted directly on the MPS expansion and the way that they have been addressed is limited to supposing a single force that is within a reasonable range for the animal [8, 66, 114, 117]. Therefore, this work shows a procedure that succeed to standardize both the preparation of expansion devices and the criteria of time of the experiment and load value, allowing to observe the changes at the cellular and molecular level produced by the expansion. According to this research, the recommended parameters for the force magnitude and time of treatment application are 0.42N and 7 days, respectively.

2.5 Conclusions

- The maxillary expansion promotes the bone formation and remodeling processes through the activation of osteoblastic and osteoclastic migration and proliferation and the increase of molecular expressions related to this type of phenomena.

- The results obtained from the histological and qPCR analysis suggest that the investigations developed, and the reported findings, on cranial sutures could be used to analyze and understand in greater depth the behavior of facial sutures, such as the midpalatal suture, when they are subjected to tensile loads.
- The expansion procedure presented is a suitable procedure to observe the effect of the maxillary expansion on the morphology of the bone–suture–bone interface and on the cellular and molecular phenomena that occurs within the suture. In addition, it allowed to standardize the preparation of the expansion devices and to calculate, in a methodological way, some parameters of the experiment such as optimum load values (0.42N) and treatment time (7 days).

Chapter 3

Mechanobiological model

Mathematical models have been used to describe a wide variety of biological phenomena such as endochondral ossification [123], skull formation [22, 54, 76], bone remodeling [124–126], long bone development [127, 128], dentinal tubules location [129], bone regeneration [130], tissue genesis [60, 131], among others. As mentioned in Section 1.1.3, some authors have worked in numerical simulations looking to establish a representation of the suture formation process and its response to mechanical loads [25, 72–75]. These studies employed different mathematical approaches, like reaction–diffusion [73] or transport–diffusion systems [25], and their results have been able to approximate suture interdigitation patterns and some cellular activity and molecular processes inside the tissue. Analyzing the aforementioned investigations, it is possible to observe that the models are designed for cranial sutures and differ from some fundamental aspects, such as the midpalatal suture morphology or ossification percentage. With respect to the morphology, it does not correspond to a line between two bone margins but is characterized by having a Y-shape [6, 20, 102]. In relation to the ossification, it has been found that this suture tends not to fuse, reaching an ossification percentage with an average of 3.11% and a maximum of 13.1% [105]. Hence, the current chapter presents a mechanobiological model that describes the MPS formation process and its biological response to a mechanical stimulus, as those generated in the maxillary expansion. To this end, a reaction–diffusion model, based on the experimental data and the literature review, is developed. In the following sections a brief explanation of the reaction–diffusion equation and of the biological models commonly used will be presented, as well as the proposed model and its solution by the finite element method. Finally, the results obtained will be shown and discussed.

3.1 Reaction–diffusion systems

3.1.1 Reaction–diffusion equation

Diffusion can be interpreted as the movement that a species performs to reach the equilibrium distribution of its concentration in the environment that contains it. Mathematically, this can be described by Fick’s Law (Equation 3-1), which represents the movement from points of higher concentration to points of lower concentration [129, 132–134]. In Equation 3-1, $u(\mathbf{x}, t)$ is the species concentration, \mathbf{J} corresponds to the diffusive flux vector and D is the diffusion coefficient.

$$\mathbf{J}(\mathbf{x}, t) = -D\nabla u(\mathbf{x}, t) \tag{3-1}$$

On the other hand, reaction is the variation of the species concentration due to the interaction effect with other species and with itself. That effect could be related with production, proliferation, degradation,

consumption, among other processes [129, 132–134] and can be represented by the function $f(\mathbf{u}, \mathbf{x}, t)$. Now, if a volume V limited by a surface S is defined, the principle of conservation states that the rate of change of the amount of mass contained in volume V is equivalent to the sum of the total mass flow through the surface S with the amount of mass that is transformed, due to the presence of the reactive term, inside the volume V . It can be seen in Equation 3-2, where the \bar{n} vector is the normal vector to the surface S .

$$\frac{\partial}{\partial t} \int_V \mathbf{u}(\mathbf{x}, t) dV = - \int_S (\mathbf{J} \cdot \bar{n}) dS + \int_V f(\mathbf{u}, \mathbf{x}, t) dV \quad (3-2)$$

As it is possible to see in Equation 3-2, the first term on the right side is in the surface domain, so the divergence theorem is used to bring the diffusive term to the volume domain. Also, replacing Equation 3-1 in Equation 3-2 the following expression is obtained:

$$\frac{\partial}{\partial t} \int_V \mathbf{u}(\mathbf{x}, t) dV = \int_V \nabla \cdot (D \nabla \mathbf{u}(\mathbf{x}, t)) dV + \int_V f(\mathbf{u}, \mathbf{x}, t) dV \quad (3-3)$$

The Neumann boundary conditions were configured as null to guarantee that the spatial patterns formation are the product only of the interaction between the species within the domain. Thus, the final reaction–diffusion equation, written in differential form, is given by Equation 3-4 [129, 133, 134]:

$$\frac{\partial \mathbf{u}(\mathbf{x}, t)}{\partial t} = \underbrace{\nabla \cdot (D \nabla \mathbf{u}(\mathbf{x}, t))}_{\text{Diffusion}} + \underbrace{f(\mathbf{u}, \mathbf{x}, t)}_{\text{Reaction}} \quad (3-4)$$

3.1.2 Biological models

The reaction–diffusion biological systems generate spatial–temporal patterns that allow to represent real phenomena like feather formation, hair follicles location, skin pigmentation, angiogenesis, among others [135–138]. Generally, these systems can be represent by chemical or cell movement interactions models. The first ones are related to cellular or molecular processes of synthesis, transport and degradation. For their part, the cell movement models describe the changes in cell concentration due to the attraction and repulsion between the cells or as a consequence of chemical signals present in the environment [133, 134]. In the following sections, the three most known and used models will be described: The Shnakenberg or morphogenesis model, the glycolysis model and the chemotaxis model.

Schnakenberg model

The Schnakenberg model has been widely used in molecular chemical systems and morphogenesis [129, 133]. This model was developed to represent the behavior of a chemical activator (u) when it interacts with a chemical inhibitor (v) [132–134]. The model is described, in a non–dimensional way, by the following system of equations:

$$\begin{aligned} \frac{\partial u}{\partial t} &= \nabla^2 u + \gamma(a - u + u^2 v) \\ \frac{\partial v}{\partial t} &= d \nabla^2 v + \gamma(b - u^2 v) \end{aligned} \quad (3-5)$$

The diffusive part of the equations represents the movement of both chemical substances, where d is the diffusion constants ratio ($d = D_u/D_v$). With respect to the reaction part, the terms a and b are related with the production of u and v , respectively; the $-u$ term is the consumption of u and the $u^2 v$

is a nonlinear kinetic reaction that describes the u production in presence of v and the v consumption in presence of u [129, 132, 133].

Glycolysis model

Glycolysis is the process that allows the energy supply to a cell through the synthesis of the glucose molecule. In this case, u represents the glucose concentration and v the pyruvate concentration. The pyruvate is a product of the glucose reaction sequences. Mathematically, this process can be described, in a dimensionless way, by the following system of equations [129, 133]:

$$\begin{aligned}\frac{\partial u}{\partial t} &= D_u \nabla^2 u + \delta - ku - u^2 v \\ \frac{\partial v}{\partial t} &= D_v \nabla^2 v + ku + uv^2 - v\end{aligned}\tag{3-6}$$

where D_u and D_v regulate the diffusion behavior of the glucose and pyruvate, respectively. The reactive part of the first equation is made up by a constant production (δ), a proportional consumption and a nonlinear consumption of u due to the interaction with v . In relation to the reactive part of the second equation, it is composed of a proportional production, a nonlinear activation as a consequence of the interaction between u and v and a linear consumption described by the $-v$ term. In both cases, k is the proportionality constant [129, 133].

Chemotaxis model

Chemotaxis models are part of the cell movement models and represent the cell migration as a response to the concentration of a chemical stimulus that is present in the environment surrounding the cells. The chemical substance is commonly known as the chemoattractant. Thus, the following system of equations describes the phenomena [133, 139, 140]:

$$\begin{aligned}\frac{\partial u}{\partial t} &= \nabla \cdot [D_u \nabla u - \alpha u \nabla v] + f(u, v) \\ \frac{\partial v}{\partial t} &= D_v \nabla^2 v + g(u, v)\end{aligned}\tag{3-7}$$

In Equation 3-7, u corresponds to the cell density and v to the chemoattractant concentration. D_u and D_v are the diffusion coefficients, α is the chemotaxis sensitivity, the $f(u, v)$ function represents the cell growth and death stages and the $g(u, v)$ function describes the production and degradation processes of the chemoattractant [129, 133, 140].

3.2 Materials and Methods

3.2.1 Mathematical model proposed

Based on the information obtained in the literature review and in the experimental data presented in Chapter 2, it was identified that the suture formation process can be modeled under two scenarios that differ from each other by the presence, or not, of external mechanical stimuli. If the suture subjected to tensile load is assumed, then the phenomenon to be modeled is the biological response characterized by cell migration from the periosteum into the suture. On the other hand, if the absence of external loads is assumed, then the process to be studied is the remodeling present at the bone margins; which is associated with the formation of interdigitation patterns.

First scenario: Cellular migration

As explained by Colsonaro *et al.* [20] and corroborated by histological images (Figures 2-9 and 2-10), the cellular response of the midpalatal suture when it is exposed to a tension load can be described in four stages. The first two are the stage before the application of the expansion force and the stage when the load is applied and the tissue becomes disorganized. The third one is the tissue recovery stage, where the migration of osteoprogenitor cells from the periosteum to the bone margins occurs. Finally, the four stage is the emergence of new bone layers adjacent to the bone margins due to cell differentiation. The above is a basic explanation of the suture behavior that simplifies the conception of the model; a more detailed explanation can be found in Section 2.1.

The process mentioned above is described in Figure 3-1. As can be seen, when the expansion load is applied (red arrows), molecular factors that signalize the process are activated and the periosteum interprets that signal as the beginning of the migration of the osteoprogenitor cells towards the inside of the suture. When the osteoblastic cells get into the sutural tissue, they are attracted by the molecular signals found in the bone margins. Once located in the margins, they agglomerate and differentiate forming new bone layers.

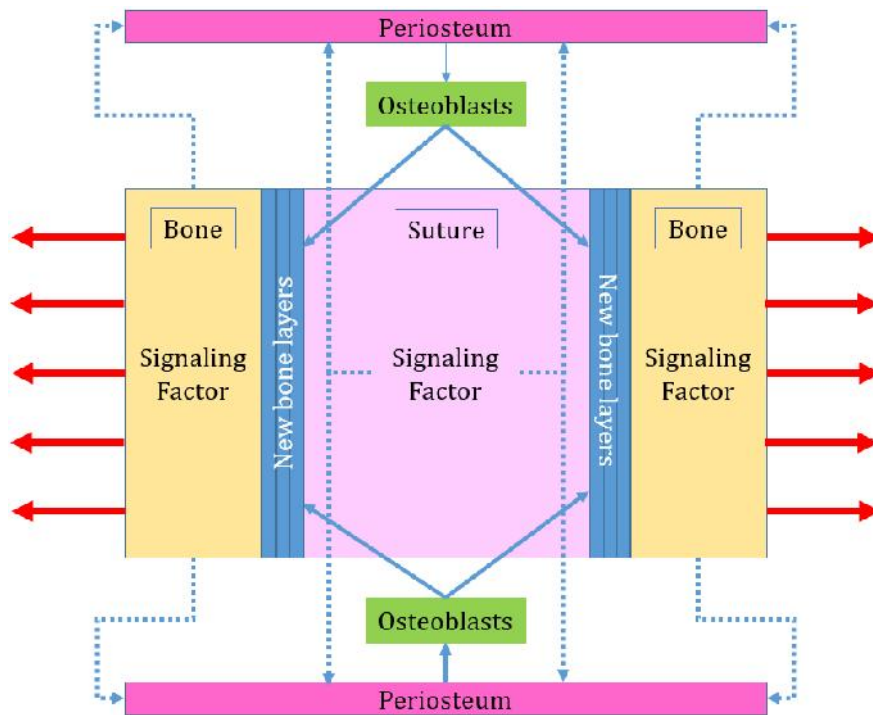


Figure 3-1: Outline of the cell migration process caused by mechanical stimuli. Red arrows mean external loads, dotted lines signage and solid lines activation.

Mathematically, the phenomena is described by the system of equations 3-8; where S_w is the osteoblastic cells density and S_p is the concentration of the chemoattractant molecule. This is a simplified model of chemotaxis that only takes into account the diffusive part of the cell density, the sensitivity to chemotaxis and the diffusive part of the chemoattractant. It is probable that the molecular factors that are responsible for signaling the onset of cell migration, and attracting the osteoblastic cells towards the bone margin, are related to the factors belonging to the *Wnt* family. The reason is that their signaling

function in the ossification processes of cranial sutures has been proven [57, 75, 141] and, in the experimental results, an increase in their expression can be observed during the expansion procedure (Figure 2.13(c)).

$$\begin{aligned}\frac{\partial S_w}{\partial t} &= D_w \nabla^2 S_w - D_p \nabla^2 S_p \\ \frac{\partial S_p}{\partial t} &= D_p \nabla^2 S_p\end{aligned}\tag{3-8}$$

To establish the criteria in which the osteoblastic cells differentiate into bone, a cell concentration threshold is used. If the cell density at a given point exceeds the threshold, it is assumed that the point becomes bone; otherwise it remains as part of the suture tissue. This is expressed in the following equation:

$$f(S_{w-thr}) = \begin{cases} 1, & S_w \geq S_{w-thr} \\ 0, & \text{otherwise} \end{cases}\tag{3-9}$$

Second scenario: Bone remodeling process

The bone remodeling process is a consequence of the osteoblastic and osteoclastic activity at the bone margins [73, 75]; some studies suggest that this process occurs even when there are no mechanical stimuli on the suture tissue [73]. To describe this process, a type of reaction–diffusion system known as activator–substrate is proposed [22, 76]. This system has been widely used for processes related to bone formation [22, 54, 75, 76] and is characterized by the interaction between two molecular factors that fulfill opposite functions; one promotes ossification while the other inhibits it.

Figure 3-2 shows the scheme of the system as it was conceived for the purpose of this study. As it can be seen, the process begins in a molecule that signals the loop. In the same way that in the first scenario, it could be assumed that this molecule is part of the *Wnt* family. Then, the bone deposition and the bone reabsorption stages are carried out. In the first one, the activating factor (Activator 1) promotes the mesenchymal cells differentiation into osteoblasts and inhibits the concentration of the substrate (Inhibitor 1) while the inhibitor factor regulates the production of osteoblasts and promotes the concentration of the activating molecule. For the second stage, it is presumed that the bone formation process described above signals an activator that stimulates the mesenchymal cells differentiation into osteoclasts. In agreement with the experimental results of the qPCR analysis (Section 2.3.3), the Activator 1 could be an osteoblastic marker like *RUNX2*, *OCN* or *COL1A1*, the Inhibitor 1 could be a typical factor associated with suture patency in cranial sutures like *TGF-β3* or *SOST* and, by last, the Activator 2 could be an osteoclastic marker like *TIMP1*, *RANK* or *CTSK*. In all cases it was demonstrated the presence of their expression with and without mechanical stimuli.

The relationships described in Figure 3-2 can be expressed, mathematically, by a Schnakenberg system as follow:

$$\begin{aligned}\frac{\partial S_a}{\partial t} &= \nabla^2 S_a + \gamma(a - S_a + S_a^2 S_s) \\ \frac{\partial S_s}{\partial t} &= d \nabla^2 S_s + \gamma(b - S_a^2 S_s)\end{aligned}\tag{3-10}$$

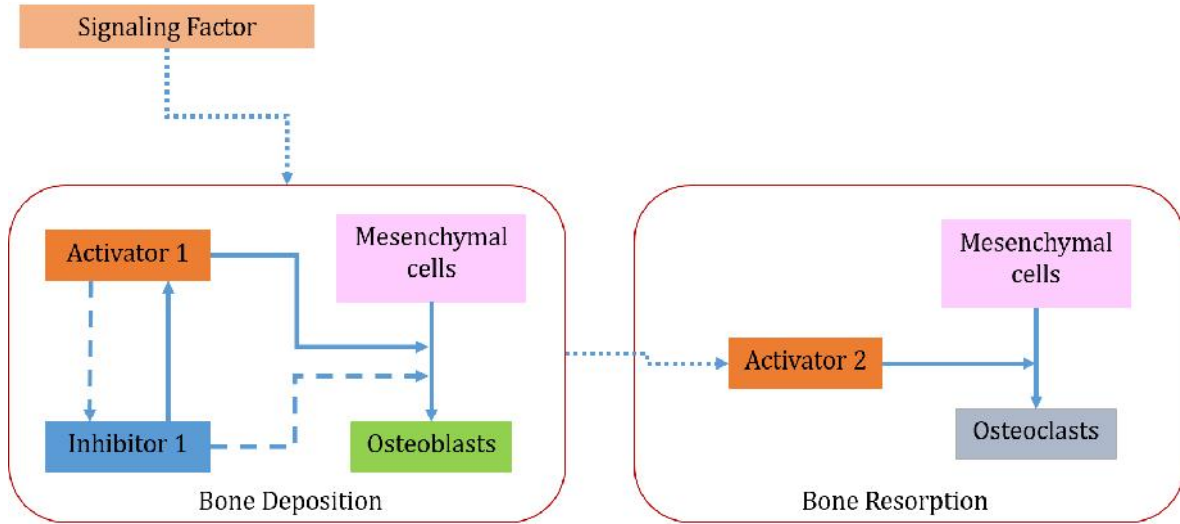


Figure 3-2: Outline of the bone remodeling process at the bone margins. Solid lines mean activation loads, dotted lines signage and dash lines inhibition.

where S_a corresponds to the concentration of the activating factor and S_s to the concentration of the substrate. Two chemical concentration thresholds are used to establish the criteria in which the osteoblastic cells differentiate into bone and the osteoclastic cells reabsorb it. If the activating factor concentration at a given point exceeds the threshold, it is assumed that the point becomes bone; otherwise it remains as part of the suture tissue. In contrast, if the substrate factor concentration at a given point exceeds the threshold, it is assumed that the adjacent bone point turns into suture tissue; otherwise it remains as part of the bone tissue. This is expressed in the following equation:

$$f(S_{x-thr}) = \begin{cases} 1, & S_x \geq S_{x-thr} \\ 0, & \text{otherwise} \end{cases} \quad (3-11)$$

where x represents the activating ($x = a$) or the substrate ($x = s$) factor.

3.2.2 Numerical Solution

The systems of equations 3-8 and 3-10 was solved using the finite element method with bilinear quadrilateral elements and a Newton–Raphson solver, for the time evolution problem, with an incremental iterative scheme.

Chemotaxis Model Solution

The system of equations 3-8 can be rewritten as follows:

$$\frac{\partial S_w}{\partial t} - D_w \nabla^2 S_w + D_p \nabla^2 S_p = 0 \quad (3-12)$$

$$\frac{\partial S_p}{\partial t} - D_p \nabla^2 S_p = 0$$

Using weighted residuals, the system of equations 3-12 becomes:

$$\int_{\Omega} w_1 \left(\frac{\partial S_w}{\partial t} - D_w \nabla^2 S_w + D_p \nabla^2 S_p \right) d\Omega = 0$$

$$\int_{\Omega} w_2 \left(\frac{\partial S_p}{\partial t} - D_p \nabla^2 S_p \right) d\Omega = 0$$
(3-13)

In Equation 3-13, Ω represents the problem domain that is limited by the border Γ and w_1 and w_2 are the weighting functions. Applying the Green's theorem and weakening the system of equations 3-13, the residue of the problem will be as follows:

$$r_{S_w} = \int_{\Omega} w_1 \frac{\partial S_w}{\partial t} d\Omega + \int_{\Omega} D_w \nabla w_1 \nabla S_w d\Omega - \int_{\Gamma} w_1 D_w (\nabla S_w \cdot \bar{n}) d\Gamma$$

$$- \int_{\Omega} D_p \nabla w_1 \nabla S_p d\Omega + \int_{\Gamma} w_1 D_p (\nabla S_p \cdot \bar{n}) d\Gamma = 0$$
(3-14)

$$r_{S_p} = \int_{\Omega} w_2 \frac{\partial S_p}{\partial t} + \int_{\Omega} D_p \nabla w_2 \nabla S_p d\Omega - \int_{\Gamma} w_2 D_p (\nabla S_p \cdot \bar{n}) d\Gamma = 0$$

As can be seen in Equations 3-14, there are two flow conditions, one for each variable. For the S_w variable, the flow condition was assigned a null value due to the fact that it is assumed that the osteoblastic population is always inside the suture and cannot penetrate the bone tissue. By the other hand, for the S_p variable, the flow conditions at the bone margins was assigned a unit value that represents the signaling done by the chemoattractant. Thus, the residue is expressed as:

$$r_{S_w} = \int_{\Omega} w_1 \frac{\partial S_w}{\partial t} d\Omega + \int_{\Omega} D_w \nabla w_1 \nabla S_w d\Omega - \int_{\Omega} D_p \nabla w_1 \nabla S_p d\Omega + 1 = 0$$
(3-15)

$$r_{S_p} = \int_{\Omega} w_2 \frac{\partial S_p}{\partial t} + \int_{\Omega} D_p \nabla w_2 \nabla S_p d\Omega - 1 = 0$$

Now, for the approximation of each variable linear shape functions will be used:

$$S_w^e = N_w S_w$$

$$S_p^e = N_p S_p$$
(3-16)

where N_w and N_p correspond to the shape functions that depend on the domain and S_w and S_p are the osteoblastic cell density and the concentrations of the chemoattractant on the nodal points, respectively. The superscript e indicates the finite element discretization. Also, a Bubnov–Galerkin formulation is used to define the weighting functions and, for this reason, the functions w take the same form of the shape functions N . Therefore, the discrete form of the residue vectors are established by:

$$r_{S_w}^e = \int_{\Omega} N^T \frac{\partial S_w}{\partial t} d\Omega + \int_{\Omega} D_w \nabla N^T \nabla S_w d\Omega - \int_{\Omega} D_p \nabla N^T \nabla S_p d\Omega + 1$$

$$r_{S_p}^e = \int_{\Omega} N^T \frac{\partial S_p}{\partial t} + \int_{\Omega} D_p \nabla N^T \nabla S_p d\Omega - 1$$
(3-17)

where ∇N is the gradient vector of the shape functions. Applying the Newton–Raphson linearization the system can be rewritten as:

$$\begin{bmatrix} \frac{\partial r_{S_w}^e}{\partial S_w} & \frac{\partial r_{S_w}^e}{\partial S_p} \\ \frac{\partial r_{S_p}^e}{\partial S_w} & \frac{\partial r_{S_p}^e}{\partial S_p} \end{bmatrix} \begin{bmatrix} \Delta S_w^e \\ \Delta S_p^e \end{bmatrix} = \begin{bmatrix} -r_{S_w}^e \\ -r_{S_p}^e \end{bmatrix} \quad (3-18)$$

where the symbol Δ denotes the difference of the nodal values between two consecutive iterations. The terms of the tangential stiffness matrix are calculated using Equations 3-17 and can be seen below:

$$\begin{aligned} \frac{\partial r_{S_w}^e}{\partial S_w} &= \frac{1}{\Delta t} \int_{\Omega} N^T N d\Omega + D_w \int_{\Omega} \nabla N^T \nabla N d\Omega \\ \frac{\partial r_{S_w}^e}{\partial S_p} &= -D_p \int_{\Omega} \nabla N^T \nabla N d\Omega \\ \frac{\partial r_{S_p}^e}{\partial S_w} &= 0 \\ \frac{\partial r_{S_p}^e}{\partial S_p} &= \frac{1}{\Delta t} \int_{\Omega} N^T N d\Omega + D_p \int_{\Omega} \nabla N^T \nabla N d\Omega \end{aligned} \quad (3-19)$$

Schnakenberg Model Solution

The system of equations 3-10 can be rewritten as follows:

$$\begin{aligned} \frac{\partial S_a}{\partial t} - \gamma(a - S_a + S_a^2 S_s) - \nabla^2 S_a &= 0 \\ \frac{\partial S_s}{\partial t} - \gamma(b - S_a^2 S_s) - d \nabla^2 S_s &= 0 \end{aligned} \quad (3-20)$$

Using weighted residuals, the system of equations 3-20 becomes:

$$\begin{aligned} \int_{\Omega} w_1 \left(\frac{\partial S_a}{\partial t} - \gamma(a - S_a + S_a^2 S_s) - \nabla^2 S_a \right) d\Omega &= 0 \\ \int_{\Omega} w_2 \left(\frac{\partial S_s}{\partial t} - \gamma(b - S_a^2 S_s) - d \nabla^2 S_s \right) d\Omega &= 0 \end{aligned} \quad (3-21)$$

In Equation 3-21, Ω represents the problem domain that is limited by the border Γ and w_1 and w_2 are the weighting functions. Applying the Green's theorem and weakening the system of equations 3-21, the residue of the problem will be as follows:

$$\begin{aligned}
r_{S_a} = & \int_{\Omega} w_1 \frac{\partial S_a}{\partial t} d\Omega - \int_{\Omega} w_1 \gamma a d\Omega + \int_{\Omega} w_1 \gamma S_a d\Omega - \int_{\Omega} w_1 \gamma S_a^2 S_s d\Omega \\
& + \int_{\Omega} \nabla w_1 \nabla S_a d\Omega - \int_{\Gamma} w_1 (\nabla S_a \cdot \bar{n}) d\Gamma = 0 \\
r_{S_s} = & \int_{\Omega} w_2 \frac{\partial S_s}{\partial t} d\Omega - \int_{\Omega} w_2 \gamma b d\Omega + \int_{\Omega} w_2 \gamma S_a^2 S_s d\Omega + \int_{\Omega} d \nabla w_2 \nabla S_s d\Omega \\
& - \int_{\Gamma} d w_2 (\nabla S_s \cdot \bar{n}) d\Gamma = 0
\end{aligned} \tag{3-22}$$

The flow conditions of both variables were set to zero because it is considered that the two molecular factors are inside the suture and cannot penetrate the bone tissue. Thus, the residue is expressed as:

$$\begin{aligned}
r_{S_a} = & \int_{\Omega} w_1 \frac{\partial S_a}{\partial t} d\Omega - \int_{\Omega} w_1 \gamma a d\Omega + \int_{\Omega} w_1 \gamma S_a d\Omega - \int_{\Omega} w_1 \gamma S_a^2 S_s d\Omega \\
& + \int_{\Omega} \nabla w_1 \nabla S_a d\Omega = 0 \\
r_{S_s} = & \int_{\Omega} w_2 \frac{\partial S_s}{\partial t} d\Omega - \int_{\Omega} w_2 \gamma b d\Omega + \int_{\Omega} w_2 \gamma S_a^2 S_s d\Omega + \int_{\Omega} d \nabla w_2 \nabla S_s d\Omega = 0
\end{aligned} \tag{3-23}$$

Now, for the approximation of each variable, linear shape functions will be used:

$$\begin{aligned}
S_a^e &= N_a S_a \\
S_s^e &= N_s S_s
\end{aligned} \tag{3-24}$$

where N_a and N_s correspond to the shape functions that depend on the domain and S_a and S_s are the molecular factors concentrations on the nodal points. The superscript e indicates the finite element discretization. Also, a Bubnov–Galerkin formulation is used to define the weighting functions and, for this reason, the functions w take the same form of the shape functions N . Therefore, the discrete form of the residue vectors are established by:

$$\begin{aligned}
r_{S_a}^e = & \int_{\Omega} N^T \frac{\partial S_a}{\partial t} d\Omega - \int_{\Omega} N^T \gamma a d\Omega + \int_{\Omega} N^T \gamma S_a d\Omega - \int_{\Omega} N^T \gamma S_a^2 S_s d\Omega \\
& + \int_{\Omega} \nabla N^T \nabla S_a d\Omega \\
r_{S_s}^e = & \int_{\Omega} N^T \frac{\partial S_s}{\partial t} d\Omega - \int_{\Omega} N^T \gamma b d\Omega + \int_{\Omega} N^T \gamma S_a^2 S_s d\Omega + \int_{\Omega} d \nabla N^T \nabla S_s d\Omega
\end{aligned} \tag{3-25}$$

where ∇N is the gradient vector of the shape functions. Applying the Newton–Raphson linearization the system can be rewritten as:

$$\begin{bmatrix} \frac{\partial r_{S_a}^e}{\partial S_a} & \frac{\partial r_{S_a}^e}{\partial S_s} \\ \frac{\partial r_{S_s}^e}{\partial S_a} & \frac{\partial r_{S_s}^e}{\partial S_s} \end{bmatrix} \begin{bmatrix} \Delta S_a^e \\ \Delta S_s^e \end{bmatrix} = \begin{bmatrix} -r_{S_a}^e \\ -r_{S_s}^e \end{bmatrix} \quad (3-26)$$

where the symbol Δ denotes the difference of the nodal values between two consecutive iterations. The terms of the tangential stiffness matrix are calculated using Equation 3-25 and can be seen below:

$$\begin{aligned} \frac{\partial r_{S_w}^e}{\partial S_w} &= \frac{1}{\Delta t} \int_{\Omega} N^T N d\Omega + \int_{\Omega} \gamma N^T N d\Omega - 2 \int_{\Omega} \gamma N^T (N^T S_a) (N^T S_s) d\Omega + \int_{\Omega} \nabla N^T \nabla N d\Omega \\ \frac{\partial r_{S_w}^e}{\partial S_p} &= - \int_{\Omega} \gamma N^T (N^T S_a)^2 \Omega \\ \frac{\partial r_{S_p}^e}{\partial S_w} &= 2 \int_{\Omega} \gamma N^T (N^T S_a) (N^T S_s) d\Omega \\ \frac{\partial r_{S_p}^e}{\partial S_p} &= \frac{1}{\Delta t} \int_{\Omega} N^T N d\Omega + \int_{\Omega} \gamma N^T (N^T S_a)^2 \Omega + \int_{\Omega} d \nabla N^T \nabla N d\Omega \end{aligned} \quad (3-27)$$

3.2.3 Parameters selection

The reaction–diffusion equations can present three types of different behavior. The first one corresponds to a uniform distribution of the species concentration. In this case, it can be said that it is an equation where the diffusive term is dominant. The second possibility is a distribution of the species concentration stable over time but unstable in space, producing patterns known as *Turing patterns* or *Turing instabilities*; this occurs when the reactive term is dominant. Finally, the third possible behavior is a system unstable both in time and space generating patterns that evolve between two different time points [129]. Therefore, the linear stability theory allows to establish the conditions under which the Turing patterns are produced in a given system [22, 76, 129, 132].

Thus, the first step is to find the values for which the homogeneous solution of the reaction–diffusion system is obtained. For this, in the Schanakenberg model (Equation 3-10), the steady–state values of the species concentrations (u^*, v^*) are calculated as shown below:

$$\begin{aligned} f(u, v) &= \gamma (a - u + u^2 v) = 0 \\ g(u, v) &= \gamma (b - u^2 v) = 0 \end{aligned} \quad (3-28)$$

where $f(u, v)$ and $g(u, v)$ are the reactive functions of the equation. Solving for u^* and v^* in Equation 3-28:

$$\begin{aligned} u^* &= a + b \\ v^* &= \frac{b}{(a + b)^2} \end{aligned} \quad (3-29)$$

In previous works, with similar non-dimensional systems, it has been prove that setting $a = 0.1$ and $b = 0.9$ produces a good response of the reaction-diffusion equation [77, 127, 129, 132]. Hence, the initial conditions were defined as perturbed concentrations around the steady-state as follows:

$$\begin{aligned} u(t=0) &= u^* + p_u \\ v(t=0) &= v^* + p_v \end{aligned} \tag{3-30}$$

where p_u and p_v are the perturbations of u^* and v^* . In this way, it is possible to find the geometric area of the possible values that the d and γ parameters can take to satisfy the necessary conditions that generate the Turing instabilities [129, 132, 134, 142]:

$$\begin{aligned} f_u g_v - f_v g_u &> 0 \\ f_u + g_v &< 0 \\ d f_u + g_v &< 0 \\ (d f_u + g_v)^2 - 4d(f_u g_v - f_v g_u) &> 0 \end{aligned} \tag{3-31}$$

where the function subscript indicates the variable by which the respective function must be partially derived.

An important fact is that the d and γ parameters are related with the spacial and temporal scale of each particular reaction-diffusion system [22, 76, 127]. Knowing some real data, like the specific diffusion coefficients or the typical concentrations of the molecular factors, it is possible to move the parameters (a , b , d and γ) from the non-dimensional model to the real one. For this study, the Schnakenberg model was worked in the non-dimensional form because with the experimental results it is not possible to establish, with absolute certainty, which molecular factor fulfills one of the three functions established in the proposed model (Activator 1, Activator 2 and Inhibitor 1, Figure 3-2). Additionally, the information of these factors with respect to the midpalatal suture is very little or nonexistent. In relation to the Chemotaxis model, the Equation 3-8 corresponds to a case where the diffusive term is dominant and, for that reason, it is not necessary to perform the calculations related to the Turing instability.

Hence, the diffusion coefficients of the models, the threshold values and the parameters d and γ where calculated by numerical experimentation. In the d and γ cases, the values used for the tests of the parameters are shown in Table 3-1 and correspond to values reported in previous research of the vibration modes found for a square domain.

Mode (m,n)	d	γ
(1,0)	10	29
(1,1)	11.5776	70.6
(2,0)	10	114
(2,1)	9.1676	176.72
(2,2)	8.6676	230.82

Table 3-1: Modes of vibrations (m,n) for different values of d and γ . Taken from [129, 134].

3.2.4 Numerical implementation

The study developed in this chapter was carried out in two different domains. The first one corresponds to a simplified domain of the mice midpalatal suture and the other one represents a simplified domain of the human midpalatal suture. In both cases, the conception of the domain and the dimensions of the CAD model (Figure 3-3) were based on histomorphometric and microscopic analyzes reported in the literature [10, 105] and in the experimental data presented in Chapter 2.

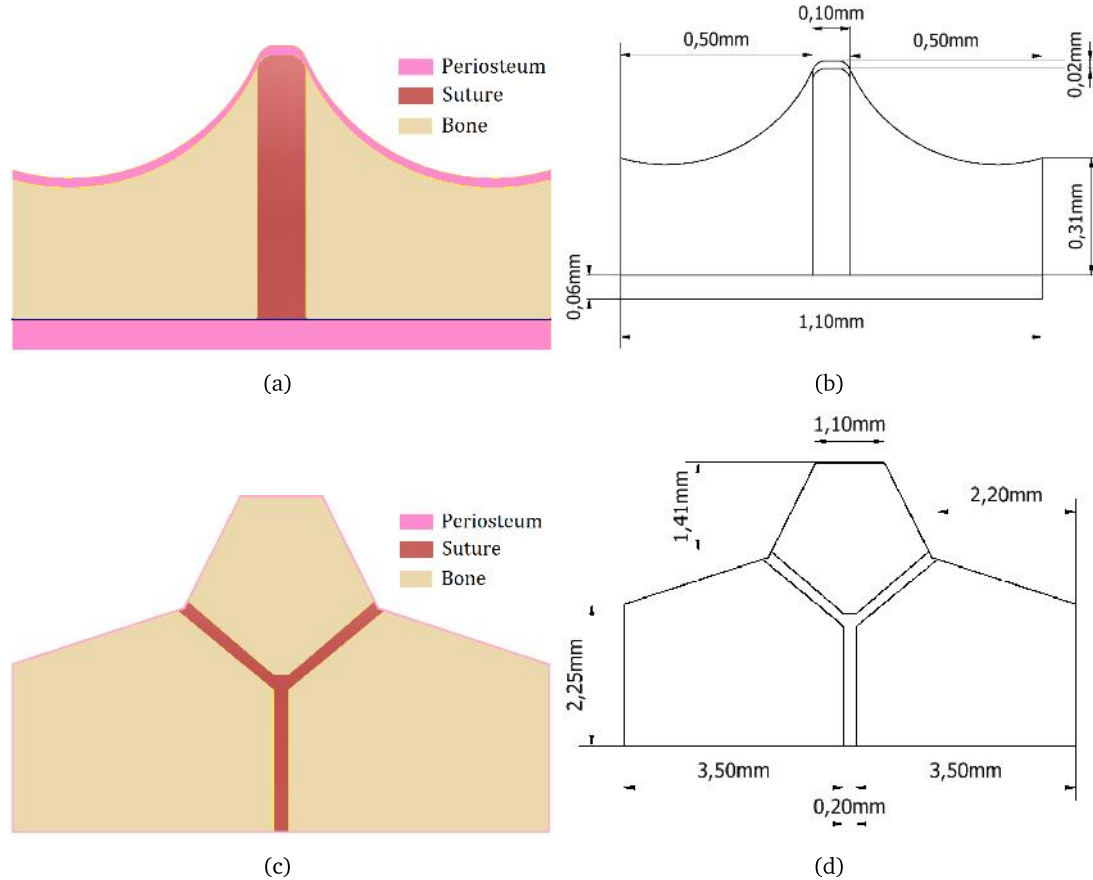


Figure 3-3: Domains developed for the mechanobiological model of the midpalatal suture: a) Simplified domain of the mice midpalatal suture. b) Dimensions of the simplified domain of the mice midpalatal suture. c) Simplified domain of the human midpalatal suture. d) Dimensions of the simplified domain of the human midpalatal suture.

The numerical solution was performed in commercial code ABAQUS software (Dassault Systèmes SE, Vélizy–Villacoublay, France) by means of a UEL FORTRAN subroutine with increments of 0.01 time units. The mesh size of the mice model had 9318 nodes and 9151 elements and the human model had 63847 nodes and 63709 elements. In both cases, the mentioned perturbations were established in a range of 0 to 10% around the steady–state values [77, 132]. For the analyzes with mechanical expansions the materials were assumed to be linear, homogeneous and isotropic and the properties were obtained from the literature. The elastic modulus for the bone and suture was 13700MPa and 1MPa , respectively. The Poisson ratio in both cases was 0.3 [82, 88, 89, 100]. A displacement was applied in the right side with a magnitude equivalent to a one activation of the maxillary expansion (0.25mm [88, 96]) and a total restriction of the left side was made. In order to guarantee a proportionality with the size of the mice MPS, the load value was reduced on a scale of 10 for these models.

3.3 Results

3.3.1 Simulation results of the mice MPS

Figure 3-4 presents the steady-state distributions, in time, for the concentrations of the Activator 1 and Inhibitor 1 in the mice midpalatal suture with different vibration modes. As it is possible to see, areas with higher concentration of the activating factor show low substrate concentration and vice versa. Comparing the different vibration modes, it is observed that the $(1, 0)$, $(2, 1)$ and $(2, 2)$ modes did not produce regular patterns while the $(1, 1)$ and $(2, 0)$ modes did. Those regular patterns had “spot” distribution and were selected to analyze the suture formation process with and without the presence of external loads.

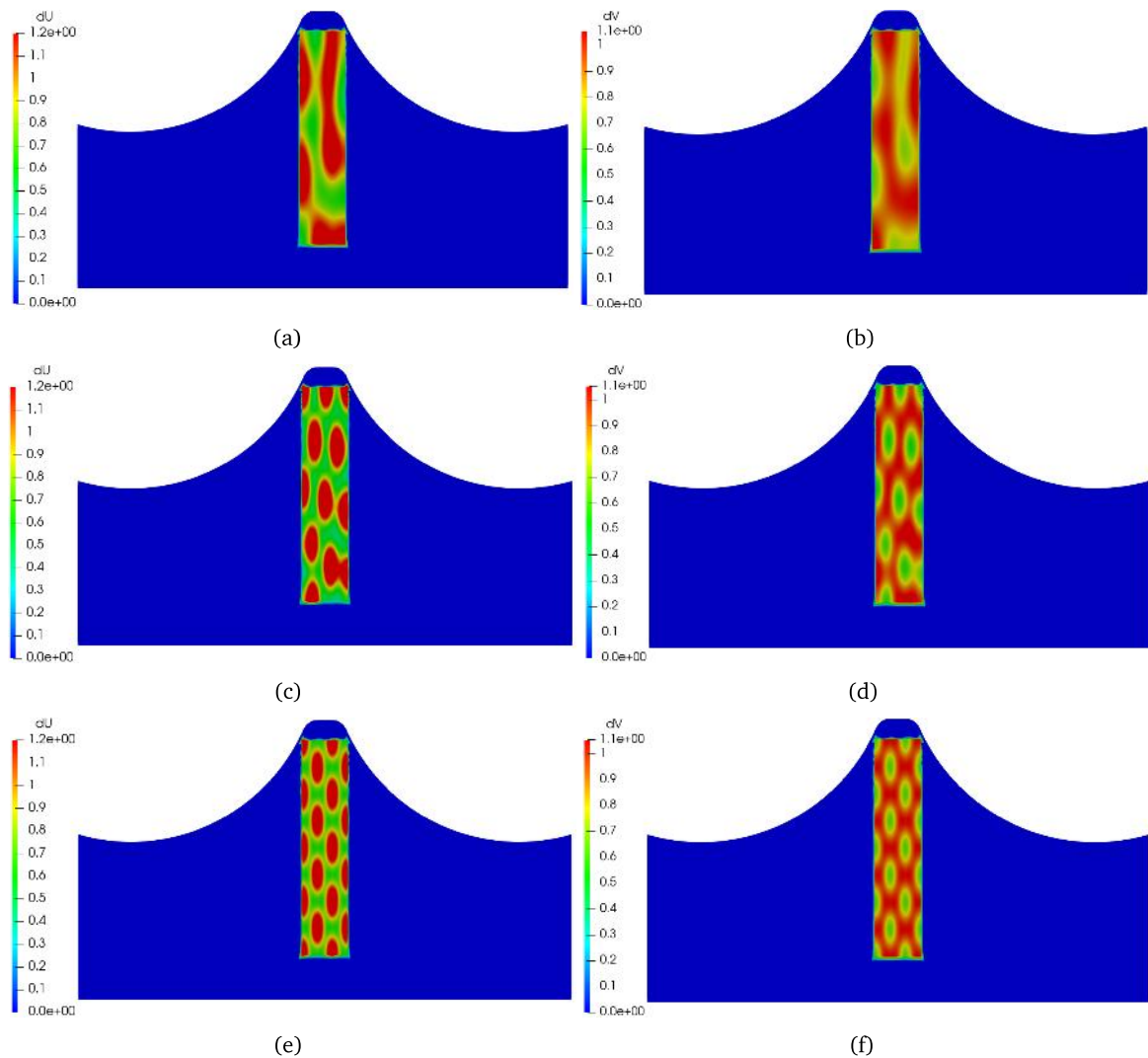


Figure 3-4: Molecular factors concentrations found in the mice MPS with different vibration modes. Concentration of a) Activator 1 and b) Inhibitor 1 with $(1, 0)$ mode. Concentration of c) Activator 1 and d) Inhibitor 1 with $(1, 1)$ mode. Concentration of e) Activator 1 and f) Inhibitor 1 with $(2, 0)$ mode.

The results of the mice MPS formation process, in absence of external mechanical stimuli, are showed in Figures 3-5 and 3-6. Figures 3.5(a) and 3.6(a) present the activating factor concentration in steady-

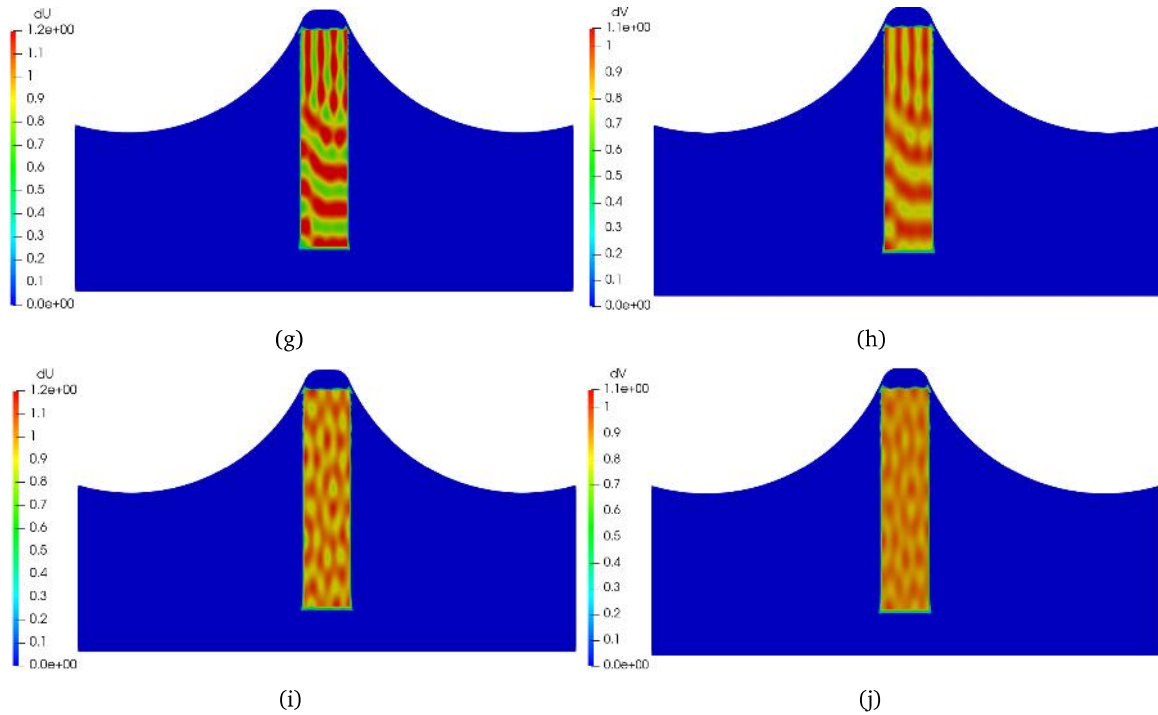


Figure 3-4 (Continued): Molecular factors concentrations found in the mice MPS with different vibration modes. Concentration of g) Activator 1 and h) Inhibitor 1 with (2, 1) mode. Concentration of i) Activator 1 and j) Inhibitor 1 with (2, 2) mode.

state after 500 time units. Figures 3.5(b) and 3.6(b) show the initial state of the MPS when the ossification algorithm begins to decide the places that must be ossified or reabsorbed, depending on the concentration values of the activating factor and the substrate. In this case, according to the numerical experimentation, the threshold values for both factors were $S_{a-thr} = S_{s-thr} = 1.3$. The other two images of each figure show the evolution of the remodeling process when t reaches 600 and 1000 units of time. After 1000 units of time the algorithm did not yield different results. Finally, in Figure 3-7 a comparison can be observed between the two final results obtained and the morphology of a mice and rabbit suture in the absence of external loads. As can be seen, the real suture does not present a regular pattern like the one that tends to give the result of the (2, 0) vibration mode. Nevertheless, it acquires an irregular shape with a prominence on the buccal side that it could resemble a little more to the result of the (1, 1) vibration mode. It is noteworthy that, unlike the human midpalatal suture, the mice suture does not have such a characteristic morphological change during growth, which can be corroborated in Figures 2.9(a) and 2.10(a).

For the models where the expansion load was taken into account, four periods of time were established: The initial state, when the cellular migration occurs due to the application of the expansion load, when the chemical factors interact in the expanded suture and the Turing instability emerges and, finally, when the ossification and reabsorption processes are carried out as a consequence of the molecular concentrations. Thus, Figures 3-8 and 3-9 present the results obtained for the models with the application of the expansion load. Figures 3.8(a) and 3.9(a) are the initial state of the suture. The next two images of each Figure show the ossification that was generated due to the cell migration process. As mentioned previously, the diffusion coefficients of the chemotaxis model were calculated by numerical experimentation and the results presented in Figures 3-8 and 3-9 were obtained with diffusion values

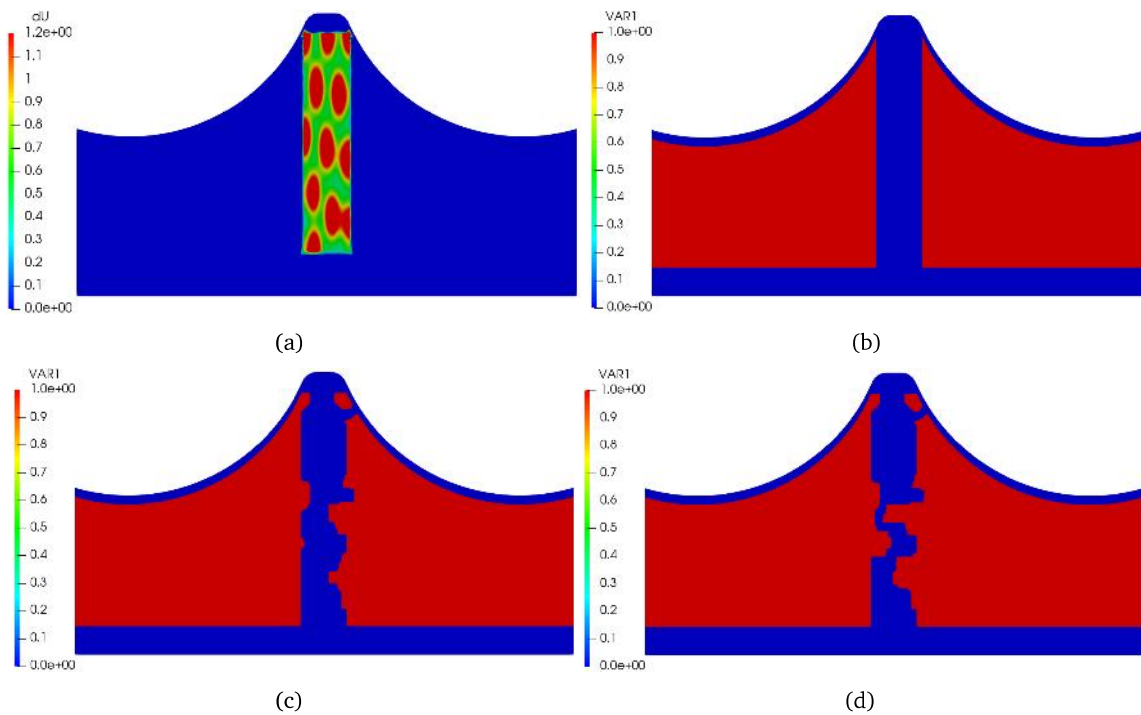


Figure 3-5: Mice MPS formation without external loads and with (1, 1) vibration mode. a) Molecular distribution of the activating factor concentration in steady-state b) $t = 500$. c) $t = 600$. d) $t = 1000$. t are in time units.

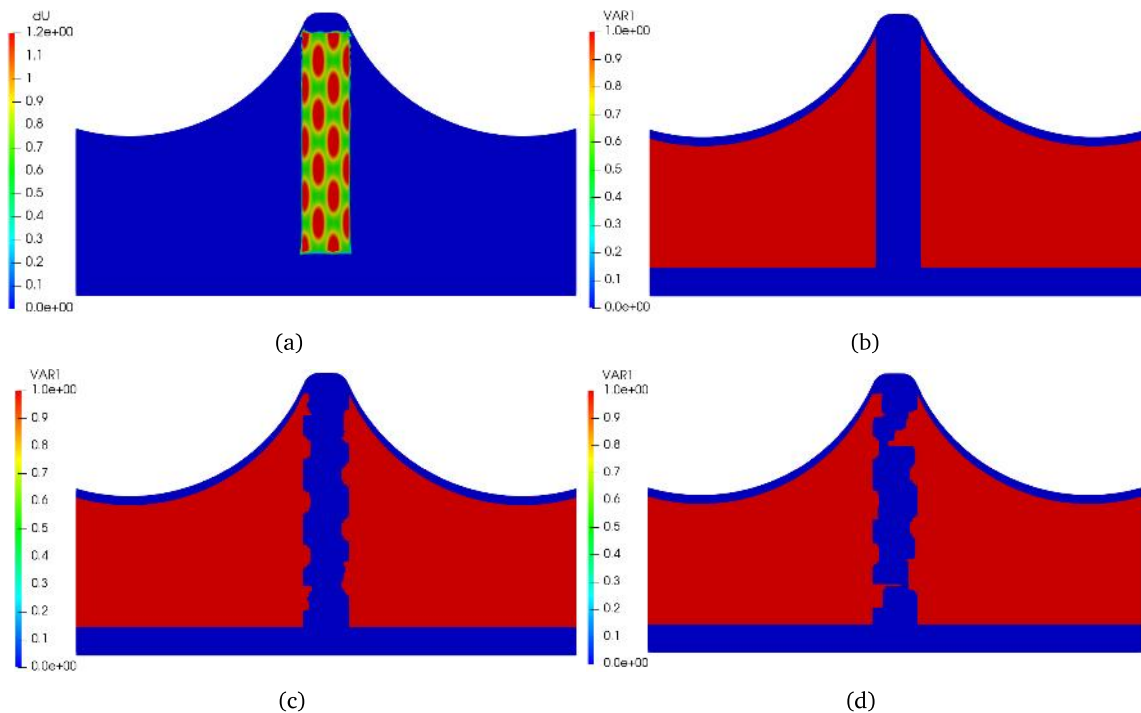


Figure 3-6: Mice MPS formation without external loads and with (2, 0) vibration mode. a) Molecular distribution of the activating factor concentration in steady-state b) $t = 500$. c) $t = 600$. d) $t = 1000$. t are in time units.

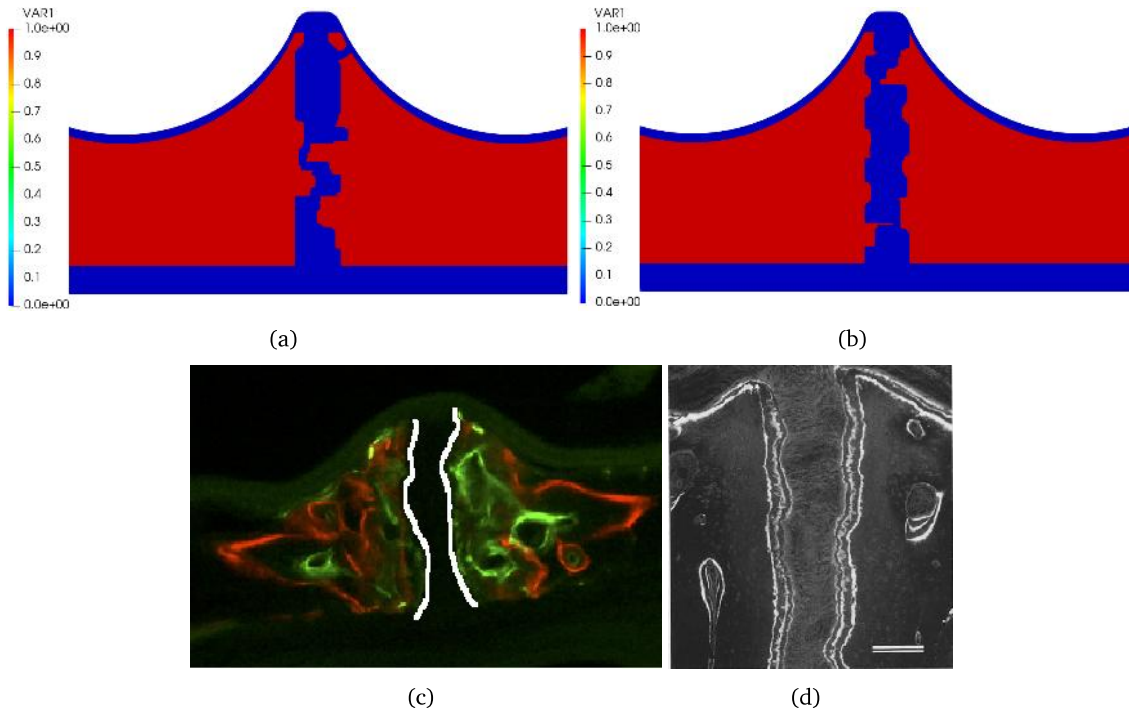


Figure 3-7: Results comparison of the mice MPS without external loads. a) Final result for the (1, 1) vibration mode. b) Final result for the (2, 0) vibration mode. c) Real mice MPS obtained from the literature. Adapted from [8]. d) Real rabbit MPS obtained from the literature. Adapted from [63].

of 0.4 and 10 for the chemoattractant and cell migration, respectively. These were the values that best represented the real phenomenon; in Appendix B is possible to find the results of the different tests performed to calculate them. Figures 3.8(d) and 3.9(d) are the Turing patterns generated of the activating factor distribution, within the expanded suture, with the vibration modes (1, 1) and (2, 0), respectively. Finally, the last two images are the results due to the deposition and reabsorption processes as a consequence of the molecular factors concentrations. The presented results show until $t = 620$ time units, after this value the software could not make the system converge, possibly because the continuity in the domain of the suture was lost.

Finally, Figure 3-10 is a comparison between the obtained results by the chemotaxis model (Figures 3.10(a) and 3.10(b)), a histological result showed in Chapter 2 (Figure 3.10(c)) and experimental results obtained by Hou *et al.* [8] (Figure 3.10(d)) and Cheng *et al.* [116] (Figure 3.10(d)). As it can be seen in the experimental data, the cellular migration produces a more accelerated ossification process at the upper (nasal side) and lower (buccal side) ends of the suture; behavior that can be reproduced by the proposed model. With respect to the process of bone remodeling that occurs after the molecular factors reach the stable state, there is no experimental or supported information in the literature to verify the reliability of the model at this stage.

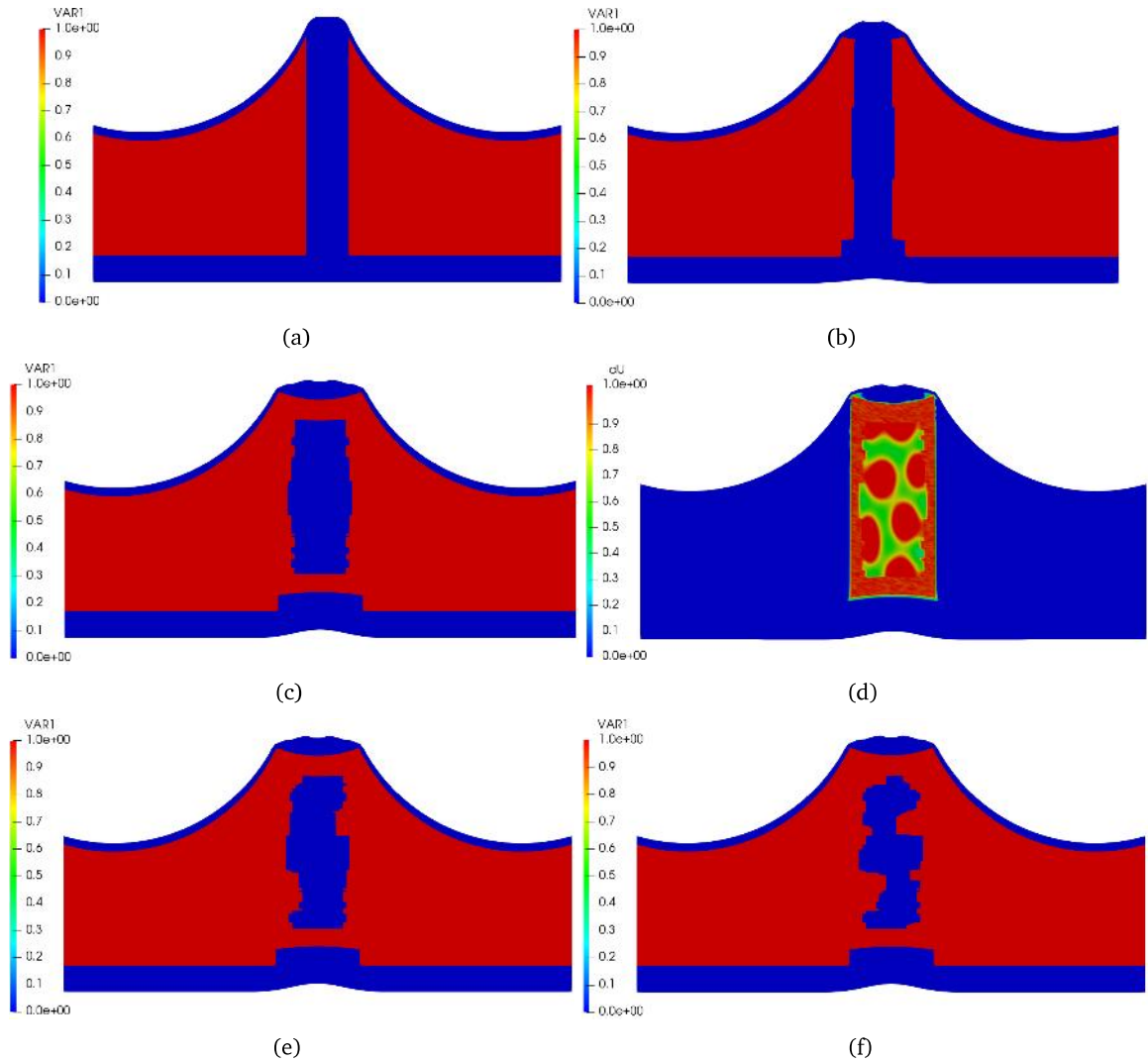


Figure 3-8: Mice MPS formation with expansion load and (1, 1) vibration mode. a) Initial state of the suture. b) Ossification due to the cellular migration process at 20 time units. c) Ossification due to the cellular migration process at 40 time units. d) Distribution of the activating factor concentration in steady-state in the expanded suture ($t = 540$ time units). e) Bone remodeling processes in the expanded suture at 580 unit times. f) Bone remodeling processes in the expanded suture at 620 time units.

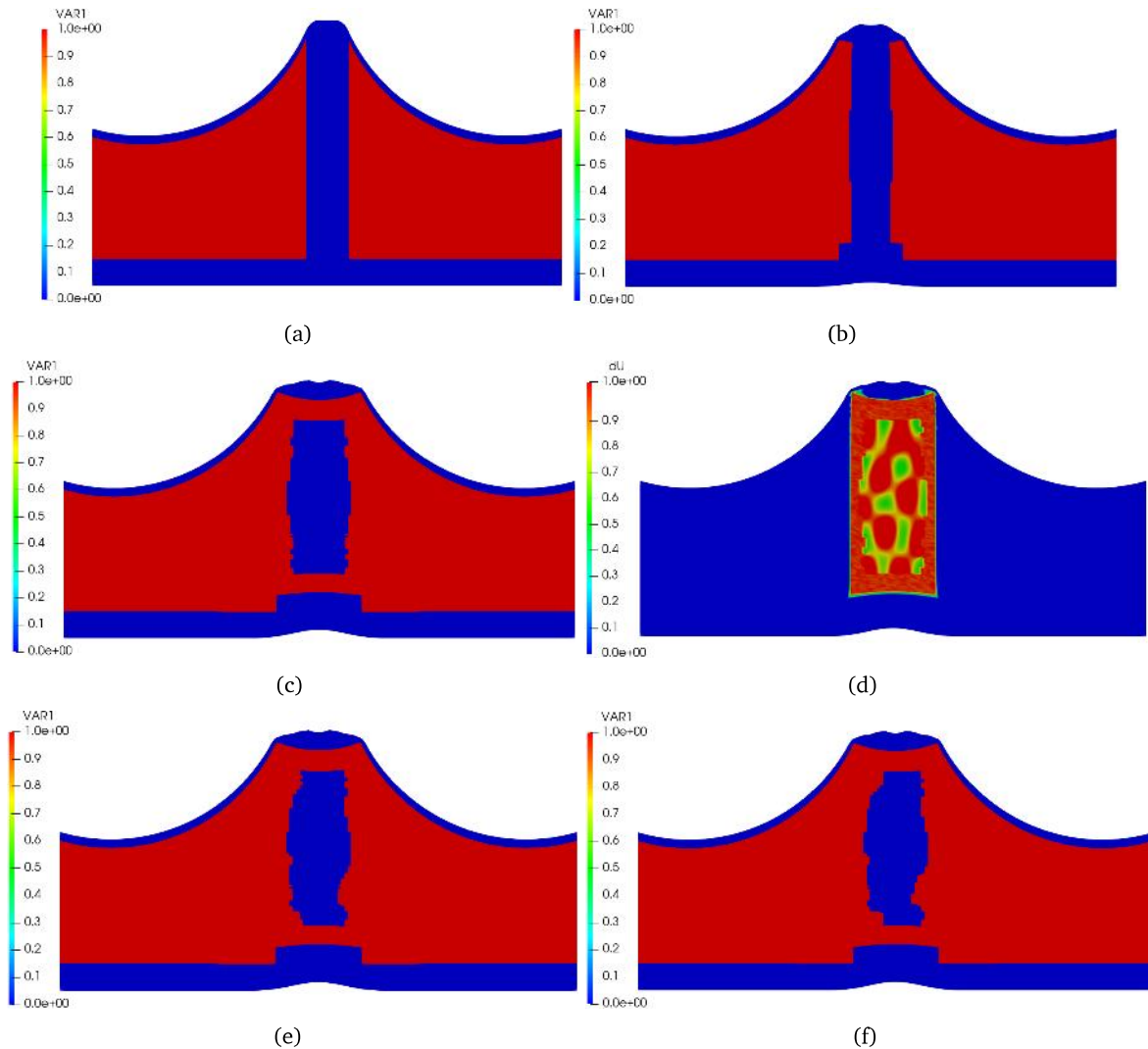


Figure 3-9: Mice MPS formation with expansion load and $(2, 0)$ vibration mode. a) Initial state of the suture. b) Ossification due to the cellular migration process at 20 time units. c) Ossification due to the cellular migration process at 40 time units. d) Distribution of the activating factor concentration in steady-state in the expanded suture ($t = 540$ time units). e) Bone remodeling processes in the expanded suture at 580 unit times. f) Bone remodeling processes in the expanded suture at 620 time units.

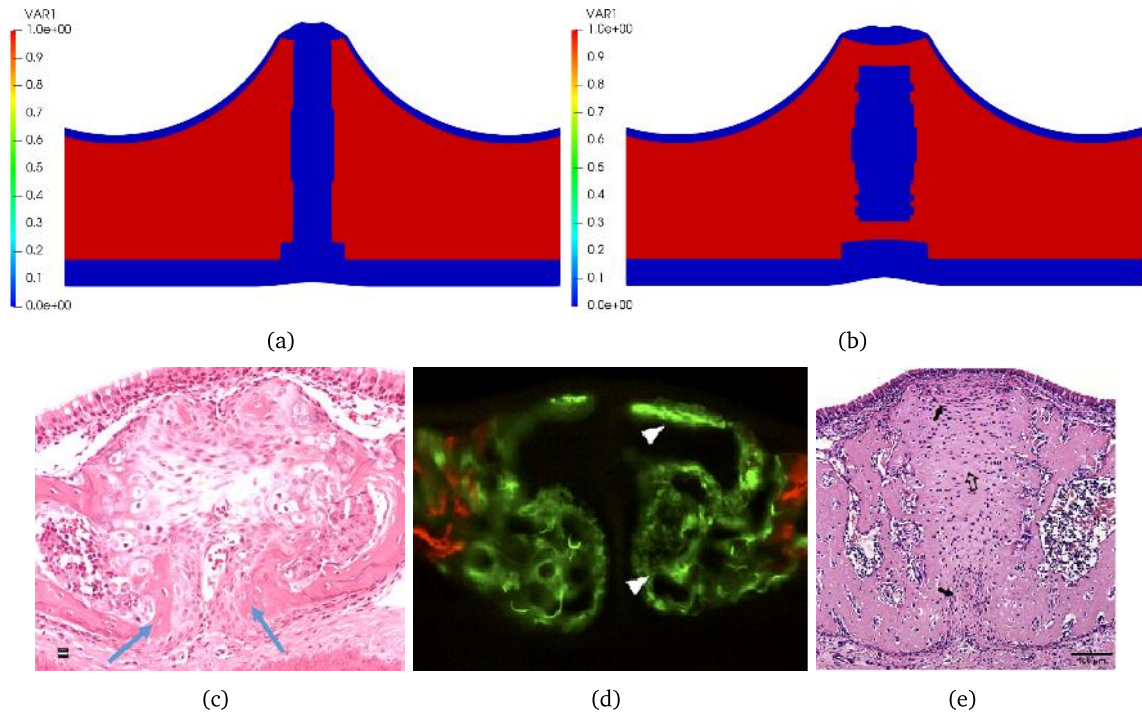


Figure 3-10: Results comparison of the mice MPS with expansion load. a) Ossification results after the cellular migration occurs at 20 time units. b) Ossification results after the cellular migration occurs at 40 time units. c) Histological image of an expanded suture obtained from the experimental results (Chapter 2) d) Real expanded MPS of mice obtained from the literature. Taken from [8]. e) Real expanded MPS of rats obtained from the literature. Taken from [116].

3.3.2 Simulation results of the human MPS

Figure 3-11 showed the steady-state concentration distributions, in time, of the Activator 1 and Inhibitor 1 in the human midpalatal suture with the vibration modes established in Table 3-1. In a similar way with the mice results, areas with higher concentration of the activating factor show low substrate concentration and vice versa. Comparing the different vibration modes, it is observed that the first four modes produce regular patterns. However, the generated patterns by the (1, 0), (2, 1) modes developed a “striped” type distribution while the (1, 1) and (2, 0) modes a “spot” distribution. The (2, 2) mode did not produce a regular pattern. Therefore, the “spot” patterns were selected to analyze the suture formation process with and without the presence of external loads because the “striped” patterns could not generate an ossification process that fit the reality.

The results of the human MPS formation process, in absence of external mechanical stimuli, are shown in Figures 3-12 and 3-13 for the (1, 1) and (2, 0) modes, respectively. Figures 3.12(a) and 3.13(a) present the activating factor concentration in steady-state after 500 time units. Figures 3.12(b) and 3.13(b) show the initial state of the MPS when the ossification algorithm begins to decide the places that must be ossified or reabsorbed, depending on the concentration values of the activating and the substrate factors. In this case, according to the numerical experimentation, the threshold values for activating factor was $S_{a-thr} = 1.35$ and for the substrate factor was $S_{s-thr} = 1.11$. The other images of each figure show the evolution of the remodeling process when t reaches 525, 550, 575 and 600 time units. After 600 time units, the algorithm was not able to converge or showed results that were far from a real suture. This is probably due to the fact that, with the ossification generated within the suture, the domain on which the chemical factors were interacting lost continuity. In Figure 3-14 is possible to observe the final results obtained in the computational simulations and compare them with a simplified outline of the morphology evolution of the MPS reported by Kumar *et al.* [6] and with histological images reported in the literature [105, 107]. As it can be seen, the two vibration modes can reproduce possible scenarios of the suture morphology evolution. Nevertheless, the vibration mode (1, 1) presents a behavior that is more in line with that described by Kumar *et al.* [6] and with the real suture images, generating an interdigitation pattern that could be considered scalloped. This vibration mode will be considered to the model with expansion loads.

In the same way as it was done with mice, for the models where the expansion load was taking into account, four periods of time were established: the initial state, when the cellular migration occurs due to the application of the expansion load, when the chemical factors interact in the expanded suture and the Turing instability emerges and, finally, when the ossification and reabsorption processes are carried out as a consequence of the molecular concentrations. In agreement with this, Figure 3-15 presents the results obtained for the models with the application of the expansion load. The first image (Figure 3.15(a)) shows the initial state of the suture. Figure 3.15(b) and Figure 3.15(c) correspond to the suture when the cellular migration processes occurs and the steady-state of the molecular factors was reached, respectively. In the lower part of the Figure 3.15(b), two blue marks can be seen that highlight the advance of the bone margins as a consequence of the chemotaxis model. In the last four images (Figures 3.15(d) to 3.15(g)) the suture morphology evolution can be observed. The changes in the morphology at the bone margins is due to the bone deposition and reabsorption processes as a result of the Schankenberg model. The presented results show until $t = 900$ time units, after this value the software could not make the system converge; as explained in the models without expansion loads, this is possibly due to the loss of continuity in the suture domain.

Figure 3.16(a) shows the final state of the model in presence of expansion loads but highlighting the sutural tissue. The purpose of this image is to allow the comparison with histological images obtained

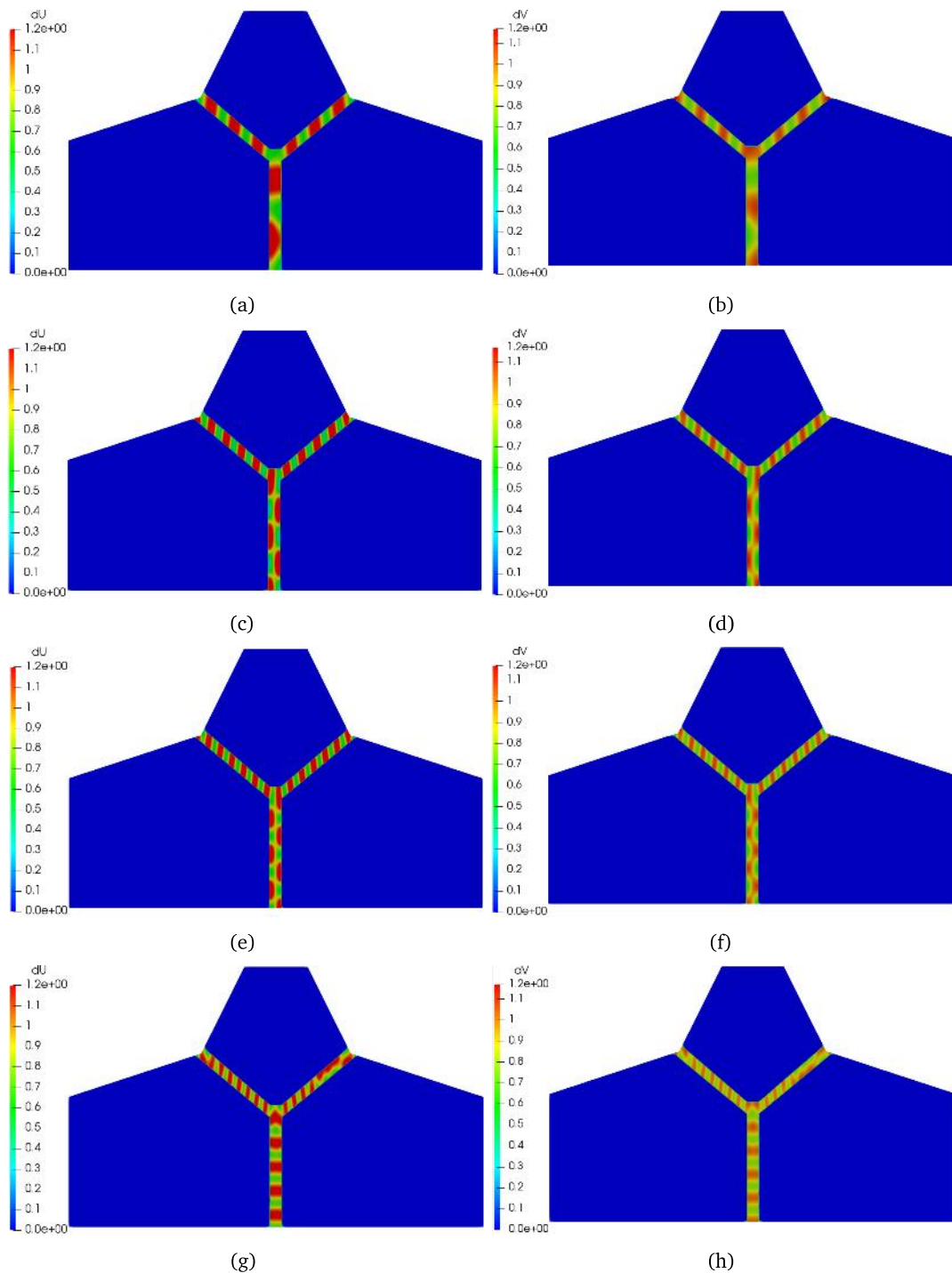


Figure 3-11: Molecular factors concentrations found in the human MPS with different vibration modes. Concentration of a) Activator 1 and b) Inhibitor 1 with $(1, 0)$ mode. Concentration of c) Activator 1 and d) Inhibitor 1 with $(1, 1)$ mode. Concentration of e) Activator 1 and f) Inhibitor 1 with $(2, 0)$ mode. Concentration of g) Activator 1 and h) Inhibitor 1 with $(2, 1)$ mode.

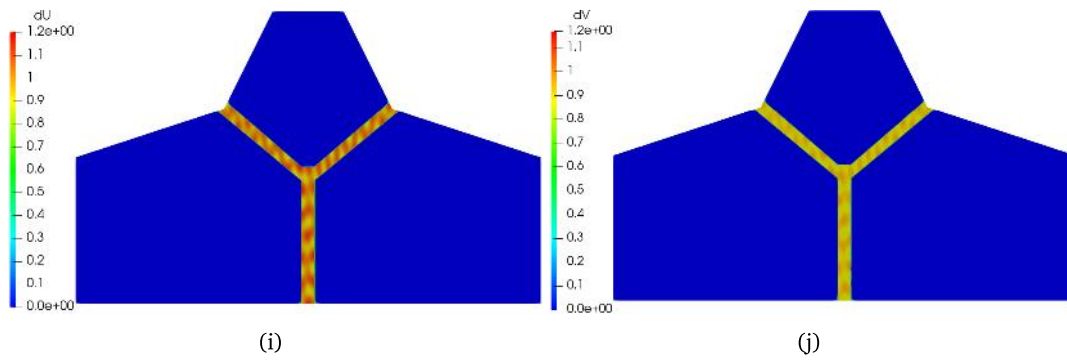


Figure 3-11 (Continued): Molecular factors concentrations found in the human MPS with different vibration modes. Concentration of i) Activator 1 and j) Inhibitor 1 with (2, 2) mode.

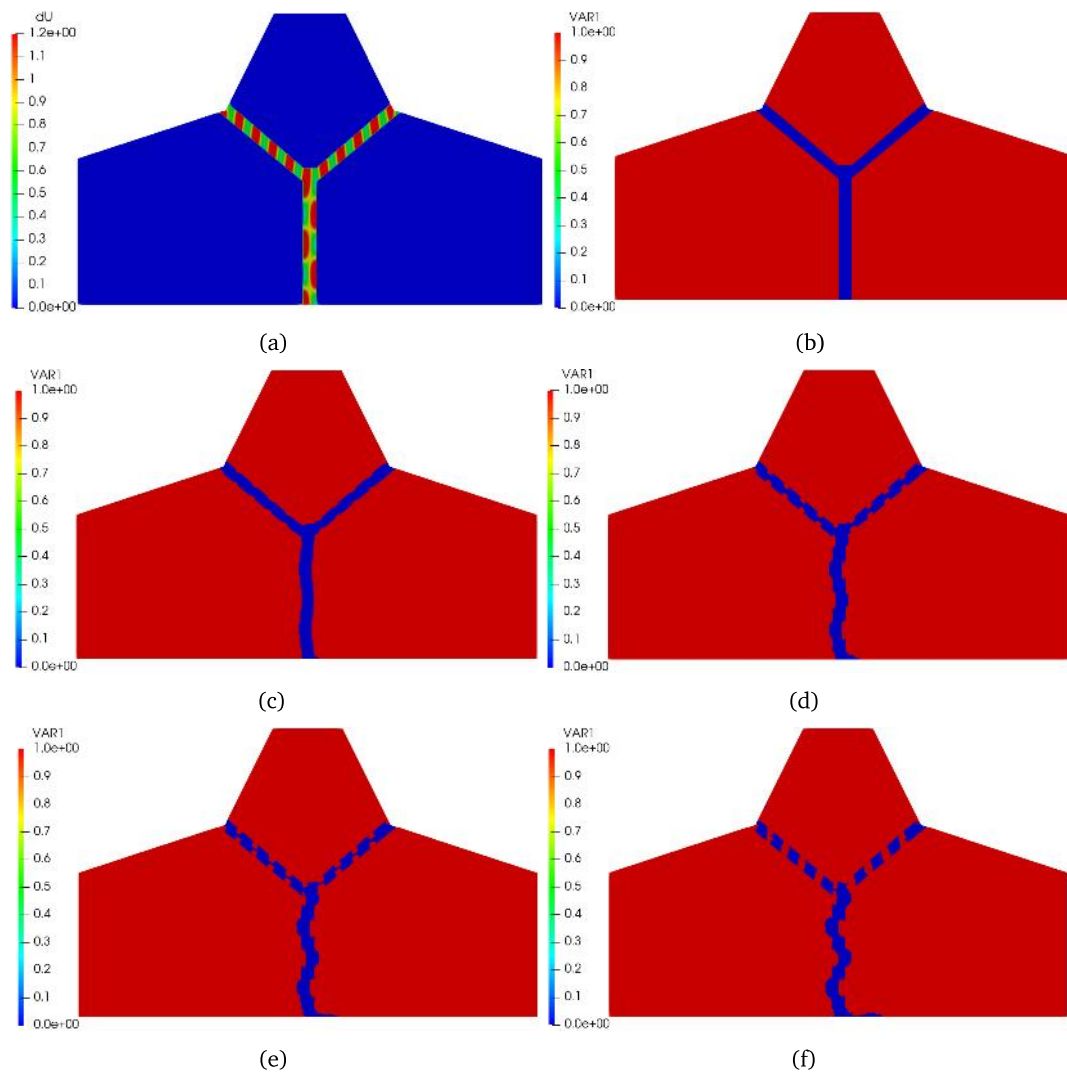


Figure 3-12: Human MPS formation without external loads and with (1, 1) vibration mode. a) Molecular distribution of the activating factor concentration in steady-state b) $t = 500$. c) $t = 525$. d) $t = 550$. e) $t = 575$. f) $t = 600$. t are in time units.

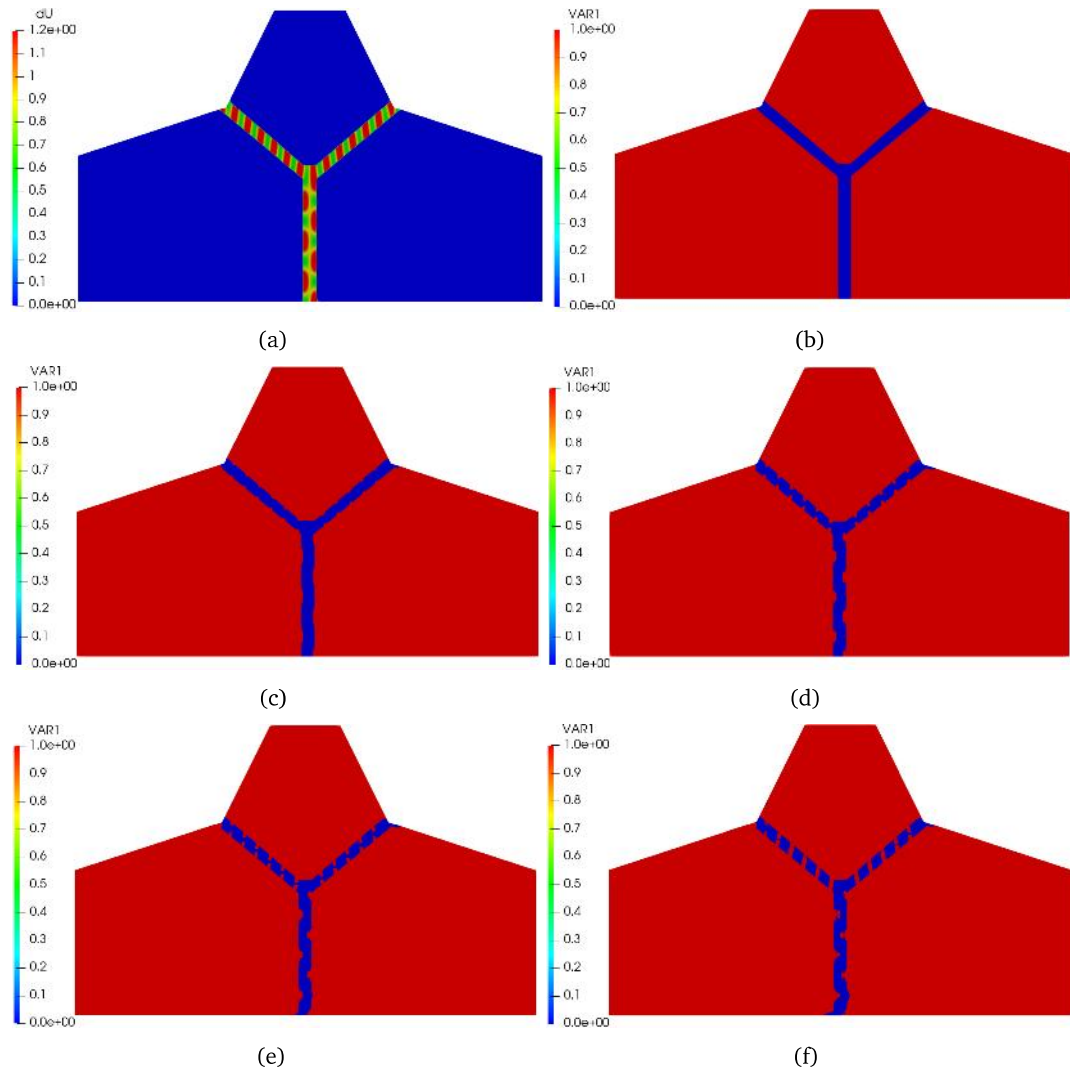


Figure 3-13: Human MPS formation without external loads and with $(2,0)$ vibration mode. a) Molecular distribution of the activating factor concentration in steady-state b) $t = 500$. c) $t = 525$. d) $t = 550$. e) $t = 575$. f) $t = 600$. t are in time units.

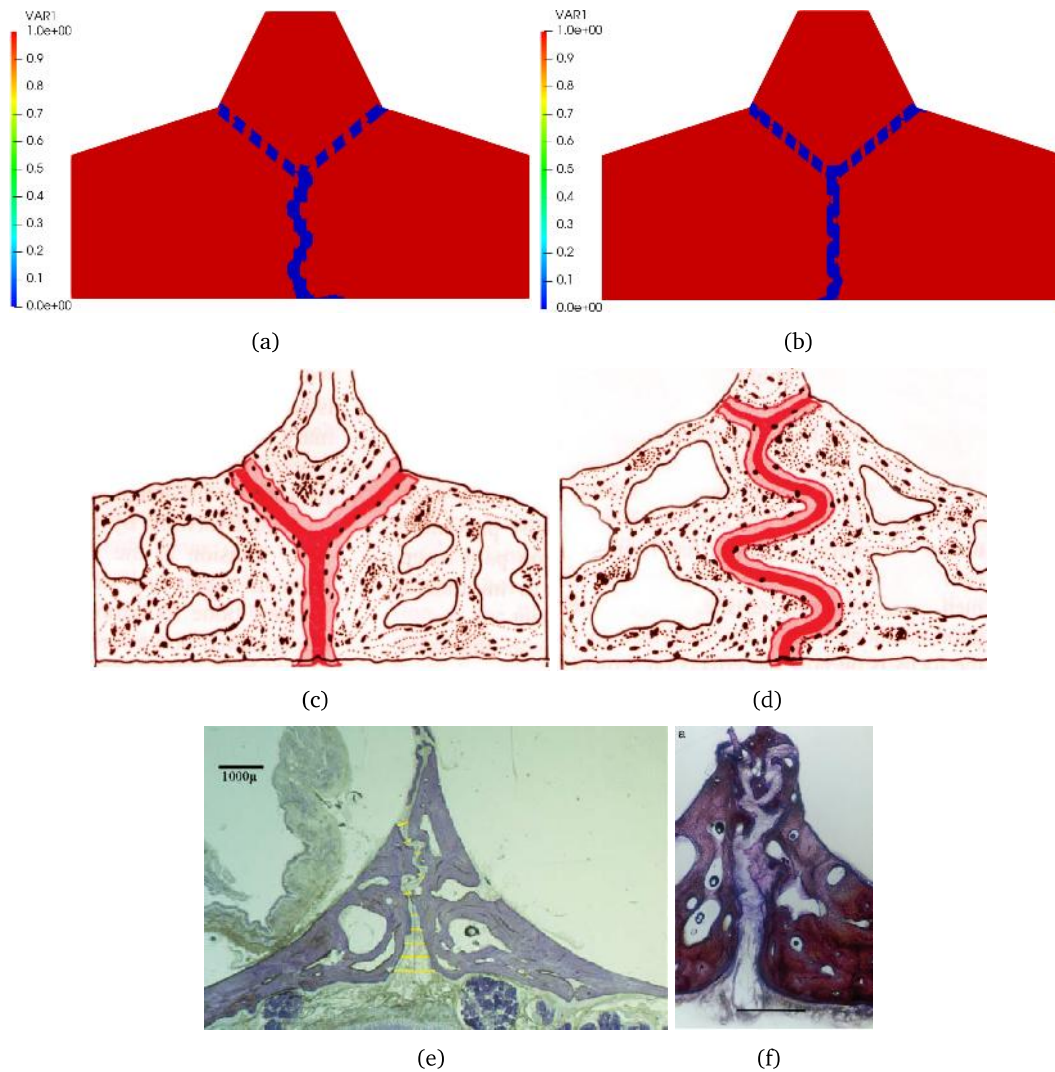


Figure 3-14: Results comparison of the human MPS without external loads. a) Result obtained with the (1, 1) vibration mode. b) Result obtained with the (2, 0) vibration mode. c) Outline of the initial state of the suture reported by Kumar *et al.*. Taken from [6]. d) Outline of the the suture in early adolescence reported by Kumar *et al.*. Taken from [6]. e) Real human MPS obtained from the literature. Taken from [105]. f) Real human MPS obtained from the literature. Taken from [107].

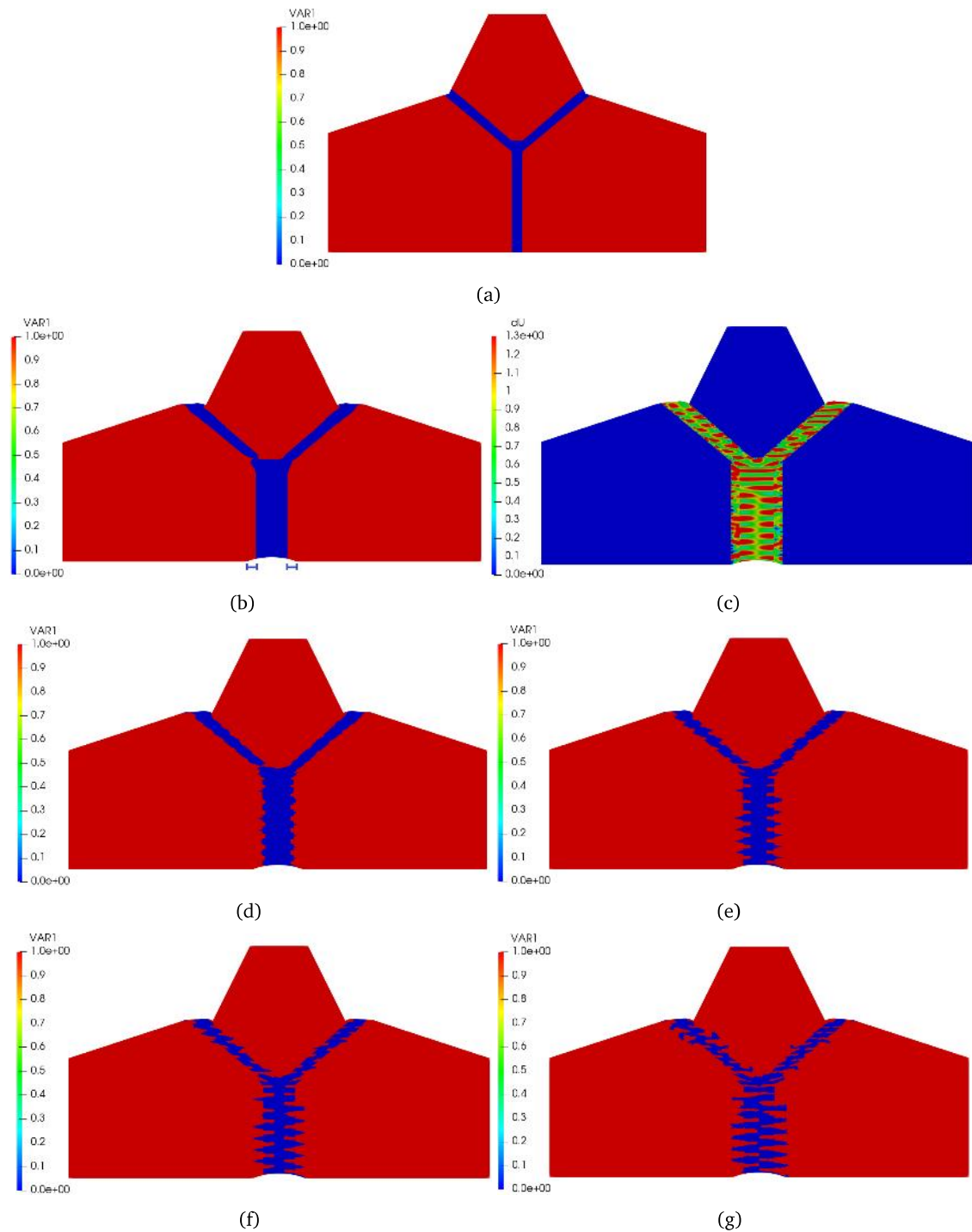


Figure 3-15: Human MPS formation with expansion load and (1, 1) vibration mode. a) Initial state of the suture. b) Expanded suture with advancement of the bone margin due to cell migration at 800 time units (the blue markers highlight the advance of the bone margins). c) Distribution of the activating factor concentration in steady-state in the expanded suture ($t = 800$ time units). Bone remodeling processes in the expanded suture at d) 825, e) 850, f) 875 and g) 900 time units.

in the literature (Figures 3.16(b) and 3.16(c)). In the case of the mice MPS, the experimental images available in the literature correspond to expanded sutures and MPS morphology images without loads are very few. In contrast, in the human case, the images reported in the literature are related with sutures in the absence of expansion loads and it was not possible to find images that show a real human MPS, or a real MPS of similar species, after a expansion procedure. Therefore, the comparison was made with images where possible interdigitation patterns are observed. These images were taken from swine (Figure 3.16(b)) and apes (Figure 3.16(c)), animals that have a certain degree of similarity with humans [102].

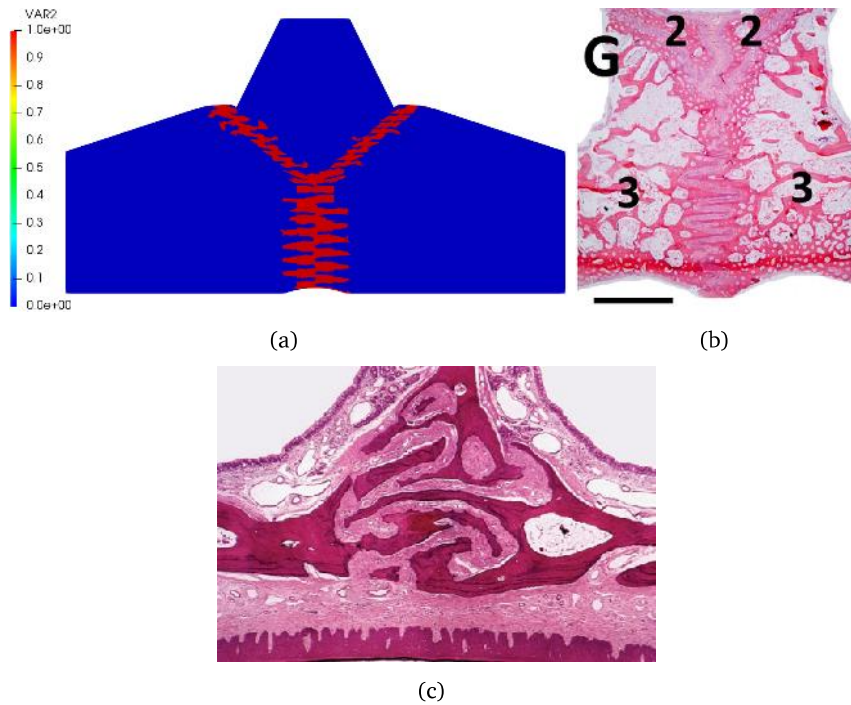


Figure 3-16: Results comparison of the human MPS morphology. a) Suture morphology after the expansion and the bone remodeling process obtained by the computational simulation. b) Real swine MPS of obtained from the literature. Taken from [101]. c) Real ape MPS of obtained from the literature. Taken from [102].

3.4 Discussion

This chapter presents a mechanobiological model of the midpalatal suture formation process in two different scenarios; with and without external expansion loads. The difference between these scenarios is that in presence of tensile forces, the biological system generates a cellular migration from the periosteum into the suture to produce bone layers adjacent to the bone margins and, in this way, compensate the separation generated due to the expansion [20, 63]. Thus, a mathematical model, based on Chemotaxis and Schnakenberg biological models, was proposed to describe the cellular and molecular behaviors inside the suture tissue and their influence in the bone–suture–bone interface. The Chemotaxis part of the model sought to reproduce the aforementioned cellular migration phenomenon while the Schnakenberg part tried to simulate the characteristic morphological changes that the suture could have during the growth [4]. Both parts of the mathematical model were proven in mice and human MPS domains.

The results obtained show that the proposed model is a good approximation of the advancement and remodeling processes of the bone margins in the midpalatal suture. As shown in Figure 3-10, the model achieves to reproduce the cells concentration, which come from the periosteum, at the ends of the mice suture, both on the buccal and nasal sides. In humans, the advance of the bone margin is given in a more uniform way (Figure 3.15(b)); in spite of not finding experimental evidence of this, it can be seen that it coincides with the theoretical approach postulated by different authors such as Consolaro [20] or Sawada [63]. Additionally, it can be observed that the interaction between the molecular factors defined by the model results in Turing instabilities, both in the mice domain (Figure 3-4) and in humans domain (Figure 3-11). Several authors have related the formation of this type of patterns with processes of morphogenesis [54, 73, 75, 123]; which allowed that, based on the factors concentration, the suture ossification and bone reabsorption criteria were established. The results in mice do not allow to conclude anything in particular about the performance of this part of the model. However, when carrying out the analysis in humans it is observed that the model is able to reproduce the suture morphological changes. In the absence of external loads, the initial formation of the suture interdigitation was obtained while, in the expanded suture, morphologies with more complex interdigitations were achieved. This can be attributed to the fact that the unexpanded suture causes that ossification bridges to be generated more quickly, preventing the domain continuity in which the molecular factors interact. In consequence, the model does not allow more iterations over time due to a lack of convergence or produces results that are far from the morphology of a real suture. It should be noted that even when the histological image of Figure 3.16(b) corresponds to a swine tissue without expansion loads, a high similarity can be observed between the pattern generated by the simulation and the real biological tissue.

Previous investigations of mechanobiological models developed in cranial sutures have been reported [25, 72–75]. However, according to the literature review performed for the elaboration of this work, no evidence has been found of models that describe the cellular and molecular processes in facial sutures such as the midpalatal suture. This aspect is of great importance since there are certain anatomical, morphological and biological variables that are fundamental to be able to reproduce the formation processes of the MPS as such. For example, the presence of the Dura mater in the skull, the Y form that the MPS has, the low ossification percentage of this suture during the growth (on average 3.11% [105]), among others. Therefore, according to the above, this would be the first mechanobiological model developed to represent the biological processes present specifically in the midpalatal suture. However, as explained previously, a strong limitation of this study has been the scarce information that is found regarding the midpalatal suture; both to feed and to validate the model. Evidence of this is that it was not possible to define exactly the molecular factors that fulfill the signaling functions (Figure 3-1) or the roles of Activator 1, Inhibitor 1 and Activator 2 (Figure 3-2). Nevertheless, due to the experimental results it was possible to propose some candidates that could carry out these tasks. This would open a research door focused on establishing exactly those factors and determining particular properties of them, within the MPS, that would allow to take the proposed model of its non-dimensional form to a model fed by real parameters.

3.5 Conclusions

- The results show that the proposed mathematical model successfully reproduces the phenomenon of cellular migration that occurs as a consequence of the expansion loads application. Therefore, the choice of an approach based on the chemotaxis biological model can be considered appropriate.
- The mathematical model developed in this chapter allows to generate distributions of the mo-

lecular factors concentrations characterized by spatial instabilities known as Turing instabilities. These distributions, as in other investigations reported in the literature, were used to simulate remodeling processes at bone margins. In agreement with the results evidenced in the human midpalatal suture, it seems that this approach properly simulates the initial states of the morphological changes suffered by the suture during the growth and allows to reproduce interdigitation patterns of greater complexity in expanded sutures.

- According to the literature review, it seems that the mathematical model proposed in this chapter is the first mechanobiological model developed specifically in the midpalatal suture. Despite the limitations, the model achieves to simulate the formation processes of this suture as a result of the migration and cellular activity at the bone margins.

Chapter 4

Biomechanical 2D model

From an anatomical point of view, particularly when studying sutures, interdigitation is a term used to describe the interlocking that exists between the bone margins [24]. This morphological characteristic can be measured by the interdigitation index (I.I.), which is the ratio between the length of the line that describes the bone margin and the distance calculated from end to end of the suture [92]. In previous studies the influence of the interdigitation in the mechanical response of the sutures has been analyzed [24, 90–92]; however those analysis are made with the assumption that the suture corresponds to a cranial one and do not take into account the particularities of the midpalatal suture. The objective of this chapter is to evaluate the influence of the interdigitation degree and the presence of the collagen fibers in the suture biomechanical response to tension and compression loads. Therefore, throughout this chapter, the methodology used to reach the proposed objective will be explained and the results obtained will be shown and discussed.

4.1 Materials and Methods

For this analysis four geometrical domains, of a simplified bone–suture–bone interface, were elaborated with different interdigitation levels; the dimensions are shown in Figure 4.1(a). The degrees of interdigitation considered were null, moderate, complex and fractal (Figures 4.1(b) to 4.1(e)) with an interdigitation index of 1, 1.23, 2.79 and 4.92, respectively. The moderate, complex and fractal interdigitations were calculated as sinusoidal functions (Equations 4-1 to 4-3). The fractal interdigitation was estimated using the Weierstrass cosine function [143].

$$f(x) = \sin(x) \quad \text{Moderate Interdigitation} \quad (4-1)$$

$$f(x) = \sin(4x) \quad \text{Complex Interdigitation} \quad (4-2)$$

$$f(x) = \sum_{n=0}^M \gamma^{-n\alpha} \cos(2\pi\gamma^n t) \quad \text{Fractal Interdigitation} \quad (4-3)$$

The finite element analysis was carried out in ANSYS Mechanical APDL 17.0 (Bela Engineering Group, Downers Grove, IL, USA) by a macro in APDL language. The analysis was performed in a plane stress state with 3mm of thickness [10]. The element type used for the bone and suture was *PLANE182* that corresponds to a quadrilateral defined by four nodes. The macro was made to work in two scenarios: with and without the presence of the collagen fibers. To insert the fibers, *LINK180* type elements attached to the nodes of the bone margins (Figure 4.2(a)) were implemented, taking into account the constant diameter of the collagen fibers reported by Lodish *et al.* (200 μ m) [144]. The material properties were defined as linear, homogeneous and isotropic. A typical elastic modulus and Poisson's ratio

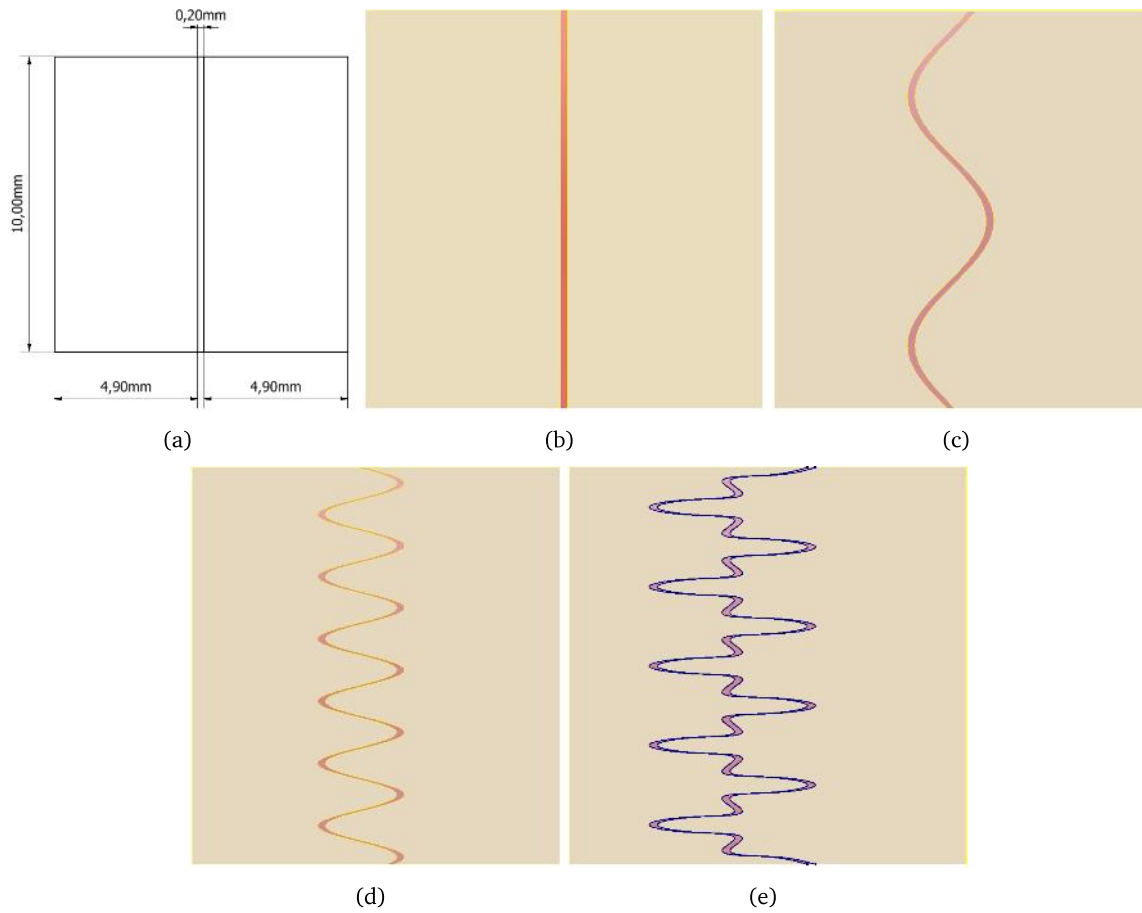


Figure 4-1: Idealized models of the bone-suture-bone interface: a) Dimensions of the idealized models. b) Model with null interdigitation. c) Model with moderate interdigitation. d) Model with complex interdigitation. e) Model with fractal interdigitation.

reported by the literature were used. For the bone, E and ν were 6000MPa and 0.27 [90] and, for the suture, 1MPa and 0.3 [82].

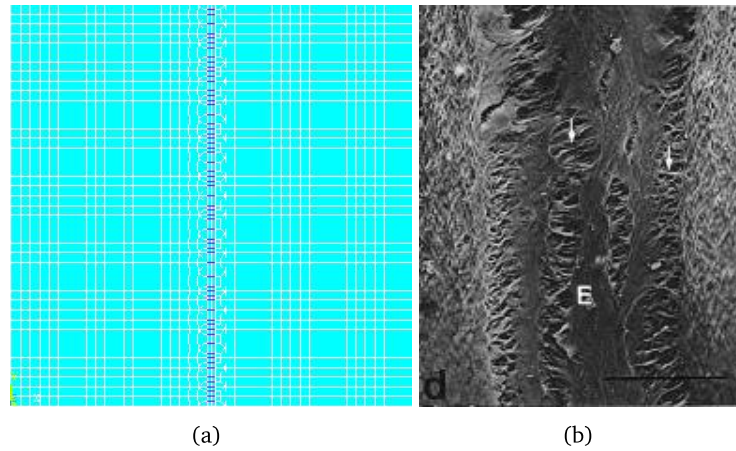


Figure 4-2: a) Configuration of the collagen fibers in the finite element model b) Scanning Electron Microscopy of the MPS (image scale: $200\mu\text{m}$). Taken from [104]

To obtain the material constants of the collagen fibers it was necessary to establish a relation with the number of fibers that could have each model, in order to calculate an equivalence between the quantity of the fibers of a real MPS and those that have each modeled suture. Thus, an image of Scanning Electron Microscopy of the MPS (Figure 4.2(b)) was used to quantify the number of fibers present in a real suture of 10mm long, the result was approximately 620 fibers. Therefore, knowing that the Young's modulus of a collagen fiber is 50MPa [90], the approximate stiffness value of the fibers set is 31000MPa. Then, to define an equivalent stiffness value for the fibers present in the different models, the calculated stiffness value was divided by the number of fibers that each model has; the results are shown in Table 4-1. Poisson's ratio employed for the fibers was 0.3 [90].

Interdigitation type	Number of links in the model	Elastic Modulus of each fiber in MPa
Null	85	364.7
Moderate	109	284.4
Complex	712	43.5
Fractal	1283	24.2

Table 4-1: Elastic modulus of the collagen fibers obtained for each model

With regard to the boundary conditions, a distributed load of 100KPa was applied in the right side of the domain [90,91]. A total restriction of the left side and a partial restriction (just in vertical direction) of the upper and bottom edges are made too. Figure 4-3 shows the described conditions. For all models, the tension and compression analysis was performed and the first and second principal stresses and the first and second principal strains were obtained.

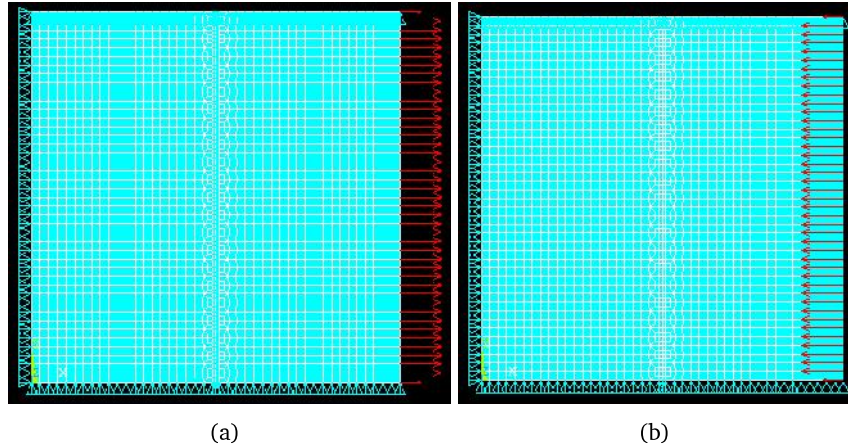


Figure 4-3: Boundary conditions to the biomechanical 2D model in a) tension and b) compression.

4.2 Results

Figure 4-4 shows the behavior of the first principal stresses for different degrees of interdigitations, without the presence of the collagen fibers. It is possible to observe that the highest values were 33.3KPa, 37.1KPa, 49.3KPa and 89.1KPa for the null, moderate, complex and fractal interdigitation, respectively. Particularly, in the case of the straight suture, the maximum value was present throughout the entire domain in an homogeneous way. In the other three cases, the maximum value was located on the bone margins and the minimum into the suture.

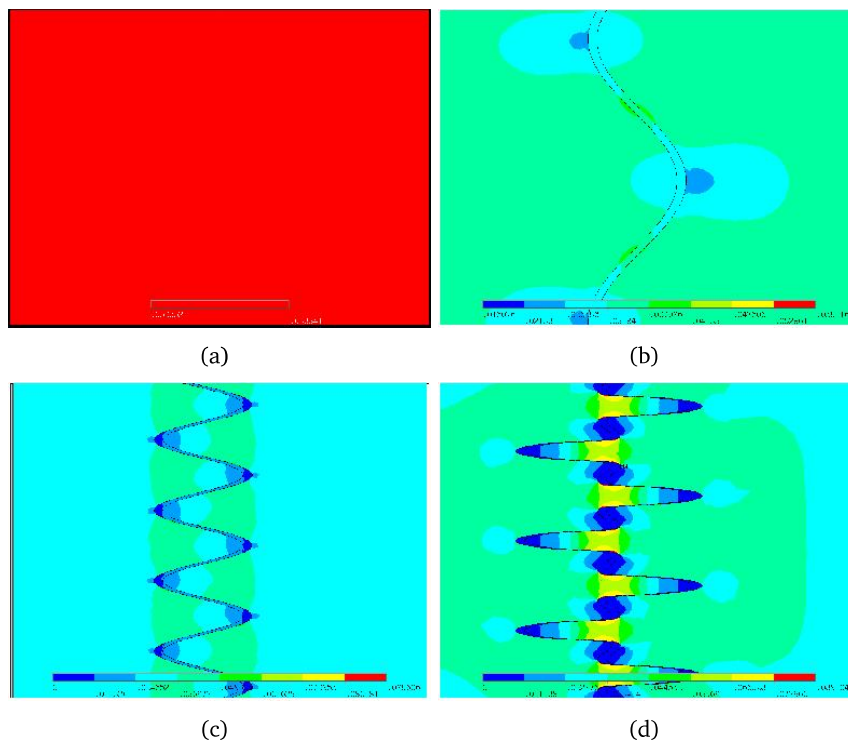


Figure 4-4: Behavior of the first principal stress between the different suture interdigitations (without collagen fibers): a) null, b) moderate, c) complex and d) fractal.

Figure 4-5 presents the behavior of the first principal strain on the different interdigitations degree, without the presence of the collagen fibers. The highest values were present into the suture with magnitudes of 0.0303, 0.0296, 0.0195 and 0.0218 for null, moderate, complex and fractal interdigitation, respectively. In this case, the minimum values were approximately zero and were located along the entire bone, including the bone margins.

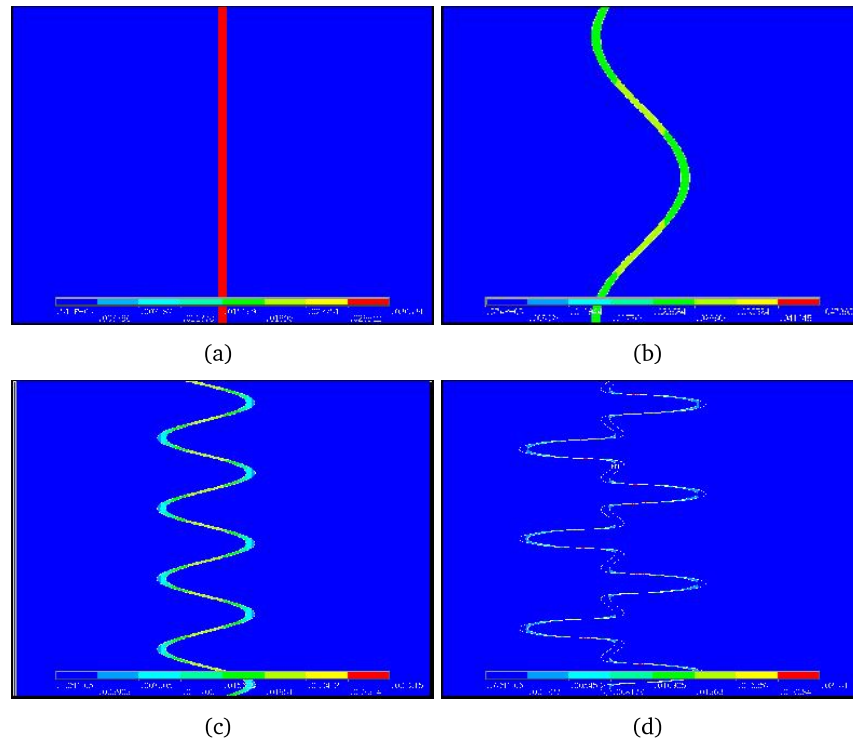


Figure 4-5: Behavior of the first principal strain between the different suture interdigitations (without collagen fibers): a) null, b) moderate, c) complex and d) fractal.

Tables 4-2 and 4-3 are presented the numerical results for the models in tension (Table 4-2) and in compression (Table 4-3), without the presence of the collagen fibers. Also, all graphical results obtained of these analysis can be visualized in the Appendix C, with and without the collagen fibers. By last, to evaluate the contribution of the collagen fibers on the suture mechanical behavior, a visual inspection and a numerical quantification were made. Figure 4-6 shows the moderate and fractal interdigitation models with absence of the collagen fibers (Figure 4.6(a) and 4.6(c)) and with the incorporation of the collagen fibers (Figure 4.6(b) and 4.6(d)). With respect to the moderate interdigitation is possible to perceive that the fibers slightly helped to homogenize the first principal stress distribution. In contrast, in the fractal interdigitation model, changes are imperceptible or non-existent. In table (4-4) the percentage variation between the model without and with the presence of the fibers are presented, in all cases the percentages were calculated with respect to variation inside the suture.

		Null	Moderate	Complex	Fractal
First principal stress (KPa)	Bone	33.341	31.841	36.977	44.552
	Bone Margin	33.341	37.096	49.303	89.104
	Suture	33.341	31.841	12.326	11.138
Second principal stress (KPa)	Bone	8.999	16.643	9.79	8.707
	Bone Margin	8.999	19.416	11.749	26.196
	Suture	10	8.321	1.954	-3.78e-02
First principal strain (mm/mm)	Bone	5.15e-06	3.74e-06	1.06e-06	3.76e-07
	Bone Margin	5.15e-06	3.74e-06	1.06e-06	3.76e-07
	Suture	0.0303	0.0296	0.0195	0.0218
Second principal strain (mm/mm)	Bone	5.96e-10	1.75e-06	1.95e-05	1.23e-05
	Bone Margin	1.02e-11	1.75e-06	1.95e05	1.23e-05
	Suture	-8.74e-11	-6.07e-03	-4.556e-03	-9.44e-4

Table 4-2: Values obtained for the models in tension

		Null	Moderate	Complex	Fractal
First principal stress (KPa)	Bone	0	0	0	0
	Bone Margin	0	15.002	0	47.108
	Suture	0	0	6.183	11.777
Second principal stress (KPa)	Bone	-8.999	-19.416	-11.749	-13.079
	Bone Margin	-8.999	-19.416	-13.708	-26.196
	Suture	-10	-11.095	-3.913	-4.335
First principal strain (mm/mm)	Bone	1.90e-06	1.13e-06	5.56e-07	1.14e-07
	Bone Margin	1.90e-06	1.13e-06	5.56e-07	1.14e-07
	Suture	0.013	0.0105	0.0142	0.020
Second principal strain (mm/mm)	Bone	-5.96e-10	-1.75e-06	-1.95e-05	-1.23e-05
	Bone Margin	-2.05e-10	-1.75e-06	-1.95e-05	-1.23e-05
	Suture	-1.02e-11	5.057e-03	3.641e-03	1.518e-03

Table 4-3: Values obtained for the models in compression

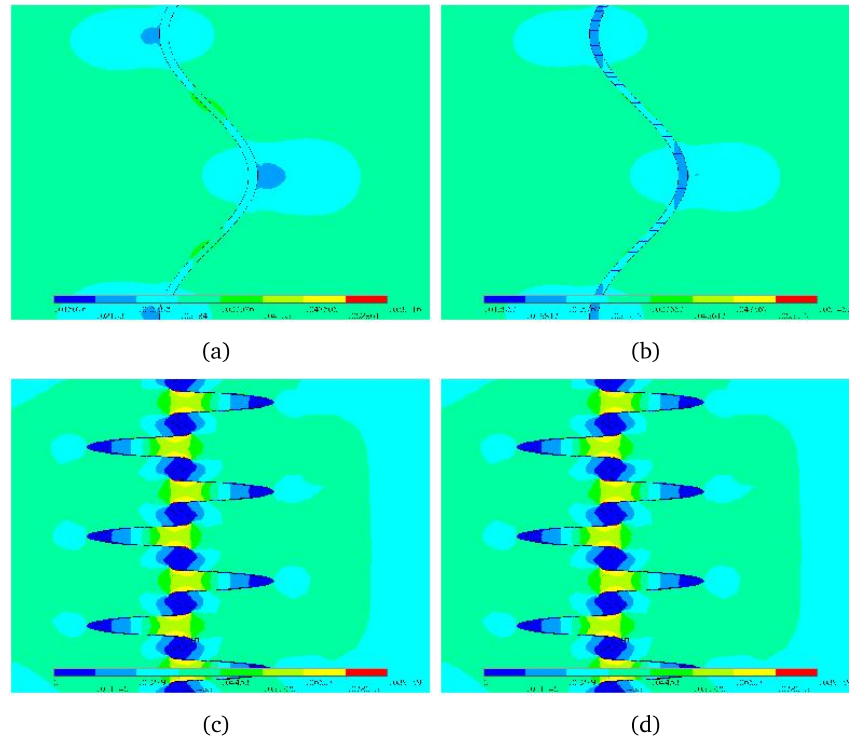


Figure 4-6: Comparative analysis between the model with and without suture. First principal stress in models with: Moderate interdigitation a) without and b) with the presence of collagen fibers; Fractal interdigitation c) without and d) with the presence of the collagen fibers.

		Null	Moderate	Complex	Fractal
Tension	First principal stress	15.85%	19.08%	4.34%	0.06%
	Second principal stress	15.83%	38.38%	0.36%	0.30%
	First principal strain	15.82%	13.74%	4.79%	2.84%
	Second principal strain	0.00%	13.74%	4.70%	2.97%
Compression	First principal stress	0.00%	0.00%	3.49%	3.20%
	Second principal stress	15.83%	30.69%	0.49%	2.77%
	First principal strain	15.82%	13.74%	4.88%	2.91%
	Second principal stress	0.00%	13.76%	4.70%	2.90%

Table 4-4: Percentage variation of the values obtained inside the midpalatal suture, between the models without and with the presence of the collagen fibers

4.3 Discussion

This study was developed in order to establish what is the influence of the interdigitation degree and the presence of the collagen fibers in some mechanical variables such as stresses and strains distribution. For this, a two dimensional simplified model was constructed and two configurations of external loads was applied. Both tension and compression loads are forces that the suture can experience in a real scenario, for example during expansion procedures or chewing. The analysis results were compared with similar investigations reported in the literature such as the research published by Jasinowski *et al.* [90]. The authors found that, for the model with null interdigitation, the highest value of the first principal stress was 100KPa which totally agrees with the results presented in Figures 4.4(a) and C-1, taking into account the difference in the suture type of each model. That difference is due to the fact that Jasinowski *et al.* assumed a 1mm of thickness that could correspond to a cranial suture while here the assigned thickness was 3mm since that value is in agreement with the MPS morphological study developed by Ennes *et al.* [10]. Another interesting work is the one made by Maloul *et al.* [24]. In this case, the domain and boundary conditions did not match those presented in the section 4.1; however, it is possible to see that the response of the moderate and complex interdigitation models is adjusted with the distributions presented in the section 4.2 and in the appendix C. Proof of this is the high similarity in the behavior of the first principal stress inside the suture; minimum values in the apex and maximum in the limbs.

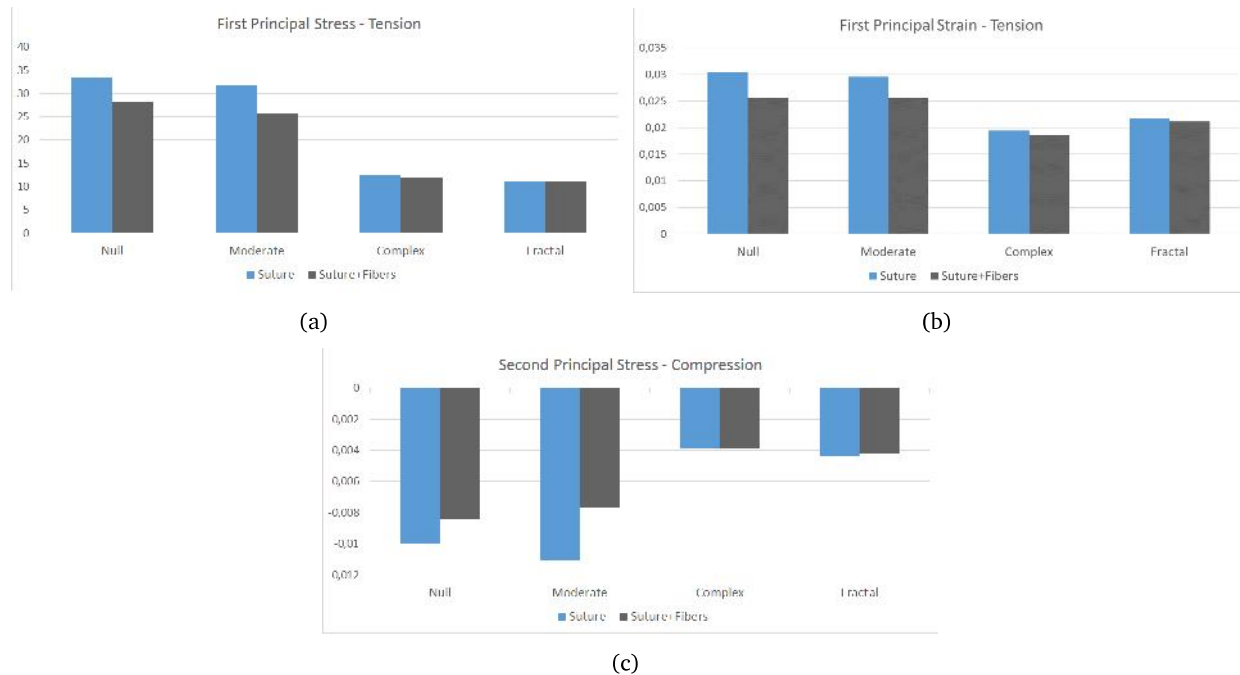


Figure 4-7: Comparative graphics of the MPS mechanical behavior in the different configurations: a) First principal stress in tension (KPa), b) First principal strain in tension (mm/mm), c) Second principal stress in compression (KPa).

Figure 4-7 was included to facilitate the comparison between the results inside the suture and, in this way, to establish the possible effect of fibers and interdigitation in the tissue mechanical behavior. Thus, it was possible to observe that the presence of the collagen fibers produces a reduction in the stress and strain values, but just in the null and moderate interdigitation cases. This can be interpreted as an

increase in the level of interdigitation will have a direct impact on the contribution of the fibers to the biomechanical response of the MPS to external stimuli, decreasing their relevance. In consequence, it is the interdigitation and not the collagen fibers that has the greatest influence in the reaction that the suture could have when it is exposed to a tension or compression loads.

4.4 Conclusions

- By carrying out the corresponding adjustments, it is possible to take advantage of the analyzes performed on cranial sutures to study the MPS due to their similarities in mechanical behavior.
- It is evident that, of the variables analyzed, the one that has the greatest impact on the suture biomechanical response is the interdigitation.
- The effect of collagen fibers on the MPS biomechanical behavior is directly related to the interdigitation degree. The higher the degree of interdigitation, the lower the effect of the collagen fibers.

Chapter 5

Biomechanical 3D model

As mentioned in Chapter 1, the biomechanics of maxillary expansion has been studied by several authors seeking to evaluate different variables such as the type of anchorage [96, 98, 99], the location of the expander screw [94], the type of suture material [5, 86, 88, 89] or variations in the design of the distractor device [95]. Nevertheless, according to the literature review a variable that has been less analyzed is the effect of interdigitation on the mechanical response of the oral cavity. To address this feature of the sutures, two-dimensional simplified models have been employed where the expansion loads are applied directly to the bone–suture–bone interface [24, 90–92]. The results obtained have a limited scope since the domain of the problem does not approach the real environment where the orthodontic treatment is carried out. Therefore, the objective of this chapter is to establish, through finite element analysis, the influence of MPS interdigitation in the biomechanical behavior of the oral cavity when a maxillary expansion treatment is performed, taking into account different types of expander devices. In the following sections will be showed the methodology that was used to the finite element analysis and the results obtained in the simulation. Thereafter, a discussion of the findings and some conclusions will be presented.

5.1 Materials and Methods

The finite element analyzes were carried out in three-dimensional domains conformed by a bone structure, the MPS and an expansion device. The bone structure included the upper maxilla, the teeth of the upper maxilla and the zygomatic, nasal and sphenoid bones; it was obtained from a computed tomography (Carestream Health/CS 9300) that was available in the research group repository. This tomography had 203 frames taken every 0.657mm and was reconstructed in the Mimics software 10.01 (Materialize, Belgium). Subsequently, the result of the reconstruction was imported into the Autodesk Inventor software (Autodesk, California, USA) where some details were corrected, such as noise, small parts generated as independent pieces that did not belong to the domain of interest, or rough contours that come from the filters used in the reconstruction process. The CAD model obtained for the bone structure (Figure 5-1) was the basis for the elaboration of the geometric models of the MPS and expander devices.

In the Autodesk Inventor software (Autodesk, California, USA) a parallel plane to the palate was generated and, in that plane, the sketch of the suture morphology was elaborated taking into account the changes that it presents during the growth, starting with a straight shape until reaching a interdigitated shape [24]. Three types of interdigitation were defined: null, moderate and scalloped; coinciding with the classification made by other authors [9, 24, 90, 91]. The sketch was used as the basis for the extru-

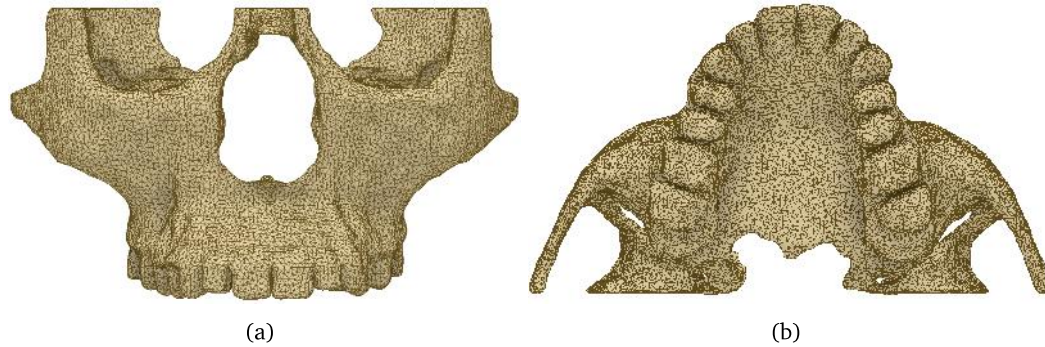


Figure 5-1: Geometric model of the bone structure obtained from the reconstruction process: a) Front view. b) Bottom view.

sion cutting operation, which made it possible to obtain the suture models that can be seen in Figure 5-2.

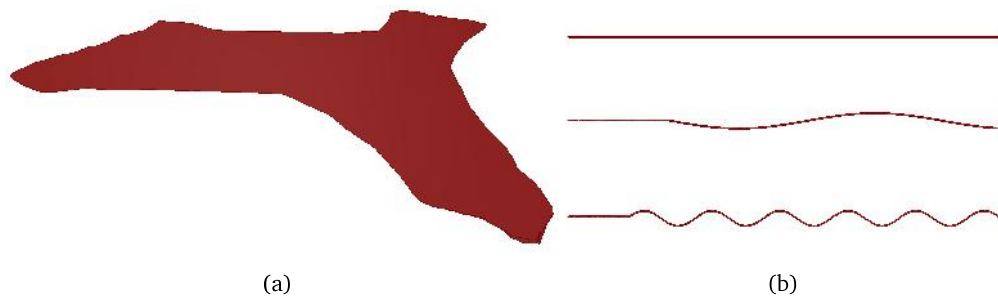


Figure 5-2: Geometric models of the sutures obtained from the bone structure: a) Side view. b) Bottom view of the suture with null, moderate and scalloped interdigitation.

As for the expansion device, the analyzes were carried out with 4 different designs; all based on the Dentaurem company catalogue [145]. The first device used was the most popular expansion device [88, 89, 96, 98], the conventional Hyrax with dental anchorage (Figure 5.3(a)). The second one was a hybrid Hyrax expander, with dental and skeletal anchorage (Figure 5.3(b)). The third one corresponded to an expander that was anchored only skeletally (Figure 5.3(c)). The fourth and last of the devices was a variation of the conventional Hyrax where the expansion screw was located in the anterior part of the maxilla (Figure 5.3(d)). The expanders with dental anchorage were supported on the first premolars and molars while the skeletal anchorage was carried out by dental mini-implants located on the mucosa of the palate.

The finite element analysis was performed using ANSYS 17.0 software (Bela Engineering Group, Downers Grove, IL, USA). To begin the configuration of the study, the material behavior of all pieces that made up the models was defined as linear, homogeneous and isotropic [95, 99, 146]. A single modulus of elasticity was used for the bone calculated as a weighted average of cortical and trabecular bone in the skull, with a value of $10000MPa$ [89, 96]. The elastic modulus used in the suture, the expansion device and the mini-implants were $1MPa$ [5, 82, 96], $200000MPa$ [96, 146, 147] and $110000MPa$ [95], respectively. The Poisson ratio assigned was 0.3 for all materials. Once the definition stage of the material properties was finished, the meshing stage was developed. The mesh size obtained, after using the ANSYS mesh quality criterion and performing a convergence analysis with the total deformation of the

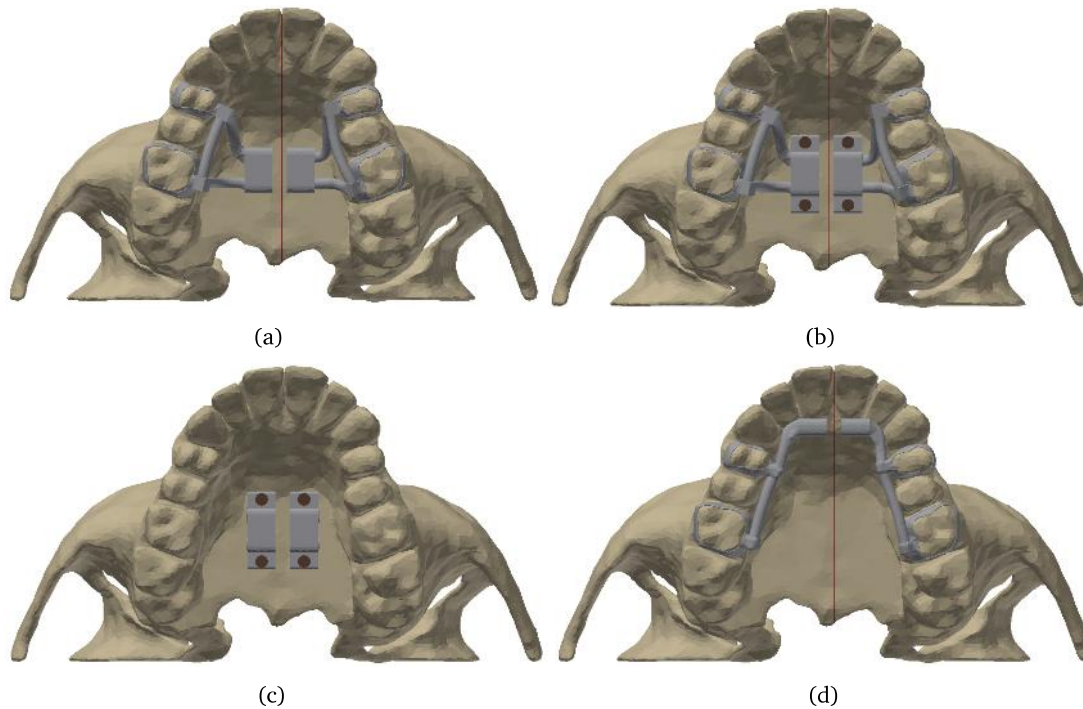


Figure 5-3: Final geometric models with null interdigitation and the expander devices: a) Model with conventional Hyrax. b) Model with hybrid expander. c) Model with a modified Hyrax to produce just skeletal anchorage. d) Model with the variation of the screw location

model, was 715008 nodes and 433185 elements. The quality criterion showed a mesh quality higher than 75% and the convergence analysis carried out on two consecutive refinements with a last change of 2.97%.

The activation of the expander device was simulated by the direct application of a displacement condition, in the transverse direction, on the internal faces of the designed devices. The applied displacement value was 0.125mm on each side, which is equivalent to a quarter turn of the screw [88, 96]. For the models with only dental anchorage, the displacement in perpendicular direction to the expansion was also restricted, simulating the presence of the device expansion screw (Figure 5.4(b)). For the analysis, chewing loads were taken into account, modeled as static forces on the first and second molars and on the first premolars. All loads were defined with a magnitude of 70N in the normal direction to the occlusal plane (Figure 5.4(c)) [148]. Finally, two displacement conditions on the bone structure were applied. The first one was a condition of “fixed support” located in the posterosuperior region, simulating the restriction of the skull base. The second one was a partial condition on the upper surface that represented the restriction of the cranial structure (Figures 5.4(d)) [89, 96, 146].

Finally, the maximum principal stresses in the maxilla and in the SMP and the equivalent stresses in the expansion devices were evaluated. Also, the suture displacement in the expansion direction was assessed. From now on, the following notation will be used for the different analyzed models: null interdigitation (NI), moderate interdigitation (MI), scalloped interdigitation (SI), dental anchorage models (DA), dento–skeletal anchorage models (DSA), skeletal anchorage models (SA) and models with the variation of the conventional Hyrax (HVDA).

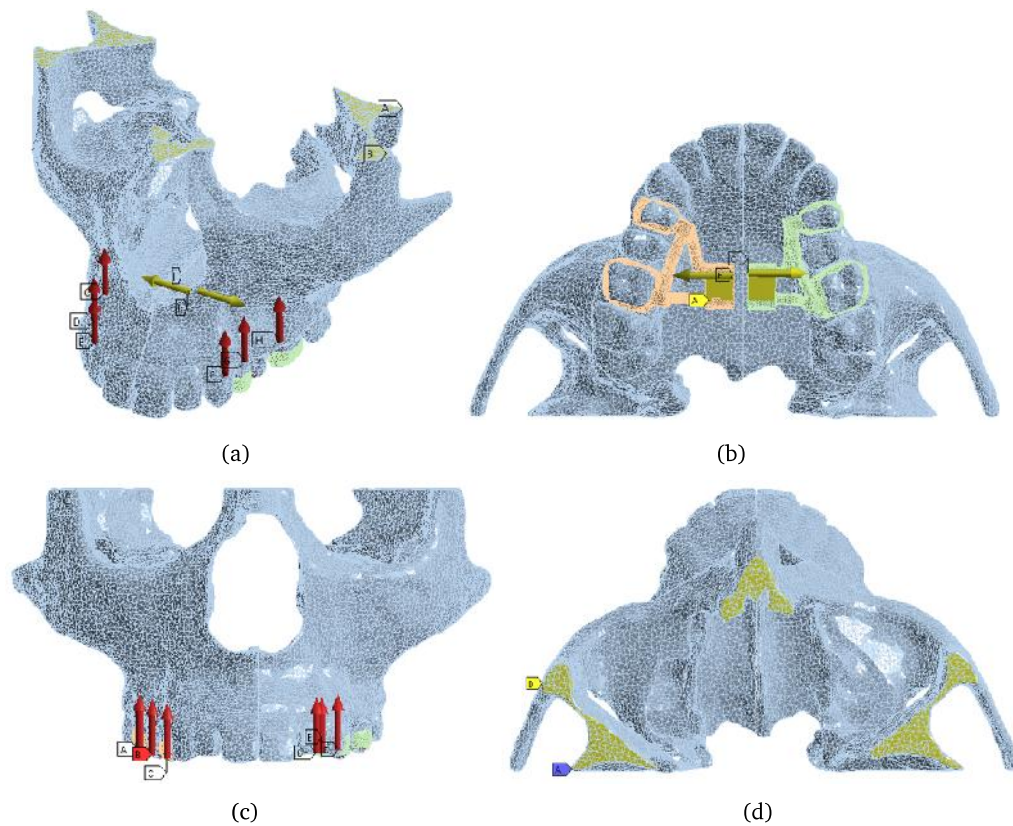


Figure 5-4: Boundary conditions for the finite element analysis: a) General view of boundary conditions. b) Boundary conditions to simulate the devices activation. c) Chewing loads applied in the first and second molars and in the first premolars (red arrows). d) Displacement restrictions on the bone structure

5.2 Results

5.2.1 Dental anchorage models (DA)

Figure 5-5 shows the maximum principal stresses behavior in the bone structure. The highest values were 59.7, 56.8 and 56.7MPa for null, moderate and scalloped interdigitation, respectively. These values were located near to the posterosuperior restriction. Around the suture area, the stresses were in the range of 0 to 5MPa.

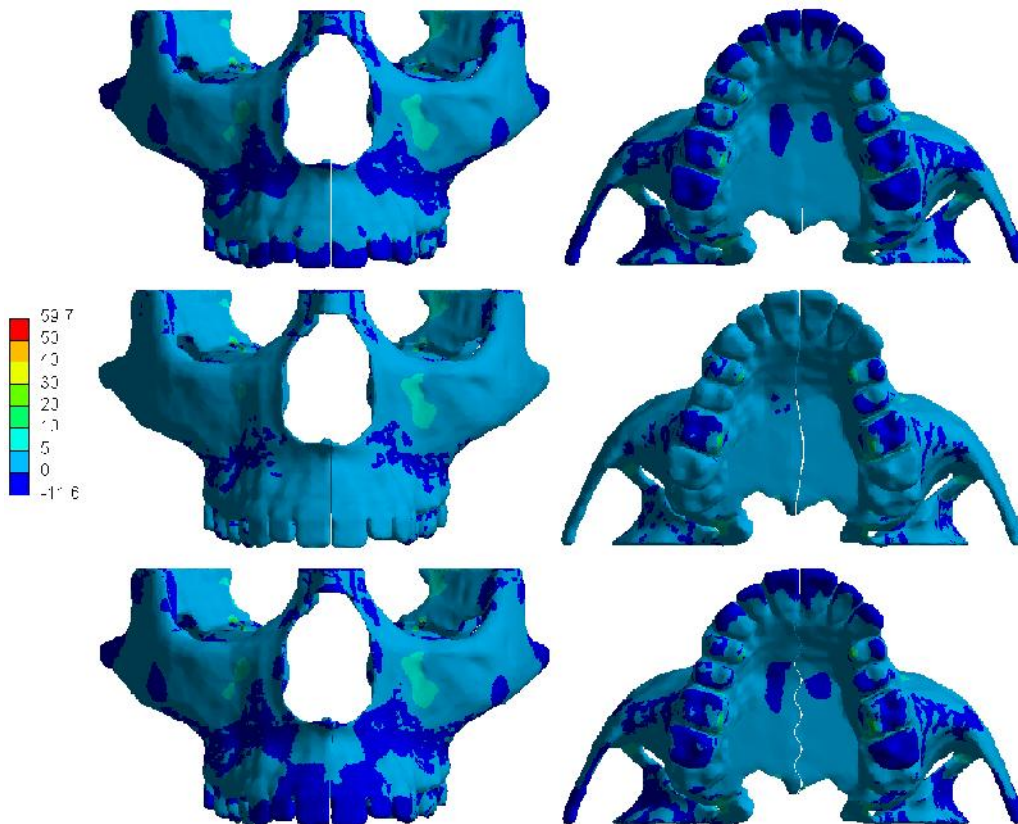


Figure 5-5: Maximum Principal Stresses (MPa) obtained for the bone structure in DA models and the three types of interdigitation modeled.

In relation to the MPS, Figure 5-6 presents the maximum principal stresses (Figure 5.6(a)) and the directional displacements (Figure 5.6(b)) in the suture for the models with the conventional Hyrax and dental anchorage. The highest values for the first variable were 1.36MPa with null interdigitation, 1.11MPa with moderate interdigitation and 1.22MPa with scalloped interdigitation. In all cases, the highest magnitude of the directional displacements was 0.07mm. Both, the maximum stress and maximum displacement were located in the posterior region.

By last, the equivalent stresses obtained in the conventional Hyrax can be seen in Figure 5-7. 408.9, 449.2 and 445.6MPa were the maximum equivalent stress values observed for the null, moderate and scalloped interdigitations, respectively. In all cases, these values were found in the device arms.

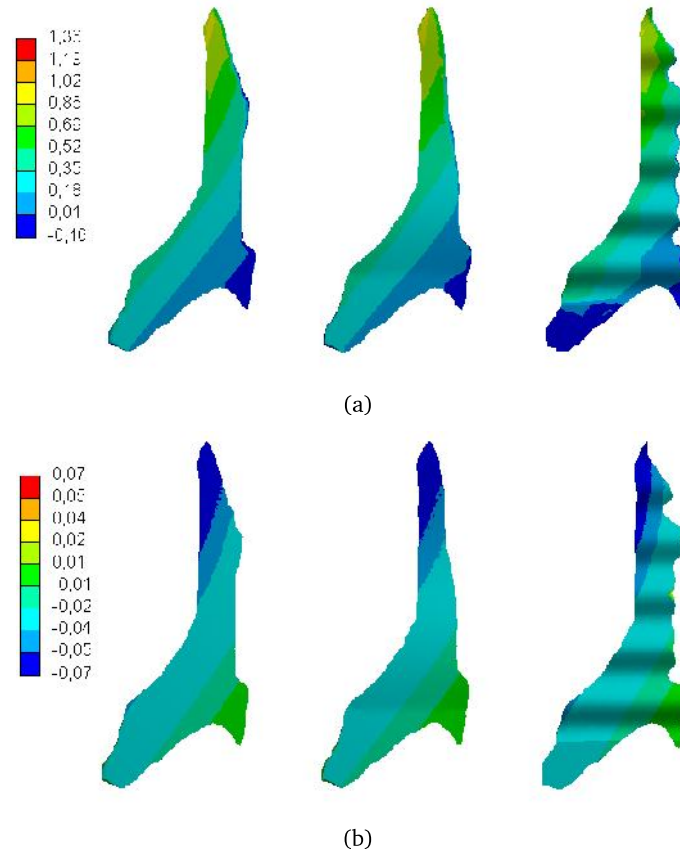


Figure 5-6: Results obtained for the midpalatal suture in DA models and the three types of interdigitation modeled. a) Maximum Principal Stresses (*MPa*). b) Directional Displacements (*mm*)

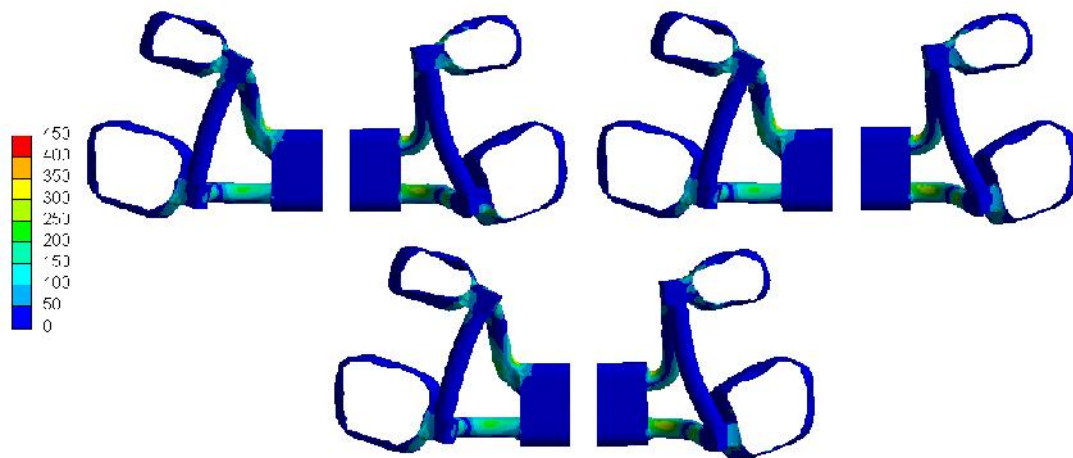


Figure 5-7: Equivalent stresses (*MPa*) obtained for the conventional Hyrax and the three types of interdigitation modeled.

5.2.2 Dento–skeletal anchorage models (DSA)

The highest values of the maximum principal stresses on the dento–skeletal models were 181.8, 163.7 and 187.6 MPa for null, moderate and scalloped interdigitation, respectively. As can be seen in Figure 5-8, these values are located close to the skeletal support area.

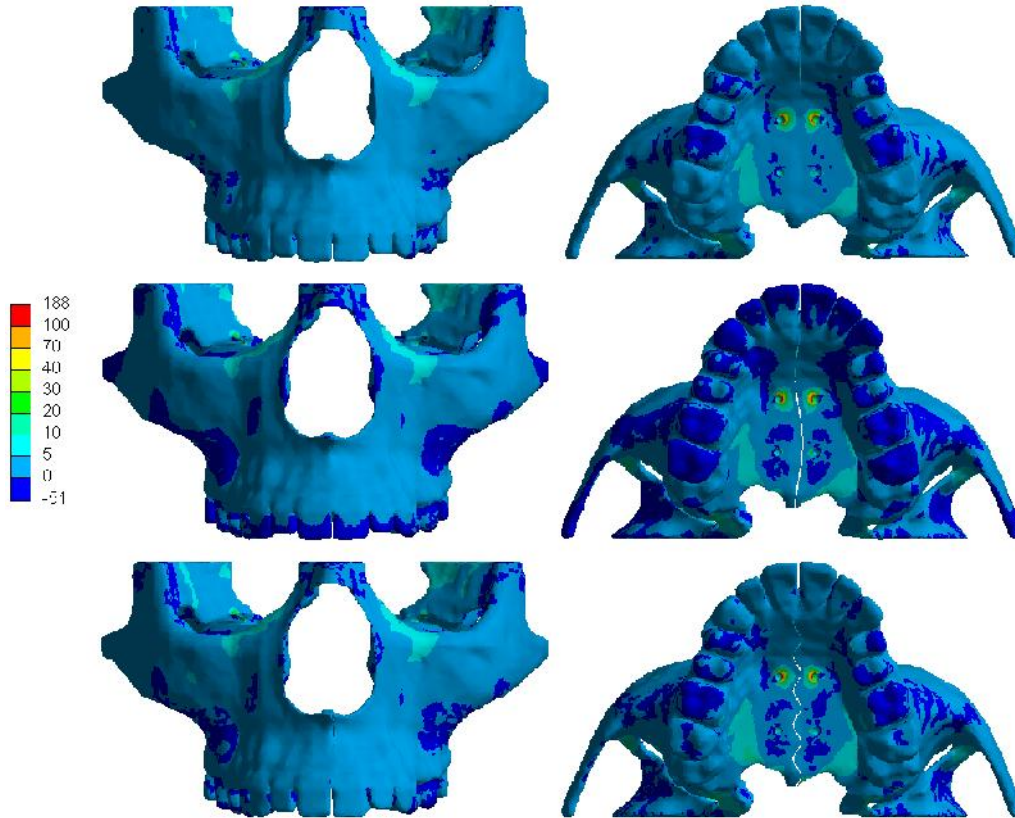


Figure 5-8: Maximum Principal Stresses (MPa) obtained for the bone structure in DSA models and the three types of interdigitation modeled.

The maximum principal stress and the directional displacement distributions on the suture are presented in Figure 5-9. The highest stress values were 2.45, 2.14 and 2.18 MPa for the null, moderate and scalloped interdigitations, respectively. With respect to the directional displacements, the null interdigitation showed a highest magnitude of 0.13 mm while the value for the moderate and scalloped interdigitation was 0.12 mm . Both, the maximum stress and the maximum displacement, were located in the posterior region.

Finally, Figure 5-10 presents the results obtained for the hybrid expander device. The maximum equivalent stresses were 424.2, 423.3 and 444.1 MPa for null, moderate and scalloped interdigitation, respectively. These values were found in the junction of the arms with the device base.

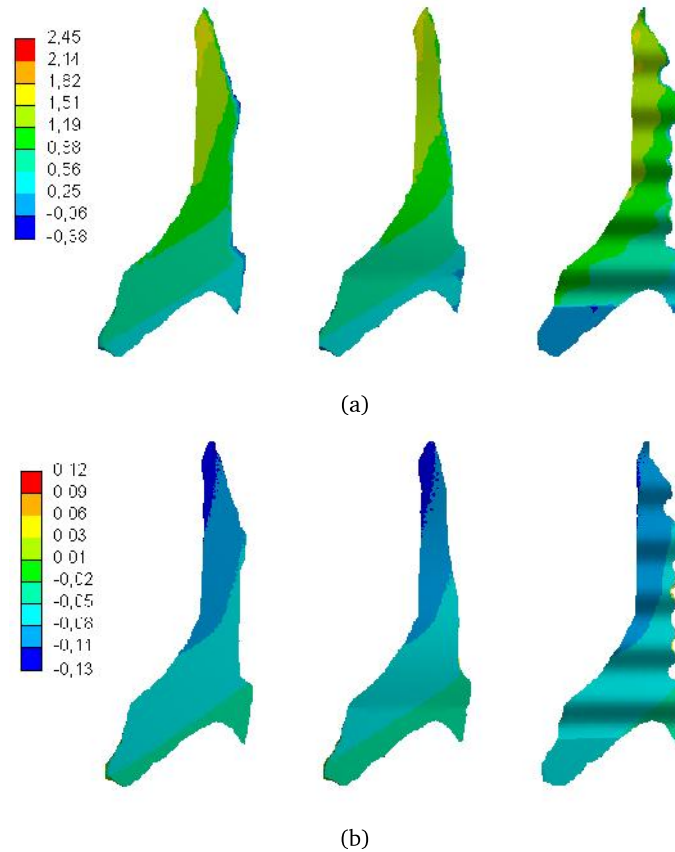


Figure 5-9: Results obtained for the midpalatal suture in DSA models and the three types of interdigitation modeled. a) Maximum Principal Stresses (*MPa*). b) Directional Displacements (*mm*)

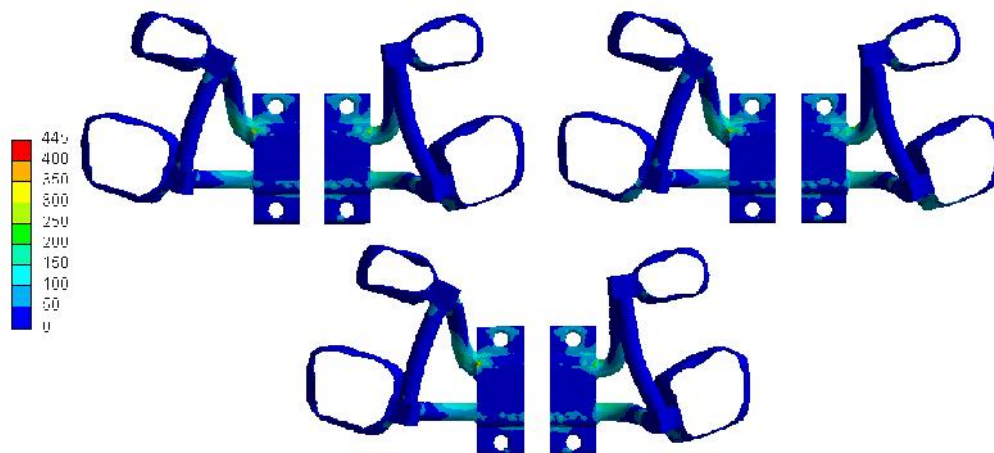


Figure 5-10: Equivalent stresses (*MPa*) obtained for the hybrid Hyrax and the three types of interdigitation modeled.

5.2.3 Skeletal anchorage models (SA)

The distribution of the maximum principal stresses on the bone structure, for the skeletal models, are presented in the Figure 5-11. In the same way that with the hybrid anchorage, the highest values were located close to the support area in the palate with magnitudes of 211.3, 175.2 and 219.8MPa for null, moderate and scalloped interdigitation, respectively.

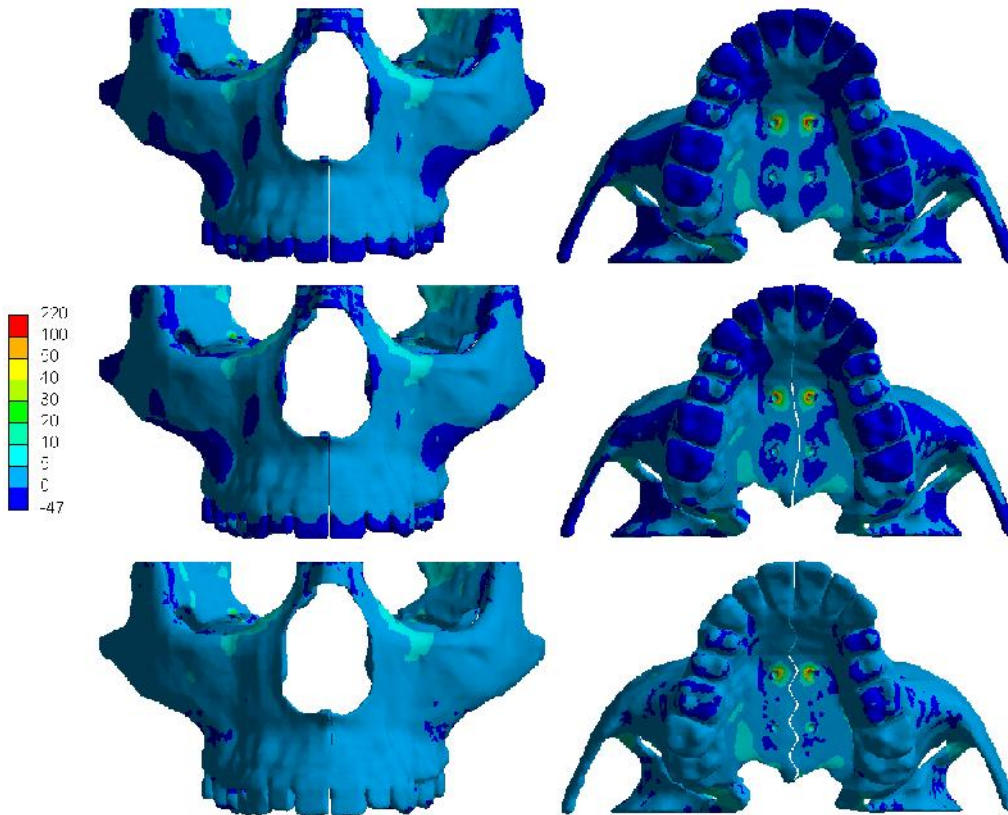


Figure 5-11: Maximum Principal Stresses (MPa) obtained for the bone structure in SA models and the three types of interdigitation modeled.

In the MPS the highest values for the maximum principal stresses were 2.34, 2.05 and 2.08MPa and for the directional displacement were 0.13, 0.12 and 0.12mm for null, moderate and scalloped interdigitation, respectively. These values were located in the posterior region. Figure 5-12 shows the distributions for both variables.

As for the expander device, the highest values of the equivalent stress were found around the anchorage points with values of 334.3, 339.1 and 330.0MPa for null, moderate and scalloped interdigitation, respectively. In Figure 5-13 is possible to see the equivalent stress distribution for the device.

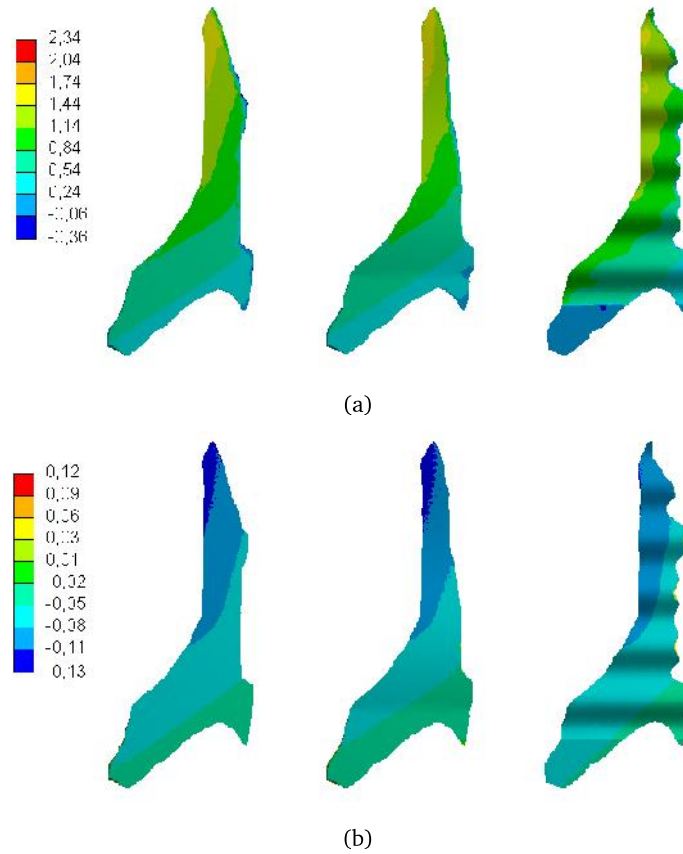


Figure 5-12: Results obtained for the midpalatal suture in SA models and the three types of interdigitation modeled. a) Maximum Principal Stresses (MPa). b) Directional Displacements (mm)

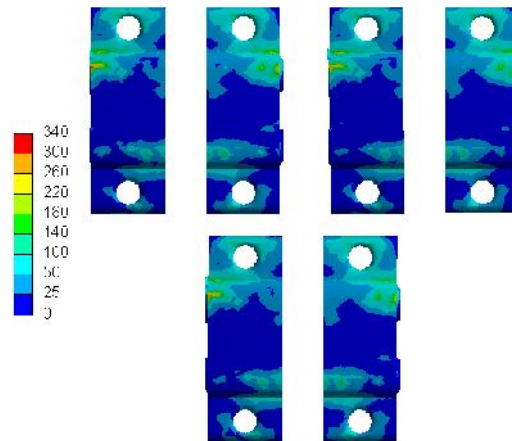


Figure 5-13: Equivalent stresses (MPa) obtained for the Hyrax with skeletal anchorage and the three types of interdigitation modeled.

5.2.4 Models with the variation of the conventional Hyrax (HVDA)

The maximum equivalent stress distribution of the bone structure in the HVDA models is presented in Figure 5-14. It is possible to observe that the maximum value obtained for the null interdigitation was 37.2, for the moderate interdigitation was 34.2 and for the scalloped interdigitation was 30.0 MPa . In the three cases, the maximum values were located in the anchorage area of the first premolars.

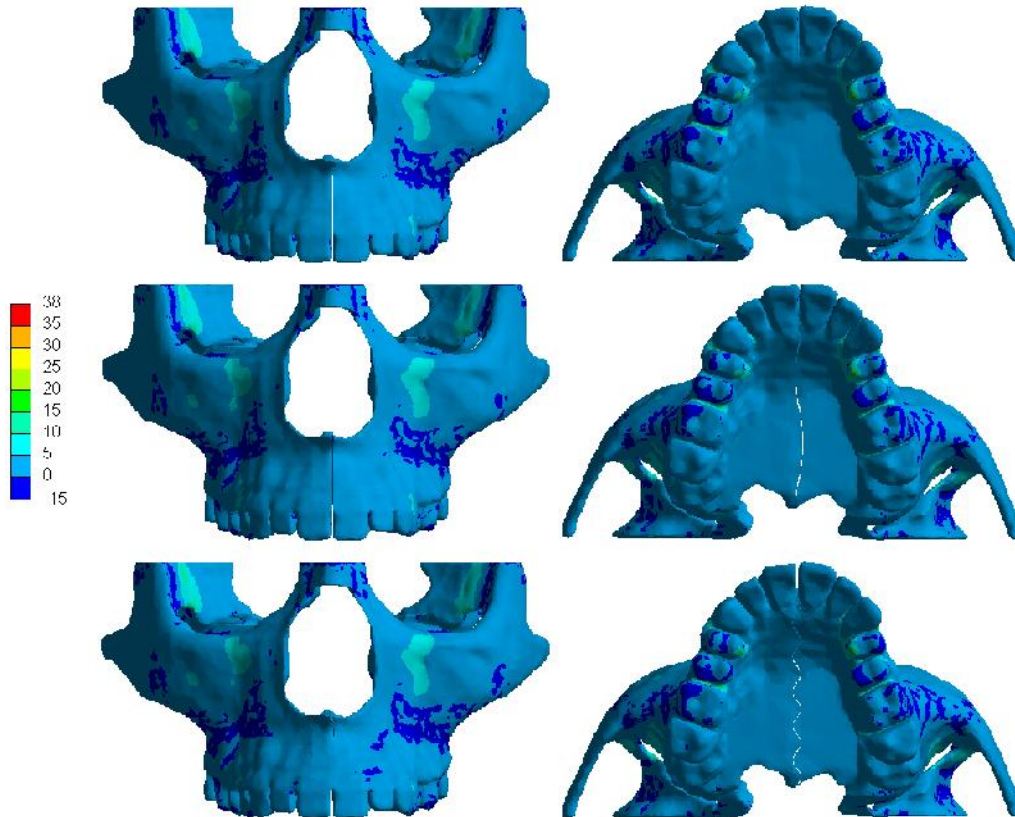


Figure 5-14: Maximum Principal Stresses (MPa) obtained for the bone structure in HVDA models and the three types of interdigitation modeled.

Figure 5-15 shows the maximum principal stress and directional displacement distributions for the MPS in the HVDA models. The highest values for the maximum principal stress were 1.15, 1.24 and 1.10 MPa and for the directional displacement were 0.06, 0.06 and 0.07 mm with null, moderate and scalloped interdigitation, respectively. In this case, the maximum values were found in the lower part of the anterior region.

Finally, the expander device of the HVDA models presented their highest equivalent stresses in the arms of the device; the results can be seen in the Figure 5-16. The highest stresses were 466.9, 458.0 and 422.1 MPa for the null, moderate and scalloped interdigitation, respectively.

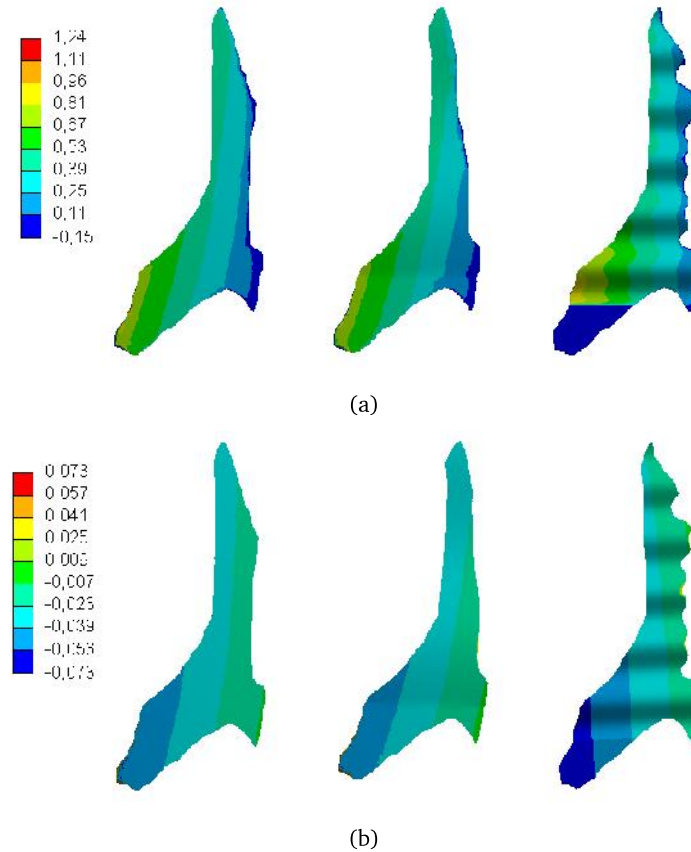


Figure 5-15: Results obtained for the midpalatal suture in HVDA models and the three types of interdigitation modeled. a) Maximum Principal Stresses (MPa). b) Directional Displacements (mm)

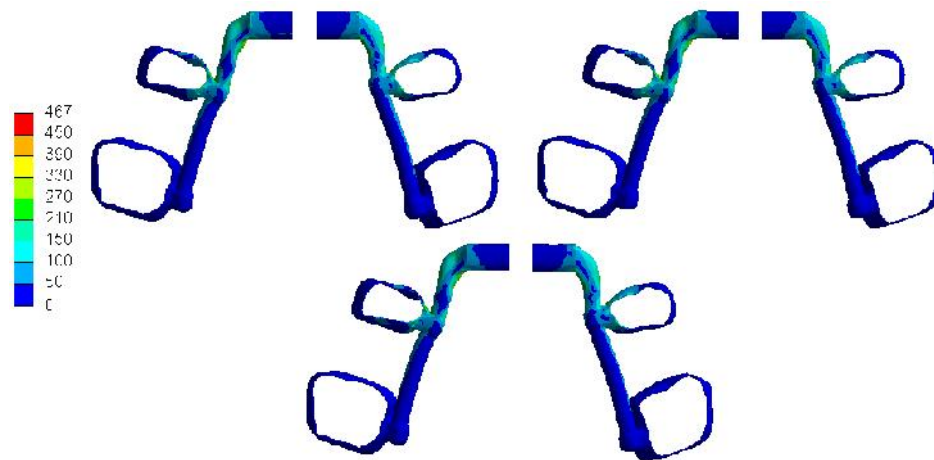


Figure 5-16: Equivalent stresses (MPa) obtained for the variation of the conventional Hyrax and the three types of interdigitation modeled.

5.3 Discussion

This Chapter presents a biomechanical study of the oral cavity when it is exposed to a maxillary expansion. For this purpose, 12 domains were developed with variations of the type of the expander device and the MPS interdigitation level. Thus, a finite element analysis was carried out and the behavior of the maximum principal stress on the bone structure and suture were obtained. Also, the equivalent stress on the expander device and the displacement in the expansion direction on the suture were observed too. As it is possible to see in the results section, the bone structure presented a stress concentration in the region close to nasal cavity, at the anchorage points and in the region between the maxilla and the zygomatic bones. Both the aforementioned behavior and the range of stress magnitudes found are in agreement with previous studies reported in the literature [84, 89, 98]. In the particular cases of the skeletal anchorage, the palatal area close to the anchorage points evidenced greater stresses of those that the bone can support [96, 99, 149]. In a real scenario, these values are lower due to the fact that the bone carries out a relaxation process after activation and this phenomena was not taking into account in this work [5, 89].

As it is possible to see in Figure 5-17, the skeletal anchorage generates the highest values for the maximum principal stress on the bone structure, being the moderate interdigitation that produces the lower values between the three interdigitation levels. In relation to the models with dental anchorage, the DA models showed higher values than the HVDA models; however, no significant differences are found in these models caused by the interdigitation degree. Regarding the MPS, the null interdigitation showed higher values than the moderate and scalloped interdigitation for the DA, DSA and SA models. For their part, the HVDA models did not show significant variations between the three types of interdigitation. In the same way that in the bone structure, the skeletal anchorage evidenced higher maximum principal stresses than the dental one. By last, with respect to the expander device, the lowest values of the equivalent stress were found in the SA models; similar magnitudes were observed in the other ones. The maximum equivalent stress for the DA, DSA and HVDA models were located in the arms of the device that transmit the mechanical signal from the base to the dental anchorage points, in agreement with the stress behavior reported by Ludwig *et al.* [88]. The above is reasonable if it is considered that the arms are the weakest part of the structure.

Figure 5-18 shows the maximum principal stress on the anterior, middle and posterior region of the bone-suture interface, for all models. It is possible to see the influence of the anchorage type and the expander device in the stress behavior in that region. Reaffirming what has been said previously, both the bone structure and the suture present higher values when the anchorage is skeletal. In the bone structure, the highest points were seen in the middle and posterior region while, in the suture, a more evident linear increase trend was observed, from the anterior to the posterior region. For the DA models, the highest point was in the posterior region and similar values were found in the middle and anterior region. For the HVDA models the behavior was opposite to the DA ones; highest stress in the anterior area and similar values in the other two.

On the other hand, in Figure 5.19(a) it is possible to see that the interdigitation degree does not have significant influence in the reaching values for the directional displacement, but the anchorage type does. Between skeletal and dental anchorage, the first one generated the highest values. In the particular case of the models without any type of skeletal anchorage, even when they produced similar displacement magnitudes, the distributions were quite different. As it is possible to see in Figures 5.6(b) and 5.15(b), the displacements were homogeneous, in vertical direction, in the DA models while in the HVDA models they were not. The above can be interpreted as the first are more efficient than the

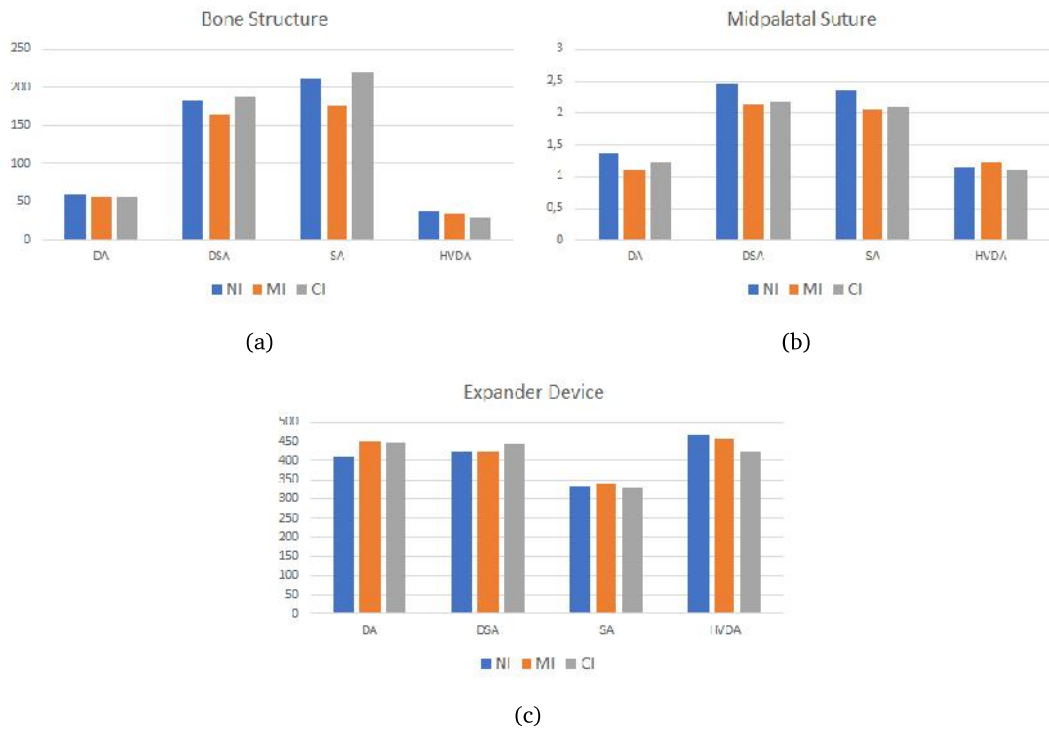


Figure 5-17: Comparative graphs of the stress behavior in the oral cavity. a) Maximum Principal Stresses on the bone structure (MPa). b) Maximum Principal Stresses on the midpalatal suture (MPa). c) Equivalent Stresses on the expander device (MPa).

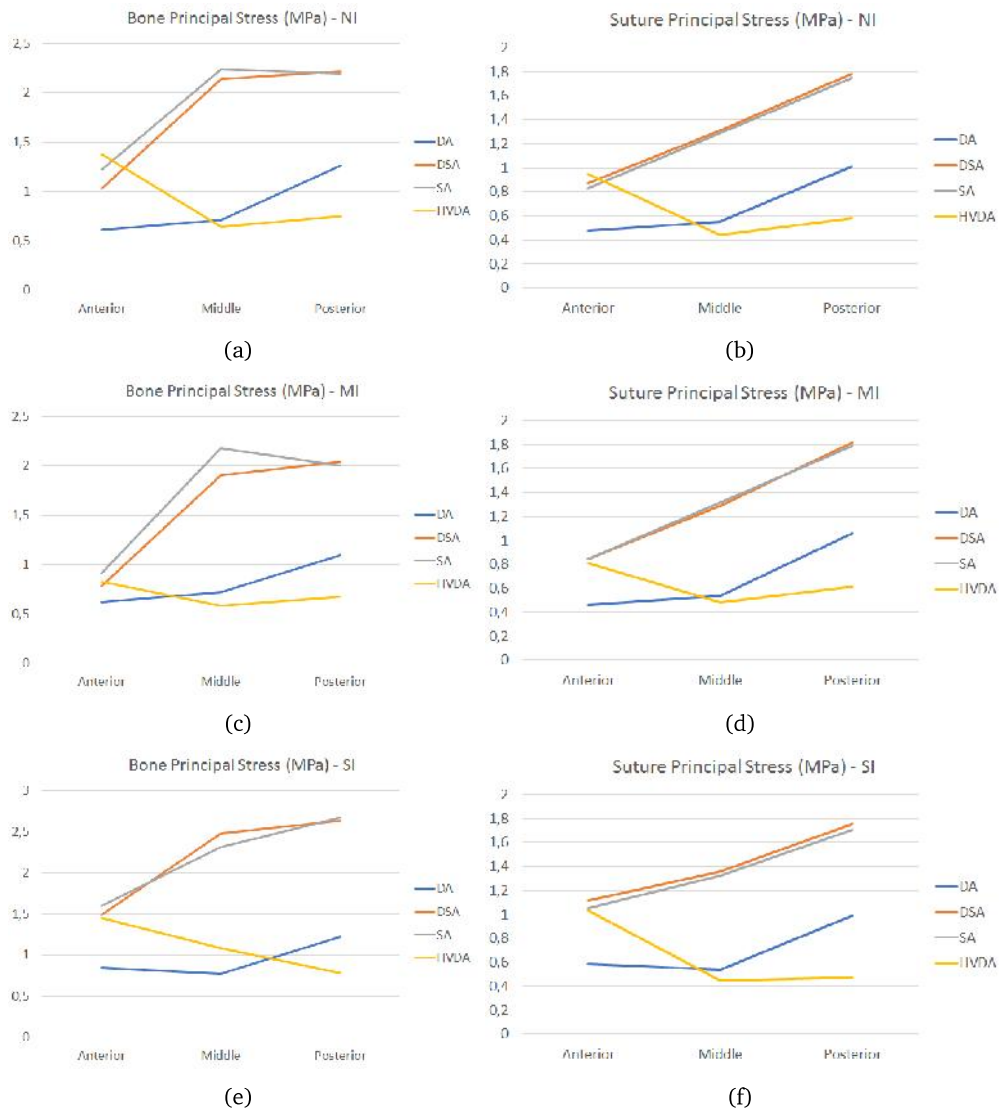


Figure 5-18: Comparative graphs of the stress behavior in the bone–suture interface. Maximum Principal Stresses on a) the bone structure and b) suture with null interdigitation. Maximum Principal Stresses on c) the bone structure and d) suture with moderate interdigitation. Maximum Principal Stresses on e) the bone structure and f) suture with scalloped interdigitation.

second ones because the maxillary expansion had effect through the entire suture and not just in the palatal surface. The displacement distribution in the skeletal models showed the lowest values in the anterior region with increase in anteroposterior direction, similar to what was observed in the DA models. This reaffirms the effectiveness of the skeletal anchorage over the dental anchorage because the skeletal ones produces similar distributions but higher displacement magnitudes. In addition to this, Figure 5.19(b) presents an approximation of the dental inclination in the anchorage teeth. To calculate that values, the directional displacements in the normal direction to the occlusal plane were observed. Then, the displacement values in the lingual and buccal surface were obtained and subtracted. According to this approximation, the skeletal anchorage transfers the mechanical expansion in a better way than the dental anchorage due to the fact that produces less dental inclination.

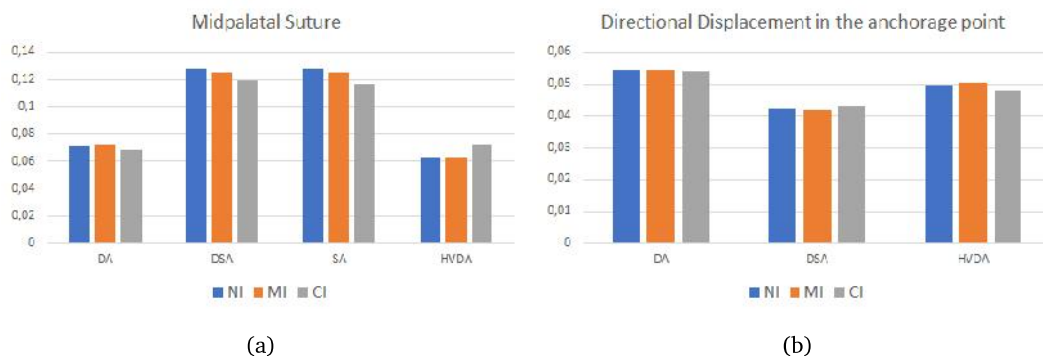


Figure 5-19: Comparative graphs of the a) MPS displacements and b) inclination teeth

Figure 5-20 shows the displacement behaviour in the bone–suture interface on the palatal surface. As can be seen in the graphs presented, the skeletal anchorage produces a similar behavior in the bone structure and in the suture, with a linear tendency that increase in the anteroposterior direction. With respect to the dental anchorage, the DA and HVDA models evidenced opposite curves. Highest values in the posterior, for the DA models, and in the anterior part, for HVDA models and similar magnitudes in the other two analyzed regions. In the DA cases, a slight decrease in the anterior region in comparison with the middle region can be seen.

This study demonstrated that the skeletal anchorage can be a good option to the maxillary expansion orthodontic treatment due to the capacity to produce greater skeletal expansion, to reduce the undesired tipping effect and to generate similar stress values than the dental anchorage. The above is consistent with the clinical and radiographic analyzes developed by Lee *et al.* [150] and Oh *et al.* [44]. The first one established that the treatment with bone support ends with a stable expansion and a healthy periodontal ligament [150]. The second one concluded that the expansion with palatal anchorage results in a greater skeletal change and in a lower buccal tipping [44]. In contrast, some investigations, like the reported by Lagravère *et al.* [40], found that there are not variations in the displacement reached between the two types of anchorage. Nevertheless, the discrepancy in the results could be related with differences in some treatment parameters such as the expander base location, the palatal place where the device is supported, the type of expander device, etc. For example, in this work the mini-implants were located close to the bone–suture interface, in a similar way that the first two studies, while the third study anchored the expander near to the teeth root. Therefore, the biomechanical analysis exposed in this chapter can simulate clinical outcomes and could be useful to evaluate modifications of some variables in the clinical protocol.

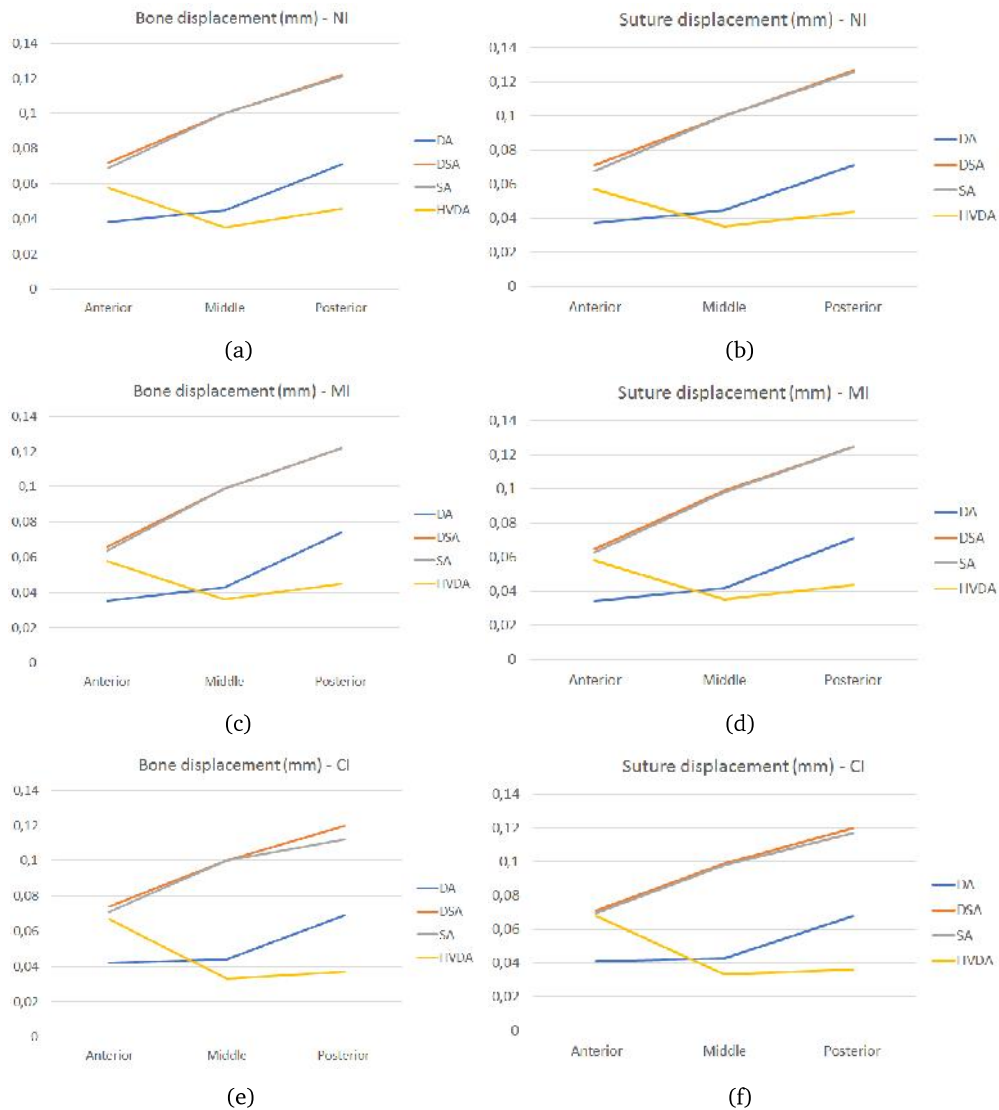


Figure 5-20: Comparative graphs of the displacement behavior in the bone-suture interface. Directional displacement on a) the bone structure and b) suture with null interdigitation. Directional displacement on c) the bone structure and d) suture with moderate interdigitation. Directional displacement on e) the bone structure and f) suture with scalloped interdigitation.

5.4 Conclusions

- The results obtained show that the MPS interdigitation level does not affect, in a significant way, the reached displacements. By the other hand, this parameter has a direct influence in the stress behavior, producing local changes in the stress distribution. This could be observed to a greater extent when the expansion was transmitted directly to the suture, as in the case of the skeletal anchorage.
- The skeletal anchorages presented the greatest effectiveness for the expansion due to their capacity to transmit most of the displacement produced by the expander device to the MPS. However, this type of anchorage generates stress levels, which must be taken into account in a real scenario, reviewing the clinical protocols.
- According to the literature review, it seems that this study is the first to analyze the influence of the interdigitation degree in the MPS response to a mechanical stimulus, like those produced by maxillary expansions and chewing, taking into account a more realistic domain by a computed tomography reconstruction of the maxilla and part of the skull.

Chapter 6

Conclusions and future work

The midpalatal suture is a fibrous tissue that is located in the middle of the two halves of the palate. Due to its importance in orthodontic treatments, such as maxillary expansion, it is necessary to understand its formation process and its response, both biological and structural, to mechanical stimuli. The main objective of the research presented in this work is the development of a biomechanical and mechanobiological model that describes the midpalatal suture formation process, using computational simulations. Thus, an experimental, a mechanobiological and a biomechanical models were carried out in order to reach this goal. For the experimental model, an *in vivo* procedure on *(WT)(C57BL/6)* mice was performed. The experiment consisted in the application of an expansion spring in the oral cavity of the animals and took into account variations in the load magnitude and in the treatment duration. The procedure allowed analysis at the cellular and molecular level. With respect to the mechanobiological component, a mathematical model that describes two biological processes present in the suture was proposed. The first one is the cellular migration generated by the expansion forces. The second one is the remodeling process present at the bone margins that produces the characteristic morphological changes of the suture during growth. Finally, in relation to the biomechanical part, a two-dimensional and a three-dimensional domain were modeled and analyzed to establish the structural response of the oral cavity to expansion procedures, taking into account some parameters such as the interdigitation level, the presence of collagen fibers and the anchorage type.

According to the results obtained from the experimental model, it is evident that the expansion loads influence the cellular and molecular activity inside the suture. As a consequence of the treatment, a cell migration process was generated, from the periosteum to the sutural tissue, which is activated after the expansion load has been applied. Also, an increase in the population of osteoprogenitor cells and in the expression of molecular factors considered as osteoblasts and osteoclasts markers could be perceived. In addition, the qPCR analysis allowed to detect the presence, and the increase in its expression due to the expansion, of molecular factors that have been related to fusion and patency of cranial sutures; suggesting that the results found by investigations developed in cranial sutures could be used in facial sutures such as the midpalatal suture. On the whole, morphometric analysis using microCT, histological analysis and molecular analysis allow us to state that the experimental procedure standardized in this work successfully performs the expansion of the maxilla and shows a reliable methodology that future research can use to deepen knowledge of the midpalatal suture and in its response to expansion procedures. By last, it should be noted that this experimental model opens the door for subsequent studies to focus on the particular effect of each of the molecular factors detected and, thus, can estimate those responsible for different anomalies such as the transverse maxillary deficiency or cleft palate, providing information for the prevention or treatment of this type of pathologies.

As it can be seen in the simulations carried out using the mechanobiological model, the proposed system of equations succeeds in simulating the cellular migration process detected in the experimental analysis and the processes of remodeling that occur at the suture margins. Therefore, it can be inferred that the approach based on the biological models of Chemotaxis and Schnakenberg was adequate. The results show that it was possible to simulate the new bone layers formation as shown by the histological analyzes carried out in mice and as different authors have established in the humans suture. Additionally, it can be seen how a distribution of the molecular factors that interact within the suture, that correspond to what is described as Turing instabilities, is achieved. These instabilities have been associated with morphogenesis processes and allowed to reproduce the initial states of the characteristic morphological changes of the midpalatal suture and to obtain more complex interdigitation patterns in sutures that have already been expanded. According to the literature review, it seems that this approach is the first mechanobiological model developed for the midpalatal suture as such. This proposal marks a way to carry out experimental research that will allow to feed the model and, consequently, to be able to take from its non-dimensional state to a real state. The mathematical model developed is a first approximation of the simulated phenomena abstraction and allows to understand them, numerically, in a better way.

Finally, the resulting biomechanical component of this work allows to have an idea about the influence of certain parameters on the structural behavior of the oral cavity, during maxillary expansion processes. According to the results, the interdigitation degree and the anchorage type used for the expansion are the variables that have the greatest impact on the mechanical response of the structure. As evidenced, both two-dimensional and three-dimensionally, the interdigitation level has little influence on the displacements but does affect the stress levels to which the bone-suture-bone interface is exposed when subjected to expansion loads. On the other hand, the anchorage type affects the distribution and magnitude of both displacements and stresses. It was found that the skeletal anchorage is more effective in terms of the expansion achieved but generates significant increases in the stress levels of the tissue that surrounds the bone supports. This study is able to simulate clinical outcomes and can be considered as a basis to analyze variations in the clinical protocol or the effect of other parameters such as the viscoelastic properties of the suture.

Appendix A

Certificate of ethical approval of the experimental protocol


 UFMG	<p>UNIVERSIDADE FEDERAL DE MINAS GERAIS</p> <p>CEUA COMISSÃO DE ÉTICA NO USO DE ANIMAIS</p>
<p>CERTIFICADO Certificamos que o Protocolo nº. 152 / 2016, relativo ao projeto intitulado "Determinação da relação de causalidade entre a magnitude das forças de expansão e a separação e ossificação da sutura palatina mediana em ca", que tem como responsável Tarcília Aparecida Silva, está de acordo com os Princípios Éticos da Experimentação Animal, adotados pela Comissão de Ética no Uso de Animais (CEUA/UFMG), tendo sido aprovado na reunião de 07/06/2016. Este certificado espira-se em 07/06/2021.</p>	
<p>CERTIFICATE We hereby certify that the Protocol nº. 152 / 2016, related to the Project entitled "Determination of the causal relationship between the magnitude of the expansion forces and the separation and ossification of the midpalatal", under the supervision of Tarcília Aparecida Silva, is in agreement with the Ethical Principles in Animal Experimentation, adopted by the Ethics Committee in Animal Experimentation (CEUA/UFMG), and was approved in 07/06/2016. This certificate expires in 07/06/2021.</p>	
<p>Cleuza Maria de Faria Rezende Coordenador(a) da CEUA/UFMG Belo Horizonte, 07/06/2016.</p>	
<p>Atenciosamente.</p>	
<p>Sistema CEUA-UFMG https://www.ufmg.br/bioetica/cetea/ceua/</p>	<p>Universidade Federal de Minas Gerais Avenida Antônio Carlos, 6627 – Campus Pampulha Unidade Administrativa II – 2º Andar, Sala 2005 31270-901 – Belo Horizonte, MG – Brasil Telefone: (31) 3499-4516 – Fax: (31) 3499-4592 www.ufmg.br/bioetica/cetea - cetea@prpq.ufmg.br</p>

Figure A-1: Certificate of ethical approval of the experimental protocol.

Appendix B

Results of the tests carried out to calculate the diffusion coefficients

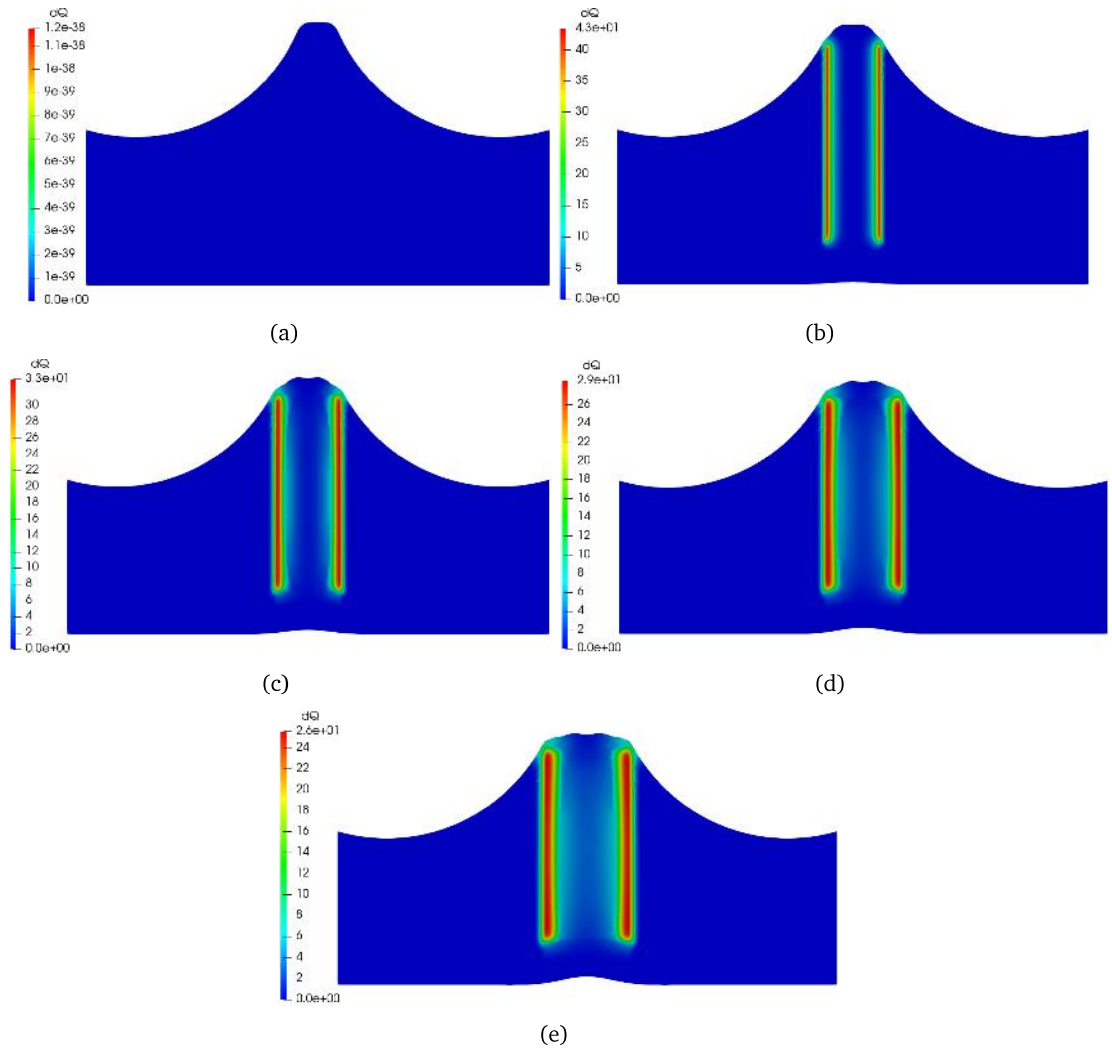


Figure B-1: Results obtained for the chemoattractant concentration with $D_p = 0.1$. a) $t = 0$ time units. b) $t = 10$ time units. c) $t = 20$ time units. d) $t = 30$ time units. e) $t = 40$ time units.

APPENDIX B. RESULTS OF THE TESTS CARRIED OUT TO CALCULATE THE
DIFFUSION COEFFICIENTS

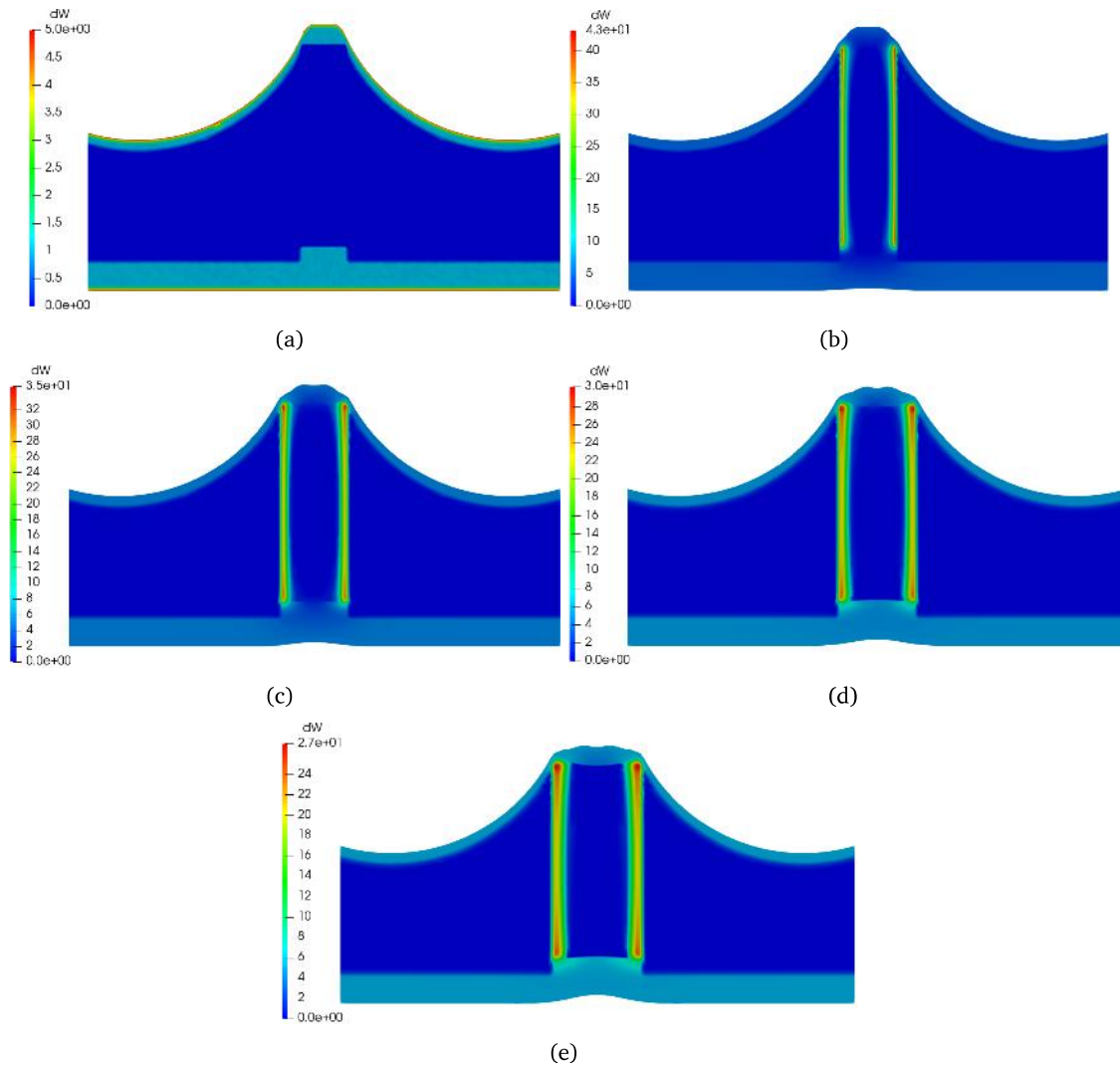


Figure B-2: Results obtained for the cellular migration with $D_p = 0.1$. a) $t = 0$ time units. b) $t = 10$ time units. c) $t = 20$ time units. d) $t = 30$ time units. e) $t = 40$ time units.

APPENDIX B. RESULTS OF THE TESTS CARRIED OUT TO CALCULATE THE DIFFUSION COEFFICIENTS

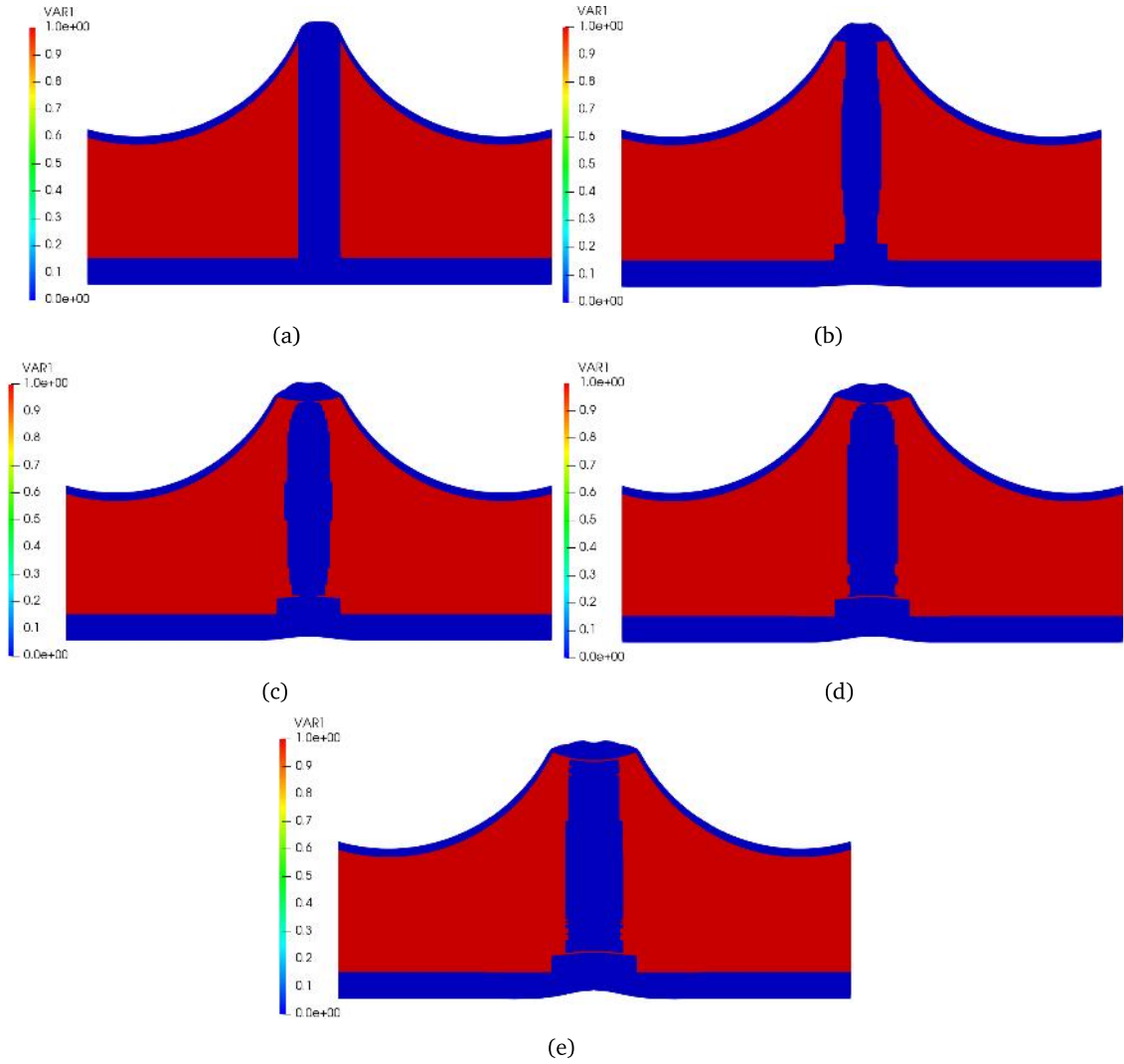


Figure B-3: Results obtained for the ossification with $D_p = 0.1$. a) $t = 0$ time units. b) $t = 10$ time units. c) $t = 20$ time units. d) $t = 30$ time units. e) $t = 40$ time units.

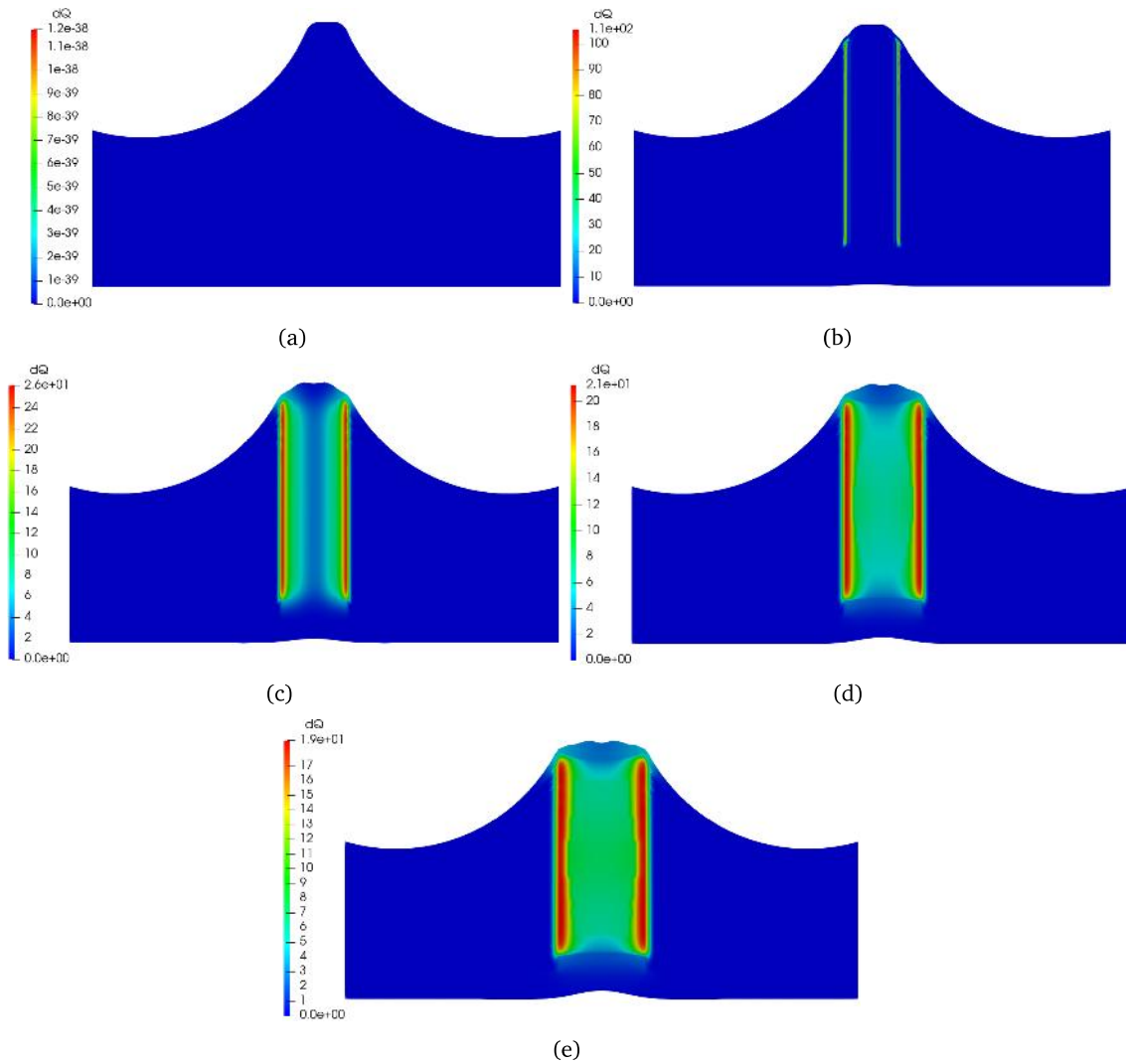


Figure B-4: Results obtained for the chemoattractant concentration with $D_p = 0.4$. a) $t = 0$ time units. b) $t = 10$ time units. c) $t = 20$ time units. e) $t = 30$ time units. e) $t = 40$ time units.

APPENDIX B. RESULTS OF THE TESTS CARRIED OUT TO CALCULATE THE DIFFUSION COEFFICIENTS

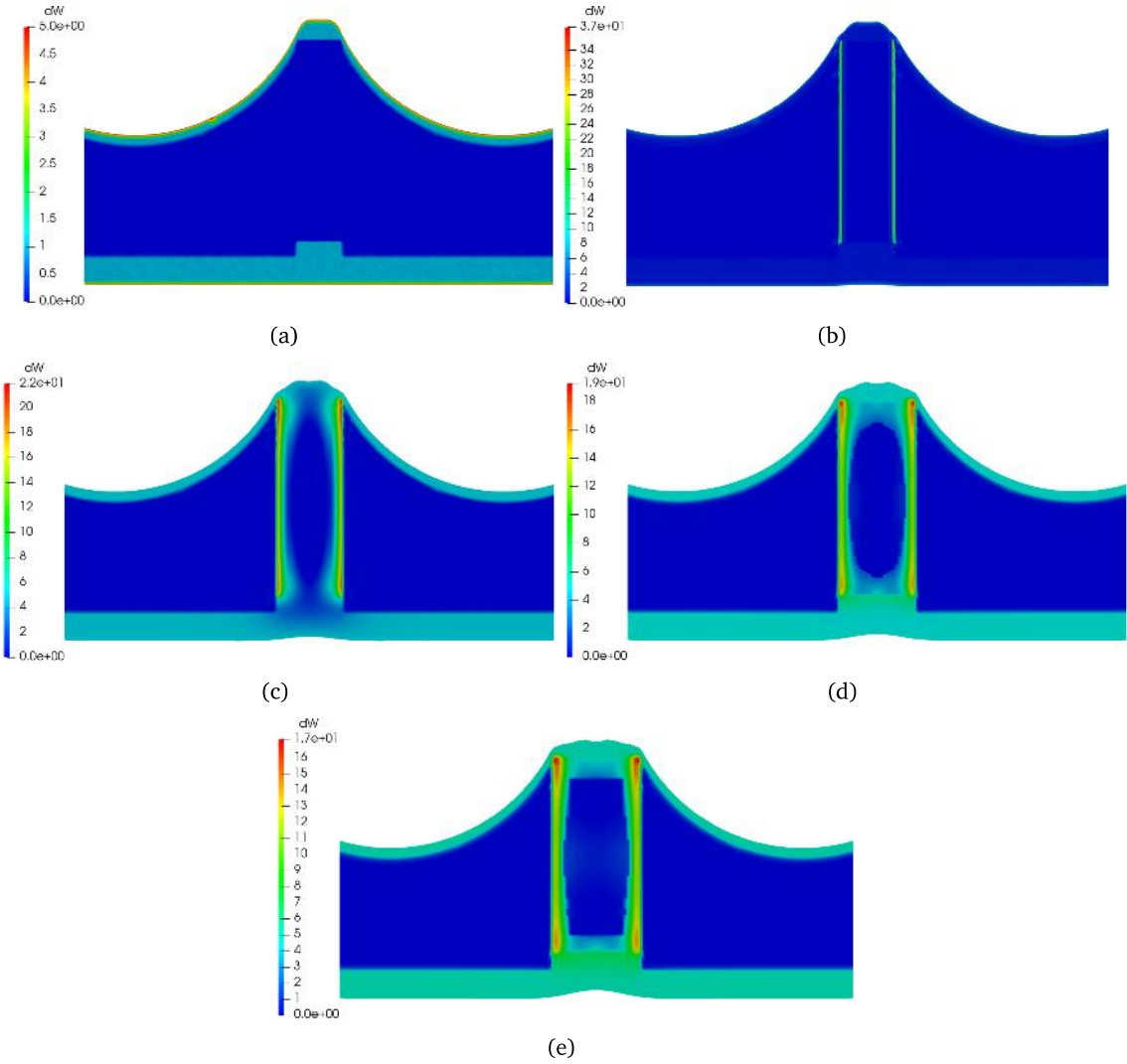


Figure B-5: Results obtained for the cellular migration with $D_p = 0.4$. a) $t = 0$ time units. b) $t = 10$ time units. c) $t = 20$ time units. e) $t = 30$ time units. e) $t = 40$ time units.

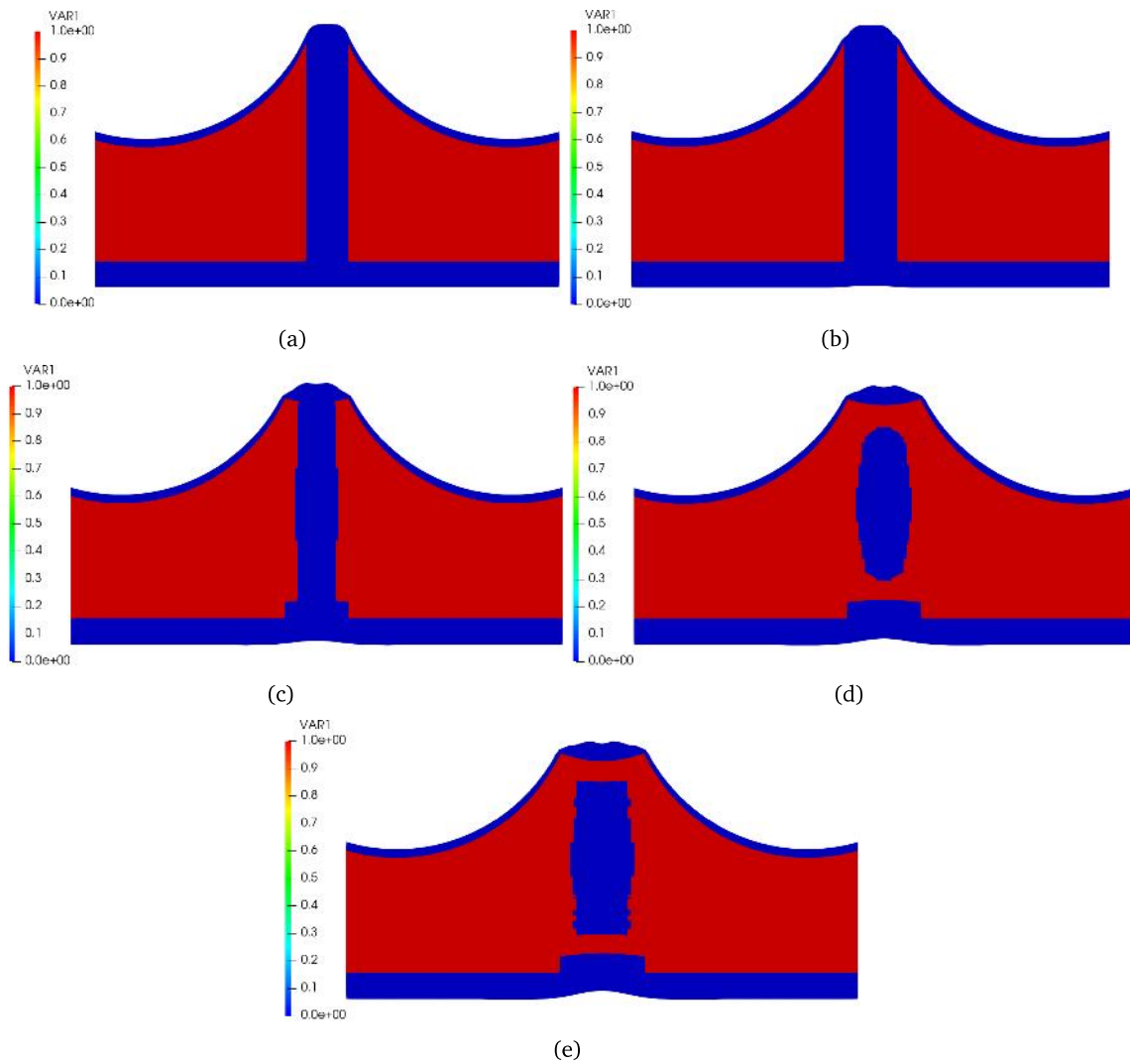


Figure B-6: Results obtained for the ossification with $D_p = 0.4$. a) $t = 0$ time units. b) $t = 10$ time units. c) $t = 20$ time units. d) $t = 30$ time units. e) $t = 40$ time units.

APPENDIX B. RESULTS OF THE TESTS CARRIED OUT TO CALCULATE THE DIFFUSION COEFFICIENTS

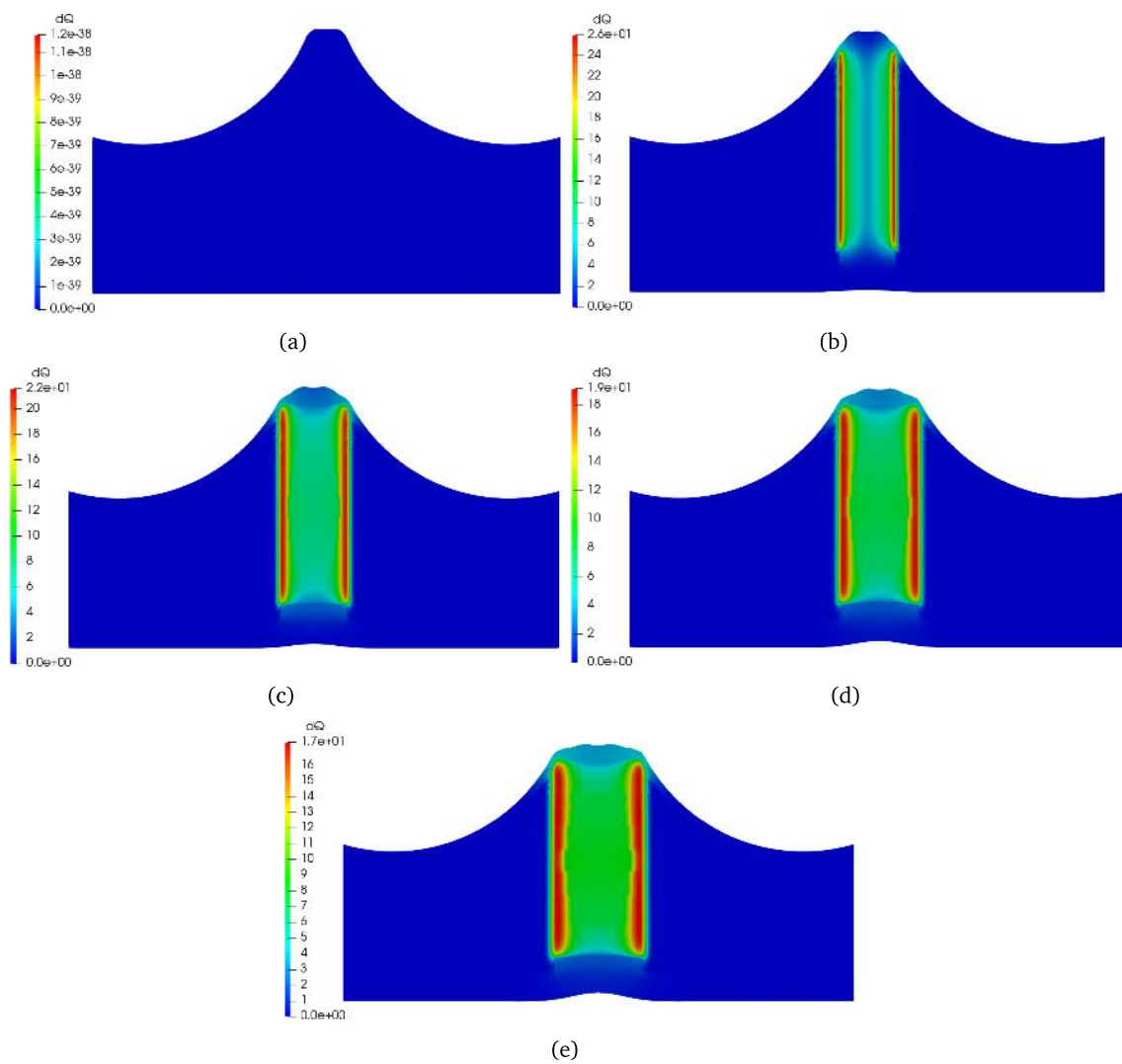


Figure B-7: Results obtained for the chemoattractant concentration with $D_p = 0.5$. a) $t = 0$ time units. b) $t = 10$ time units. c) $t = 20$ time units. e) $t = 30$ time units. e) $t = 40$ time units.

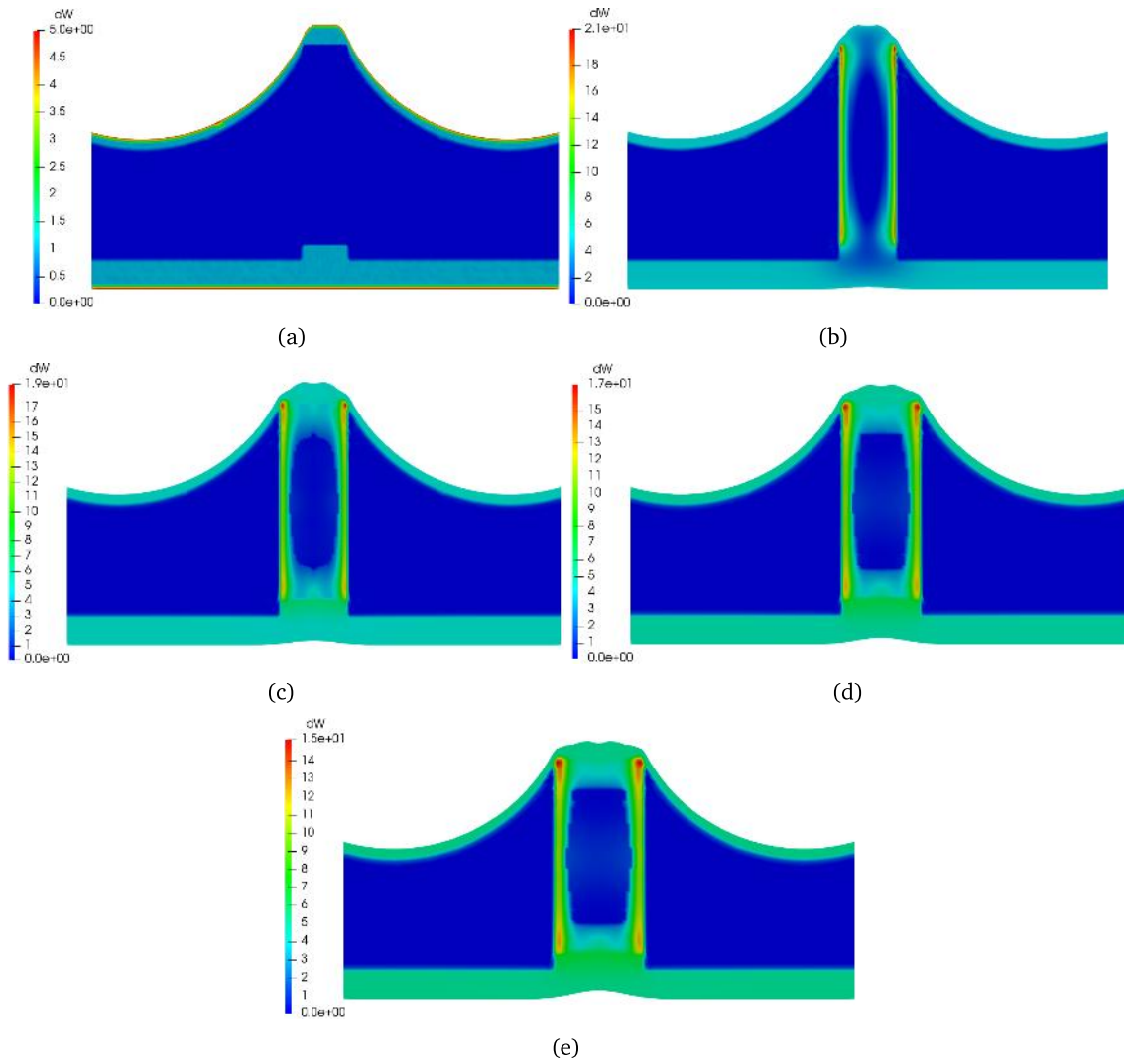


Figure B-8: Results obtained for the cellular migration with $D_p = 0.5$. a) $t = 0$ time units. b) $t = 10$ time units. c) $t = 20$ time units. d) $t = 30$ time units. e) $t = 40$ time units.

APPENDIX B. RESULTS OF THE TESTS CARRIED OUT TO CALCULATE THE DIFFUSION COEFFICIENTS

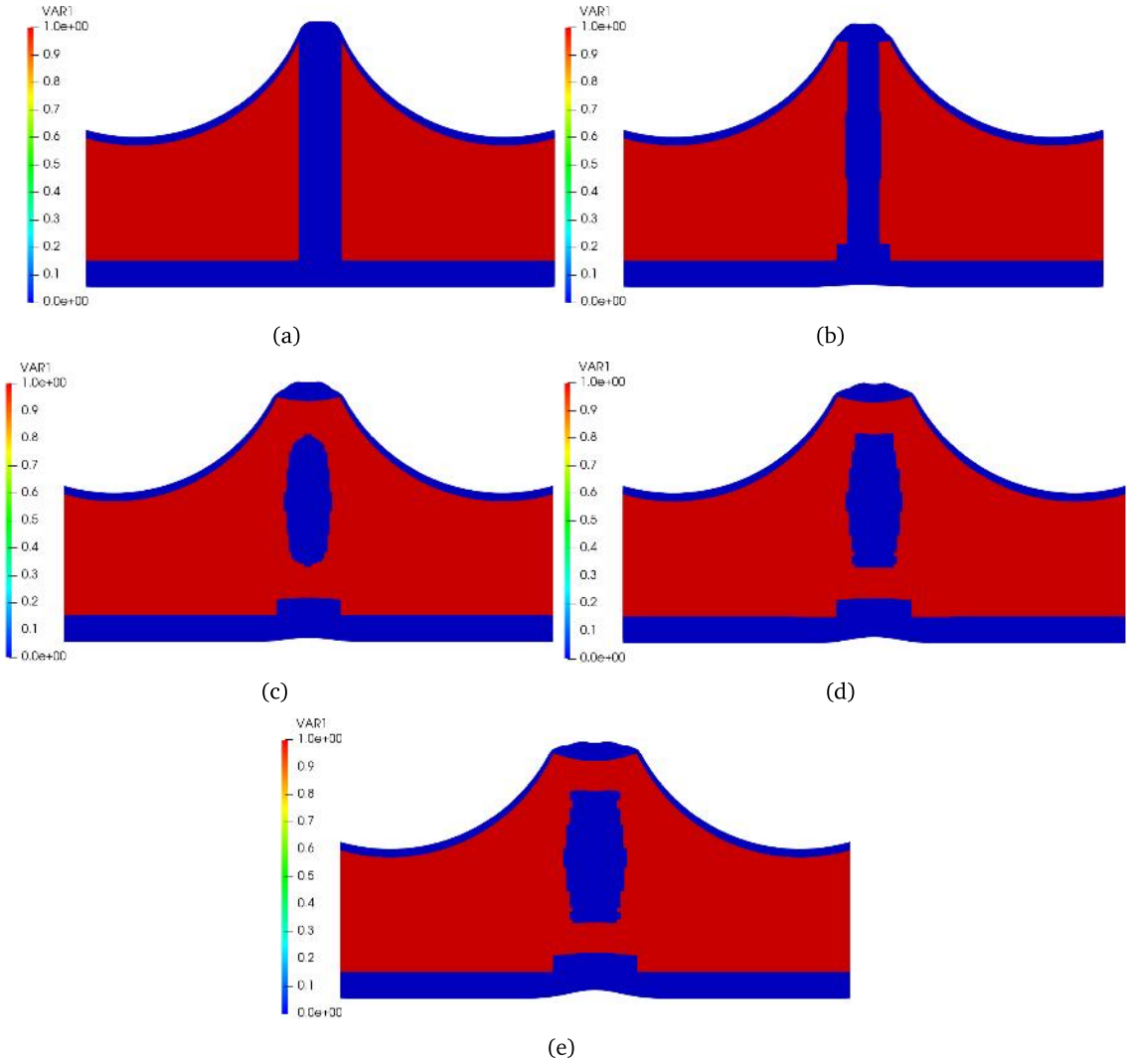


Figure B-9: Results obtained for the ossification with $D_p = 0.5$. a) $t = 0$ time units. b) $t = 10$ time units. c) $t = 20$ time units. d) $t = 30$ time units. e) $t = 40$ time units.

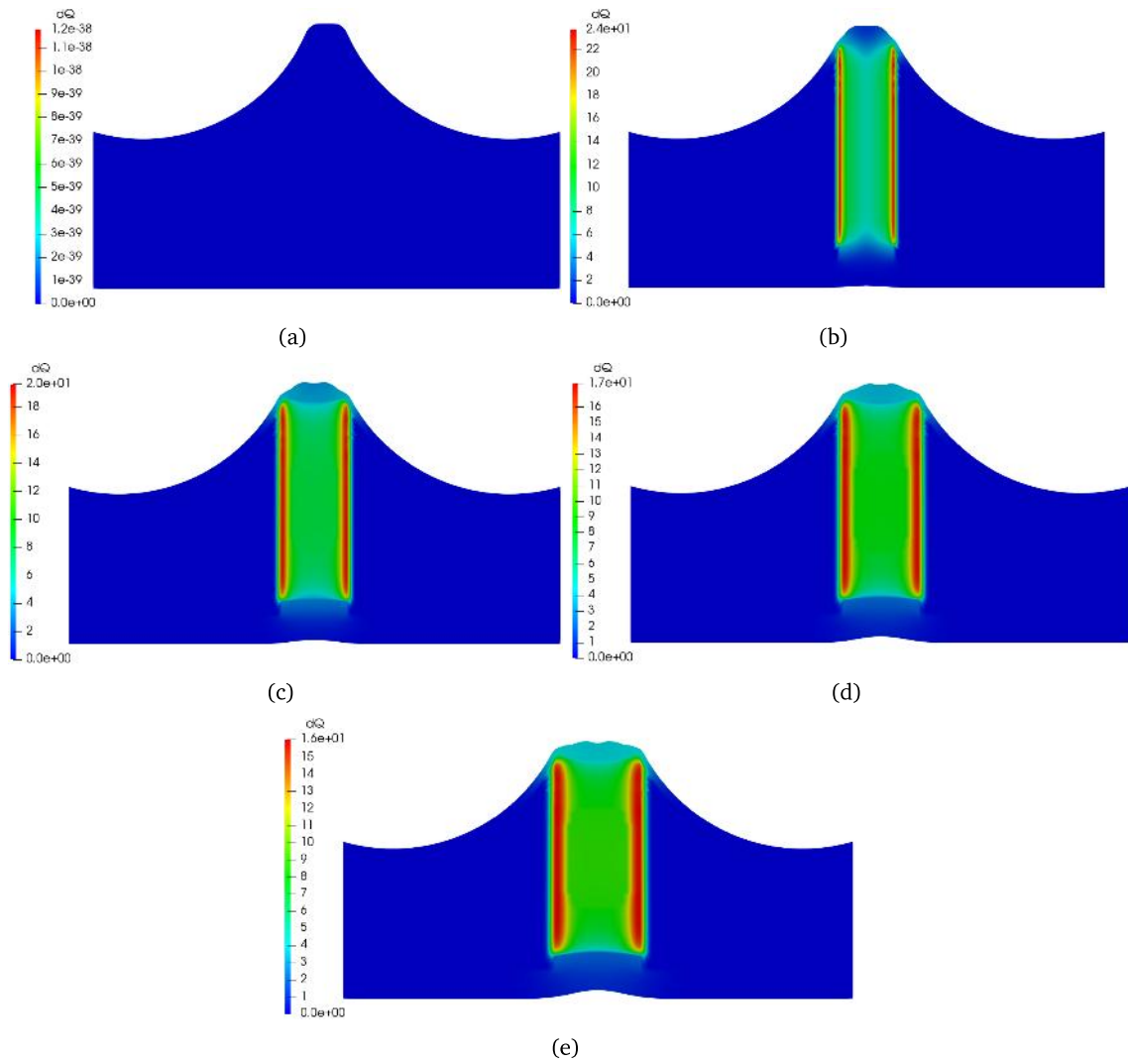


Figure B-10: Results obtained for the chemoattractant concentration with $D_p = 0.7$. a) $t = 0$ time units. b) $t = 10$ time units. c) $t = 20$ time units. d) $t = 30$ time units. e) $t = 40$ time units.

APPENDIX B. RESULTS OF THE TESTS CARRIED OUT TO CALCULATE THE
 DIFFUSION COEFFICIENTS

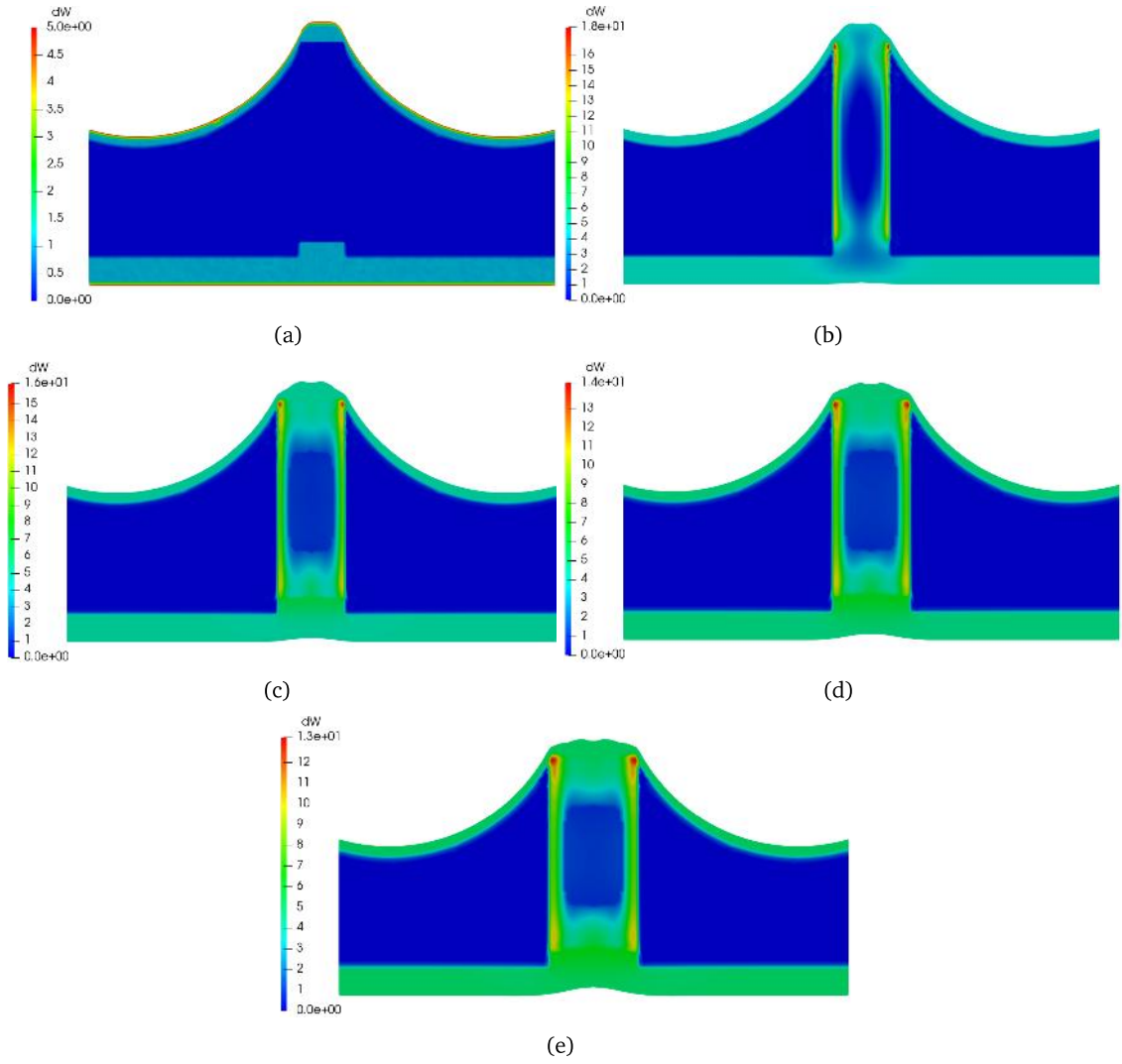


Figure B-11: Results obtained for the cellular migration with $D_p = 0.7$. a) $t = 0$ time units. b) $t = 10$ time units. c) $t = 20$ time units. e) $t = 30$ time units. e) $t = 40$ time units.

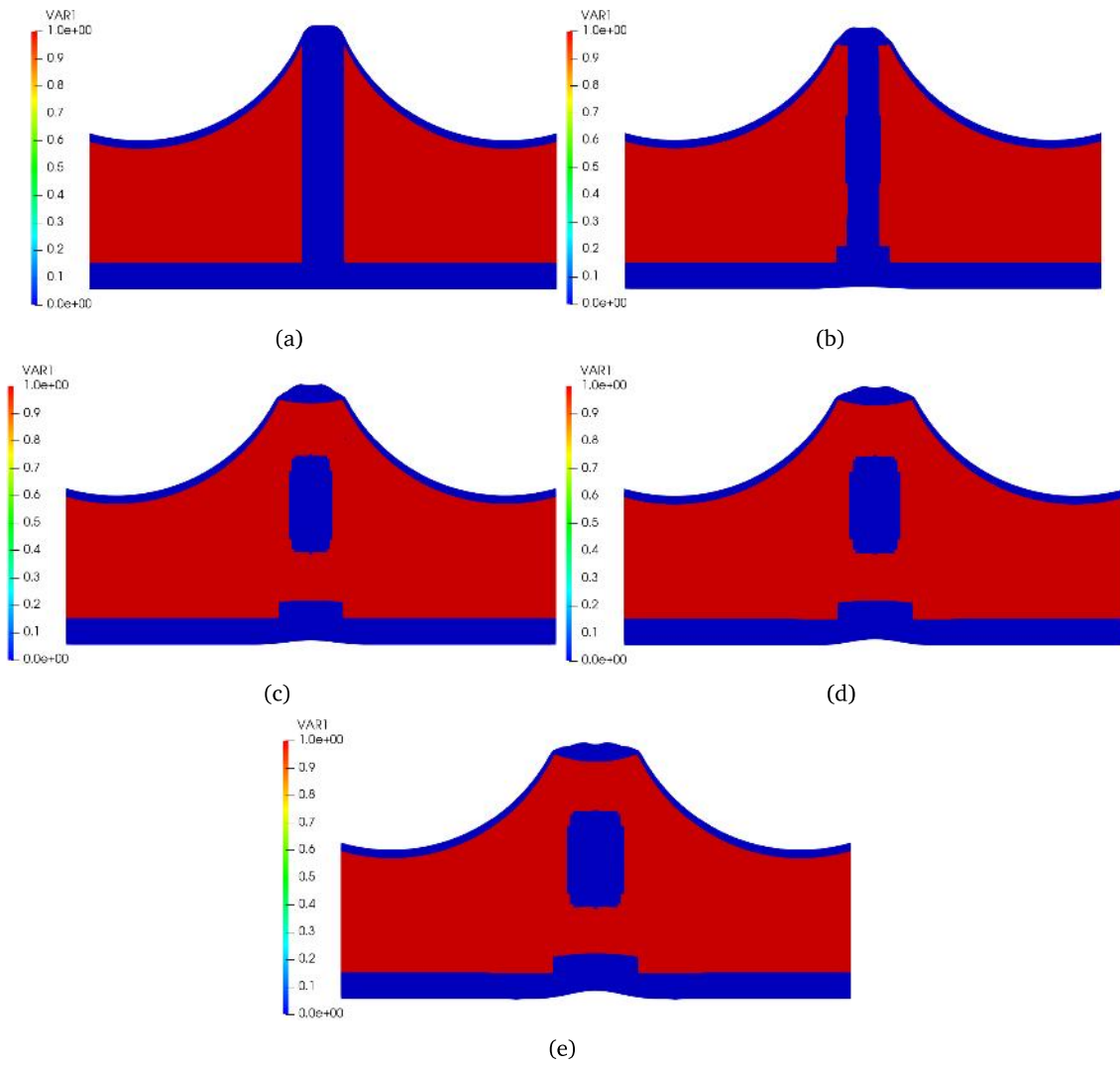


Figure B-12: Results obtained for the ossification with $D_p = 0.7$. a) $t = 0$ time units. b) $t = 10$ time units. c) $t = 20$ time units. d) $t = 30$ time units. e) $t = 40$ time units.

APPENDIX B. RESULTS OF THE TESTS CARRIED OUT TO CALCULATE THE DIFFUSION COEFFICIENTS

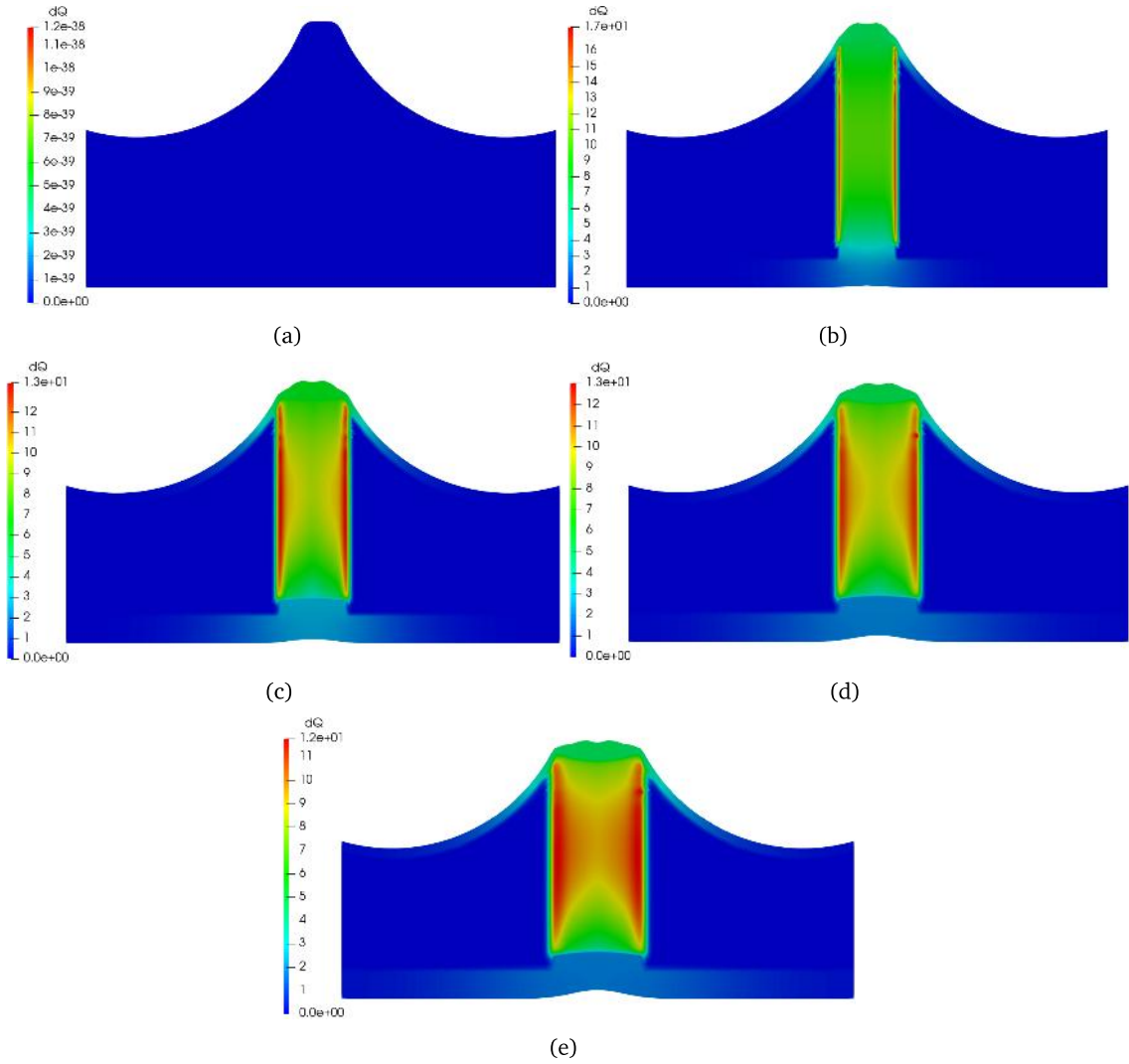


Figure B-13: Results obtained for the chemoattractant concentration with $D_p = 1.0$. a) $t = 0$ time units. b) $t = 10$ time units. c) $t = 20$ time units. d) $t = 30$ time units. e) $t = 40$ time units.

APPENDIX B. RESULTS OF THE TESTS CARRIED OUT TO CALCULATE THE
DIFFUSION COEFFICIENTS

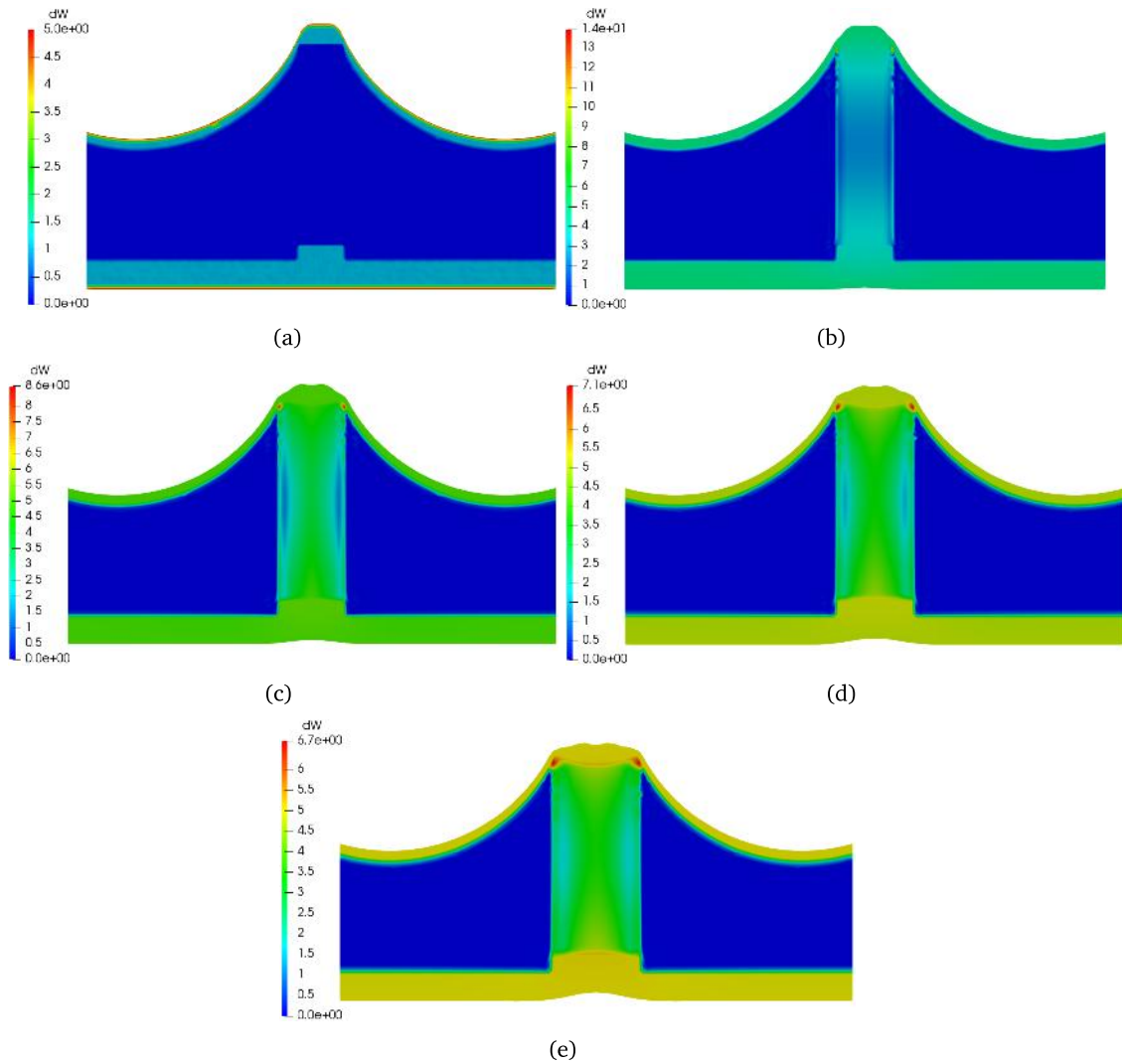


Figure B-14: Results obtained for the cellular migration with $D_p = 1.0$. a) $t = 0$ time units. b) $t = 10$ time units. c) $t = 20$ time units. d) $t = 30$ time units. e) $t = 40$ time units.

APPENDIX B. RESULTS OF THE TESTS CARRIED OUT TO CALCULATE THE DIFFUSION COEFFICIENTS

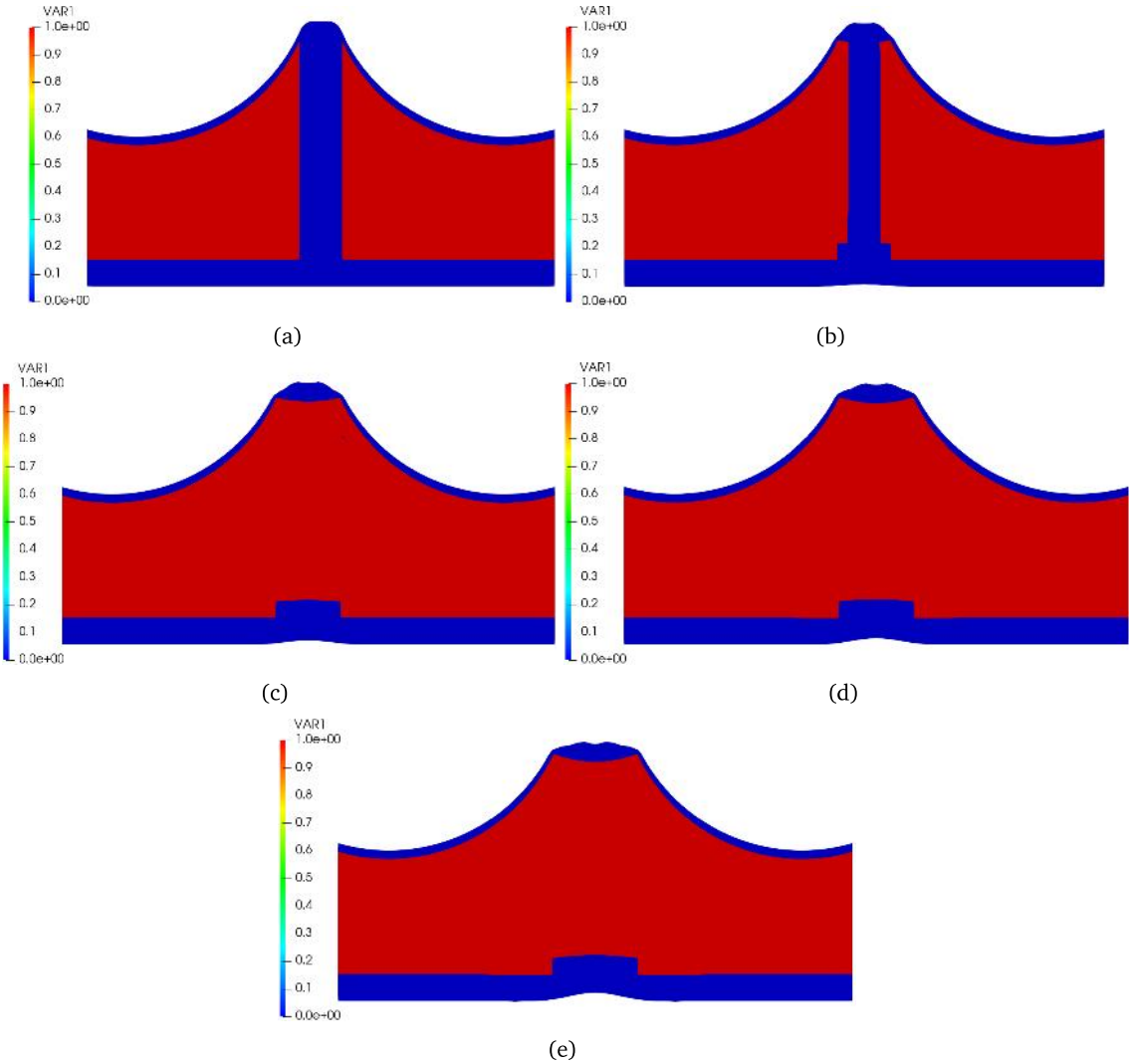


Figure B-15: Results obtained for the ossification with $D_p = 1.0$. a) $t = 0$ time units. b) $t = 10$ time units. c) $t = 20$ time units. d) $t = 30$ time units. e) $t = 40$ time units.

Appendix C

Graphical results obtained for the biomechanical 2D model

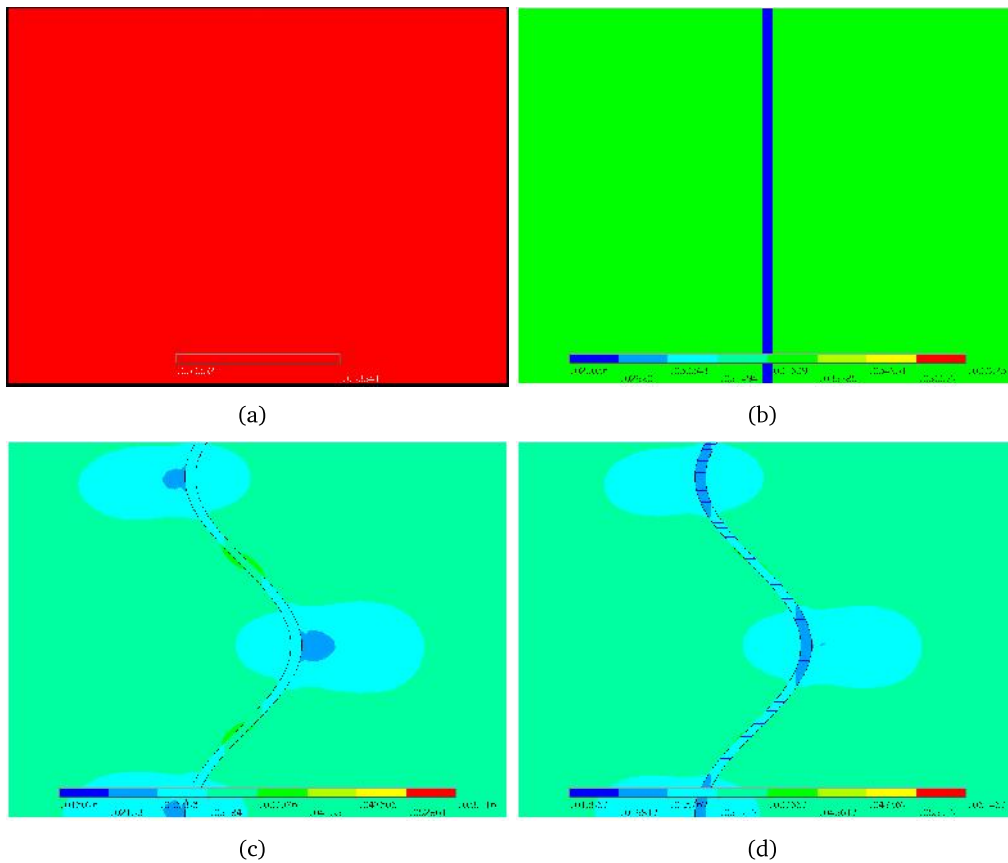


Figure C-1: First principal stress obtained for the models in tension: Null interdigitation a) without and b) with collagen fibers; Moderate interdigitation c) without and d) with collagen fibers.

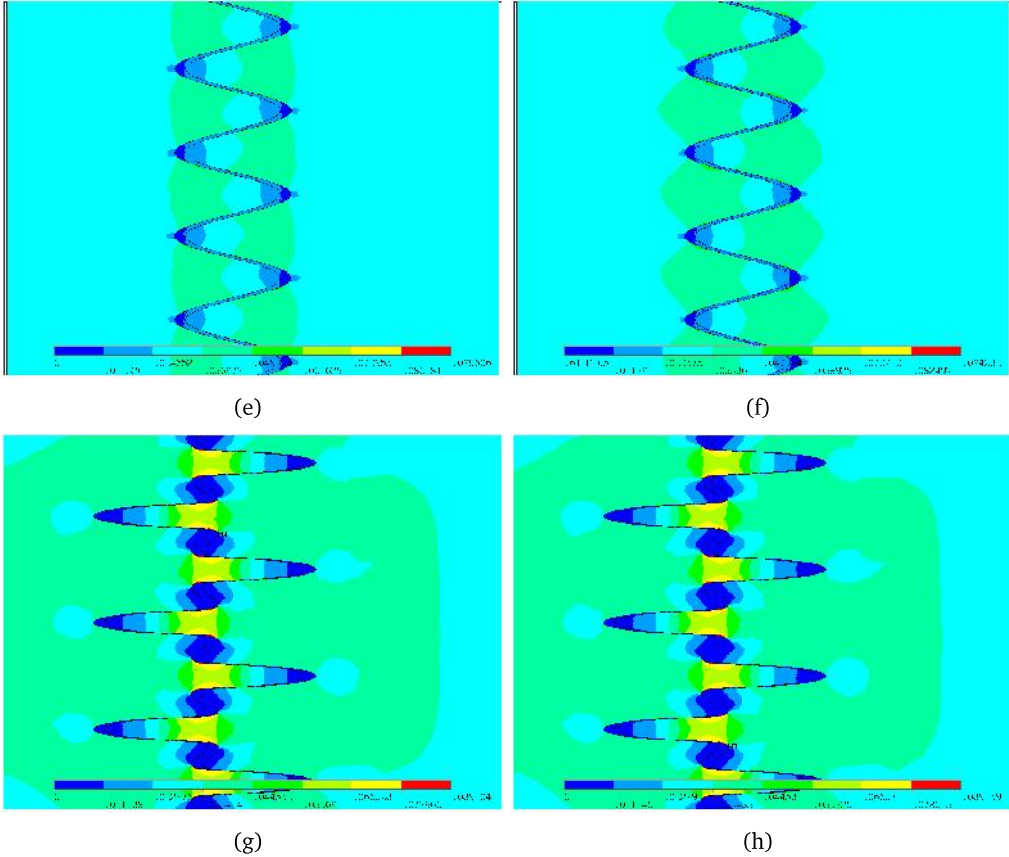


Figure C-1 (Continued): First principal stress obtained for the models in tension: Complex interdigitation e) without and f) with collagen fibers; Fractal interdigitation g) without and h) with collagen fibers.

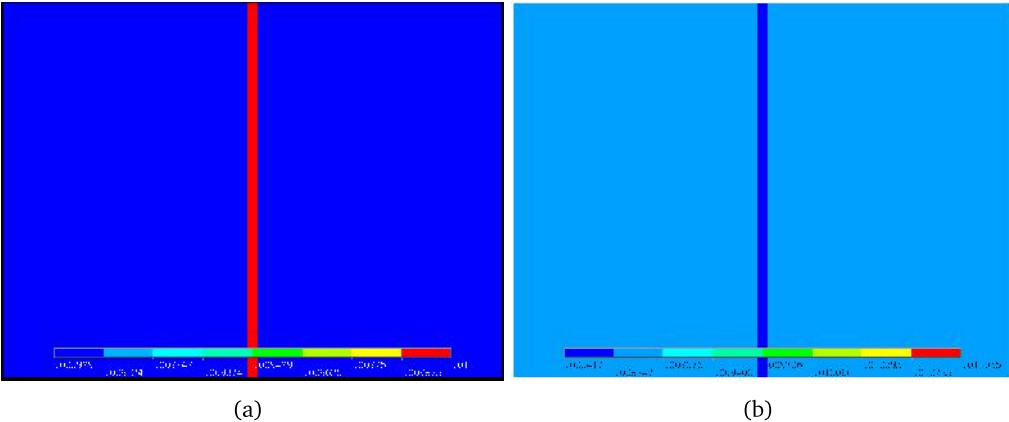


Figure C-2: Second principal stress obtained for the models in tension: Null interdigitation a) without and b) with collagen fibers.

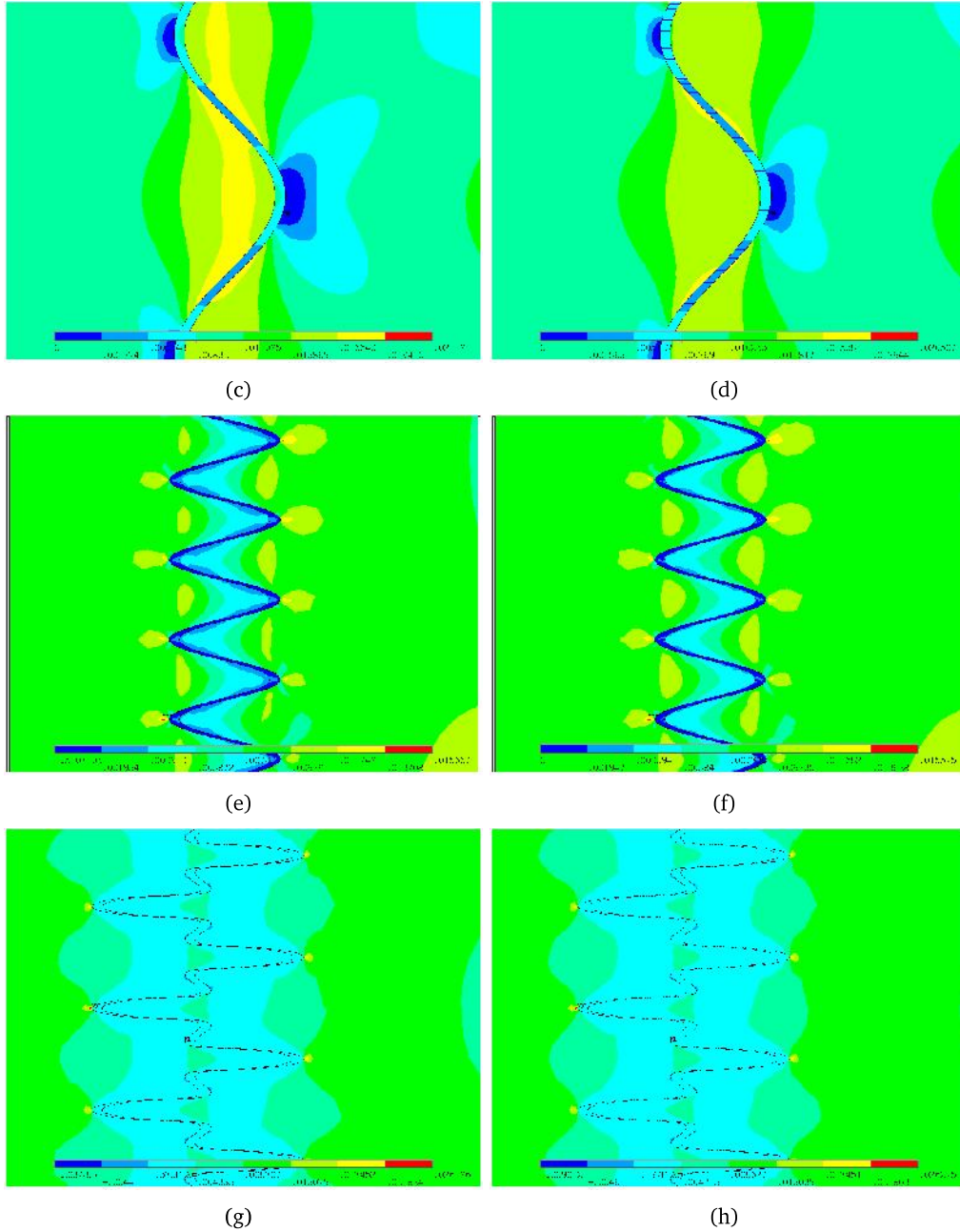


Figure C-2 (Continued): Second principal stress obtained for the models in tension: Moderate interdigitation c) without and d) with collagen fibers; Complex interdigitation e) without and f) with collagen fibers; Fractal interdigitation g) without and h) with collagen fibers.

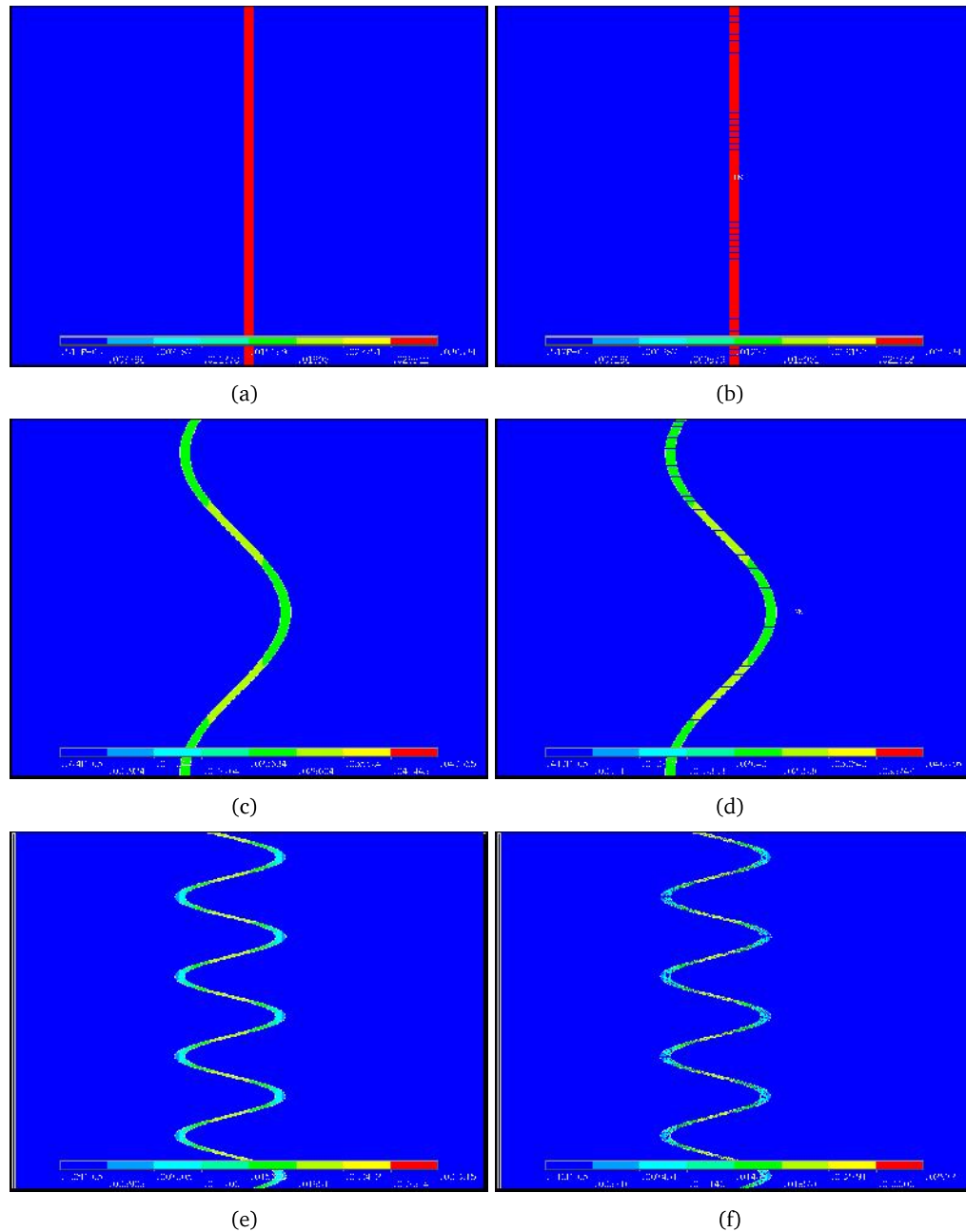


Figure C-3: First principal strain obtained for the models in tension: Null interdigitation a) without and b) with collagen fibers; Moderate interdigitation c) without and d) with collagen fibers; Complex interdigitation e) without and f) with collagen fibers.

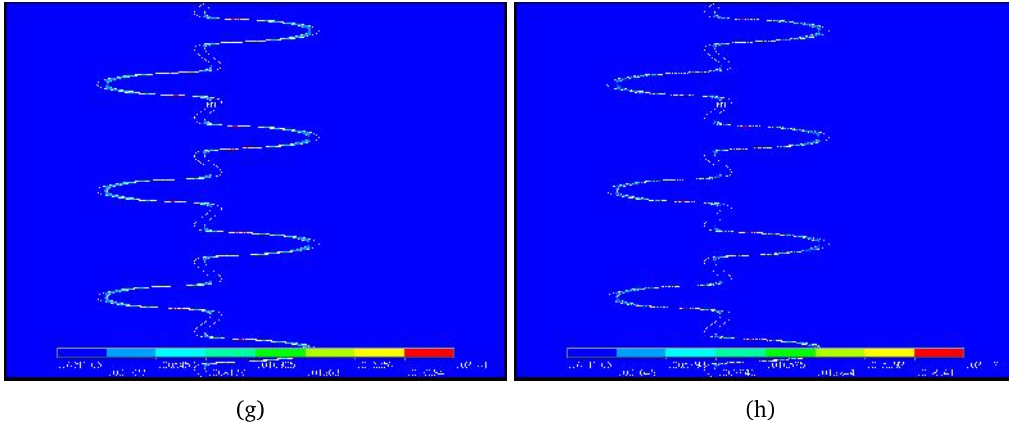


Figure C-3 (Continued): First principal strain obtained for the models in tension: Fractal interdigitation g) without and h) with collagen fibers.

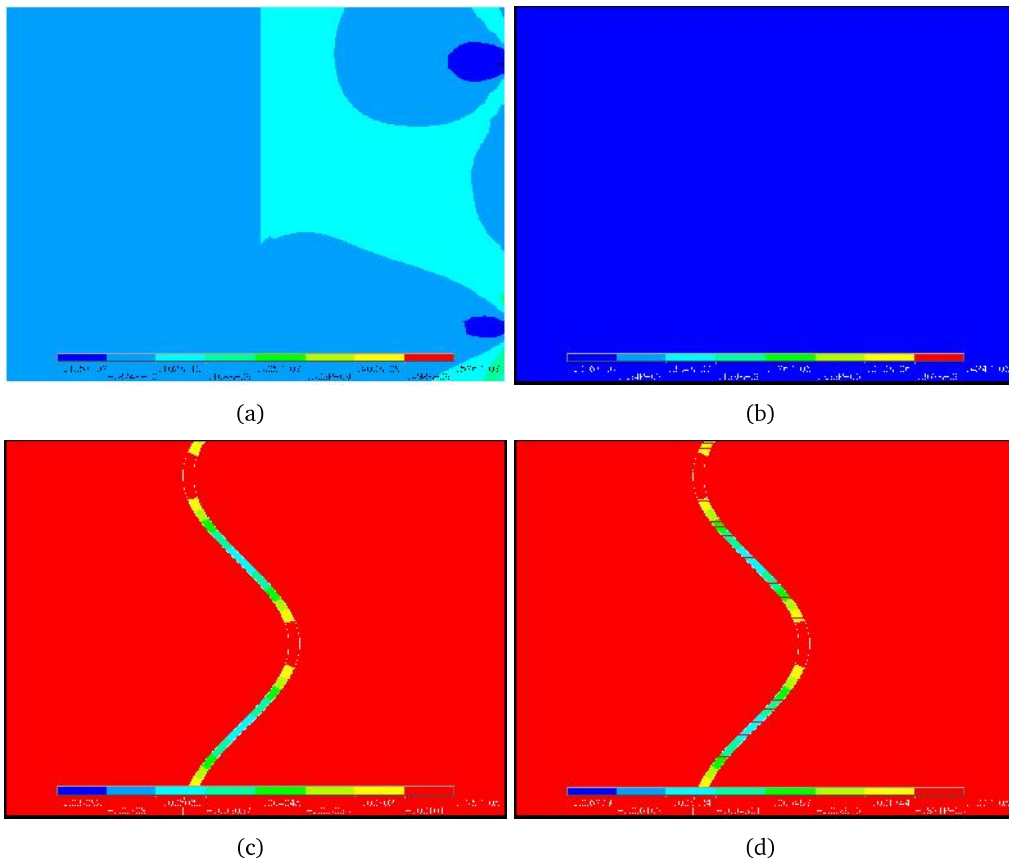


Figure C-4: Second principal strain obtained for the models in tension: Null interdigitation a) without and b) with collagen fibers; Moderate interdigitation c) without and d) with collagen fibers.

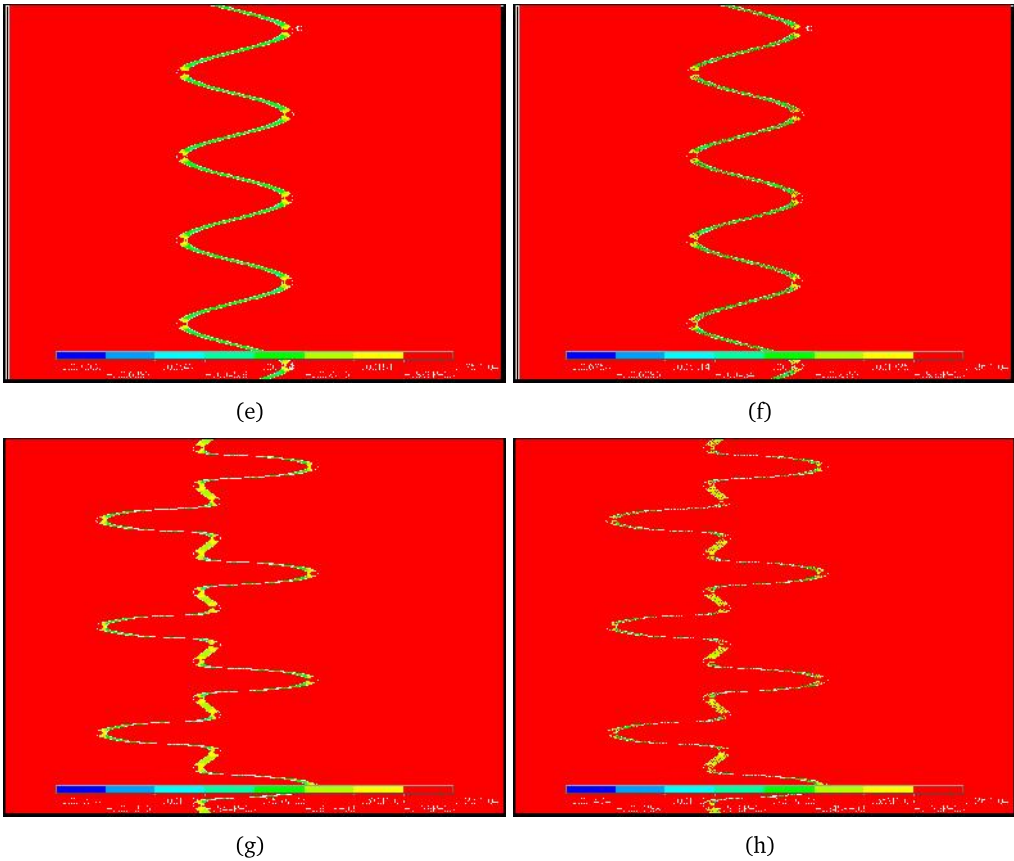


Figure C-4 (Continued): Second principal strain obtained for the models in tension: Complex interdigitation e) without and f) with collagen fibers; Fractal interdigitation g) without and h) with collagen fibers.

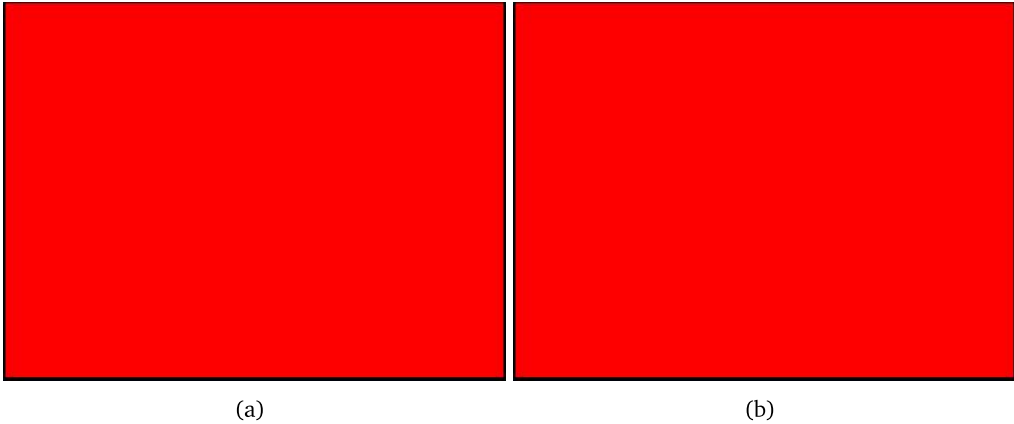


Figure C-5: First principal stress obtained for the models in compression: Null interdigitation a) without and b) with collagen fibers.

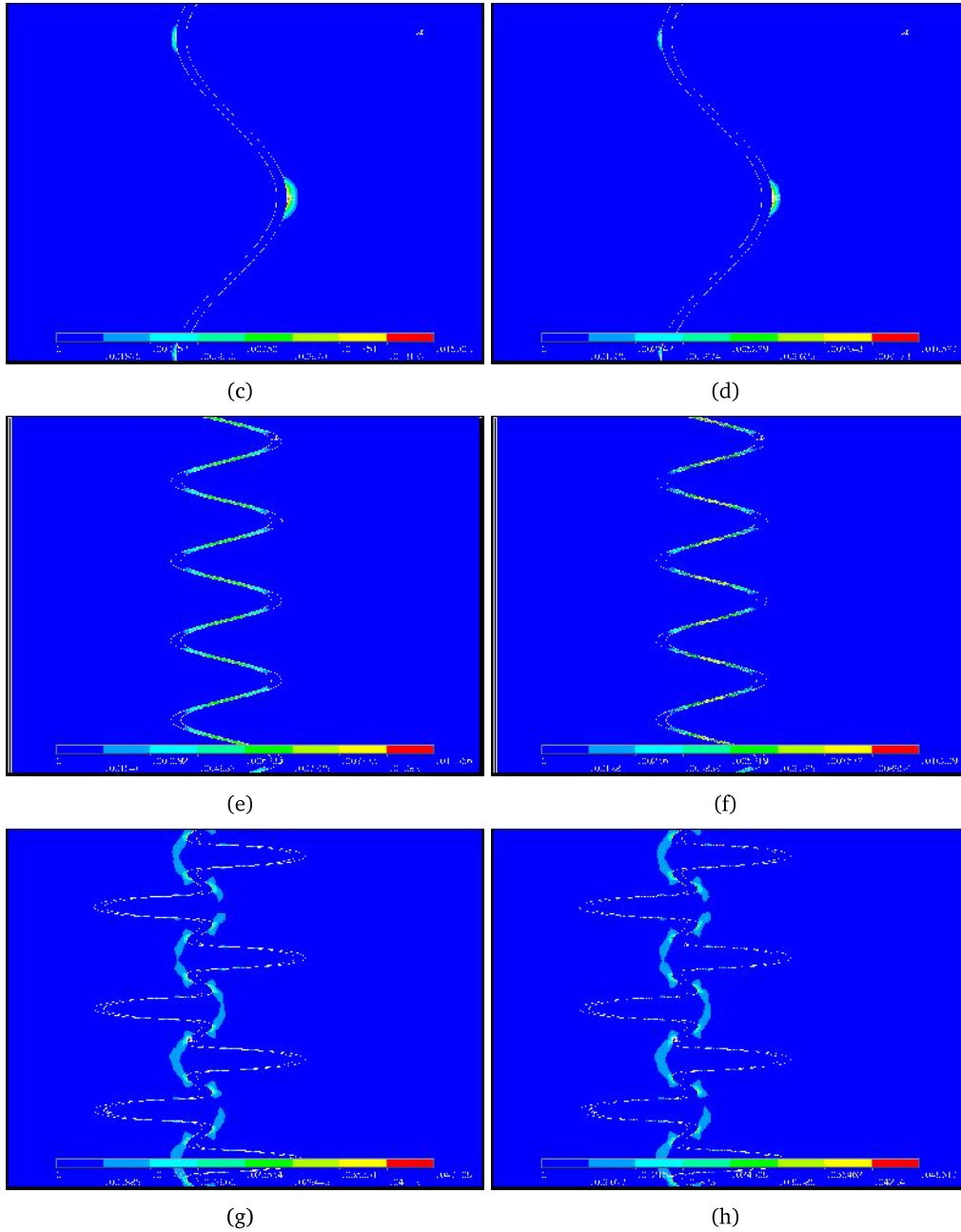


Figure C-5 (Continued): First principal stress obtained for the models in compression: Moderate interdigitation c) without and d) with collagen fibers; Complex interdigitation e) without and f) with collagen fibers; Fractal interdigitation g) without and h) with collagen fibers.

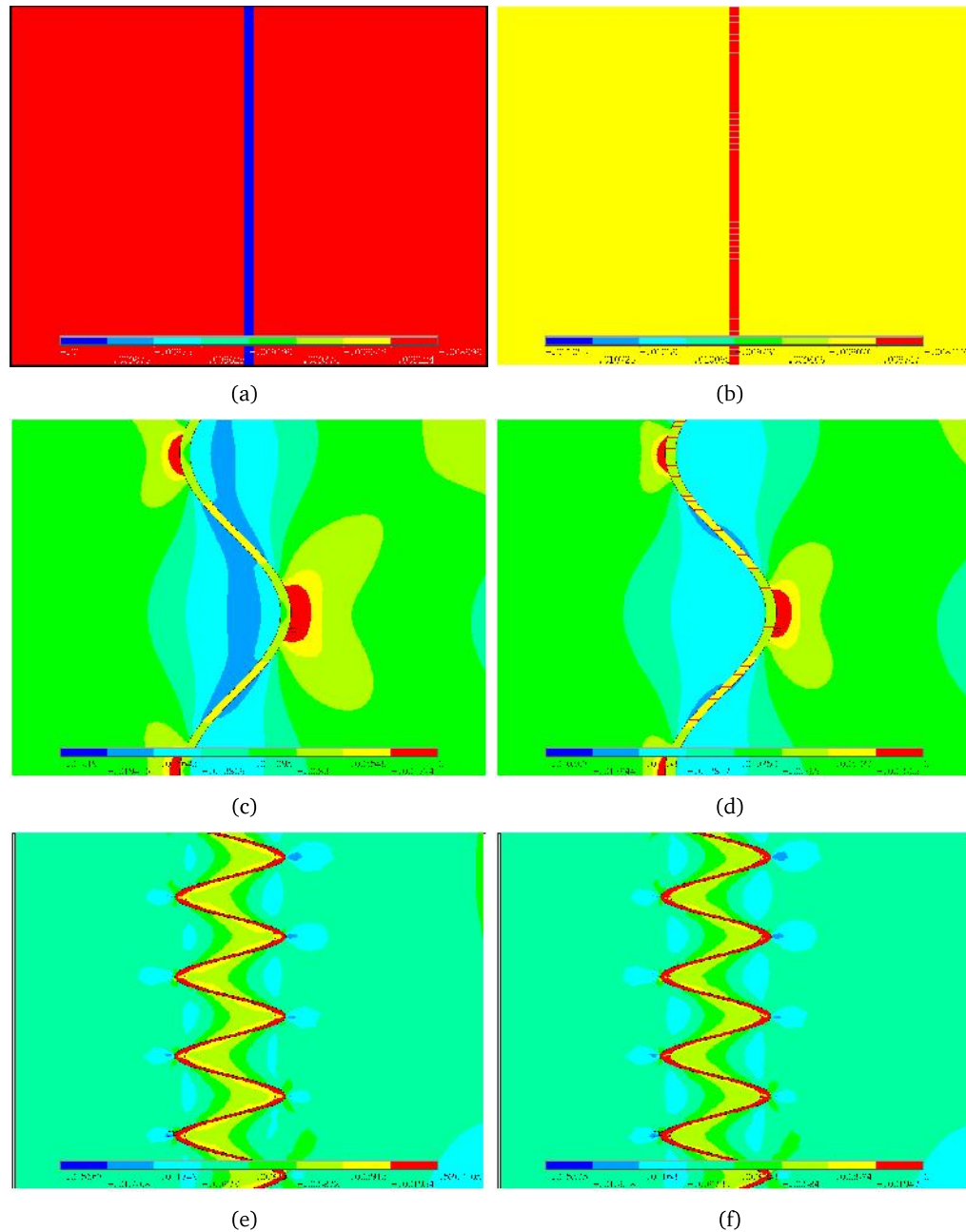


Figure C-6: Second principal stress obtained for the models in compression: Null interdigitation a) without and b) with collagen fibers; Moderate interdigitation c) without and d) with collagen fibers; Complex interdigitation e) without and f) with collagen fibers.

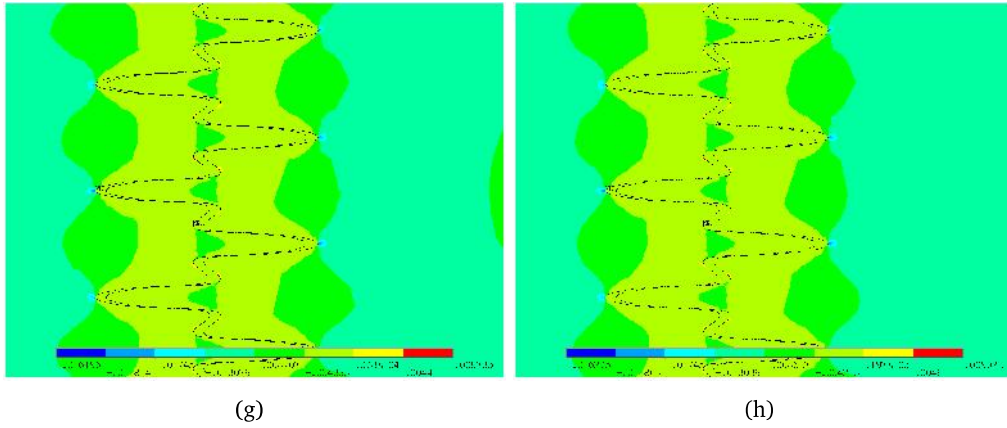


Figure C-6 (Continued): Second principal stress obtained for the models in compression: Fractal interdigitation g) without and h) with collagen fibers.

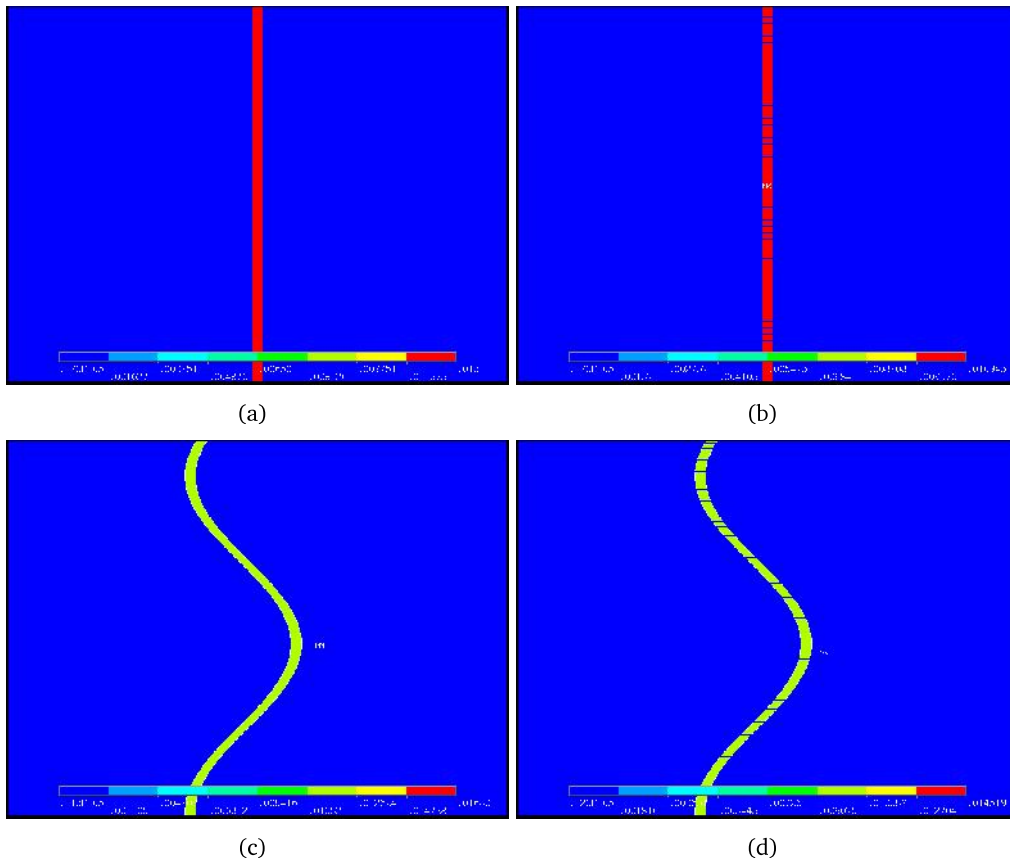


Figure C-7: First principal strain obtained for the models in compression: Null interdigitation a) without and b) with collagen fibers; Moderate interdigitation c) without and d) with collagen fibers.

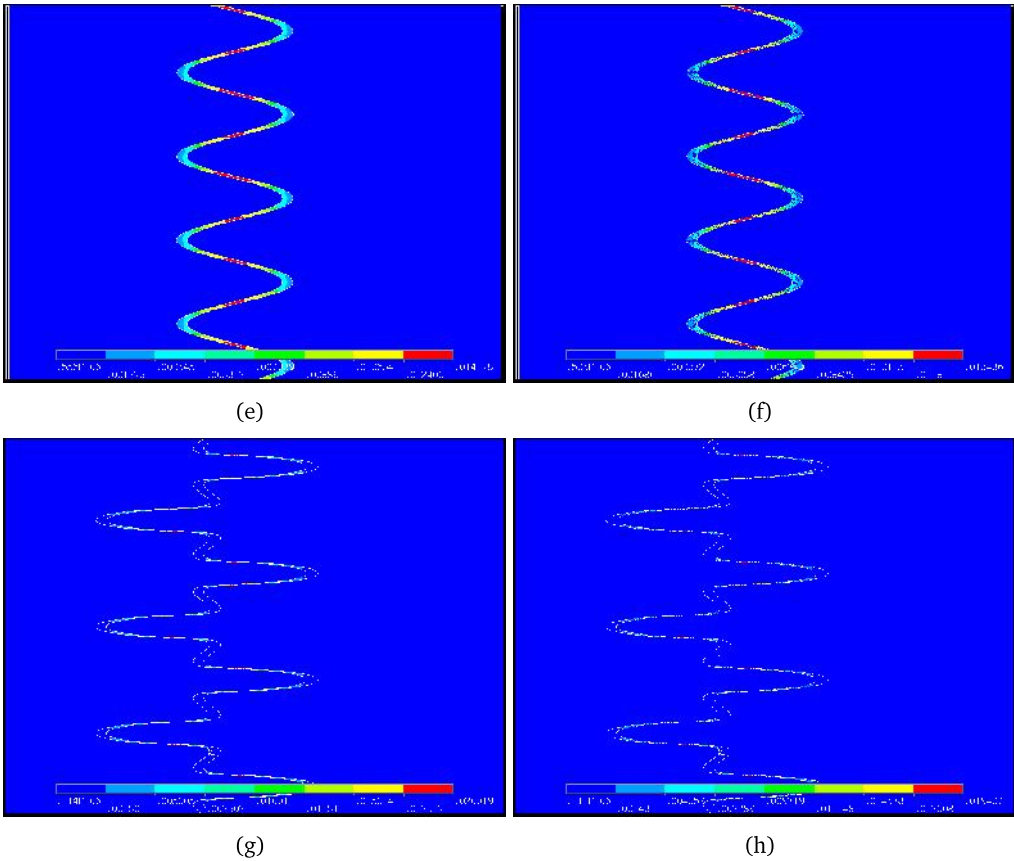


Figure C-7 (Continued): First principal strain obtained for the models in compression: Complex interdigitation e) without and f) with collagen fibers; Fractal interdigitation g) without and h) with collagen fibers.

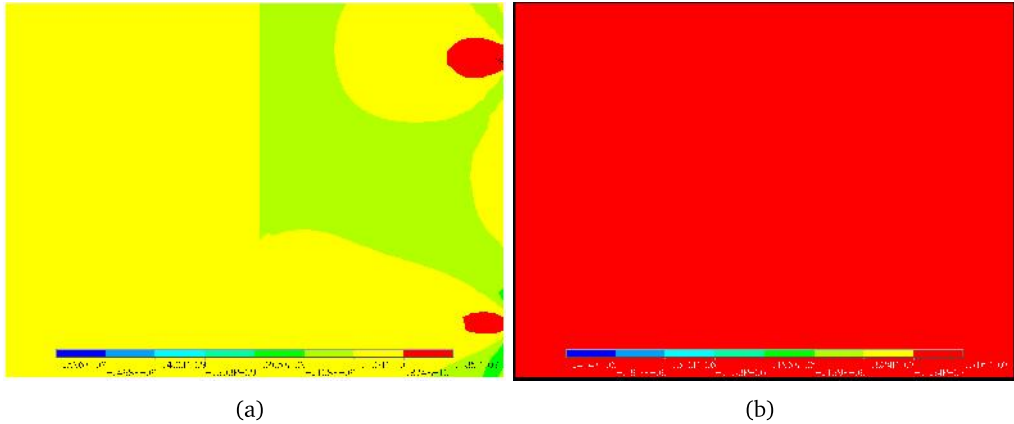


Figure C-8: Second principal strain obtained for the models in compression: Null interdigitation a) without and b) with collagen fibers.

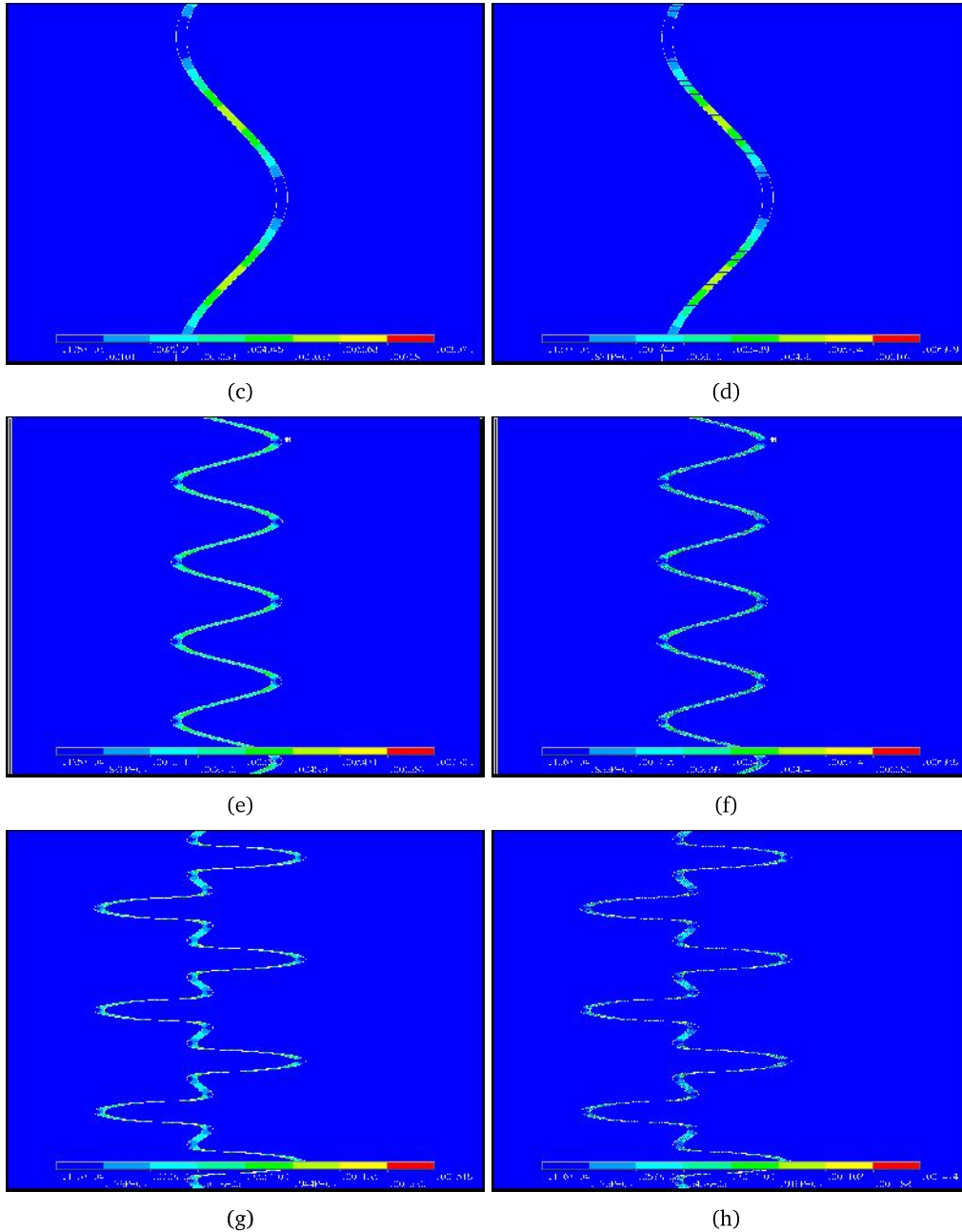


Figure C-8 (Continued): Second principal strain obtained for the models in compression: Moderate interdigitation c) without and d) with collagen fibers; Complex interdigitation e) without and f) with collagen fibers; Fractal interdigitation g) without and h) with collagen fibers.

Bibliography

- [1] G. A. Ramieri, M. C. Spada, M. Austa, S. D. Bianchi, and S. Berrone, "Transverse maxillary distraction with a bone-anchored appliance: Dento-periodontal effects and clinical and radiological results," *International Journal of Oral and Maxillofacial Surgery*, vol. 34, no. 4, pp. 357–363, 2005.
- [2] E. Garreau, J. Bouscaillou, S. Rattier, J. Ferri, and G. Raoul, "Bone-borne distractor versus tooth-borne distractor for orthodontic distraction after surgical maxillary expansion: The patient's point of view," *International Orthodontics*, vol. 14, no. 2, pp. 214–232, 2016.
- [3] V. A. Pereira-Filho, M. S. Monnazzi, M. A. C. Gabrielli, R. Spin-Neto, E. R. Watanabe, C. M. M. Gimenez, A. Santos-Pinto, and M. F. R. Gabrielli, "Volumetric upper airway assessment in patients with transverse maxillary deficiency after surgically assisted rapid maxillary expansion," *International journal of oral and maxillofacial surgery*, vol. 43, no. 5, pp. 581–586, 2014.
- [4] R. Lione, L. Franchi, and P. Cozza, "Does rapid maxillary expansion induce adverse effects in growing subjects?," *Angle Orthodontist*, vol. 83, no. 1, pp. 172–182, 2013.
- [5] C. Provatidis, B. Georgiopoulos, A. Kotinas, and J. P. McDonald, "On the FEM modeling of craniofacial changes during rapid maxillary expansion," *Medical Engineering and Physics*, vol. 29, no. 5, pp. 566–579, 2007.
- [6] A. Kumar, D. Gurunathan, Muruganandham, and S. Sharma, "Rapid Maxillary Expansion : A Unique Treatment Modality in Dentistry," *Journal of Clinical and Diagnostic Research*, vol. 5, no. 4, pp. 906–911, 2011.
- [7] D. Anderson, *Mosby's Pocket Dictionary of Medicine, Nursing & Health*. Mosby Elsevier, 7th ed., 2013.
- [8] B. Hou, N. Fukai, and B. R. Olsen, "Mechanical force-induced midpalatal suture remodeling in mice," *Bone*, vol. 40, no. 6, pp. 1483–1493, 2007.
- [9] F. Angelieri, L. H. S. Cevidanes, L. Franchi, J. R. Gonçalves, E. Benavides, and J. A. McNamara, "Midpalatal suture maturation: Classification method for individual assessment before rapid maxillary expansion," *American Journal of Orthodontics and Dentofacial Orthopedics*, vol. 144, no. 5, pp. 759–769, 2013.
- [10] J. P. Ennes and A. Consolaro, *Análise morfológica da sutura palatina mediana de ratos, de coelhos, de macacos e homens em diferentes fases do desenvolvimento cronológico*. PhD thesis, Universidade de São Paulo, 2002.
- [11] H. Suzuki, W. Moon, L. H. Previdente, S. S. Suzuki, A. S. Garcez, and A. Consolaro, "Miniscrew-assisted rapid palatal expander (MARPE): the quest for pure orthopedic movement," *Dental Press Journal of Orthodontics*, vol. 21, no. 4, pp. 17–23, 2016.

- [12] A. J. Haas, "Palatal expansion: Just the beginning of dentofacial orthopedics," *American Journal of Orthodontics*, vol. 57, no. 3, pp. 219–255, 1970.
- [13] C. Ciambotti, P. Ngan, M. Durkee, K. Kohli, H. Kim, and D. R. Musich, "A comparison of dental and dentoalveolar changes between rapid palatal expansion and nickel-titanium palatal expansion appliances," *American Journal of Orthodontics and Dentofacial Orthopedics*, vol. 119, no. 1, pp. 11–20, 2001.
- [14] Z. Sun, S. Hueni, B. C. Tee, and H. Kim, "Mechanical strain at alveolar bone and circummaxillary sutures during acute rapid palatal expansion," *American Journal of Orthodontics and Dentofacial Orthopedics*, vol. 139, no. 3, pp. e219–e228, 2011.
- [15] D. G. Garib, J. F. C. Henriques, G. Janson, M. R. de Freitas, and A. Y. Fernandes, "Periodontal effects of rapid maxillary expansion with tooth-tissue-borne and tooth-borne expanders: A computed tomography evaluation," *American Journal of Orthodontics and Dentofacial Orthopedics*, vol. 129, no. 6, pp. 749–758, 2006.
- [16] N. Erverdi, I. Okar, N. Küçükkeles, and S. Arbak, "A comparison of two different rapid palatal expansion techniques from the point of root resorption.," *American journal of orthodontics and dentofacial orthopedics : official publication of the American Association of Orthodontists, its constituent societies, and the American Board of Orthodontics*, vol. 106, no. 1, pp. 47–51, 1994.
- [17] M. Ferreira and V. Malmström, *Avaliação da informação óssea na sutura palatina mediana por meio de radiografia digitalizada após a expansão assistida cirurgicamente*. PhD thesis, Universidade de São Paulo, 2005.
- [18] S. Petrick, T. Hothan, V. Hietschold, M. Schneider, W. Harzer, and E. Tausche, "Bone density of the midpalatal suture 7 months after surgically assisted rapid palatal expansion in adults," *American Journal of Orthodontics and Dentofacial Orthopedics*, vol. 139, no. 4 SUPPL., pp. S109–S116, 2011.
- [19] J. Rodrigues Laureano Filho, M. Allais de Maurette, P. E. Maurette O'Brien, and H. Nicodemos da Cruz, "Expansión rápida del maxilar quirúrgicamente asistida, abordaje unilateral," *Acta Odontológica Venezolana*, vol. 45, no. 2, pp. 1–12, 2007.
- [20] A. Consolaro and M. F. M.-O. Consolaro, "Protocolo semanal repetitivo de Expansão Rápida da Maxila e Constrição Alternadas e técnica da Protração Maxilar Ortopédica Efetiva : Por que ? Como ?," vol. 2, pp. 106–111, 2008.
- [21] W. L. Nowinski, T. S. L. Thaug, B. C. Chua, S. H. W. Yi, V. Ngai, Y. Yang, R. Chrzan, and A. Urbanik, "Three-dimensional stereotactic atlas of the adult human skull correlated with the brain, cranial nerves, and intracranial vasculature," *Journal of Neuroscience Methods*, vol. 246, pp. 65–74, 2015.
- [22] D. A. Garzón-Alvarado, "A hypothesis on the formation of the primary ossification centers in the membranous neurocranium: A mathematical and computational model," *Journal of Theoretical Biology*, vol. 317, pp. 366–376, 2013.
- [23] D. Renier, É. Lajeunie, M. Catala, É. Arnaud, and D. Marchac, "Craneoostenosis," *EMC - Pédiatrie*, vol. 43, no. 2, pp. 1–19, 2008.
- [24] A. Maloul, J. Fialkov, D. Wagner, and C. M. Whyne, "Characterization of craniofacial sutures using the finite element method," *Journal of Biomechanics*, vol. 47, no. 1, pp. 245–252, 2014.

- [25] R. H. Khonsari, J. Olivier, P. Vigneaux, S. Sanchez, P. Tafforeau, P. E. Ahlberg, F. Di Rocco, D. Bresch, P. Corre, A. Ohazama, P. T. Sharpe, and V. Calvez, "A mathematical model for mechanotransduction at the early steps of suture formation," *Proceedings of the Royal Society B: Biological Sciences*, vol. 280, no. 1759, pp. 20122670–20122670, 2013.
- [26] A. I. Peptan, A. Lopez, R. A. Kopher, and J. J. Mao, "Responses of intramembranous bone and sutures upon in vivo cyclic tensile and compressive loading," *Bone*, vol. 42, no. 2, pp. 432–438, 2008.
- [27] K. Vij and J. J. Mao, "Geometry and cell density of rat craniofacial sutures during early postnatal development and upon in vivo cyclic loading," *Bone*, vol. 38, no. 5, pp. 722–730, 2006.
- [28] J. Craven, "Anatomy of the skull," *Anaesthesia and Intensive Care Medicine*, vol. 15, no. 4, pp. 146–148, 2014.
- [29] D. Fontes, Ó. Natoli, and J. Pinyot, "Estudio de la craneosinostosis por tomografía computarizada," *Imagen Diagnóstica*, vol. 2, no. 2, pp. 47–52, 2011.
- [30] R. Bristol and S. Beals, "Craniosynostosis," in *Encyclopedia of the Neurological Sciences (Second Edition)*, vol. 1, pp. 894–895, Academic Press, 2014.
- [31] J. Ennes and A. Consolaro, "Sutura palatina mediana: avaliação do grau de ossificação em crânios humanos," *Revista Dental Press de Ortodontia e Ortopedia Facial*, pp. 64–73, 2004.
- [32] M. Thadani, U. Shenoy, B. Patle, A. Kalra, S. Goel, and N. Toshinawal, "Midpalatal Suture Ossification and Skeletal Maturation: A Comparative Computerized Tomographic Scan and Roentgenographic Study," *Journal of Indian Academy of Oral Medicine and Radiology*, vol. 22, no. 2, pp. 81–87, 2010.
- [33] L. Franchi, T. Baccetti, R. Lione, E. Fanucci, and P. Cozza, "Modifications of midpalatal sutural density induced by rapid maxillary expansion: A low-dose computed-tomography evaluation," *American Journal of Orthodontics and Dentofacial Orthopedics*, vol. 137, no. 4, pp. 486–488, 2010.
- [34] M. Schauseil, C. Waldeyer, B. Zorkun, B. Ludwig, A. Hellak, and W. Kater, "Three-Dimensional Quantification of the Effects between Different Types of RME," *Dentistry*, vol. 05, no. 09, 2015.
- [35] O. G. Silva Filho, G. F. Graziani, R. D. C. M. C. Lauris, and T. S. Lara, "Ossificação da sutura palatina mediana após o procedimento de expansão rápida da maxila: estudo radiográfico," *R Dental Press Ortodon Ortop Facial*, vol. 12, pp. 124–131, 2008.
- [36] J. A. McNamara, R. Lione, L. Franchi, F. Angelieri, L. H. Cevidanez, M. A. Darendeliler, and P. Cozza, "The role of rapid maxillary expansion in the promotion of oral and general health," *Progress in orthodontics*, vol. 16, p. 33, 2015.
- [37] P. Velazquez, E. Benito, and L. A. Bravo, "Rapid maxillary expansion. A study of the long-term effects," *American Journal of Orthodontics & Dentofacial Orthopedics*, vol. 109, pp. 361–367, 1996.
- [38] H. N. Chang, L. P. Garetto, R. H. Potter, T. R. Katona, C. H. Lee, and W. E. Roberts, "Angiogenesis and osteogenesis in an orthopedically expanded suture.," *American journal of orthodontics and dentofacial orthopedics : official publication of the American Association of Orthodontists, its constituent societies, and the American Board of Orthodontics*, vol. 111, no. 4, pp. 382–390, 1997.

- [39] M. Sandikçioğlu and S. Hazar, "Skeletal and dental changes after maxillary expansion in the mixed dentition," *American Journal of Orthodontics and Dentofacial Orthopedics*, vol. 111, no. 3, pp. 321–327, 1997.
- [40] M. O. Lagravère, J. P. Carey, G. Heo, R. W. Toogood, and P. W. Major, "Transverse, vertical, and anteroposterior changes from bone-anchored maxillary expansion vs traditional rapid maxillary expansion: A randomized clinical trial," *American Journal of Orthodontics and Dentofacial Orthopedics*, vol. 137, no. 3, pp. 304–305, 2010.
- [41] M. Gunyuz Toklu, D. Germec-Cakan, and M. Tozlu, "Periodontal, dentoalveolar, and skeletal effects of tooth-borne and tooth-bone-borne expansion appliances," *American Journal of Orthodontics and Dentofacial Orthopedics*, vol. 148, no. 1, pp. 97–109, 2015.
- [42] E. Kayalar, M. Schauseil, S. V. Kuvat, U. Emekli, and S. Firatli, "Comparison of tooth-borne and hybrid devices in surgically assisted rapid maxillary expansion: A randomized clinical cone-beam computed tomography study," *Journal of Cranio-Maxillofacial Surgery*, vol. 44, no. 3, pp. 285–293, 2016.
- [43] A. Weissheimer, L. M. E. De Menezes, M. Mezomo, D. M. Dias, E. M. S. De Lima, and S. M. D. Rizzato, "Immediate effects of rapid maxillary expansion with Haas-type and hyrax-type expanders: A randomized clinical trial," *American Journal of Orthodontics and Dentofacial Orthopedics*, vol. 140, no. 3, pp. 366–376, 2011.
- [44] H. Oh, J. Park, and M. O. Lagravere-Vich, "Comparison of traditional RPE with two types of micro-implant assisted RPE: CBCT study," *Seminars in Orthodontics*, vol. 25, no. 1, pp. 60–68, 2019.
- [45] M. Schauseil, B. Ludwig, B. Zorkun, A. Hellak, and H. Korbmacher-Steiner, "Density of the mid-palatal suture after RME treatment - a retrospective comparative low-dose CT-study," *Head and Face Medicine*, vol. 10, no. 1, pp. 6–10, 2014.
- [46] H. M. Lim, Y. C. Park, K. J. Lee, K. H. Kim, and Y. J. Choi, "Stability of dental, alveolar, and skeletal changes after miniscrew-assisted rapid palatal expansion," *Korean Journal of Orthodontics*, vol. 47, no. 5, pp. 313–322, 2017.
- [47] J. H. Henderson, L. Y. Chang, H. M. Song, M. T. Longaker, and D. R. Carter, "Age-dependent properties and quasi-static strain in the rat sagittal suture," *Journal of Biomechanics*, vol. 38, no. 11, pp. 2294–2301, 2005.
- [48] J. A. Parr, L. P. Garetto, M. E. Wohlford, G. R. Arbuckle, and W. E. Roberts, "Sutural expansion using rigidly integrated endosseous implants an experimental study in rabbits.pdf," *The Angle Orthodontist*, vol. 67, no. 4, pp. 283–290, 1997.
- [49] S. S. Y. Liu, L. A. Opperman, H. M. Kyung, and P. H. Buschang, "Is there an optimal force level for sutural expansion?," *American Journal of Orthodontics and Dentofacial Orthopedics*, vol. 139, no. 4, pp. 446–455, 2011.
- [50] A. J. Oppenheimer, S. T. Rhee, S. A. Goldstein, and S. R. Buchman, "Force-induced craniosynostosis via paracrine signaling in the murine sagittal suture," *Journal of Craniofacial Surgery*, vol. 23, no. 2, pp. 573–577, 2012.

- [51] E. Tanaka, Y. Miyawaki, R. Del Pozo, and K. Tanne, "Changes in the biomechanical properties of the rat interparietal suture incident to continuous tensile force application," *Archives of Oral Biology*, vol. 45, no. 12, pp. 1059–1064, 2000.
- [52] E. Tanaka, Y. Miyawaki, M. Tanaka, M. Watanabe, K. Lee, R. Del Pozo, and K. Tanne, "Effects of tensile forces on the expression of type III collagen in rat interparietal suture," *Archives of Oral Biology*, vol. 45, no. 12, pp. 1049–1057, 2000.
- [53] L. A. Opperman, "Cranial Sutures as Intramembranous Bone Growth Sites," *Journal of Bone and Mineral Research*, vol. 485, no. September, pp. 472–485, 2000.
- [54] C. Lee, J. T. Richtsmeier, and R. H. Kraft, "A Computational Analysis of Bone Formation in the Cranial Vault in the Mouse," *Frontiers in Bioengineering and Biotechnology*, vol. 3, no. March, pp. 1–11, 2015.
- [55] M. Beederman, E. M. Farina, and R. R. Reid, "Molecular basis of cranial suture biology and disease: Osteoblastic and osteoclastic perspectives," *Genes and Diseases*, vol. 1, no. 1, pp. 120–125, 2014.
- [56] K. B. S. Paiva and J. M. Granjeiro, "Bone tissue remodeling and development: Focus on matrix metalloproteinase functions," *Archives of Biochemistry and Biophysics*, vol. 561, pp. 74–87, 2014.
- [57] M. A. Katsianou, C. Adamopoulos, H. Vastardis, and E. K. Basdra, "Signaling mechanisms implicated in cranial sutures pathophysiology: Craniosynostosis," *BBA Clinical*, vol. 6, pp. 165–176, 2016.
- [58] E. Yilmaz, E. Mihci, B. Nur, Ö. M. Alper, and ü. Taçoy, "Recent Advances in Craniosynostosis," *Pediatric Neurology*, 2019.
- [59] E. Van Otterloo, W. Feng, K. L. Jones, N. E. Hynes, D. E. Clouthier, L. Niswander, and T. Williams, "MEMO1 drives cranial endochondral ossification and palatogenesis," *Developmental Biology*, vol. 415, no. 2, pp. 278–295, 2016.
- [60] S. R. Moore, G. M. Saidel, U. Knothe, and M. L. Knothe Tate, "Mechanistic, Mathematical Model to Predict the Dynamics of Tissue Genesis in Bone Defects via Mechanical Feedback and Mediation of Biochemical Factors," *PLoS Computational Biology*, vol. 10, no. 6, 2014.
- [61] M. L. Rodriguez, P. J. McGarry, and N. J. Sniadecki, "Review on Cell Mechanics: Experimental and Modeling Approaches," *Applied Mechanics Reviews*, vol. 65, no. 6, p. 060801, 2013.
- [62] D. A. Roth, L. I. Gold, V. K. Han, J. G. McCarthy, J. J. Sung, J. H. Wisoff, and M. T. Longaker, "Immunolocalization of transforming growth factor beta 1, beta 2, and beta 3 and insulin-like growth factor I in premature cranial suture fusion.," *Plastic and reconstructive surgery*, vol. 99, pp. 300–9; discussion 310–6, feb 1997.
- [63] M. Sawada and N. Shimizu, "Stimulation of bone formation in the expanding mid-palatal suture by transforming growth factor-S , in the rat," *European Journal of Orthodontics*, vol. 18, no. 2, pp. 169–179, 1996.
- [64] S. S. Y. Liu, H. Xu, J. Sun, E. Kontogiorgos, P. R. Whittington, K. G. Misner, H. M. Kyung, P. H. Buschang, and L. A. Opperman, "Recombinant human bone morphogenetic protein-2 stimulates bone formation during interfrontal suture expansion in rabbits," *American Journal of Orthodontics and Dentofacial Orthopedics*, vol. 144, no. 2, pp. 210–217, 2013.

- [65] K. Hirukawa, K. Miyazawa, H. Maeda, Y. Kameyama, S. Goto, and A. Togari, "Effect of tensile force on the expression of IGF-I and IGF-I receptor in the organ-cultured rat cranial suture," *Archives of Oral Biology*, vol. 50, no. 3, pp. 367–372, 2005.
- [66] B. Hou, E. Kolpakova-Hart, N. Fukai, K. Wu, and B. R. Olsen, "The polycystic kidney disease 1 (Pkd1) gene is required for the responses of osteochondroprogenitor cells to midpalatal suture expansion in mice," *Bone*, vol. 44, no. 6, pp. 1121–1133, 2009.
- [67] A. Burn, S. Herring, R. Hubbard, K. Zink, K. Rafferty, and D. Lieberman, "Dietary consistency and the midline sutures in growing pigs," *Orthodontics & Craniofacial Research*, vol. 13, pp. 106–113, may 2010.
- [68] M. C. Van der Meulen and R. Huiskes, "Why mechanobiology? A survey article," *Journal of Biomechanics*, vol. 35, no. 4, pp. 401–414, 2002.
- [69] J. A. Guerrero, J. C. Vanegas, D. A. Garzón, M. Casale, and H. Arzate, "Mechanobiology of Oral Implantable Devices," in *Biomaterials Science and Engineering* (Rosario Pignatello, ed.), ch. 15, pp. 309–336, InTech, 2011.
- [70] J. Klein-Nulend, R. G. Bacabac, and M. G. Mullender, "Mechanobiology of bone tissue," *Pathologie Biologie*, vol. 53, no. 10, pp. 576–580, 2005.
- [71] N. K. Srinivasan, "Computer Based Modelling and Simulation 1.," *Resonance*, vol. 6, no. March, pp. 46–54, 2001.
- [72] C. P. Zollikofer and J. D. Weissmann, "A bidirectional interface growth model for cranial interosseous suture morphogenesis," *Journal of Anatomy*, vol. 219, no. 2, pp. 100–114, 2011.
- [73] T. Miura, C. A. Perlyn, M. Kinboshi, N. Ogihara, M. Kobayashi-Miura, G. M. Morriss-Kay, and K. Shiota, "Mechanism of skull suture maintenance and interdigitation," *Journal of Anatomy*, vol. 215, no. 6, pp. 642–655, 2009.
- [74] K. Yoshimura, R. Kobayashi, T. Ohmura, Y. Kajimoto, and T. Miura, "A new mathematical model for pattern formation by cranial sutures," *Journal of Theoretical Biology*, vol. 408, pp. 66–74, 2016.
- [75] F. J. Burgos-Flórez, M. E. Gavilán-Alfonso, and D. A. Garzón-Alvarado, "Flat bones and sutures formation in the human cranial vault during prenatal development and infancy: A computational model," *Journal of Theoretical Biology*, vol. 393, pp. 127–144, 2016.
- [76] D. A. Garzón-Alvarado, A. González, and M. L. Gutiérrez, "Growth of the flat bones of the membranous neurocranium: A computational model," *Computer Methods and Programs in Biomedicine*, vol. 112, no. 3, pp. 655–664, 2013.
- [77] D. A. Garzón-Alvarado, C. H. Galeano, and J. M. Mantilla, "Turing pattern formation for reaction-convection-diffusion systems in fixed domains submitted to toroidal velocity fields," *Applied Mathematical Modelling*, vol. 35, no. 10, pp. 4913–4925, 2011.
- [78] E. J. de Oliveira, *Biomecânica avançada no controle de efeitos colaterais em ortodontia*. Belo Horizonte: Real Produções Gráficas Ltda, 2005.
- [79] M. Nordin, *Biomecánica Basica del Sistema Musculoesquelético*. Madrid: McGraw-Hill, tercera ed., 2004.

- [80] G. R. Suarez, *Biomecánica deportiva y control del entrenamiento*. Medellín: Funámbulo Editores, primera ed., 2009.
- [81] M. S. Commisso Cuñarro, *Biomecánica de mandíbula humana*. PhD thesis, Universidad de Sevilla, 2010.
- [82] D. L. Romanyk, C. R. Collins, M. O. Lagravere, R. W. Toogood, P. W. Major, and J. P. Carey, "Role of the midpalatal suture in FEA simulations of maxillary expansion treatment for adolescents: A review," *International Orthodontics*, vol. 11, no. 2, pp. 119–138, 2013.
- [83] J. Priyadarshini, C. M. Mahesh, B. S. Chandrashekar, A. Sundara, A. V. Arun, and V. P. Reddy, "Stress and displacement patterns in the craniofacial skeleton with rapid maxillary expansion—a finite element method study," *Progress in Orthodontics*, vol. 18, no. 1, 2017.
- [84] H. Lee, K. Ting, M. Nelson, N. Sun, and S. J. Sung, "Maxillary expansion in customized finite element method models," *American Journal of Orthodontics and Dentofacial Orthopedics*, vol. 136, no. 3, pp. 367–374, 2009.
- [85] D. L. Romanyk, S. S. Liu, R. Long, and J. P. Carey, "Considerations for determining relaxation constants from creep modeling of nonlinear suture tissue," *International Journal of Mechanical Sciences*, vol. 85, pp. 179–186, 2014.
- [86] D. L. Romanyk, C. Shim, S. S. Liu, M. O. Lagravere, P. W. Major, and J. P. Carey, "Viscoelastic response of the midpalatal suture during maxillary expansion treatment," *Orthodontics and Craniofacial Research*, vol. 19, no. 1, pp. 28–35, 2016.
- [87] D. L. Romanyk, S. S. Liu, M. G. Lipsett, R. W. Toogood, M. O. Lagravère, P. W. Major, and J. P. Carey, "Towards a viscoelastic model for the unfused midpalatal suture: Development and validation using the midsagittal suture in New Zealand white Rabbits," *Journal of Biomechanics*, vol. 46, no. 10, pp. 1618–1625, 2013.
- [88] B. Ludwig, S. Baumgaertel, B. Zorkun, L. Bonitz, B. Glasl, B. Wilmes, and J. Lisson, "Application of a new viscoelastic finite element method model and analysis of miniscrew-supported hybrid hyrax treatment," *American Journal of Orthodontics and Dentofacial Orthopedics*, vol. 143, no. 3, pp. 426–435, 2013.
- [89] L. Carvalho Trojan Serpe, E. Barbosa de Las Casas, A. C. Toyofuku Moreira Melo, and L. A. González-Torres, "A bilinear elastic constitutive model applied for midpalatal suture behavior during rapid maxillary expansion," *Revista Brasileira de Engenharia Biomedica*, vol. 31, no. 4, pp. 319–327, 2015.
- [90] S. C. Jasinowski, B. D. Reddy, K. K. Louw, and A. Chinsamy, "Mechanics of cranial sutures using the finite element method," *Journal of Biomechanics*, vol. 43, no. 16, pp. 3104–3111, 2010.
- [91] S. C. Jasinowski and B. D. Reddy, "Mechanics of cranial sutures during simulated cyclic loading," *Journal of Biomechanics*, vol. 45, no. 11, pp. 2050–2054, 2012.
- [92] L. Liu, Y. Jiang, M. Boyce, C. Ortiz, J. Baur, J. Song, and Y. Li, "The effects of morphological irregularity on the mechanical behavior of interdigitated biological sutures under tension," *Journal of Biomechanics*, vol. 58, pp. 71–78, 2017.

- [93] U. A. Han, Y. Kim, and J. U. Park, "Three-dimensional finite element analysis of stress distribution and displacement of the maxilla following surgically assisted rapid maxillary expansion," *Journal of Cranio-Maxillofacial Surgery*, vol. 37, no. 3, pp. 145–154, 2009.
- [94] R. M. de Sousa Araugio, J. Landre Jr, D. d. L. A. Silva, W. Pacheco, M. M. Pithon, and D. D. Oliveira, "Influence of the expansion screw height on the dental effects of the hyrax expander: A study with finite elements," *American Journal of Orthodontics and Dentofacial Orthopedics*, vol. 143, no. 2, pp. 221–227, 2013.
- [95] Y. Matsuyama, M. Motoyoshi, N. Tsurumachi, and N. Shimizu, "Effects of palate depth, modified arm shape, and anchor screw on rapid maxillary expansion: A finite element analysis," *European Journal of Orthodontics*, vol. 37, no. 2, pp. 188–193, 2014.
- [96] L. Carvalho Trojan, L. Andrés González-Torres, A. Claudia Moreira Melo, and E. Barbosa de Las Casas, "Stresses and Strains Analysis Using Different Palatal Expander Appliances in Upper Jaw and Midpalatal Suture," *Artificial Organs*, vol. 41, no. 6, pp. E41–E51, 2017.
- [97] V. Jain, T. R. Shyagali, P. Kambalyal, Y. Rajpara, and J. Doshi, "Comparison and evaluation of stresses generated by rapid maxillary expansion and the implant-supported rapid maxillary expansion on the craniofacial structures using finite element method of stress analysis," *Progress in Orthodontics*, vol. 18, no. 3, pp. 1–12, 2017.
- [98] M. Macginnis, H. Chu, G. Youssef, K. W. Wu, A. W. Machado, and W. Moon, "The effects of micro-implant assisted rapid palatal expansion (MARPE) on the nasomaxillary complex – a Finite Element Method (FEM) analysis," *Progress in orthodontics*, pp. 1–15, 2014.
- [99] H. K. Lee, M. Bayome, C. S. Ahn, S. H. Kim, K. B. Kim, S. S. Mo, and Y. A. Kook, "Stress distribution and displacement by different bone-borne palatal expanders with micro-implants: A three-dimensional finite-element analysis," *European Journal of Orthodontics*, vol. 36, no. 5, pp. 531–540, 2014.
- [100] S. C. Lee, J. H. Park, M. Bayome, K. B. Kim, E. A. Araujo, and Y. A. Kook, "Effect of bone-borne rapid maxillary expanders with and without surgical assistance on the craniofacial structures using finite element analysis," *American Journal of Orthodontics and Dentofacial Orthopedics*, vol. 145, no. 5, pp. 638–648, 2014.
- [101] F. Savoldi, B. Xu, J. K. Tsoi, C. Paganelli, and J. P. Matinlinna, "Anatomical and mechanical properties of swine midpalatal suture in the premaxillary, maxillary, and palatine region," *Scientific Reports*, vol. 8, no. 1, pp. 1–12, 2018.
- [102] A. Consolaro and M. F. M.-O. Consolaro, "Expansão Rápida da Maxila e Constricção Alternadas (ERMC-Alt) e técnica de Protração Maxilar Ortopédica Efetiva : extrapolação de conhecimentos prévios para fundamentação biológica," *Dental Press Ortodon Ortop Facial*, vol. 13, no. 1, pp. 18–23, 2008.
- [103] A. Di Ieva, E. Bruner, J. Davidson, P. Pisano, T. Haider, S. S. Stone, M. D. Cusimano, M. Tschabitscher, and F. Grizzi, "Cranial sutures: A multidisciplinary review," *Child's Nervous System*, vol. 29, no. 6, pp. 893–905, 2013.
- [104] M. Del Santo, A. M. Minarelli, and E. A. Liberti, "Morphological aspects of the mid-palatal suture in the human foetus: A light and scanning electron microscopy study," *European Journal of Orthodontics*, vol. 20, no. 1, pp. 93–99, 1998.

- [105] B. Knaup, F. Yildizhan, and H. Wehrbein, "Altersveränderungen der Sutura palatina mediana: Eine histomorphometrische Studie," *Journal of Orofacial Orthopedics*, vol. 65, no. 6, pp. 467–474, 2004.
- [106] H. Korbmacher, A. Schilling, K. Püschel, M. Amling, and B. Kahl-Nieke, "Dreidimensionale mikro-computertomographische Analyse der humanen Sutura palatina mediana in Abhängigkeit vom Alter," *Journal of Orofacial Orthopedics*, vol. 68, no. 5, pp. 364–376, 2007.
- [107] H. Wehrbein and F. Yildizhan, "The mid-palatal suture in young adults. A radiological-histological investigation," *European Journal of Orthodontics*, vol. 23, no. 2, pp. 105–114, 2001.
- [108] M. Dobrzyński, K. Miśków, and K. Dowgierd, "Selected palatal suture expansion techniques in the treatment of transvers maxillary narrowings-literature review," *Polish Annals of Medicine*, vol. 20, no. 2, pp. 160–163, 2013.
- [109] K. A. Schlegel, F. Kinner, and K. D. Schlegel, "The anatomic basis for palatal implants in orthodontics.," *The International journal of adult orthodontics and orthognathic surgery*, vol. 17, no. 2, pp. 133–9, 2002.
- [110] S. W. Herring, "Mechanical Influences on Suture Development and Patency," *Front Oral Biol*, vol. 7446, pp. 1–15, 2010.
- [111] D. Cantarella, R. Dominguez-Mompell, C. Moschik, L. Sfogliano, I. Elkenawy, H. C. Pan, S. M. Mallya, and W. Moon, "Zygomaticomaxillary modifications in the horizontal plane induced by micro-implant-supported skeletal expander, analyzed with CBCT images," *Progress in Orthodontics*, vol. 19, no. 1, 2018.
- [112] S. M. Alaqeel, R. J. Hinton, and L. A. Opperman, "Cellular response to force application at craniofacial sutures," *Orthodontics and Craniofacial Research*, vol. 9, no. 3, pp. 111–122, 2006.
- [113] J. C. Yu, J. L. Borke, and G. Zhang, "Brief synopsis of cranial sutures: Optimization by adaptation," *Seminars in Pediatric Neurology*, vol. 11, no. 4, pp. 249–255, 2004.
- [114] J. Chen, J. Zhou, F. Li, J. Sun, G. Li, S. Zou, and Q. Ye, "Expression of MMP-2 and TIMP-1 during rapid maxillary expansion in rats," *Archives of Oral Biology*, vol. 76, pp. 30–35, 2017.
- [115] J. Fernando Ramírez Patiño, J. Andrea Isaza, and J. Andrés Vélez Zea, "Unidades Hounsfield como instrumento para la evaluación de la desmineralización ósea producida por el uso de exoprótesis," *Rev. Fac. Ing. Univ. Antioquia*, vol. 66, pp. 159–167, 2013.
- [116] Y. Cheng, J. Sun, Z. Zhou, J. Pan, S. Zou, and J. Chen, "Effects of lactoferrin on bone resorption of midpalatal suture during rapid expansion in rats," *American Journal of Orthodontics and Dentofacial Orthopedics*, vol. 154, no. 1, pp. 115–127, 2018.
- [117] B.-H. Wu, X.-X. Kou, C. Zhang, Y.-M. Zhang, Z. Cui, X.-D. Wang, Y. Liu, D.-W. Liu, and Y.-H. Zhou, "Stretch force guides finger-like pattern of bone formation in suture," *Plos One*, vol. 12, no. 5, p. e0177159, 2017.
- [118] B. F. Boyce and L. Xing, "Bruton and Tec: New Links in Osteoimmunology," *Cell Metabolism*, vol. 7, no. 4, pp. 283–285, 2008.
- [119] S. Aoki, M. Honma, Y. Kariya, Y. Nakamichi, T. Ninomiya, N. Takahashi, N. Udagawa, and H. Suzuki, "Function of OPG as a traffic regulator for RANKL is crucial for controlled osteoclastogenesis," *Journal of Bone and Mineral Research*, vol. 25, no. 9, pp. 1907–1921, 2010.

- [120] V. Krishnan and Z. Davidovitch, "Cellular, molecular, and tissue-level reactions to orthodontic force," *American Journal of Orthodontics and Dentofacial Orthopedics*, vol. 129, no. 4, pp. 469.e1–469.e32, 2006.
- [121] G. E. Wise and G. J. King, "Mechanisms of tooth eruption and orthodontic tooth movement," *Journal of Dental Research*, vol. 87, no. 5, pp. 414–434, 2008.
- [122] E. M. Greenfield, Y. Bi, and A. Miyauchi, "Regulation of osteoclast activity," *Life Sciences*, vol. 65, no. 11, pp. 1087–1102, 1999.
- [123] J. M. Guevara, Y. Hata, and S. J. Shefelbine, "Mechanobiological modeling of endochondral ossification : an experimental and computational analysis," *Biomechanics and Modeling in Mechanobiology*, 2018.
- [124] Y. Kameo, T. Adachi, and M. Hojo, "Effects of loading frequency on the functional adaptation of trabeculae predicted by bone remodeling simulation," *Journal of the Mechanical Behavior of Biomedical Materials*, vol. 4, no. 6, pp. 900–908, 2011.
- [125] J. Li, H. Li, L. Shi, A. S. Fok, C. Ucer, H. Devlin, K. Horner, and N. Silikas, "A mathematical model for simulating the bone remodeling process under mechanical stimulus," *Dental Materials*, vol. 23, no. 9, pp. 1073–1078, 2007.
- [126] J. R. Fernández, J. M. García-Aznar, R. Martínez, and J. M. Viaño, "Numerical analysis of a strain-adaptive bone remodelling problem," *Computer Methods in Applied Mechanics and Engineering*, vol. 199, no. 23-24, pp. 1549–1557, 2010.
- [127] D. A. Garzón-Alvarado, J. M. García-Aznar, and M. Doblaré, "A reaction-diffusion model for long bones growth," *Biomechanics and Modeling in Mechanobiology*, vol. 8, no. 5, pp. 381–395, 2009.
- [128] J. M. Guevara, M. A. Moncayo, J. J. Vaca-González, M. L. Gutiérrez, L. A. Barrera, and D. A. Garzón-Alvarado, "Growth plate stress distribution implications during bone development: A simple framework computational approach," *Computer Methods and Programs in Biomedicine*, vol. 118, no. 1, pp. 59–68, 2015.
- [129] J. Nino-Barrera, J. Guerrero, G. Nino, M. Cerrolaza, E. de las Casas, A. Ramírez Martínez, and D. Garzón-Alvarado, "Finite Element Modeling of Turing Pattern Formation," in *Numerical Methods and Advanced Simulation in Biomechanics and Biological Processes*, ch. 5, pp. 77–94, Elsevier, 2018.
- [130] H. Isaksson, O. Comas, C. C. van Donkelaar, J. Mediavilla, W. Wilson, R. Huiskes, and K. Ito, "Bone regeneration during distraction osteogenesis: Mechano-regulation by shear strain and fluid velocity," *Journal of Biomechanics*, vol. 40, no. 9, pp. 2002–2011, 2007.
- [131] E. Reina-Romo, M. J. Gómez-Benito, J. M. García-Aznar, J. Domínguez, and M. Doblaré, "Growth mixture model of distraction osteogenesis: Effect of pre-traction stresses," *Biomechanics and Modeling in Mechanobiology*, vol. 9, no. 1, pp. 103–115, 2010.
- [132] L. A. González, J. C. Vanegas, and D. A. Garzón, "Formación de patrones en sistemas de reacción-difusión en dominios crecientes," *Universidad Politécnica de Catalunya*, vol. 25, pp. 145–161, 2009.

- [133] J. C. Vanegas-Acosta and D. A. Garzón-Alvarado, "Biological modelling and computational implementation using the finite elements method," *Computational and Applied Mathematics*, vol. 33, no. 3, pp. 621–640, 2013.
- [134] D. A. Garzón Alvarado, *Simulación de procesos de reacción-difusión: aplicación a la morfogénesis del tejido óseo*. PhD thesis, Universidad de Zaragoza, 2007.
- [135] M. Watanabe and S. Kondo, "Is pigment patterning in fish skin determined by the Turing mechanism?," *Trends in Genetics*, vol. 31, no. 2, pp. 88–96, 2015.
- [136] D. G. Míguez and A. P. Muñuzuri, "On the orientation of stripes in fish skin patterning," *Biophysical Chemistry*, vol. 124, no. 2, pp. 161–167, 2006.
- [137] L. Marcon and J. Sharpe, "Turing patterns in development: What about the horse part?," *Current Opinion in Genetics and Development*, vol. 22, no. 6, pp. 578–584, 2012.
- [138] N. V. Mantzaris, S. Webb, and H. G. Othmer, "Mathematical modeling of tumor-induced angiogenesis," *Journal of Mathematical Biology*, vol. 49, no. 2, pp. 111–187, 2004.
- [139] L. Ritter and A. Texas, "A Short Course In the Modeling of Chemotaxis," *Texas A & M University*, 2004.
- [140] T. Hillen and K. J. Painter, "A user's guide to PDE models for chemotaxis," *Journal of Mathematical Biology*, vol. 58, no. 1-2, pp. 183–217, 2009.
- [141] S. R. F. Twigg and A. O. M. Wilkie, "A Genetic-Pathophysiological Framework for Craniosynostosis," *American Journal of Human Genetics*, vol. 97, no. 3, pp. 359–377, 2015.
- [142] D. A. Garzón-Alvarado and A. M. Ramírez Martínez, "A biochemical hypothesis on the formation of fingerprints using a turing patterns approach," *Theoretical Biology and Medical Modelling*, vol. 8, no. 1, pp. 1–10, 2011.
- [143] P. Chamorro-Posada, "A simple method for estimating the fractal dimension from digital images: The compression dimension," *Chaos, Solitons and Fractals*, vol. 91, pp. 562–572, 2016.
- [144] H. Lodish, A. Berk, S. L. Zipursky, P. Matsudaira, D. Baltimore, and J. Darnell, *Molecular Cell Biology*. New York: W. H. Freeman, 4th ed., 2000.
- [145] Dentaurum, "Expansion screws," tech. rep., Dentaurum, Ispringen, 2018.
- [146] O. M. Tanaka, A. Y. Saga, M. M. Pithon, and M. A. Argenta, "Stresses in the midpalatal suture in the maxillary protraction therapy: A 3D finite element analysis," *Progress in Orthodontics*, vol. 17, no. 1, 2016.
- [147] S. Bosiakov, A. Vinokurova, and A. Dosta, "Craniofacial Stress Patterns and Displacements After Activation of Hyrax Device: Finite Element Modelling," *Facta Universitatis, Series: Mechanical Engineering*, vol. 15, no. 3, pp. 517–533, 2017.
- [148] L. C. Trojan-serpe, L. S. Dorneles, A. Claudia, M. Melo, E. Barbosa, and D. L. Casas, "Strain Level At Midpalatal Suture-Correlation With Mechanobiological Concepts," *22nd International Congress of Mechanical Engineering*, no. Cobem, pp. 8523–8531, 2013.
- [149] J. H. Park, M. Bayome, J. J. Zahrowski, and Y. A. Kook, "Displacement and stress distribution by different bone-borne palatal expanders with facemask: A 3-dimensional finite element analysis," *American Journal of Orthodontics and Dentofacial Orthopedics*, vol. 151, no. 1, pp. 105–117, 2017.

-
- [150] K. J. Lee, Y. C. Park, J. Y. Park, and W. S. Hwang, “Miniscrew-assisted nonsurgical palatal expansion before orthognathic surgery for a patient with severe mandibular prognathism,” *American Journal of Orthodontics and Dentofacial Orthopedics*, vol. 137, no. 6, pp. 830–839, 2010.